Marcus Großmann

Transmission Strategies for Broadband Wireless Systems with MMSE Turbo Equalization

Transmission Strategies for Broadband Wireless Systems with MMSE Turbo Equalization

Marcus Großmann

Universitätsverlag Ilmenau
2012

Impressum

Bibliografische Information der Deutschen Nationalbibliothek
Die Deutsche Nationalbibliothek verzeichnet diese Publikation in der Deutschen Nationalbibliografie; detaillierte bibliografische Angaben sind im Internet über http://dnb.d-nb.de abrufbar.

Diese Arbeit hat der Fakultät für Elektrotechnik und Informationstechnik der Technischen Universität Ilmenau als Dissertation vorgelegen.

Tag der Einreichung:	9. Dezember 2011
1. Gutachter:	Prof. Dr.-Ing. habil. Reiner Thomä (Technische Universität Ilmenau)
2. Gutachter:	Prof. Dr.-Ing. habil. Volker Kühn (Universität Rostock)
3. Gutachter:	Dr.-Ing. Werner Teich (Universität Ulm)
Tag der Verteidigung:	6. Juli 2012

Technische Universität Ilmenau/Universitätsbibliothek
Universitätsverlag Ilmenau
Postfach 10 05 65
98684 Ilmenau
www.tu-ilmenau.de/universitaetsverlag

Herstellung und Auslieferung
Verlagshaus Monsenstein und Vannerdat OHG
Am Hawerkamp 31
48155 Münster
www.mv-verlag.de

ISBN 978-3-86360-040-2 (Druckausgabe)
URN urn:nbn:de:gbv:ilm1-2012000014

Titelfoto: photocase.com | AlexFlint

Acknowledgments

I gratefully acknowledge all the people who helped me to finalize my dissertation at the Ilmenau University of Technology. Foremost, I owe my thanks to Prof. Reiner Thomä for the opportunity of being a part of his research group, the academic freedom he provided me with and the guidance and assistance during the past years at his lab.

I would like to express my sincere gratitude to Prof. Tad Matsumoto for the fruitful discussions and his very kind support and encouragement during my research visits at the Center for Wireless Communications in Oulu, Finland and the Japan Advanced Institute of Technology in Kanazawa, Japan. Tad was an invaluable source of ideas and inspiration for my research work and I highly appreciate his enormous effort for unofficially supervising my thesis work. I have learned a huge amount of new things from him not only on a scientific level, but also on a personal level. I will also remember Tad for his fantastic cooking he almost daily prepared for me when he was staying as a Visiting Professor at the Ilmenau University of Technology.

Furthermore, I would like to thank Prof. Volker Kühn and Dr. Werner Teich for acting as referees for this work and their helpful comments and constructive suggestions for improving the quality of this dissertation. I am grateful to Mario Lorenz for carefully proofreading the manuscript.

I am thankful to all my colleagues at the Electronic Measurement Research Lab and especially to Christian Schneider, Dr.-Ing Aihua Hong and Dr. Alexis Paolo Garcia Ariza. I spent a great time working together with them. I also acknowledge the friendly support from Henning Schwanbeck for all the issues related to the use of the compute cluster.

Last, but not least, my deepest gratitude goes to my wife, Andrea, and my children, Elise Lotte and Gustav Sander, for their understanding and endless love. My parents, Inge and Reiner, as well as my brother, Sascha, receive my sincere gratitude for their dedication, love and the constant moral support during my academic life.

Zusammenfassung

Die vorliegende Arbeit beschäftigt sich mit dem Entwurf und der Analyse von effizienten Übertragungskonzepten für drahtlose, breitbandige Einträger-Kommunikationssysteme mit iterativer (Turbo-) Entzerrung und Kanaldekodierung. Dies beinhaltet einerseits die Entwicklung von empfängerseitigen Frequenzbereichsentzerrern mit geringer Komplexität basierend auf dem Prinzip der Soft Interference Cancellation Minimum-Mean Squared-Error (SC-MMSE) Filterung und andererseits den Entwurf von senderseitigen Konzepten, die durch Ausnutzung von Kanalzustandsinformationen die Bandbreiten- und Leistungseffizienz von Ein- und Mehrnutzersystemen mit Mehrfachantennen (sog. Multiple-Input Multiple-Output (MIMO)) verbessern.

Im ersten Teil dieser Arbeit wird ein allgemeiner Ansatz für Verfahren zur Turbo-Entzerrung nach dem Prinzip der MMSE-Schätzung sowie der kombinierten MMSE- und Maximum-a-Posteriori (MAP)-Schätzung vorgestellt. In diesem Zusammenhang werden zwei neue Empfängerkonzepte, die eine Steigerung der Leistungsfähigkeit und Verbesserung der Konvergenz in Bezug auf existierende SC-MMSE Turbo-Entzerrer in verschiedenen Kanalumgebungen erzielen, eingeführt. Der erste Empfänger - PDA SC-MMSE - stellt eine Kombination aus dem Probabilistic-Data-Association (PDA) Ansatz und dem bekannten SC-MMSE Entzerrer dar. Im Gegensatz zum SC-MMSE nutzt der PDA SC-MMSE eine interne Entscheidungsrückführung, so dass zur Unterdrückung von Interferenzen neben den *a priori* Informationen der Kanaldekodierung auch weiche Entscheidungen der vorherigen Detektionsschritte berücksichtigt werden. Durch die zusätzlich interne Entscheidungsrückführung erzielt der PDA SC-MMSE einen wesentlichen Gewinn an Performance in räumlich unkorrelierten MIMO-Kanälen gegenüber dem SC-MMSE, ohne dabei die Komplexität des Entzerrers wesentlich zu erhöhen. Der zweite Empfänger - HY SC-MMSE - bildet eine Verknüpfung von gruppenbasierter SC-MMSE Frequenzbereichsfilterung und MAP-Detektion. Dieser Empfänger besitzt eine skalierbare Berechnungskomplexität und weist eine hohe Robustheit gegenüber räumlichen Korrelationen in MIMO-Kanälen auf. Die numerischen Ergebnisse von Simulationen basierend auf Messungen mit einem Channel-Sounder in Mehrnutzerkanälen mit starken räumlichen Korrelationen zeigen eindrucksvoll die Überlegenheit des HY SC-MMSE-Ansatzes gegenüber dem konventionellen SC-MMSE-basiertem Empfänger.

Im zweiten Teil wird der Einfluss von System- und Kanalmodellparametern auf die Konvergenzeigenschaften der vorgestellten iterativen Empfänger mit Hilfe sogenannter Korrelationsdiagramme untersucht. Durch semi-analytische Berechnungen der Entzerrer- und Kanaldekoder-Korrelationsfunktionen wird eine einfache Berechnungsvorschrift zur Vorhersage der Bitfehlerwahrscheinlichkeit von SC-MMSE und PDA SC-MMSE Turbo Entzerrern für MIMO-Fadingkanäle entwickelt. Des Weiteren werden zwei Fehlerschranken für die Ausfallwahrscheinlichkeit der Empfänger vorgestellt. Die semi-analytische Methode und die abgeleiteten Fehlerschranken ermöglichen eine aufwandsgeringe Abschätzung sowie Optimierung der Leistungsfähigkeit der iterativen Systeme.

Im dritten und abschließenden Teil werden Strategien zur Raten- und Leistungszuweisung in Kommunikationssystemen mit konventionellen iterativen SC-MMSE Empfängern untersucht. Zunächst wird das Problem der Maximierung der instantanen Summendatenrate unter der Berücksichtigung der Konvergenz des iterativen Empfängers für einen Zweinutzerkanal mit fester Leistungsallokation betrachtet. Mit Hilfe des Flächentheorems von Extrinsic-Information-Transfer (EXIT)-Funktionen wird eine obere Schranke für die erreichbare Ratenregion hergeleitet. Auf Grundlage dieser Schranke wird ein einfacher Algorithmus entwickelt, der für jeden Nutzer aus einer Menge von vorgegebenen Kanalkodes mit verschiedenen Kodierraten denjenigen auswählt, der den instantanen Datendurchsatz des Mehrnutzersystems verbessert. Neben der instantanen Ratenzuweisung wird auch ein ausfallbasierter Ansatz zur Ratenzuweisung entwickelt. Hierbei erfolgt die Auswahl der Kanalkodes für die Nutzer unter Berücksichtigung der Einhaltung einer bestimmten Ausfallwahrscheinlichkeit (Outage Probability) des iterativen Empfängers. Des Weiteren wird ein neues Entwurfskriterium für irreguläre Faltungskodes hergeleitet, das die Ausfallwahrscheinlichkeit von Turbo SC-MMSE Systemen verringert und somit die Zuverlässigkeit der Datenübertragung erhöht. Eine Reihe von Simulationsergebnissen von Kapazitäts- und Durchsatzberechnungen werden vorgestellt, die die Wirksamkeit der vorgeschlagenen Algorithmen und Optimierungsverfahren in Mehrnutzerkanälen belegen. Abschließend werden außerdem verschiedene Maßnahmen zur Minimierung der Sendeleistung in Einnutzersystemen mit senderseitiger Singular-Value-Decomposition (SVD)-basierter Vorkodierung untersucht. Es wird gezeigt, dass eine Methode, welche die Leistungspegel des Senders hinsichtlich der Bitfehlerrate des iterativen Empfängers optimiert, den konventionellen Verfahren zur Leistungszuweisung überlegen ist.

Abstract

This thesis deals with the design and analysis of efficient transmission strategies for wireless single-carrier broadband communication systems with iterative (turbo) joint channel equalization and decoding. On the one hand, the investigations are focused on the development of advanced low complexity turbo frequency domain equalizer (FDE) techniques based on the principle of soft interference cancellation and minimum-mean squared-error (SC-MMSE) filtering. On the other hand, the investigations are concerned with the development of practical transmitter schemes that aim to improve spectrum and power efficiency by exploiting channel state information in single- and uplink multiple-access multiple-input multiple-output (MIMO) communication systems.

The first part of the thesis presents a generic framework for turbo equalization based on MMSE signal estimation and combined MMSE and maximum *a posteriori* (MAP) signal estimation. In this context, two novel turbo equalizer designs are devised that improve performance and exhibit a better convergence behavior over the existing standard SC-MMSE FDE in a variety of channel environments. The first receiver combines probabilistic data association (PDA) detection and frequency domain SC-MMSE filtering in one algorithm. This receiver, referred to as PDA SC-MMSE FDE, has a similar structure than the existing SC-MMSE FDE. However, additionally to the *a priori* information from channel decoding, it exploits soft-decision feedback within the equalizer for interference cancellation. The PDA SC-MMSE FDE achieves impressive performance gains over the SC-MMSE FDE in spatially-uncorrelated MIMO block-fading channels, without significantly increasing the computational complexity of the equalizer. The second receiver jointly performs groupwise frequency domain SC-MMSE filtering and MAP signal detection. This algorithm, referred to as HY SC-MMSE FDE, offers a great design flexibility in terms of complexity and robustness against spatial channel correlation. Numerical results obtained through a series of simulations using channel-sounding field measurement data demonstrate the superiority of the HY SC-MMSE FDE over the existing SC-MMSE FDE in uplink multiple-access interference environments with strong correlation between the users' channels.

In the second part of the thesis, the impact of system and channel model parameters on the convergence properties of turbo equalizers is investigated with the aid of

the recently proposed correlation chart analysis method. Based on semi-analytical computations of the equalizer and decoder correlation functions, a simple method to accurately predict the bit error probability of the SC-MMSE FDE and the PDA SC-MMSE FDE in fixed and block-fading MIMO channels is developed. Moreover, two error bounds on the outage probability of the SC-MMSE FDE are proposed. The semi-analytical approach and the derived error bounds provide simple but effective methods for estimating and optimizing the overall performance of the iterative systems.

The third part of the thesis presents efficient rate and power allocation strategies for single and multiple-access MIMO turbo communication systems employing the conventional SC-MMSE FDE. First, the problem of rate allocation maximizing the instantaneous sum rate of a two-user system subject to a convergence constraint of the turbo equalizer is investigated. By using the area property of extrinsic information transfer (EXIT) charts, an upper bound on the achievable rate region of the system is derived. With this bound, a simple rate allocation scheme is developed, involving a code selection procedure at each user, that aims to maximize the instantaneous system throughput. Further, the extension of the code selection scheme to an outage-based rate allocation approach is discussed. Novel design criteria for irregular channel codes minimizing the outage probability of turbo systems are established. Numerous results of capacity calculations and throughput simulations are presented to show the effectiveness of the proposed rate allocation and optimization techniques. Finally, transmission power minimization in single-access MIMO communication systems with singular value decomposition (SVD)-based precoding at the transmitter is studied. Several methods for allocating the power over the frequency domain channel eigenmodes are presented. Among them, a convex optimization approach which optimizes the power levels with respect to a target bit error probability of the turbo equalizer is shown to be superior over other existing power allocation methods.

Contents

1. Introduction

1.1. Motivation and Thesis Scope

The deployment of mobile audio, video and multimedia services and the possibility to access data anywhere have established wireless communications as an essential part in our everyday life. A variety of digital communication standards have been developed over the past years to support a wide range of applications in different radio environments with different system coverage, mobility, and quality-of-service (QoS) requirements. The well known existing GSM[1], WCDMA/UMTS[2] and IEEE 802.11n WLAN[3] standards are a few examples.

While there is a steadily growing demand for ever higher data rates due to the variety of high-speed multimedia services in wireless applications, the radio frequency spectrum has become an increasingly scarce resource. Future wireless single-user (single-access) and multiuser (multiple-access) broadband communication systems must therefore efficiently utilize the limited spectral resources to provide data transmissions with high spectral efficiency. Moreover, they have to support a high transmission reliability, a low power consumption, a low end-to-end-delay, and a manageable complexity.

Accordingly, achieving all of these goals is a very challenging task, since wireless broadband single-carrier transmission as considered in this thesis is typically affected by several impairments caused by multipath channel propagation, channel fading due to the mobility of the transmitter/receiver and the changing environment, thermal noise at the receiver, and interferences from other devices [PNG03].

Diversity techniques are an effective way to mitigate the detrimental effects of multipath fading channels. The main idea of diversity schemes is to increase the transmission reliability by sending and receiving the same information over multiple independently fading paths [PNG03]. In principle, the common diversity schemes can be classified into frequency, time, space/spatial, polarization and code diversity, and combinations thereof. Especially, spatial diversity techniques realized by em-

[1] GSM: Global Standard for Mobile Communications.
[2] WCDMA/UMTS: Wideband Code Division Multiple Access/Universal Mobile Telecommunications System.
[3] WLAN: Wireless Local Area Network.

ploying multiple antennas at both the transmitter and receiver side have attracted much research interest [PNG03]. Such multiple-input multiple-output (MIMO) antenna configurations promise high spectral efficiency (spatial multiplexing gain), high robustness of the transmission (diversity gain), high coverage (array gain), and interference reduction in rich multipath environments [Tel99], [FG98]. Because of the high potential of MIMO in single and multiuser systems, they have become an important part of modern digital communication standards, such as 3GPP[4] Long Term Evolution [ZM07].

Another technique for increasing transmission reliability over fading channels is error-control coding and interleaving. While a channel encoder introduces redundancy to the transmitted data which is used by a channel decoder at the receiver to correct transmission errors, an interleaver minimizes the effect of burst errors by simply randomizing the order of the data. A powerful method that serially combines channel encoding and bitwise interleaving is known as bit-interleaved coded modulation (BICM) [Zeh92], [CTB98]. BICM offers remarkable diversity gains in fading channels as well as a great design flexibility since channel encoding and symbol mapping can be optimized independently [Zeh92]. In addition, it is straightforward to combine BICM with MIMO system configurations. Therefore, this technique has been accepted in current digital communication systems and remains important in forthcoming standards.

In single and uplink multiuser MIMO system settings employing BICM signaling, the signals transmitted from the multiple sources (either from a single user or from many users) over a broadband multipath fading channel may suffer from several types of interference that have to be compensated for at the receiver. Indeed, when channel state information is unavailable at the transmitter side, channel orthogonality cannot be obtained by precoding neither in space nor in time. Then, strong multiple access interference (MAI) and co-antenna interference (CAI) may appear, both caused by a superposition of the transmitted data signals. In addition due to the channel frequency selectivity, the received data is impaired by inter-symbol interference (ISI). For such scenarios, the high computational complexity precludes the application of the optimum brute force signal detection approach at the receiver for joint equalization of the interference components and decoding of the transmitted data streams. This has motivated a number of studies on simpler suboptimal receiver structures.

Turbo equalization [DJB$^+$95], [WP99a], [TSK02], [TH02], [GM08], [AM03], [KM07], [AJL07], [KSMT05], [WP99b], [LP04], [GM07], [YGWP08], [JPSL04] is one of the most promising approaches to solve this problem. In turbo systems, channel equal-

[4] 3rd Generation Partnership Project

ization and channel decoding are separated into two independent soft-in soft-out (SfISfO) processing blocks, which exchange probabilistic information about the data symbols in an iterative manner. In contrast to the conventional two-step receiver that performs first channel equalization and then channel decoding, the turbo equalizer iteratively performs both tasks to refine the signal estimates iteration-by-iteration. By doing so, turbo equalization can achieve close-to-optimal error performance at much lower computational complexity as compared to the optimum detector. Because of the excellent performance of turbo systems, the so-called "turbo principle" has been applied to a variety of detection and decoding problems in communication systems, such as iterative joint demodulation and decoding of single-user BICM transmissions (BICM-ID) [LR97], [tBSY98a], [tBSY98b], [SGHB03], iterative joint detection and decoding of space-time BICM over fading MIMO channels [Ari00], [Ton03], and iterative multiuser detection and decoding for coded code division multiple access (CDMA) [WP99a], [SS01], [SSB06].

In its basic form, turbo equalization involves the maximum *a posteriori* probability (MAP) algorithm for channel equalization [DJB+95]. However, owing to the high complexity of this algorithm, the MAP-based turbo equalizer is only applicable to systems with few users, data transmissions with simple modulation formats like binary phase shift keying (BPSK), and channels with only a few multipath components. Throughout the past years numerous reliable alternatives have been proposed in the literature. Among them, especially soft interference cancellation minimum mean-squared error (SC-MMSE) filtering techniques [WP99a], [TSK02], [AM03], [KSMT05], [WP99b], [LP04], [JPSL04], and their frequency domain equivalents [TH02], [KM07], [AJL07], [YGWP08] appear as prospective candidates for use in turbo equalization systems. This is due to their ability to achieve good performance at relatively low computational cost. The main idea of this approach is to exploit the probabilistic-feedback from channel decoding to first estimate and cancel the interference from the received signal, and then to use linear MMSE filtering for further suppression of residual interference components. The main emphasis of this thesis is therefore on SC-MMSE filtering techniques.

A major concern that is often ignored but may prevent the application of SC-MMSE turbo equalizers in practical MIMO channel environments is their high sensitivity to spatial channel correlation. In spatially correlated MIMO channels, their error performance may significantly be deteriorated and other more sophisticated methods are required at the receiver [GM07]. Therefore, one of the main objectives of this thesis is the development of a number of advanced low complexity turbo equalizer strategies that may overcome the performance degradations of existing SC-MMSE designs in a variety of channel environments, without significantly increasing the complexity.

Furthermore, most of the research work so far has mainly concentrated on the design of turbo equalizers for (either single- or multiuser) BICM communication systems employing, irrespective of the channel conditions, a fixed allocation of resources such as transmission rate and power at the transmitter. However, in applications where the transmitter is able to acquire some form of channel state information (CSI), either indirectly through channel reciprocity, or directly through a feedback link from the receiver, a fixed allocation of resources may result in a waste of spectral and power efficiency. Hence, there is a clear motivation for incorporating the available CSI at the transmitter to adjust the transmission parameters rate and power, so that both the system efficiency and the overall performance of the turbo equalizer are improved. In particular, the allocation of resources can be formulated as optimization problem, where the objective function is either the transmission rate or the transmission power, and the corresponding constraints are defined by QoS requirements. Finding the optimal solution to such optimization problems may not be a trivial task for communication systems involving turbo equalization, as they depend on the specific transmission scheme, the level of CSI available at the transmitter and receiver as well as on the convergence properties of the turbo equalizer. Therefore, this work is also concerned with the development of practical transmission rate and power allocation and optimization strategies for communication systems employing the low complexity SC-MMSE-based turbo equalizer at the receiver.

1.2. Thesis Contributions and Organization

This section presents an outline of the main contributions of the thesis. The main body of this work consists of three parts. The first part focuses on the design of advanced turbo equalization techniques for BICM transmission over MIMO ISI fading channels. Several turbo equalizer schemes that can be efficiently implemented using the fast Fourier transform (FFT) and clearly outperform the existing SC-MMSE turbo equalizer are proposed. In the second part of the thesis, a detailed convergence analysis of the proposed receivers are presented and analytical approximations of the bit error rate (BER) and the outage probability of the overall iterative systems are derived. The analytical results obtained by the convergence analysis are the basis for the following third part of the thesis. There, the focus is on how CSI at the transmitter side can be exploited to efficiently allocate transmission rate and power in single- and multiuser systems with BICM signaling and SC-MMSE turbo equalization. For each optimization problem, practical resource allocation schemes finding the optimal or a near-optimal solution are proposed. The discussed topics and the proposed transmitter and receiver schemes in this thesis aim at achieving

higher transmission reliability, higher spectral and/or power efficiency over existing schemes for wireless broadband communications.

The individual chapters are outlined in the following.

Chapter 2 presents the relevant background material that will be used in subsequent chapters. A generic discrete-time system model for wireless communications is presented and the channel models used for system performance evaluations are introduced. The concept of block data transmission with cyclic prefix is reviewed. This transmission technique plays a crucial role throughout the thesis, as it enables the application of simplified (frequency domain) channel equalization at the receiver. Furthermore, the transmitter and iterative receiver models are presented. Thereby, some definitions and basic properties of log-likelihood ratios (LLRs) are reviewed, and some important aspects of iterative equalization of coded broadband MIMO systems as well as iterative decoding of concatenated codes are discussed. Finally, the fundamental information theoretical limits on single and multiuser data transmission with Gaussian-distributed and finite discrete inputs are studied.

Chapter 3 deals with implementation aspects of turbo equalizers in broadband MIMO communication systems with single-carrier BICM signaling. In this context, the principle of optimum MAP trellis-based equalization is reviewed, and a brief overview about other known algorithms which perform equalization of MIMO ISI channels at much lower computational complexity is provided. The main attention in this chapter is devoted to soft interference cancellation schemes. The classical time and frequency domain block-filtering concepts based on MMSE criteria as well as extensions thereof are extensively discussed. Moreover, a new alternative derivation is presented of the widely used frequency-domain SC-MMSE turbo equalizer. Furthermore, two novel iterative receiver designs are devised. In particular, the main contributions in this chapter include the following:

- A generic framework for turbo equalization based on nonlinear MMSE estimation is introduced. By formulating signal detection as a nonlinear MMSE estimation problem, an equalizer structure combining probabilistic data association (PDA) detection [LPWH01] and SC-MMSE filtering in one algorithm can be derived. A computationally efficient frequency domain implementation of such an algorithm is presented. The corresponding PDA SC-MMSE FDE has a similar structure than the existing SC-MMSE equalizer, but it possesses an additional internal feedback loop by which the symbol estimates can be further improved. Simulation results exhibit a faster convergence and better performance of the proposed scheme compared to existing methods for the transmission over spatially uncorrelated MIMO channels.

- Analytical derivations of the signal-to-noise-ratio (SNR) at the LLR output of

the MMSE-based equalizers are presented. A recursive relationship describing the SNR evolution over the internal iterations within the PDA SC-MMSE FDE is developed. Based on the SNR expressions, the performance gain of the PDA SC-MMSE FDE over SC-MMSE FDE is evaluated for single-user transmissions.

- A novel turbo equalizer, referred to as HY SC-MMSE FDE, suited for uplink multiple-access communications in spatially-correlated fading environments is proposed. Unlike to the existing SC-MMSE receiver, the novel approach adapts a two step detection process: at the first step, groupwise soft interference cancellation and linear filtering on the received data signals is performed with the aim to separate the transmitted user signals into a number of subgroups; at the second step, joint MAP detection of the signals in each subgroup is employed. The groupwise filtering stage removes interferences between subgroups, while it preserves the effective degrees of freedom of the spatial components within each subgroup. Different criteria used for the optimization of this filter are addressed. It is proven that groupwise filter designs with the objective to minimize the mean-square-error (MSE) or to maximize the signal-to-interference-plus-noise ratio (SINR) of each subgroup lead to identical equalizer structures. Moreover, by introducing an additional design criterion in the optimization, the filter can directly be derived in frequency domain. Several greedy methods for group selection are proposed and compared with respect to their performance. Numerical results from simulations in various channel conditions indicate a strong robustness of the HY SC-MMSE FDE against spatial channel correlation.

- The practicality of the proposed receiver algorithms is investigated in real channel propagation environments. Numerical results obtained through a series of Monte-Carlo bit error rate simulation experiments using multidimensional channel-sounding field measurement data are presented.

Chapter 4 analytically and numerically investigates the convergence properties of the proposed receivers in various channel environments. In particular, the correlation chart framework [TtBH02], [Hag04], [Cho07] is applied to analyze the iterative equalizers. The definition of correlation functions used to characterize the behavior of the channel equalizer and the decoders in the correlation chart is first presented. The correlation functions for the SC-MMSE and PDA SC-MMSE equalizers and the non-iterative/iterative channel decoding schemes are subsequently evaluated. Thereby, it is illustrated how variations of channel model parameters (such as spatial channel correlation) and code parameters (generator polynomials and code rate)

influence the shape of the equalizer function surfaces and the decoder function surface, respectively, in the correlation chart. Moreover, the relationship between the correlation chart and the well known extrinsic information transfer (EXIT) chart is considered. Finally, the outage performance of the standard SC-MMSE turbo equalizer in Rayleigh fading ISI channels with exponential delay-power profile is analyzed. The main contributions in this chapter are as follows:

- An analytic computation of the correlation functions for SC-MMSE and PDA SC-MMSE equalizers is proposed. By comparing the analytic correlation functions with the ones obtained by Monte-Carlo simulation, it is found that the proposed method is sufficiently accurate for predicting the correlation functions of both equalizer types in different channel configurations. It is shown how the correlation functions of the channel equalizer and channel decoder can be used to semi-analytically compute the overall BER performance of the turbo systems at low computational cost.

- A closed-form expression on the outage probability of SC-MMSE turbo equalization in Rayleigh fading ISI channels is presented. The single-user single-antenna transmission case is considered. In particular, by using a union-bounding technique and a specific central limit theorem, it is shown that the outage probability can be approximated by a sum of complementary Gaussian error functions. In addition, a generic lower bound on the outage performance of the turbo system is presented. Comparison of analytical and numerical results confirm that the proposed error bound is tight for a large range of different SNR values and different channel delay-power profiles.

Chapter 5 considers transmission rate and power allocation for single and multiuser MIMO systems with SC-MMSE turbo equalization under the assumption of perfect CSI, partial CSI (in the form of a bandwidth-limited feedback channel), or statistical CSI (channel fading distribution statistics) to be available at the transmitter side. An EXIT chart design approach for rate allocation in uplink two-user systems with fixed power allocation and partial CSI at the transmitters is first considered. Therein, the objective is to maximize the sum rate of the system subject to a successful convergence of the turbo equalizer with respect to the instantaneous channel state. The structure of the optimization problem is studied and a practical algorithm that adapts a code selection procedure at each user to approximately solve the problem is proposed. Furthermore, two fixed-rate transmission strategies optimized with respect to the channel fading distribution and the outage performance of the iterative SC-MMSE receiver are proposed. Finally, transmission power optimization for single-user MIMO systems under the assumption of perfect CSI and

a fixed rate allocation at the transmitter is considered. Several design criteria for optimizing the power levels are discussed and illustrative numerical and analytical results are presented. The main contributions of this chapter are as follows:

- Using the relationship between the rate of any linear code and the area under the corresponding decoder EXIT function [AKtB04], an upper bound on the achievable instantaneous rate region of a two-user turbo system is derived. Numerical evaluations show that the rate region, in general, is non-convex and its dominant face strongly depends on the realization of the channel coefficients. Based on the rate region upper bound, the problem of maximizing the instantaneous system sum rate subject to a convergence constraint of the SC-MMSE turbo equalizer is studied. A simple code selection algorithm that selects independently for each user from a set of rate-compatible codes the optimal one with the objective to maximize the overall rate is derived. Furthermore, the extension of the algorithm for systems with more than two users is discussed. It is demonstrated that the proposed rate allocation scheme enhances the throughput efficiency over automatic repeat request with fixed codes at each user.

- The code selection algorithm is generalized to an outage-based rate allocation approach that maximizes the sum rate of the users subject to an outage probability constraint of the turbo equalizer. Furthermore, a novel design method for irregular convolutional codes which aim to improve the outage performance of single-user single-antenna turbo systems is proposed.

- A linear transmit precoding scheme combined with transmission power optimization for single-user single-carrier transmissions over MIMO ISI fading channels is proposed. A convex optimization framework for the adjustment of the power levels at the transmitter is derived. The BER performances of precoding schemes with different power allocations are compared to each other by means of Monte Carlo simulations.

Chapter 6 concludes the thesis, and provides an overview of possible research activities for future work.

Parts of the thesis were published in journal papers and refereed conference proceedings [GM07], [GM08], [Gro09], [GOM10], [Gro11], [GS11], [SGT04], [SGK+04], [GM09], [GM10].

2. Preliminaries

This chapter introduces the fundamentals of wireless broadband communication systems and constitutes the basis for the upcoming parts of the thesis. We start by defining in Section 2.1 a generic discrete-time linear system model with multiple inputs and multiple outputs. This model covers the transmission systems considered in this work. The relationship between the transmit and received signals is expressed in compact form by matrix-vector notation.

One important aspect of wireless high-rate communications is the equalization of ISI caused by multipath propagation of the radio channel. An efficient approach to deal with the interference at the receiver is to apply the so-called block transmission technique [BDFT10]. In Section 2.2, we review this transmission principle as well as the corresponding decomposition properties of the ISI MIMO channel. Following this, several models for simulating MIMO ISI block-fading channels with different delay-power profiles and spatial channel correlation properties are introduced in Section 2.3. Moreover, the cross-correlation between the frequency domain channel gains are analyzed. We then focus in Section 2.4 on the generation of the transmit data symbols and introduce two different transmitter structures for single and multiuser transmissions. Before outlining the corresponding receiver parts, we address the definition, some relations and properties of LLRs in Section 2.5. Iterative joint channel equalization and decoding schemes following the turbo principle [Hag04] are proposed in Section 2.6. In Section 2.7, a generic MIMO system model for single-carrier block signaling is presented, which contains as special cases the transmissions with signal precoding [MP07] and no precoding at the transmitter side. Some important parameters used for performance evaluation of wireless communication systems such as the SNR and the energy-per-bit-to noise power spectral density ratio for fixed and time-varying MIMO ISI block-fading channels are discussed as well. Finally, the mutual information and the capacity of single-carrier MIMO systems under the constraint of Gaussian and finite input constellations is reviewed in Section 2.8. The analytical expressions obtained in this section serve as the information-theoretic performance bounds of the communication systems considered in this thesis.

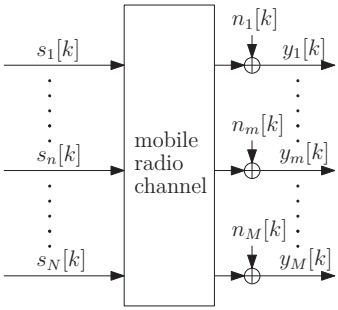

Figure 2.1.: Complex baseband system model for MIMO communication with N inputs and M outputs.

2.1. System Model

Consider the discrete-time equivalent complex baseband model of a MIMO communication system with N inputs and M outputs in Fig. 2.1. Hereby $s_n[k]$, $1 \leq n \leq N$ represents the real- or complex-valued kth data sample transmitted by the nth antenna, and $y_m[k]$ and $n_m[k]$, $1 \leq m \leq M$ represent the kth received and noise sample at the mth receive antenna, respectively. The N inputs of the MIMO system can be either the transmit signals from multiple users each equipped with a single transmit antenna, or the transmit signals from a single user equipped with multiple transmit antennas. The M outputs correspond to the signals arriving at the same time at the receive antennas of a common receiver.

Thus, this MIMO system model covers the following two specific transmission setups considered in this thesis: 1) the multiuser single-input multiple-output (SIMO) transmission with space-division multiple access (SDMA) and 2) the single-user MIMO point-to-point (P2P) transmission. The former setup typically arises in the uplink of a wireless cellular system when multiple users, which cannot directly communicate with each other, send data simultaneously at the same time and frequency band to a single base station. The latter setup occurs when only a single user transmits data simultaneously from multiple antennas to a single base station or an access point of a WLAN system.

The radio channel of the MIMO system in Fig. 2.1 is characterized by multipath signal propagation and fading. The transmitted signals arrive at the multiple receive antennas via multiple paths with different delays, amplitudes, and phases due to reflections, diffuse scattering, and diffraction [Jak94], [Bel63]. In addition, due to the movement of the receiver, transmitters and changing environment, the radio channel appears as a time-varying system. For high-rate data communications, as considered

in this thesis, the symbol duration is small compared to the multipath time delay spread of the channel and the received signals experience severe ISI. This means the transmission bandwidth certainly exceeds the channel coherence bandwidth. Hence, the channel is characterized by a frequency-selective fading. Although the channel frequency selectivity complicates the extraction of the transmitted signals at the receiver, it also provides an additional diversity gain that can be used in the design of robust transceivers.

The physical channel between the nth transmit antenna to the mth receive antenna of a MIMO communication system is modeled by a time-variant continuous-time impulse response [Pro01]

$$g_{m,n}(t,t') \equiv \sum_{p=1}^{N_p} a_{m,n,p}(t)\delta(t'-t'_p), \tag{2.1}$$

where t, N_p, t', $a_{m,n,p}(t)$, denote the absolute time, the total number of resolvable (not necessarily uniformly spaced) discrete delays t'_p at the receiver, the propagation delay and the time-variant complex gain associated with discrete delay t'_p, respectively. The complex gain factors $a_{m,n,p}(t)$ are obtained by a superposition of the individual path components of the physical channel associated with the delay t'_p. Obviously, they depend on the physical channel characteristics, such as the propagation environment and scatterer distribution as well as on the communication system parameters, such as the antenna beam pattern and the carrier frequency, etc. A detailed description of these quantities is beyond the scope of this work, and we refer the interested reader to [Jak94]. [Bel63]. Without loss of generality, we assume in the following that $t'_1 < t'_2 < ...t'_{N_p}$. Moreover, the discrete delays t'_p are supposed to be identical for all transmit and receive antenna pairs (n,m). Mathematically, it was shown by Forney in [For72] that the equivalent discrete-time channel model to (2.1), including the transmit pulse-shaping, the receive-matched filtering as well as the effects of symbol-rate sampling and sampling phase, can be represented by a time-varying finite impulse response (FIR) filter. Following the approach in [For72], the discrete-time channel impulse response (CIR) between the nth input and the mth output of the MIMO channel can be represented by

$$h_{m,n}[k,l] \equiv \sum_{p=1}^{N_p} g_{m,n}(kT,t'_p)d(lT-t'_p), l=0,...,L-1, \tag{2.2}$$

where $d(t)$ denotes the overall impulse response of the transmit/receive filtering, and T and $L-1$ designate the symbol duration and the effective discrete-time channel memory length, respectively. The overall impulse response $d(t)$ is supposed to be identical for all links and to satisfy the first Nyquist criterion [Pro01]. Hence, when

the maximum channel delay t'_{N_p} is smaller than the symbol duration T, the channel fading is frequency-flat and $L = 1$. In the other case of $t'_{N_p} \gg T$, the channel fading is frequency-selective and $L > 1$. Since we assume identical transmit and receive filters for all links as well as the same discrete delays t'_p, the discrete-time channel memory length $L - 1$ is identical for all transmit/receive antenna pairs.

For convenience, the channel coefficients $h_{m,n}[k, l]$ are arranged into the vector

$$\mathbf{h}_{m,n}[k] = \Big[h_{m,n}[k, 0], ..., h_{m,n}[k, l], ..., h_{m,n}[k, L-1]\Big]^T \in \mathbb{C}^{L\times 1}. \tag{2.3}$$

Similarly, all $N \cdot M$ CIRs of the MIMO channel are stacked into the vector

$$\mathbf{h}_{\text{vec}}[k] = \Big[\mathbf{h}^T_{1,1}[k], ..., \mathbf{h}^T_{1,N}[k], ..., \mathbf{h}^T_{M,1}[k], ..., \mathbf{h}^T_{M,N}[k]\Big]^T \in \mathbb{C}^{NML\times 1}. \tag{2.4}$$

Throughout the thesis, we consider a coherent transmission where all N transmitters and the receiver are perfectly synchronized and carrier frequency offsets are compensated in an ideal manner. The received signal $y_m[k]$ at the mth antenna can therefore be expressed by the following superposition of the multiple transmit antenna signals $s_n[k]$:

$$y_m[k] = \sum_{n=1}^{N} \sum_{l=0}^{L-1} h_{m,n}[k, l]s_n[k - l] + n_m[k], m = 1, ..., M. \tag{2.5}$$

Moreover, the noise samples $n_m[k]$ in (2.5) are assumed to be independent identically distributed (i.i.d.), spatially uncorrelated, zero-mean, complex Gaussian random variables with variance σ_0^2, i.e.,

$$\mathbb{E}\Big[n_m[k]n^*_{m'}[k + z]\Big] = \begin{cases} \sigma_0^2 \text{ for } m = m', \text{ and } z = 0, \\ 0 \text{ else.} \end{cases} \tag{2.6}$$

2.2. Block Transmission with Guard Interval

To employ an efficient block detection algorithm at the receiver the concept of block transmission [BDFT10] can be applied. For this, the data stream to be transmitted at each transmit antenna is grouped into several fixed-length blocks of data symbols. In addition, to avoid inter-block interference between successive blocks, a guard-interval is inserted in front of each transmit block. The length of the guard-interval (P in samples) has to be greater or equal to the channel memory length $L-1$. Several options have been considered in the literature for the structure of the guard-interval:

- The guard interval contains a copy of the last P symbols of the successive transmit block. This method is the most commonly used one and called cyclic

prefix (CP) extension.

- The guard interval contains the all-zero symbol sequence. This method is called zero padding (ZP) extension.

- The guard interval contains a known symbol sequence that can be used for example for synchronization and channel estimation. This method is called unique word (UW) extension.

For a more in-depth comparison between these three transmit block extension schemes, we refer the interested reader to [MWG+02], [PS04], [WMG02], [DGE01], [RLM06], [SM07]. Within the scope of this work, we will make use of the first method and use the CP as the guard interval. The corresponding CP-assisted MIMO block transmission scheme is described in the following.

Consider a frame of N_s data symbols at each transmit antenna, which are grouped into N_b equal-sized blocks. Suppose that the block length $Q = N_s/N_b$ is identical for all N transmit antennas and that $Q \geq L$. The kth data block at the nth antenna can then be represented by the symbol-data vector

$$\mathbf{d}_n(k) \equiv \Big[d_{0,n}[k], ..., d_{q,n}[k], ..., d_{Q-1,n}[k]\Big]^T \in \mathbb{C}^{Q\times 1}, k = 1, ..., N_b, \tag{2.7}$$

where the qth signal component $d_{q,n}[k]$ is related to symbol $s_n[k]$ by $d_{q,n}[k] \equiv s_n\Big[(k-1)Q+q\Big]$ for $q = 0, ..., Q-1$ and $k = 1, ..., N_b$. Similarly, the received and noise signals at the mth receive antenna, respectively, are arranged into the vectors

$$\mathbf{r}_m(k) \equiv \Big[r_{0,m}[k], ..., r_{q,m}[k], ..., r_{Q-1,m}[k]\Big]^T \in \mathbb{C}^{Q\times 1}, \tag{2.8}$$

$$\mathbf{n}_m(k) \equiv \Big[n_{0,m}[k], ..., n_{q,m}[k], ..., n_{Q-1,m}[k]\Big]^T \in \mathbb{C}^{Q\times 1}, k = 1, ..., N_b, \tag{2.9}$$

where $r_{q,m}[k] \equiv y_m\Big[(k-1)Q+q\Big]$ and $n_{q,m}[k] \equiv n_m\Big[(k-1)Q+q\Big]$ for $q = 0, ..., Q-1$ and $k = 1, ..., N_b$.

Assume that the block grouping of the data symbols is aligned with the channel coherence time such that the channel coefficients $h_{m,n}[k, l]$ can reasonable be regarded as being time-invariant during the transmission of a complete frame of N_b subsequently transmitted blocks. This inherently leads to a so called (quasi-) static MIMO channel [Tel99], [FG98], where the N_b transmit blocks from all antennas experience the same channel realization over the duration of a frame. Within a single frame, the time index k of the CIRs $\mathbf{h}_{m,n}[k]$, $\forall m, n$ can thus be dropped, and we can write $\mathbf{h}_{m,n} = \mathbf{h}_{m,n}[k]$, for all $k = 1, ..., N_b$.

Fig. 2.2 illustrates the block structure and the use of the CP as guard interval. Each data block $\mathbf{b}_n(k)$ is preceded by a CP of length $P = L-1$ before transmission,

•••	data symbol block $k-1$	cyclic prefix	data symbol block k	•••
		$d_{Q-L+1,n}[k]$ ••• $d_{Q-1,n}[k]$	$d_{0,n}[k]$ ••• $d_{q,n}[k]$ ••• $d_{Q-1,n}[k]$	

Figure 2.2.: Frame structure of block transmission with cyclic prefix as guard interval.

where the CP is a copy of the last P data symbols of the block. The total number of samples per transmitted block and antenna is, thus, $P+Q$. At the receiver, the P received samples associated to the CP are discarded to ensure that the kth received block is not affected from the last $L-1$ samples from the prior transmission block. Based on Eqn. (2.5), the received vector of the kth data block at antenna m can be written as

$$\mathbf{r}_m(k) = \sum_{n=1}^{N} \mathbf{H}_{m,n}\mathbf{d}_n(k) + \mathbf{n}_m(k), \tag{2.10}$$

where $\mathbf{H}_{m,n} \in \mathbb{C}^{Q\times Q}$ is the circulant matrix constructed from the entries of vector $\mathbf{h}_{m,n}$,

$$\mathbf{H}_{m,n} \equiv \begin{bmatrix} h[0] & 0 & \dots & 0 & 0 & h[L-1] & \dots & h(1) \\ h[1] & h(0) & 0 & \dots & 0 & 0 & \ddots & \vdots \\ \vdots & h[1] & h[0] & 0 & 0 & \ddots & 0 & h[L-1] \\ h[L-1] & \vdots & h[1] & \ddots & 0 & \ddots & 0 & 0 \\ 0 & h[L-1] & \vdots & \ddots & h[0] & \ddots & \ddots & 0 \\ \vdots & 0 & h[L-1] & \ddots & h[1] & h[0] & 0 & 0 \\ \vdots & \vdots & 0 & \ddots & \vdots & \ddots & \ddots & 0 \\ 0 & 0 & \dots & 0 & h[L-1] & \dots & h[1] & h[0] \end{bmatrix}. \tag{2.11}$$

For notational simplicity, the antenna indices n and m have been skipped in (2.11) and are omitted in the following. Considering (2.10) and (2.11), we observe that the CP is useful for two reasons: first, it eliminates inter-block interference caused by the multipath components of the channel, and second, it converts the linear channel convolution in (2.5) into a circular convolution [RG75] over a block of Q samples. Finally, by defining

$$\mathbf{d}(k) \equiv \left[\mathbf{d}_1^T(k), ..., \mathbf{d}_n^T(k), ..., \mathbf{d}_N^T(k)\right]^T \in \mathbb{C}^{NQ\times 1} \tag{2.12}$$

as the overall transmit block at time instant k, the corresponding overall received vector can be expressed by

$$\begin{aligned}\mathbf{r}(k) &\equiv \left[\mathbf{r}_1^T(k), ..., \mathbf{r}_m^T(k), ..., \mathbf{r}_M^T(k)\right]^T \\ &= \sum_{n=1}^{N} \mathbf{H}_n \mathbf{d}_n(k) + \mathbf{n}(k) \\ &= \mathbf{H}\mathbf{d}(k) + \mathbf{n}(k), \end{aligned} \tag{2.13}$$

where the noise vector $\mathbf{n}(k) \equiv \left[\mathbf{n}_1^T(k), ..., \mathbf{n}_m^T(k), ..., \mathbf{n}_M^T(k)\right]^T$ is defined accordingly. The covariance matrix of the additive complex Gaussian noise $\mathbf{n}(k)$ is with (2.6) obtained as $\mathbb{E}[\mathbf{n}(k)\mathbf{n}^H(k)] = \sigma_0^2 \mathbf{I}_{MQ}$. Further, the channel matrix $\mathbf{H}_n \in \mathbb{C}^{MQ \times Q}$ and the overall MIMO channel matrix $\mathbf{H} \in \mathbb{C}^{MQ \times NQ}$ are defined by $\mathbf{H}_n \equiv \left[\mathbf{H}_{1,n}^H, ..., \mathbf{H}_{m,n}^H, ..., \mathbf{H}_{M,n}^H\right]^H$ and $\mathbf{H} \equiv \left[\mathbf{H}_1, ..., \mathbf{H}_n, ..., \mathbf{H}_N\right]$, respectively.

Fig. 2.3 depicts the block diagram of the CP-assisted MIMO block transmission scheme that corresponds to the signal model (2.13). We remark that (2.13) is a general model that can be used to describe the relationship between transmit and received signals for single-carrier and multi-carrier CP-based MIMO communication systems.

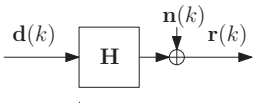

Figure 2.3.: Matrix-vector model for MIMO block transmission.

Property of Circulant MIMO Channel Matrices

An inherent property of circulant matrices is that their eigenvectors are the columns of the normalized discrete Fourier transform (DFT) matrix [RG75]. Based on this property, the eigenvalue decomposition of the block-circulant overall MIMO channel matrix in (2.13) can be expressed as

$$\mathbf{H} = \mathbf{F}_M^H \boldsymbol{\Xi} \mathbf{F}_N, \tag{2.14}$$

where $\mathbf{F}_M$ and $\mathbf{F}_N$ are block-Fourier matrices

$$\begin{aligned}\mathbf{F}_M &= \mathbf{I}_M \otimes \mathbf{F}, \\ \mathbf{F}_N &= \mathbf{I}_N \otimes \mathbf{F}\end{aligned}$$

with $\otimes$ being the Kronecker product, and $\mathbf{F} \in \mathbb{C}^{Q\times Q}$ being the Q-point DFT matrix with elements

$$\Big[\mathbf{F}\Big]_{lj} = \frac{1}{\sqrt{Q}}\exp\left[-\sqrt{-1}\frac{2\pi}{Q}lj\right], \text{ for } 0 \le l, j \le Q-1.$$

As $\mathbf{F}$ is unitary, $\mathbf{F}\mathbf{F}^H = \mathbf{I}_Q$. Here, the matrix $\mathbf{\Xi} \in \mathbb{C}^{MQ\times NQ}$ contains the frequency response of the MIMO channel. Due to its block-diagonal structure, it can be partitioned into smaller diagonal sub-matrices $\mathbf{\Xi}_{m,n} \in \mathbb{C}^{Q\times Q}$,

$$\begin{aligned}\mathbf{\Xi} &\equiv \Big[\mathbf{\Xi}_1, ..., \mathbf{\Xi}_n, ..., \mathbf{\Xi}_N\Big],\\ \mathbf{\Xi}_n &\equiv \Big[\mathbf{\Xi}_{1,n}^H, ..., \mathbf{\Xi}_{m,n}^H, ..., \mathbf{\Xi}_{M,n}^H\Big]^H \in \mathbb{C}^{MQ\times Q}, n = 1, ..., N.\end{aligned}$$

The diagonal elements of $\mathbf{\Xi}_{m,n}$ represent the frequency channel response $\boldsymbol{\tau}_{m,n} \equiv [\tau_{m,n}(0), .., \tau_{m,n}(q), ..., \tau_{m,n}(Q-1)]^T$ between receive antenna m and transmit antenna n. The values $\tau_{m,n}(q)$ are obtained by applying the (non-unitary) DFT to the first column of $\mathbf{H}_{m,n}$,

$$\tau_{m,n}(q) \equiv \Big[\mathbf{\Xi}_{m,n}\Big]_{q,q} = \sum_{l=0}^{L-1} h_{m,n}[l]\exp\left[-\sqrt{-1}\frac{2\pi}{Q}lq\right] \text{ for } q = 0, .., Q-1. \qquad (2.15)$$

In the following, we refer to $\boldsymbol{\tau}_{m,n}$ and $\tau_{m,n}(q)$ as the frequency domain channel response and the qth frequency domain channel coefficient between the nth transmit and mth receive antenna pair, respectively. For convenience, we also define by $\mathbf{\Xi}(q) \in \mathbb{C}^{M\times N}$ the matrix whose elements represent the spatial response of the MIMO ISI channel at the qth subchannel as

$$\begin{aligned}\mathbf{\Xi}(q) &\equiv \Big[\mathbf{\Xi}_1(q), ..., \mathbf{\Xi}_n(q), ..., \mathbf{\Xi}_N(q)\Big],\\ \mathbf{\Xi}_n(q) &\equiv \Big[\tau_{1,n}(q), ..., \tau_{m,n}(q), ..., \tau_{M,n}(q)\Big]^T \in \mathbb{C}^{M\times 1}, n = 1, ..., N.\end{aligned}$$

The circulant property in (2.14) of the channel matrix $\mathbf{H}$ enables the application of efficient frequency domain equalization schemes at the receiver as it is used for single-carrier block signaling or multi-carrier modulation employing orthogonal frequency-division multiplexing (OFDM).

2.3. Channel Model

In order to assess the performance of communication systems and to obtain analytical insight into the system behavior, it is important to specify the channel model and its parameters used for system simulation. The topic of channel modeling has

received much interest in recent years and a broad variety of different models exist in the literature, see [PGNB04], [GSS+03] and [KSP+03] for an overview.

In this work, we restrict our self to two particular models of the MIMO channel: 1) the widely-used stochastic Rayleigh block-fading MIMO channel and 2) the deterministic block-fading MIMO channel. The Rayleigh block-fading MIMO channel model is accurate for a wide range of practical scenarios and often used to predict the theoretical limits of communication systems. Specifically, the stochastic Rayleigh channel model is used to design novel transmitter and receiver structures. However, a serious drawback of this model is the impossibility of direct evaluating the system performance in specific real-field environments. For this, we use in this work a measurement data-based channel model that is parametrized to the specific measured scenario. This model is based on results of extensive measurement campaigns, which are gathered from double-directional real-time radio channel sounding experiments [THR+01].

In the following sections, we review the statistical properties of the Rayleigh block-fading MIMO channel, and introduce the Kronecker model for modeling the spatial correlation of the MIMO ISI channel. Moreover, as a novel contribution, we present a rigorous analysis and a closed form derivation for the cross-correlation coefficients of the frequency domain MIMO channel gains. The measurement-data based channel model used for the performance evaluation will be described in Chapter 3.

2.3.1. Rayleigh Block-fading Channel and Antenna Correlation Matrices

The Rayleigh block-fading model is widely used in the literature to model communication systems in rich-scattering environments. The channel is assumed to be constant over the duration of one frame, comprised of N_b transmit blocks, but varying randomly and independently frame-by-frame. The channel coefficients $h_{m,n}[l]$ are modeled as circularly-symmetric, zero-mean, complex-valued Gaussian random variables,

$$h_{m,n}[l] \sim \mathcal{CN}(0, \sigma_l^2) \text{ for } l = 0, ..., L-1, \forall n, m \tag{2.16}$$

with $|h_{m,n}[l]|$ being Rayleigh distributed. The Gaussian assumption on the coefficients $h_{m,n}[l]$, in general, is well justified in rich-scattering propagation environments, where no line-of-sight component is available between the transmitter and receiver, and a large number of propagation paths with different amplitudes and phases from different scatterers contribute to each resolvable path [Skl97], [Jak94], [Bel63]. The channel variances σ_l^2 in (2.16) are assumed to be identical for all transmit/receive

antenna pairs of the MIMO system. This assumption is reasonable in single-user P2P MIMO systems, where all channel links experience on average the same physical environment and have the same delay-power profile. The delay-power profile may be different from one link to another in multiuser setups due to the different distances between the users and base station. To reduce the simulation effort of the channel model, however, we suppose in the following that even in multiuser setups all channel links have identical delay-power profiles.

A sufficiently large number of scatterers is supposed to be present, so that the channel coefficients with respect to different tap-delays l can be modeled as statistically independent. We remark that inter-tap correlation between channel coefficients typically occurs due to the convolution of the impulse responses of the physical channel and the transmit and receive filters [XWL+04], [PNG03]. However, to simplify the simulation model, we ignore inter-tap correlation and always suppose that

$$\mathbb{E}\Big[h_{m,n}[l]h^*_{m,n}[l']\Big] = 0 \text{ for } l \neq l'. \tag{2.17}$$

The delay-power profile of the channel defines the values of the channel variances σ_l^2. Two common schemes often found in the literature are the uniform and the exponential decay delay-power profiles. For the exponential profile, the values of σ_l^2 are defined by

$$\sigma_l^2 = c_{\exp}\frac{1}{\tau_d}\exp(-l/\tau_d) \text{ for } l = 0, ..., L-1, \tag{2.18}$$

where $c_{\exp} \equiv \left(\sum_{l=0}^{L-1}\tau_d^{-1}\exp[-l/\tau_d]\right)^{-1}$ is an appropriate normalization constant, and τ_d is the root mean square (RMS) channel delay spread (c.f. [Cox72]). Similarly, for the uniform channel delay-power profile, the values of σ_l^2 are defined as

$$\sigma_l^2 = \frac{1}{L} \text{ for } l = 0, ..., L-1. \tag{2.19}$$

Spatial Channel Correlation Properties: The spatial-temporal correlation matrix $\mathbf{J} \equiv \mathbb{E}\Big[\mathbf{h}_{\text{vec}}\mathbf{h}_{\text{vec}}^H\Big]$ of the MIMO channel coefficient vector $\mathbf{h}_{\text{vec}}$ (see (2.4)) is supposed to follow the well-known Kronecker spatial correlation model which can be expressed in Kronecker product form [KSP+03]:

$$\mathbf{J} = \mathbf{R} \otimes \mathbf{S} \otimes \mathbf{C}, \tag{2.20}$$

where $\mathbf{R} \in \mathbb{C}^{M\times M}$, $\mathbf{S} \in \mathbb{C}^{N\times N}$ and $\mathbf{C} \in \mathbb{C}^{L\times L}$ denote the hermitian, positive-definite receive correlation coefficient matrix, the hermitian, positive-definite transmit correlation coefficient matrix and the diagonal variance matrix, respectively. Corre-

spondingly, the entries $[\mathbf{R}]_{m,m'}$ $\left(0 \leq |[\mathbf{R}]_{m,m'}| \leq 1\right)$ and $[\mathbf{S}]_{n,n'}$ $\left(0 \leq |[\mathbf{S}]_{n,n'}| \leq 1\right)$ denote the receive and transmit cross-correlation coefficients between receive antennas m and m' and transmit antennas n and n', respectively. Also, the entries of the variance matrix $\mathbf{C}$ are defined by

$$\mathbf{C} = \begin{bmatrix} \sigma_0^2 & 0 & \dots & 0 \\ 0 & \sigma_1^2 & \dots & \vdots \\ \vdots & \ddots & \ddots & 0 \\ 0 & \dots & 0 & \sigma_{L-1}^2 \end{bmatrix}. \tag{2.21}$$

Based on the spatial separation property of (2.20), a simple method for generating Rayleigh block-fading MIMO channels with spatial and frequency selectivity can be devised. The Rayleigh block-fading MIMO channel coefficients can be generated according to

$$\mathbf{h}_{\text{vec}} = \left(\mathbf{R}^{1/2} \otimes \mathbf{S}^{1/2} \otimes \mathbf{C}^{1/2}\right)\mathbf{h'}_{\text{vec}}, \tag{2.22}$$

where $(\cdot)^{1/2}$ is the matrix square-root computed by the Cholesky decomposition [Kre05], and $\mathbf{h'}_{\text{vec}} \in \mathbb{C}^{MNL\times 1}$ denotes an i.i.d., circularly-symmetric, zero-mean, Gaussian random vector with covariance $\mathbb{E}\left[\mathbf{h'}_{\text{vec}}\mathbf{h'}^{H}_{\text{vec}}\right] = \mathbf{I}_{MNL}$. We remark that the vectors $\mathbf{h'}_{\text{vec}}$ must be generated in such a way that they are statistically independent from one frame to the following one. The Kronecker model (2.20) is preferred in this thesis due to its simplicity. However, it should be noted that results with measured channels show that the Kronecker model has some deficiencies in terms of modeling accuracy [OHW+03], [JW04], [RKS10].

2.3.2. Cross-Correlations of Frequency Domain Channel Coefficients

Next, we analyze the cross-correlation coefficients of the frequency domain channel gains $\tau_{m,n}(q)$. The results derived in the following will be used in Chapter 5 to design channel coding schemes for transmission systems employing iterative receivers.

According to (2.15) and (2.16), the frequency domain channel gains $\tau_{m,n}(q)$ are a weighted sum of zero-mean, circularly-symmetric, complex Gaussian distributed random variables, and hence, the distribution of $\tau_{m,n}(q)$ is Gaussian as well. The real and imaginary parts of $\tau_{m,n}(q)$,

$$\tau_{m,n}(q) = \Re\{\tau_{m,n}(q)\} + \sqrt{-1}\Im\{\tau_{m,n}(q)\}, \tag{2.23}$$

are thus also zero-mean, real-valued, Gaussian random variables with variance $\frac{1}{2}$

for all q, n, m. Utilizing the decoupling property of the spatial-temporal correlation matrix (2.20), the cross-correlations between the real and imaginary parts of two frequency domain channel coefficients $\tau_{m,n}(q_1)$ and $\tau_{m',n'}(q_2)$ can be expressed as

$$\begin{aligned}
\mathbb{E}\Big[\Re\{\tau_{m,n}(q_1)\}\Im\{\tau_{m',n'}(q_1)\}\Big] &= \mathbb{E}\Big[\Re\{\tau_{m,n}(q_2)\}\Im\{\tau_{m',n'}(q_2)\}\Big] = 0 \\
\mathbb{E}\Big[\Re\{\tau_{m,n}(q_1)\}\Re\{\tau_{m',n'}(q_2)\}\Big] &= \mathbb{E}\Big[\Im\{\tau_{m,n}(q_1)\}\Im\{\tau_{m',n'}(q_2)\}\Big] \\
&= \frac{1}{4}[\mathbf{R}]_{m,m'}[\mathbf{S}]_{n,n'}\Big(w(\Delta q) + w(-\Delta q)\Big) \\
\mathbb{E}\Big[\Re\{\tau_{m,n}(q_1)\}\Im\{\tau_{m',n'}(q_2)\}\Big] &= -\mathbb{E}\Big[\Im\{\tau_{m,n}(q_1)\}\Re\{\tau_{m',n'}(q_2)\}\Big] \\
&= \frac{1}{4}[\mathbf{R}]_{m,m'}[\mathbf{S}]_{n,n'}\sqrt{-1}\Big(w(\Delta q) - w(-\Delta q)\Big), \qquad (2.24)
\end{aligned}$$

where $w(\Delta q)$ is the cross-correlation function of the complex channel coefficients $\tau_{m,n}(q_1)$ and $\tau_{m',n'}(q_2)$, defined by

$$\begin{aligned}
w(\Delta q) &= \frac{1}{[\mathbf{R}]_{m,m'}[\mathbf{S}]_{n,n'}} \sum_{l=0}^{L-1}\sum_{l'=0}^{L-1} \mathbb{E}\Big[h_{m,n}[l]h^*_{m',n'}[l']\Big]\exp\left(-\sqrt{-1}\frac{2\pi}{Q}l\Delta q\right) \\
&= \sum_{l=0}^{L-1} \sigma_l^2 \exp\left(-\sqrt{-1}\frac{2\pi}{Q}l\Delta q\right). \qquad (2.25)
\end{aligned}$$

Here, $\Delta q \equiv q_1 - q_2$ designates the frequency separation between the two subchannels q_1 and q_2. From (2.24), we observe that the cross correlation coefficients can be written in a product form of the spatial channel correlation coefficients and a function $w(\Delta q)$ related to the frequency correlation of the subchannels. The function $w(\Delta q)$ is given by a weighted finite sum of the channel-tap variances and depends on the particular choice of the delay-power profile, the channel-memory length L and the DFT-size Q. In order to investigate the influence of $w(\Delta q)$ on the cross-correlations in (2.24) with the aid of a simple analytic expression, we assume in the following an exponential channel delay-power profile and consider the asymptotic limit of the values Q and L as $Q, L \to \infty$.

Let $\Delta f = 1/Q$ be the normalized frequency separation between adjacent subchannels. Without loss of generality, we suppose $Q = L$, such that the block-size is chosen equal to the channel memory-length. We remark that the more general case of $Q > L$ can be derived in a straightforward manner. Suppose that, as L and Q increase, the product of Δf and τ_d remains fixed. Then, we can state the following lemma.

Lemma 2.1. In the limit of $L, Q \to \infty$, the function $w(\Delta q)$ is given by

$$w(\Delta q) = \frac{1 - \sqrt{-1}2\pi\Delta f\tau_d\Delta q}{1 + (2\pi\Delta f\tau_d\Delta q)^2}. \qquad (2.26)$$

Proof. See Appendix A.1. □

Using this result, we can rewrite (2.24), as $L, Q \to \infty$, as

$$\begin{aligned}
\mathbb{E}\Big[\Re\{\tau_{m,n}(q_1)\}\Im\{\tau_{m',n'}(q_1)\}\Big] &= \mathbb{E}\Big[\Re\{\tau_{m,n}(q_2)\}\Im\{\tau_{m',n'}(q_2)\}\Big] = 0 \\
\mathbb{E}\Big[\Re\{\tau_{m,n}(q_1)\}\Re\{\tau_{m',n'}(q_2)\}\Big] &= \mathbb{E}\Big[\Im\{\tau_{m,n}(q_1)\}\Im\{\tau_{m',n'}(q_2)\}\Big] \\
&= [\mathbf{R}]_{m,m'}[\mathbf{S}]_{n,n'}\frac{1/2}{1+(2\pi\Delta f\tau_d\Delta q)^2} \\
\mathbb{E}\Big[\Re\{\tau_{m,n}(q_1)\}\Im\{\tau_{m',n'}(q_2)\}\Big] &= -\mathbb{E}\Big[\Im\{\tau_{m,n}(q_1)\}\Re\{\tau_{m',n'}(q_2)\}\Big] \\
&= -[\mathbf{R}]_{m,m'}[\mathbf{S}]_{n,n'}\frac{\pi\Delta f\tau_d\Delta q}{1+(2\pi\Delta f\tau_d\Delta q)^2}. \qquad (2.27)
\end{aligned}$$

Fig. 2.4 shows the cross-correlation coefficients $q_1(\Delta q)$ and $q_2(\Delta q)$, $q_1(\Delta q) \equiv \mathbb{E}\Big[\Re\{\tau_{m,n}(q_1)\}\Re\{\tau_{m',n'}(q_2)\}\Big]$ and $q_2(\Delta q) \equiv \mathbb{E}\Big[\Re\{\tau_{m,n}(q_1)\}\Im\{\tau_{m',n'}(q_2)\}\Big]$, for the same channel link (i.e., $n = n'$ and $m = m'$) over the frequency separation Δq. The product of Δf and τ_d is set to 0.0625. We observe that with increasing Δq, the cross correlation $q_2(\Delta q)$ decreases by factor $(\Delta q)^{-1}$, which exhibits a strong channel correlation. This strong correlation does not allow the use of the classical central limit theorem [PP02] on functions of the frequency domain subchannel gains [CST07], [Arc94].

We remark that the distribution of the frequency domain channel gains $\kappa_{m,n}(q) \equiv |\tau_{m,n}(q)|^2$, $q = 0, ..., Q-1$ follows an exponential distribution with unit-mean and unit-variance and correlation coefficient [Mal03]:

$$\delta_{\Delta q} \equiv \mathrm{Corr}[\kappa_{m,n}(q_1), \kappa_{m,n}(q_2)] = \frac{1}{1+(2\pi\Delta f\tau_d\Delta q)^2}. \qquad (2.28)$$

2.4. Transmitter Models

Having introduced the basic structure of the block transmission system and the channel model, it is necessary to specify the generation of the data symbols at the transmitter. Inspecting the two system setups used in this work, it turns out that we require two different transmitter structures for the single- and the multiuser transmission. To achieve a good overall performance, we apply the standard encoding and mapping technique BICM. As shown by Caire *et. al.* in [CTB98], BICM is a simple approach that reveals in combination with simple Gray mapping a nearly-optimum performance very close to capacity. As also shown in [LR97], [tBSY98a] [tBSY98b] and [SGHB03], a close to optimum performance can be achieved by iterative detection and decoding of BICM (BICM-ID) over additive white Gaussian noise (AWGN)

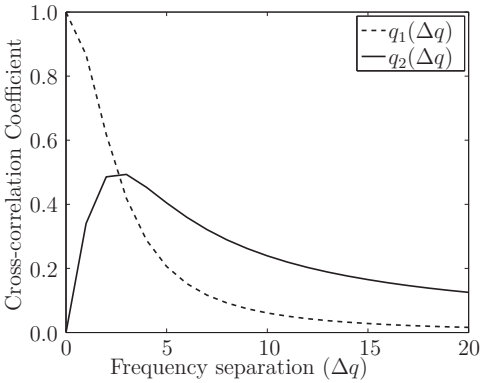

Figure 2.4.: Frequency domain cross-correlation coefficients versus frequency separation Δq for $\Delta f \tau_d = 0.0625$.

channels with very simple channel coding and symbol mappings different from Gray. The BICM scheme is therefore a common method for bandwidth efficient coding on fading channels and today already used in several wireless local area network standards, e.g., in IEEE 802.11n [80207].

In this section, we present the transmitter models for both system setups and give an overview of the basic aspects of BICM.

2.4.1. Transmitter Model for Single-User MIMO Coded Transmission

Fig 2.5 illustrates a common single-carrier single-user MIMO BICM transmitter employing N antennas. The information bits $a_i \in \{0,1\}$, $i = 1, ..., N_i$ are independent and identically distributed with $\Pr(a_i = 1) = \Pr(a_i = 0) = 1/2$ $\forall i$ and organized in frames. Each frame consists of N_i bits which are arranged into a vector $\mathbf{a} = [a_1, ..., a_i, ..., a_{N_i}]^T$, $a_i \in \{0,1\}$, $\forall i$. The bit sequence $\mathbf{a}$ is ideally compressed and does not contain any redundancy. The binary encoder (represented in Fig. 2.5 by the block "ENC") maps the information bit vector $\mathbf{a}$ to an N_c-length coded bit vector $\mathbf{c} = [c_1, c_2, ..., c_{N_c}]^T$, $c_j \in \{0,1\}$, $\forall j$. Hence, the overall rate of the channel code is $r_c = N_i/N_c$ bits per MIMO channel use. After channel encoding, the encoded bit vector $\mathbf{c}$ is interleaved by a random bit-interleaver π_1, producing the permuted bit vector $\mathbf{e}$. The purpose of the interleaver is to remove the correlation introduced due to the channel coding between successive coded bits. The independence between these bits is an essential requirement for the signal processing

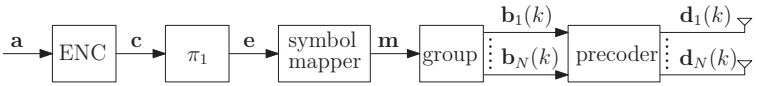

Figure 2.5.: Transmitter model for single-carrier single-user MIMO BICM.

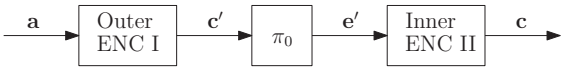

Figure 2.6.: SCCC encoder.

in the iterative receivers proposed in Chapter 3. The encoder can be in this work either a single convolutional code (SCC) or a serially concatenated convolutional code (SCCC) [Tüc04].

In the case of a SCCC, the encoder comprises two sub-encoders which are separated by a random bit-interleaver, as shown in Fig. 2.6. These two sub-encoders are referred to as encoder I (or outer encoder) and encoder II (or inner encoder); the overall encoder is called SCCC encoder. The information bit sequence $\mathbf{a}$ is mapped to a coded bit sequence $\mathbf{c}$ as follows: The sequence $\mathbf{a}$ is first encoded by a rate-$r'_{c,1}$ convolutional encoder I. The resulting encoded bit sequence $\mathbf{c}'$ is bit-interleaved by a random bit-interleaver π_0, yielding the permuted bits $\mathbf{e}'$, which are then fed through the rate-$r'_{c,2}$ convolutional encoder II. This produces the double-encoded bit sequence $\mathbf{c}$. As inner component code we employ a simple SCC with rate $r'_{c,2} = 1$, so that the overall code rate of the SCCC is $r_c = r'_{c,1} r'_{c,2} = r'_{c,1}$. The inner component code introduces no redundancy and is recursive in order to maximize the attainable interleaver gain and to avoid the BER floor in iterative decoding [BDMP98]. As shall be shown later, the use of the inner code provides a remarkable performance gain when used in combination with an iterative decoding scheme compared to the single convolutional-coded system.

After interleaving of the coded bits, the interleaved sequence $\mathbf{e}$ is mapped to a binary phase shift keying (BPSK) symbol vector $\mathbf{m} = [m_1, ..., m_i ..., m_{N_c}]^T$, $m_i \in \{-1, +1\}$ and de-multiplexed into N independent subsequences $\mathbf{b}_n(k)$, $n = 1, .., N$, $k = 1, ..., N_b$. We apply the component-wise mapping rule $m_i = 1 - 2e_i$, $i = 1, ..., N_c$. In general, we consider only BPSK modulation, however, the extension to more generic modulation formats is rather straightforward. The $N_s = N_c/N$ data symbols of each subsequence are arranged into $N_b = N_s/Q$ equal-sized blocks each containing

Q data symbols,

$$\mathbf{b}_n(k) \equiv \left[b_{0,n}[k], ..., b_{q,n}[k], ..., b_{Q-1,n}[k]\right]^T \in \{-1,+1\}^{Q\times 1}, n = 1, ..., N. \quad (2.29)$$

The N data blocks in time slot k are collected in vector

$$\mathbf{b}(k) = [\mathbf{b}_1^T(k), \mathbf{b}_2^T(k), ..., \mathbf{b}_N^T(k)]^T \in \{-1,+1\}^{NQ\times 1}. \quad (2.30)$$

Prior to transmission, the symbol vector $\mathbf{b}(k)$ is multiplied by a weighting matrix $\mathbf{T} \in \mathbb{C}^{NQ\times NQ}$. In this way we obtain the overall kth transmit block $\mathbf{d}(k)$ (see (2.12)) as

$$\mathbf{d}(k) = \mathbf{T}\mathbf{b}(k). \quad (2.31)$$

Depending on the level of CSI available at the transmitter and receiver, the entries of $\mathbf{T}$ can be chosen to optimize the transmit powers of the signal streams, or to direct the transmit signals from the N antennas along orthogonal modes of the frequency-selective MIMO channel with a specific power allocation. The weighting matrix $\mathbf{T}$ is therefore referred to as precoding matrix (and represented by the block "precoder" in Fig. 2.5) and its specific realization will be discussed in Chapter 5.

2.4.2. Transmitter Model for Multiuser SIMO Coded Transmission

Consider a single-carrier multiuser uplink system, where a base station having M receive antennas receives signals from N active users, each equipped with a single transmit antenna. The block-diagram of the transmitter-end of such a communication system is shown in Fig. 2.7. The transmission of each user is organized in frames and is based on BICM. The information bit sequence $\mathbf{a}_n = [a_{n,1}, ..., a_{n,i}, ..., a_{n,N_i(n)}]^T$ of the nth user of length $N_i(n)$ is independently encoded by a rate-$r_{c,n}$ binary encoder, yielding the equal length $N_c = N_i(n)/r_{c,n}$ encoded bit sequences $\mathbf{c}_n = [c_{n,1}, c_{n,2}, ..., c_{n,N_c}]^T$ for all users. We consider SCC or SCCC as channel error correction at each user. After channel encoding, $\mathbf{c}_n$ is randomly bit-interleaved at each user, yielding the sequence $\mathbf{e}_n$, BPSK-modulated, and grouped into N_b equal-sized Q-length blocks $\mathbf{b}_n(k)$ (see (2.29)). We remark that the channel encoders (ENC_n) and the interleavers ($\pi_{1,n}$) shown in Fig. 2.7 are specific to each user.

Each data block $\mathbf{b}_n(k)$ is multiplied by a user-specific precoding matrix $\mathbf{T}_n \in \mathbb{C}^{Q\times Q}$. The precoder is used for transmit power optimization, or for controlling the spectrum of the user's transmitted signal. Similar to the single-user case, the N data blocks $\mathbf{b}_n(k)$ are collected in the vectors $\mathbf{b}(k)$, $\forall k$. The overall transmit signal

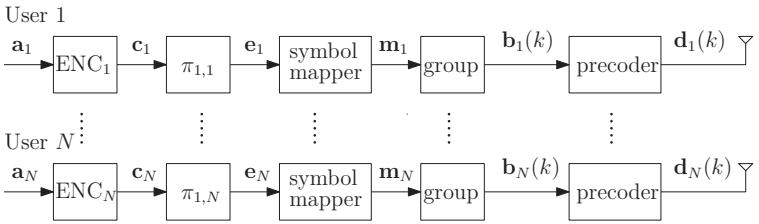

Figure 2.7.: Transmitter model for single-carrier multiuser BICM.

vector is given by

$$\mathbf{d}(k) = \mathbf{T}\mathbf{b}(k), \tag{2.32}$$

where $\mathbf{T}$ is the $QN \times QN$ overall precoding matrix. Since no cooperation between the N users is assumed, the matrix $\mathbf{T}$ is constrained to be block-diagonal, i.e.,

$$\mathbf{T} = \begin{bmatrix} \mathbf{T}_1 & 0 & \dots & 0 \\ 0 & \mathbf{T}_2 & \dots & \vdots \\ \vdots & \ddots & \ddots & 0 \\ 0 & \dots & 0 & \mathbf{T}_N \end{bmatrix}. \tag{2.33}$$

The particular choice of matrix $\mathbf{T}$, in general, depends on the transmit and receive strategy and the system requirements and is discussed more in detail in Chapter 5.

2.5. Log Likelihood Ratio

Log-likelihood ratios of binary random variables are used in the context of iterative detection, decoding and equalization. In the following, we provide some definitions and properties of LLRs. These properties will be exploited in subsequent sections and chapters. We further discuss the application of LLRs for soft-output MIMO detection and soft-output channel decoding in iterative receivers. A more detailed information about LLR algebra and relations to probabilities can be found in [HOP96], [Hub02].

2.5.1. Definition and Properties of LLRs

Consider a binary random variable X with elements $\{+1, -1\}$. The LLR of X, $L(x)$, is defined as

$$L(x) \equiv \log\left(\frac{\text{Prob}(x = +1)}{\text{Prob}(x = -1)}\right) \in \mathbb{R}, \tag{2.34}$$

where $\text{Prob}(x = c)$ denotes the probability that X takes on the value $c = \pm 1$. The sign of $L(x)$ provides an estimate of the binary symbol (also called the hard decision) and the magnitude $|L(x)|$ represents a measure for the reliability of the estimate. Thus an LLR near zero corresponds to an unreliable estimate. The LLR $L(x)$ is therefore denoted as soft value, or soft information of the random variable X. The definition of the LLR in (2.34) can also be interpreted as a conversion of two probabilities to a real value. Obviously, this relation can be inverted and the corresponding bit probabilities are obtained from the LLR as

$$\text{Prob}(x = c) = \frac{1}{1 + e^{-cL(x)}}. \tag{2.35}$$

Let us now consider a binary random variable X that is conditioned on a real-valued random variable $Y \in \mathbb{R}$. The random variable Y may be associated with the received symbol of a coded bit X transmitted over a binary-input (not necessarily memory-less) channel. Similar to (2.34), we define the conditioned LLR $L(x|y)$ as

$$L(x|y) \equiv \log\left(\frac{\text{Prob}(x = +1|y)}{\text{Prob}(x = -1|y)}\right) \in \mathbb{R}. \tag{2.36}$$

Using Bayes' theorem for probabilities, we can express (2.36) as a sum of two independent LLRs,

$$\begin{aligned} L(x|y) &= \log\left(\frac{\text{Prob}(x = +1)}{\text{Prob}(x = -1)}\right) + \log\left(\frac{p(y|x = +1)}{p(y|x = -1)}\right) \\ &= L(x) + L(y|x). \end{aligned} \tag{2.37}$$

Here $p(y|x = c)$ denotes the probability density function of Y conditioned on $X = c$. Equation (2.37) is a fundamental principle used in iterative decoding schemes and also known as chain rule for LLRs [Lan05]. Note that if X is uniformly distributed, i.e., $L(x)$ is equal to zero, we obtain $L(x|y) = L(y|x)$.

2.5.2. Application to Soft-Output MIMO Detection and Channel Decoding

As an application of (2.37), let us consider the problem of signal detection in MIMO-ISI channels. Assume a single-user coded MIMO BPSK transmission based on the system model introduced in Section 2.4.1. Let us denote by $\mathbf{c}$ the length-N_c output sequence of a channel code, and the corresponding vectors of BPSK data symbols to be transmitted by $\mathbf{b}(k)$. We are interested in the probability that the BPSK data symbol $b_{q,n}[k]$ is equal to ± 1, conditioned on the received vector $\mathbf{r}(k)$, the channel state information $\mathbf{H}$ and the precoding matrix $\mathbf{T}$. As in equation (2.36), we may use the conditional LLR $L(b_{q,n}[k]|\mathbf{r}(k))$, which is defined as

$$\theta_e\Big[b_{q,n}[k]\Big] \equiv L(b_{q,n}[k]|\mathbf{r}(k)) = \log\left(\frac{\text{Prob}\Big(b_{q,n}[k]=+1|\mathbf{r}(k),\mathbf{H},\mathbf{T}\Big)}{\text{Prob}\Big(b_{q,n}[k]=-1|\mathbf{r}(k),\mathbf{H},\mathbf{T}\Big)}\right), \forall q,n,k. \quad (2.38)$$

Equation (2.38) is known as the symbol-wise MAP detection rule that is optimal in terms of minimum symbol error rate. The sign of the *a posteriori* soft value $\theta_e\Big[b_{q,n}[k]\Big]$ may be used to obtain a hard estimate $\hat{b}_{q,n}[k]$ on the BPSK data symbol $b_{q,n}[k]$. The corresponding symbol error rate is obtained from the magnitude $\Big|\theta_e\Big[b_{q,n}[k]\Big]\Big|$ as

$$\text{Prob}(\hat{b}_{q,n}[k] \neq b_{q,n}[k]) = \frac{1}{1+\exp\Big(\Big|\theta_e\Big[b_{q,n}[k]\Big]\Big|\Big)}. \quad (2.39)$$

Based on the chain rule for LLRs (2.37), we can split (2.38) into two independent terms,

$$\theta_e\Big[b_{q,n}[k]\Big] = \zeta_e\Big[b_{q,n}[k]\Big] + \lambda_e\Big[b_{q,n}[k]\Big]. \quad (2.40)$$

Here, $\zeta_e\Big[b_{q,n}[k]\Big] \equiv L(b_{q,n}[k])$ and $\lambda_e\Big[b_{q,n}[k]\Big] \equiv L(\mathbf{r}(k)|b_{q,n}[k])$ denote the *a priori* and *extrinsic* LLR on $b_{q,n}[k]$, respectively. The *extrinsic* LLR contains the channel and *a priori* information from all symbols in vector $\mathbf{b}(k)$ except the symbol $b_{q,n}[k]$. It can therefore be considered as an independent estimate from the corresponding *a priori* LLR $\zeta_e\Big[b_{q,n}[k]\Big]$ and may be used as a soft-input by a subsequent channel decoding stage, as in iterative receivers. An analytic expression for the LLR $\lambda_e\Big[b_{q,n}[k]\Big]$ will be given in Chapter 3. The algorithm directly implementing the above equation is known as the SfISfO MAP MIMO detector. This detector accepts channel observations in the form of the received sequence $\mathbf{r}(k)$ together with the *a priori* soft-inputs $\zeta_e\Big[b_{q,n}[k]\Big]$ on the BPSK data symbols and produces the corresponding *a posteriori* soft-outputs $\theta_e\Big[b_{q,n}[k]\Big]$.

Equation (2.37) can also be applied to a channel error correcting code. Then, (2.40) becomes the *a posteriori* LLR of the coded bit c_i as

$$\theta_d[c_i] = \zeta_d[c_i] + \lambda_d[c_i]. \tag{2.41}$$

The *extrinsic* LLR $\lambda_d[c_i]$ of the coded bit c_i stems from the constraint of the channel code and contains the *a priori* information from all other coded bits in the sequence $\mathbf{c}$ except c_i. The corresponding algorithm implementing the MAP-based channel decoding is called SfISfO MAP channel decoder.

The SfISfO MAP MIMO detector and SfISfO MAP channel decoder both are algorithms suited to iterative detection and decoding in concatenated coded transmission schemes.

2.5.3. Relations and Exponential Symmetry

In the analysis of iterative decoding, the conditioned LLRs $l \equiv L(y|x)$ are often considered as outcomes of a random variable L. This random variable can be described by its probability density function (PDF) $p(l)$, or equivalently, by its conditional PDFs $p(l|x = c)$, $c \in \{+1, -1\}$.

Lemma 2.2. For symmetric channel outputs, i.e., $p(y|x = +1) = p(-y|x = -1)$, the PDF and the conditional PDFs of L satisfy:

$$p(l|x = +1) = e^l p(l|x = -1) \tag{2.42}$$
$$p(l|x = +1) = e^l p(-l|x = +1) \tag{2.43}$$
$$p(l) = e^l p(-l). \tag{2.44}$$

Proof. From the definition of the LLR $L(y|x)$ in (2.37), it follows that $p(y|x = +1) = e^l p(y|x = -1)$. Hence, as a property of the two conditional PDFs of L, we obtain

$$\begin{aligned} p(l|x = +1) &= \int_{y \in \mathcal{I}} p(y|x = +1)\mathrm{d}y \\ &= e^l \int_{y \in \mathcal{I}} p(y|x = -1)\mathrm{d}y \\ &= e^l p(l|x = -1), \end{aligned} \tag{2.45}$$

where $\mathcal{I} \equiv \left\{ y \in \mathbb{R}^N \middle| L(y|x) = l \right\}$. Moreover, based on the channel symmetry condition, we obtain

$$L(y|x) = \log\left(\frac{p(y|x = +1)}{p(y|x = -1)}\right) = \log\left(\frac{p(-y|x = -1)}{p(-y|x = +1)}\right) = -L(-y|x). \tag{2.46}$$

Therefore, we can write the conditional PDF $p(l|x=+1)$ as

$$\begin{aligned} p(l|x=+1) &= \int_{y\in\mathcal{I}} p(-y|x=-1)\mathrm{d}y \\ &= p(-l|x=-1). \end{aligned} \tag{2.47}$$

Combining (2.45) with (2.47), it immediately follows (2.42)-(2.44). □

Equations (2.42)-(2.44) are known as the exponential symmetry property of the conditional probability distributions and the probability distribution of the LLR $L(y|x)$ for binary-input output-symmetric channels. This important property was first shown by Hoeher et. al. in [HLS00], and later also reported by the authors of [RU01] and [LHG03]. Notice that (2.42)-(2.44) also holds true for the LLR $L(x|y)$ if $L(x)$ is equal to zero. We will see in the sequel that the exponential symmetry property plays an important role in analyzing the convergence behavior of iterative receivers.

In general, we suppose the conditional PDFs $p(l|x=+1)$ and $p(l|x=-1)$ to be Gaussian distributed, i.e., $p(l|x=+1)\sim\mathcal{N}(m_1,\sigma_1^2)$ and $p(l|x=-1)\sim\mathcal{N}(m_2,\sigma_2^2)$. Due to the exponential symmetry constraint on the distributions, the mean and variance satisfy $m_1=-m_2=\frac{\sigma_1^2}{2}$ and $\sigma_1^2=\sigma_2^2$. Hence, the distribution of L follows a Gaussian distribution that is completely specified by a single parameter, the variance σ_1^2, that is

$$L=\frac{\sigma_1^2}{2}X+N,\ \text{where } N\sim\mathcal{N}(0,\sigma_1^2). \tag{2.48}$$

The above Gaussian model for the conditioned LLRs $L(y|x)$ has been successfully applied in the convergence analysis of iterative decoding schemes [tB01], and will extensively be used in this work to analyze the convergence behavior of iterative receivers.

2.6. Receiver Models

At the receiver side, given the channel observation in the form of the received data one is often interested in minimizing the bit error rate, that is the probability of a wrong estimate on a transmitted binary information symbol. From Bayesian decision theory, it is known that the optimal MAP-based receiver maximizes the *a-posteriori* probability of each transmitted information symbol by jointly performing the following three tasks[1]:

[1]Note that synchronization at the receiver is not explicitely mentioned here as we consider a coherent communication system with zero carrier frequency offset and perfect phase and symbol

1. the equalization of the MIMO ISI block-fading channel to separate the transmitted data symbols;

2. the decoding of the coded data symbols;

3. and the estimation of the channel coefficients and the receiver noise variance.

The design of such an optimal MAP-based estimation algorithm leads to decision metrics whose calculations are computationally demanding. Even in the case of perfect knowledge of CSI and noise variance at the receiver, it turns out that the optimum receiver is prohibitively complex for practical systems (especially in cases when a long bit-interleaver is present in the system), as it performs signal detection by means of a super-trellis, including the channel code(s), the bit-interleaver(s) and the MIMO ISI block-fading channel. Hence, in order to lower the computational complexity a standard approach is to separate channel equalization and signal detection (to be referred to simply as equalization in the sequel), channel decoding and channel parameter estimation into three main parts. Thereby, we can chose different approaches for these three parts with respect to specific performance and complexity requirements. In addition, by applying SfISfO algorithms for equalization and channel decoding, signal detection may iteratively be performed on the received signal with exchange of soft probabilistic information in the form of bit-*extrinsic* LLRs. The aim of this principle, which is widely known as "MIMO Turbo Equalization" [DJB+95], [WP99a], [TSK02], [AM03], is to iteratively refine the data estimates of the transmitted symbols, the estimates of the channel coefficients and receiver noise variance so as to achieve near-optimal performance with reasonable complexity.

Different equalization and decoding schemes can be applied for turbo equalization. Most of the equalizers are trellis-based (Viterbi-like) algorithms [DJB+95], [BF98] or soft interference cancellation and linear-filtering approaches [WP99a], [TSK02], [TH02], [GM08], [AM03], [KM07], [KSMT05], [WP99b], [LP04], [GM07] and [JPSL04]. The former equalization concepts usually have a very high computational complexity; thus they are unpractical when large signal constellations are employed, or equalization of ISI channels involving a large channel memory is considered. We therefore focus in this work mostly on the class of filtering-based turbo equalizers. Such turbo equalizers offer good performance in a variety of channel environments at low computational complexity and facilitate a simple analysis of their convergence behavior.

For the parameter estimation part, soft input iterative channel estimation [SSS04], [GPH09] can be used to refine the channel data estimates based on the channel ob-

timing.

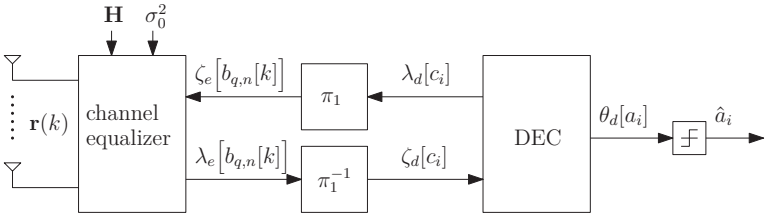

Figure 2.8.: Receiver model for single-carrier single-user MIMO BICM.

servation and the soft-feedback provided by the channel decoders. The channel estimate may be obtained using different performance criteria, such as the least squares (LS), the recursive least squares (RLS), the MMSE, the MAP, the expectation-maximization (EM), or the Kalman filtering approach. For an overview over these estimation techniques, the interested reader is referred to [Hay02]. However, as parameter estimation is not the focus of this thesis, we suppose throughout this work that the channel coefficients and the receiver noise variance both are always perfectly known at the receiver. Although the instantaneous and perfect knowledge of these parameters is not always realistic in practical systems, it can be almost achieved by using efficient iterative channel estimation techniques [SSS04], [GPH09]. Bear this in mind, we are now able to present the corresponding receiver models for the single- and multiuser transmitters with BICM signaling of Section 2.4.

2.6.1. Receiver Model for Turbo Equalization of Single-User MIMO Coded Transmission Systems

A block diagram of the iterative receiver for coded single-user transmission systems is depicted in Fig 2.8. The turbo equalizer consists of two SfiSfO stages - the equalizer and the decoder. Both components are separated by an interleaver (π_1) and a deinterleaver (π_1^{-1}). Within the iterative processing, soft probabilistic information about the coded bits are exchanged between the constituent SfISfO algorithms, until a maximum number of iterations is attained. More specifically, $\lambda_{(\cdot)}[\cdot]$ and $\zeta_{(\cdot)}[\cdot]$ in Fig. 2.8 represent the *extrinsic* and the *a priori* information, respectively, expressed in terms of LLRs of the corresponding bits, where the subscript $(\cdot)$ is used to distinguish between the SfISfO modules. The iterations between the equalizer and the decoder are referred to as turbo iterations. The total number of turbo iterations is denoted in the following by T_e.

The equalizer deals jointly with channel equalization, multiple-antenna detection and symbol-wise de-mapping, with the aim to mitigate ISI and to cancel CAI, caused by the multiple transmit data streams. Inputs to the equalizer are the received

symbol vectors $\mathbf{r}(k)$, $k = 1, ..., N_b$, the channel matrix $\mathbf{H}$, the receiver noise variance σ_0^2, the signaling strategy applied at the transmitter in the form of the precoding matrix $\mathbf{T}$, and the *a priori* LLR sequences

$$\begin{aligned}\boldsymbol{\zeta}_e[\mathbf{b}(k)] &\equiv \left[\boldsymbol{\zeta}_e^T[\mathbf{b}_1(k)], ..., \boldsymbol{\zeta}_e^T[\mathbf{b}_n(k)], ..., \boldsymbol{\zeta}_e^T[\mathbf{b}_N(k)]\right]^T, \\ \boldsymbol{\zeta}_e[\mathbf{b}_n(k)] &\equiv \left[\zeta_e\left[b_{0,n}[k]\right], ..., \zeta_e\left[b_{q,n}[k]\right], ..., \zeta_e\left[b_{Q-1,n}[k]\right]\right]^T \text{ for all } k,\end{aligned} \tag{2.49}$$

where $\zeta_e[b_{q,n}(k)] = L(b_{q,n}[k])$. It is worth mentioning that during the first iteration of turbo equalization, the LLR $\zeta_e\left[b_{q,n}[k]\right]$ is zero for all n, q, k, and later on $\zeta_e\left[b_{q,n}[k]\right]$ is provided via the de-multiplexer and interleaver in the form of *extrinsic* LLRs of the channel decoder ("DEC"). The equalizer applies MAP estimation to the data symbols, or approximations thereof, and outputs *extrinsic* LLRs of the code bits. Using the notations introduced in Section 2.5.2, the *extrinsic* LLR for symbol $b_{q,n}[k]$ can be expressed as

$$\lambda_e\left[b_{q,n}[k]\right] = \theta_e\left[b_{q,n}[k]\right] - \zeta_e\left[b_{q,n}[k]\right]. \tag{2.50}$$

Similar to (2.49), the LLRs at the equalizer output are arranged into vectors

$$\boldsymbol{\lambda}_e[\mathbf{b}(k)] \equiv \left[\lambda_e\left[b_{0,1}[k]\right], ..., \lambda_e\left[b_{q,n}[k]\right], ..., \lambda_e\left[b_{Q-1,n}[k]\right]\right]^T \text{ for all } n, k. \tag{2.51}$$

The LLR vectors $\boldsymbol{\lambda}_e[\mathbf{b}(k)]$ are multiplexed and serve after deinterleaving as *a priori* information for the binary decoder. Based on the *a priori* LLRs $\zeta_d\left[c_i\right] = L(c_i)$, $\forall i$ the decoder calculates the corresponding *extrinsic* and information-bit *a posteriori* LLRs $\lambda_d[c_i]$ and $\theta_d[a_i]$, respectively. The iterative processing of the received data is carried out until a maximum number of T_e turbo iterations is achieved. After the last turbo iteration, the *a posteriori* LLRs $\theta_d[a_i]$ are passed through a hard decision decoder to obtain estimates $\hat{a}_i$ on the information bits a_i for all $i = 1, ..., N_i$.

The decoder is implemented using the Log-MAP algorithm in the case of SCC encoding. For details on Log-MAP decoding (Bahl-Cocke-Jelinek-Raviv (BCJR) algorithm in the logarithmic domain), the reader is referred to standard literature [Han02].

When employing SCCC encoding of the information bit sequence $\mathbf{a}$ at the transmitter, an iterative decoding approach for the two constituent codes is used. Fig. 2.9 depicts a block diagram of the iterative SCCC decoder. The SCCC decoder comprises two sub-decoders, an interleaver (π_0) and a deinterleaver (π_0^{-1}). The two sub-decoders, referred to as decoder I (outer decoder) and decoder II (inner decoder), correspond to the two constitutes encoders of Fig. 2.6. Commonly, the Log-MAP algorithm is employed as constitutes decoders. The two decoders exchange *extrinsic*

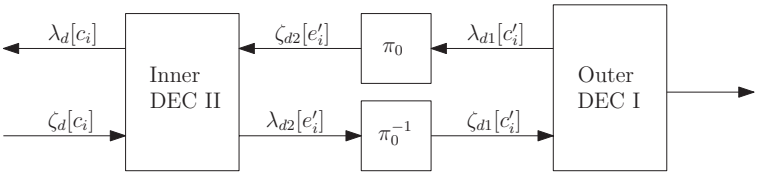

Figure 2.9.: Block diagram of the iterative SCCC decoder.

LLRs of the corresponding bits. Using the *a priori* information $\zeta_d[c_i]$ and $\zeta_{d2}[e'_i]$, and taking into account the code constraint of the inner encoder, decoder II computes *extrinsic* soft values $\lambda_d[c_i]$ and $\lambda_{d2}[e'_i]$ for its coded and information bits c_i and e'_i, respectively. In the first decoding iteration, $\zeta_{d2}[e'_i]$ is set to zero for all i, and in the other iterations, $\zeta_{d2}[e'_i]$ is provided by the *extrinsic* LLRs of decoder I after interleaving. The LLRs $\lambda_{d2}[e'_i]$ are the decoding result of decoder II. These values are deinterleaved and forwarded to decoder I. Using the *a priori* information $\zeta_{d1}[c'_i]$ and taking into account the code constraint of the outer encoder, decoder I computes the *extrinsic* soft values $\lambda_{d1}[c'_i]$ for the code bits c'_i for all i.

In order to simplify the convergence analysis of the iterative receiver (see Chapter 4), we assume a *static* activation schedule when SCCC encoding is applied, where after one activation of the equalizer, decoding proceeds iteratively for a fixed number of iterations between decoder I and decoder II. The total number of decoding iterations (after each equalizer activation) is denoted by T_d.

2.6.2. Receiver Model for Turbo Equalization of Multiuser SIMO Coded Transmission Systems

The receiver part for the multiuser setup is depicted in Fig. 2.10. It consists of N turbo loops, one for each user. Each turbo loop comprises the user-specific deinterleaver, channel decoder, and interleaver. The signal processing follows the turbo principle and is similar to the single-user transmission of Section 2.6.1. The equalizer accepts the received symbol vectors $\mathbf{r}(k)$ and the *a priori* inputs $\boldsymbol{\zeta}_e[\mathbf{b}(k)]$ of the coded bit vector $\mathbf{b}(k)$, $\forall k$ and outputs the *extrinsic* information vector $\boldsymbol{\lambda}_e[\mathbf{b}(k)]$. The vectors $\boldsymbol{\lambda}_e[\mathbf{b}(k)]$ contain after bit-interleaving the *a priori* information for the N decoders. The number of turbo iterations is again denoted by T_e. One turbo iteration comprises the activation of the equalizer and subsequently the activation of all N decoders. The receiver outputs after the last turbo iteration the hard decision bits $\hat{a}_{n,i}$ on the information bits $a_{n,i}$, $\forall n, i$.

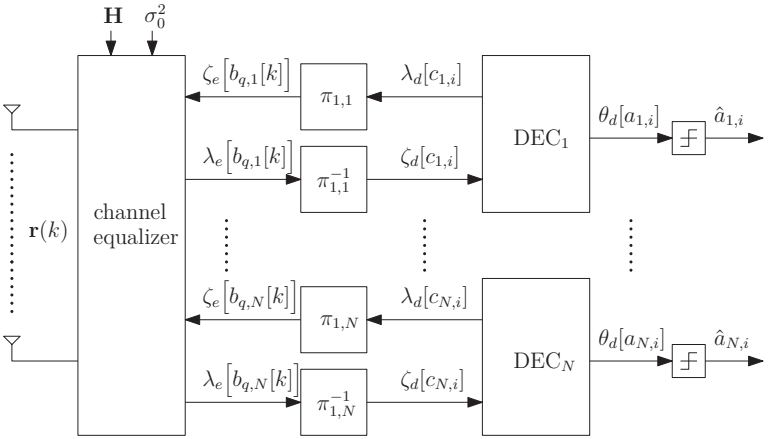

Figure 2.10.: Receiver model for single-carrier multiuser SIMO BICM.

Some Remarks

We conclude this section by noting some remarks about the turbo equalization principle.

- *Sufficient Interleaver Length:* When processing soft information for turbo equalization, the *a priori* LLRs about the code bits available at the input of each SfISfO component are supposed to be statistically independent. This ensures to calculate the soft information of each code bit without taking into account the correlation between successive bits. To satisfy the statistical independence assumption, an appropriate bit-interleaver of sufficient length at each user has to be used.

- *Extrinsic Information Processing:* In order to avoid an early convergence and a worse performance of the turbo equalizer, the independence assumption must also be satisfied for each *a priori* LLR of the same bit over several iterations. Each SfISfO algorithm must therefore provide at its output for each bit only the soft information gained from the *a priori* information about all code bits without the desired bit itself. In other words, the SfISfO algorithm has to deliver only the information increment (i.e., *extrinsic* information) about the desired bit to the other modules. As shown by (2.37), the *extrinsic* knowledge of a binary symbol can be obtained by a subtraction of the *a priori* information from the *a posterori* information on the binary symbol.

- *Turbo Equalization as Factor Graph:* The turbo equalizer can also be consid-

ered as an application of the belief propagation (also called the sum-product) algorithm on an undirected bipartite (factor) graph [KFL01], [Loe04], [TKS04], [SCG05]. The factor graph represents the factorization of the joint probability function $p\Big(\{\mathbf{a}_i\}_{i=1}^{N}, \{\mathbf{b}(k)\}_{k=1}^{N_b}, \{\mathbf{r}(k)\}_{k=1}^{N_b}\Big)$ of all binary and non-binary variables of the communication system. The factor graph is divided into several subgraphs that describe the behavior of the equalizer and the N decoders. These subgraphs consist of some blocks that exchange messages in the form of probability distributions via shared variable nodes (which model the information/code bits and modulated data symbols). The execution of the sum-product algorithm applied over the factor graph involves a finite number of operations to efficiently compute the *a posterori* probability $\text{Prob}\Big(a_{n,i} = c|\{\mathbf{r}(k)\}_{k=1}^{N_b}\Big)$, $c \in \{0,1\}$ for each information bit $a_{n,i}$. Once this probability is computed, an estimate on the information bit $a_{n,i}$ is obtained based on the calculated marginals using the MAP decision rule $\hat{a}_{n,i} = \arg\max_{c\in\{0,1\}} \text{Prob}\Big(a_{n,i} = c|\{\mathbf{r}(k)\}_{k=1}^{N_b}\Big)$.

The sum-product algorithm does not provide exact values for the calculated marginals, since the underlying graph modeling the turbo equalizer contains cycles due to the presence of finite-length interleaving at each user. The accuracy of the probability approximation, however, may be improved by increasing the length of the shortest cycle in the graph [RU06]. In this context, several authors have imposed certain constraints in the factor graph, such as improved code or interleaver designs [HEM01], [TJVW04], to eliminate short cycles. This enables the iterative receiver to achieve performance very close to the optimal joint MAP equalizer and decoder as the number of turbo iterations and the codeword (interleaver) length become very large.

2.7. System Model for Precoded Transmission

For a compact notation of the overall system model for the single- and multiuser system setups, we include the operations of the transmit signal precoding from (2.31) and (2.32) into the system model (2.13), and rewrite the received signal $\mathbf{r}(k)$ as

$$\begin{aligned}\mathbf{r}(k) &= \mathbf{H}\mathbf{d}(k) + \mathbf{n}(k) = \mathbf{H}\mathbf{T}\mathbf{b}(k) + \mathbf{n}(k)\\ &= \mathbf{H}_c\mathbf{b}(k) + \mathbf{n}(k)\\ &= \sum_{n=1}^{N} \mathbf{H}_{c,n}\mathbf{b}_n(k) + \mathbf{n}(k),\end{aligned} \tag{2.52}$$

where

$$\mathbf{H}_c \equiv \mathbf{HT} = [\mathbf{H}_{c,1}, ..., \mathbf{H}_{c,n}, ..., \mathbf{H}_{c,N}] \in \mathbb{C}^{MQ \times NQ} \tag{2.53}$$

with $\mathbf{H}_{c,n} = [\mathbf{H}_{c,n,1}^T, \mathbf{H}_{c,n,2}^T, ..., \mathbf{H}_{c,n,M}^T]^T \in \mathbb{C}^{MQ \times Q}$, $n = 1, ..., N$ denotes the compound channel and precoding matrix. The precoding matrix $\mathbf{T}$ is assumed to be block-circulant, such that $\mathbf{T} = \mathbf{F}_N^H \mathbf{\Xi}_T \mathbf{F}_M$, where $\mathbf{\Xi}_T \in \mathbb{C}^{QN \times NQ}$ is block-diagonal. As in (2.14), the compound channel matrix $\mathbf{H}_c$ is therefore block-circulant as well and may be decomposed into a block-diagonal matrix

$$\mathbf{\Xi}_c = \mathbf{F}_M^H \mathbf{H}_c \mathbf{F}_N = [\mathbf{\Xi}_{c,1}, \mathbf{\Xi}_{c,2}, ..., \mathbf{\Xi}_{c,N}] \in \mathbb{C}^{MQ \times NQ} \tag{2.54}$$

with $\mathbf{\Xi}_{c,n} = [\mathbf{\Xi}_{c,n,1}^T, \mathbf{\Xi}_{c,n,2}^T, ..., \mathbf{\Xi}_{c,n,M}^T]^T \in \mathbb{C}^{MQ \times Q}$ for $n = 1, ..., N$. Obviously, $\mathbf{\Xi}_c$ can be written in product form as $\mathbf{\Xi}_c = \mathbf{\Xi}\mathbf{\Xi}_T$. Equation (2.52) describes the general system model for precoded single-carrier block transmission that will be extensively used throughout this work.

We conclude this section by defining the SNR at the reveiver for a time-invariant and a time-variant block-fading channel. Assume that the signal energy at the transmitter has been normalized, such that $E_0 = \mathbb{E}[b_{q,n}(k)] = 1$. Consequently, the SNR per receive antenna for a time-invariant channel is given by

$$\frac{E_s}{N_0} = \frac{E_h E_0}{M\sigma_0^2} = \frac{E_h}{M\sigma_0^2}, \tag{2.55}$$

where E_s and N_0 designate the signal and noise power, respectively, and $E_h \equiv \sum_{n=1}^{N} \sum_{m=1}^{M} \sum_{l=0}^{L-1} \left| h_{m,n}[l] \right|^2$ designates the average instantaneous power of the CIR. The average SNR for a time-variant block-fading MIMO channel is defined accordingly as

$$\frac{E_s}{N_0} = \frac{\bar{E}_h}{M\sigma_0^2}, \tag{2.56}$$

where $\bar{E}_h = \mathbb{E}[E_h]$ is the average power of the channel. For the performance evaluation in the following sections, we neglect the rate loss due to transmission of the cyclic prefix. The energy per information bit, denoted by E_b, is then related to E_0 as $E_0 = r_c E_b$. Therefore, the energy-per-bit-to-noise ratios for a time-invariant and a time-variant channel, respectively, are given by

$$\frac{E_b}{N_0} = \frac{E_h}{M r_c \sigma_0^2} \text{ and } \frac{E_b}{N_0} = \frac{\bar{E}_h}{M r_c \sigma_0^2}. \tag{2.57}$$

2.8. Fundamental Limits

In this section, we give an overview of the information-theoretic performance limits of single- and multiuser wireless communication systems employing single-carrier block transmission over the fixed and the time-varying MIMO ISI channel. In detail, we analyze the mutual information under different constraints for the distribution of the input signal constellation and derive analytical expressions for the outage and ergodic rates and rate regions of the channel. We first consider the channel with unconstrained input symbols having Gaussian distributions. The obtained results are then generalized to the case of fixed and finite input constellation, as encountered in most practical systems. The derived analytical expressions in this section serve as the performance upper bounds of the communication systems considered in this thesis.

2.8.1. Mutual Information with Gaussian Signaling

Single-User Systems: To begin analyzing the mutual information for the transmission over the single-user MIMO ISI channel, we consider first the case when the channel $\mathbf{H}$ is fixed and perfectly known at the receiver. Then the average mutual information between the received signal vector sequence $\left\{\mathbf{r}(k)\right\}_{k=1}^{N_b}$ and the transmitted signal vector sequence $\left\{\mathbf{d}(k)\right\}_{k=1}^{N_b}$ is given by

$$I(\mathbf{d},\mathbf{r}) = \lim_{k\to\infty}\frac{1}{kQ}\Big(h\big(\mathbf{r}(1),\mathbf{r}(2),...,\mathbf{r}(k)\big) - h\big(\mathbf{n}(1),\mathbf{n}(2),...,\mathbf{n}(k)\big)\Big) \tag{2.58}$$

$$= Q^{-1}\log_2\det(\pi e\mathbf{Y}) - Q^{-1}\log_2\det(\pi e\sigma_0^2\mathbf{I}_{MQ}), \tag{2.59}$$

where $h(\cdot)$ denotes the differential entropy function [CT91], and $\mathbf{Y} \equiv \mathbb{E}\big[\mathbf{r}(k)\mathbf{r}^H(k)\big]$, $\forall k$ is the covariance matrix of $\mathbf{r}(k)$. For simplicity, we have omitted the conditioning on the channel realization in (2.59). The components of $\mathbf{d}(k)$ are chosen to be zero-mean, circularly symmetric, complex Gaussian random variables. It follows that the received signal vector $\mathbf{r}(k)$ is circularly symmetric, complex Gaussian random distributed as well. Moreover, with $\mathbf{d}(k)$ and $\mathbf{n}(k)$ to be independent, we obtain $\mathbf{Y} = \mathbf{HQH}^H + \sigma_0^2\mathbf{I}$, where $\mathbf{Q} \equiv \mathbb{E}\big[\mathbf{d}(k)\mathbf{d}^H(k)\big]$, $\forall k$ is the covariance matrix of $\mathbf{d}(k)$. Therefore, the mutual information in (2.59) can be expressed as

$$I(\mathbf{d},\mathbf{r}) = Q^{-1}\log_2\det\left(\mathbf{I}_{MQ} + \rho_{\text{SNR}}\mathbf{HQH}^H\right), \tag{2.60}$$

where $\rho_{\text{SNR}} = \sigma_0^{-2}$. Besides, using the channel decomposition property in (2.14), Eqn. (2.60) can further be written as $\mathrm{I}(\mathbf{d},\mathbf{r}) = Q^{-1}\log_2\det\left(\mathbf{I}_{MQ} + \rho_{\text{SNR}}\mathbf{\Xi Q}_F\mathbf{\Xi}^H\right)$, where $\mathbf{Q}_F \equiv \mathbf{F}_N^H\mathbf{QF}_N$.

Consider first the case of perfect CSI available at the transmitter. By the singular value decomposition theorem [HJ85], we can write the frequency domain channel matrix $\mathbf{\Xi}$ as $\mathbf{\Xi} = \mathbf{U}\mathbf{G}\mathbf{V}^H$, where $\mathbf{U} \in \mathbb{C}^{MQ\times MQ}$ and $\mathbf{V} \in \mathbb{C}^{NQ\times NQ}$ are unitary. Here, $\mathbf{G} \in \mathbb{C}^{MQ\times NQ}$ is a diagonal matrix with entries $[\mathbf{G}]_{i,i} = \sqrt{g_i}, 1 \leq i \leq r$ on the main diagonal, where $r = \min(NQ, MQ)$ denotes the rank of $\mathbf{\Xi}$, and g_i, $1 \leq i \leq r$ are the real non-negative eigenvalues of $\mathbf{\Xi}\mathbf{\Xi}^H$. The knowledge of the CSI at the transmitter can be used to choose the input covariance matrix $\mathbf{Q}_F$ as a function of $\mathbf{\Xi}$. The mutual information is maximized by letting $\mathbf{Q}_F = \mathbf{V}\mathbf{P}\mathbf{V}^H$, where $\mathbf{P} = \text{diag}([\mathbf{p}^T, 0, .., 0]^T) \in \mathbb{C}^{NQ\times NQ}$ is a real non-negative and diagonal matrix with $\mathbf{p} = [p_1, p_2, ..., p_r]^T$ being the power loading vector on the main diagonal. By substituting $\mathbf{Q}_F = \mathbf{V}\mathbf{P}\mathbf{V}^H$ into the expression for the mutual information, we obtain

$$I(\mathbf{d}, \mathbf{r}) = \max_{\mathbf{P}:\text{Trace}(\mathbf{P})\leq P_0} Q^{-1} \log_2 \det\left(\mathbf{I} + \rho_{\text{SNR}}\mathbf{P}\mathbf{G}^2\right). \tag{2.61}$$

It can easily be shown that the optimal solution to Eqn. (2.61) can be found via "water-filling" [Tel99], [XP03] over the frequency domain channel eigenmodes g_u,

$$p_u = \left(c_{\text{MaxMI}} - g_u^{-1}\rho_{\text{SNR}}^{-1}\right)^+, u = 1, ..., r \tag{2.62}$$

with c_{MaxMI} being a parameter chosen to satisfy the power constraint. The mutual information with CSI at the transmitter can hence be expressed as

$$Q^{-1}\sum_{u=1}^{r}\left[\log_2\left(c_{\text{MaxMI}}\rho_{\text{SNR}}g_u\right)\right]^+. \tag{2.63}$$

Consequently, to achieve the maximum mutual information, the optimal input distribution must be Gaussian with a water-filling power allocation over the eigenmodes g_u and the transmit directions of the covariance matrix $\mathbf{Q}_F$ being aligned with the right singular-vectors of the frequency domain channel $\mathbf{\Xi}$.

Consider now the case where no CSI is available at the transmitter. The optimal transmit strategy is then given by the uniform power allocation $\mathbf{Q}_F = \mathbf{I}_{(NQ)}$ [Tel99]. Using a similar derivation as for the case with CSI, the mutual information can be shown to be expressed as

$$\begin{aligned} I(\mathbf{d}, \mathbf{r}) &= Q^{-1}\log_2\det\left(\mathbf{I} + \rho_{\text{SNR}}\mathbf{\Xi}\mathbf{\Xi}^H\right) \\ &= Q^{-1}\sum_{q=0}^{Q-1}\log_2\det\left(\mathbf{I} + \rho_{\text{SNR}}\mathbf{\Xi}(q)\mathbf{\Xi}^H(q)\right). \end{aligned} \tag{2.64}$$

The expression in (2.64) can be directly related to the capacity of the MIMO ISI

channel, by letting $Q \to \infty$, yielding

$$C^{\text{MIMO}}(\boldsymbol{\Xi}) = \lim_{Q\to\infty} \sum_{q=0}^{Q-1} Q^{-1} \log_2 \det\Big(\mathbf{I} + \rho_{\text{SNR}} \boldsymbol{\Xi}(q) \boldsymbol{\Xi}^H(q)\Big). \tag{2.65}$$

The channel capacity in (2.65) gives an upper bound on the information rate (in bits/symbol) that can be reliably transmitted over the MIMO ISI channel with arbitrary small probability of error.

Finally, we analyze the situation when the MIMO ISI channel is time-varying and the channel matrix $\mathbf{H}$ is a random matrix, which will be the case for the most wireless systems. For this setup, the achievable information rate depends rather on the channel statistics than on the single channel realization. A relevant performance measure in this case is the outage mutual information, which defines the maximum information rate R at which communication is possible with error probability no higher than P_{out} [BPS98]: $C^{\text{MIMO}}_{\text{out}}(P_{\text{out}}) \equiv \Big\{R\Big|\text{Prob}(I(\mathbf{d},\mathbf{r}) < R) \leq P_{\text{out}}\Big\}$. The error or outage probability P_{out} is also as a lower bound on the achievable pairwise codeword error probability when communicating with information rate R [CTB99].

Furthermore, whenever the fading statistics of the channel are revealed within one transmit frame, such that the long-term ergodic properties of the channel can be observed, we use the ergodic mutual information to characterize the maximum information rate $R = C^{\text{MIMO}}_{\text{erg}} \equiv \mathbb{E}\Big[C^{\text{MIMO}}(\boldsymbol{\Xi})\Big]$ that can be transmitted over the MIMO ISI channel with vanishing probability of error.

Multi-User Systems: A communication scenario where uncoordinated multiple users send independent information to a common receiver is referred to as a multiple access channel. The set of information rate vectors $\mathbf{R} \equiv [R_1, R_2, ..., R_N]^T$ achievable for the multiple access channel with single carrier block transmission and each user having a single antenna, as it is considered in this thesis, can be derived from the mutual information and is given for the fixed frequency domain channel $\boldsymbol{\Xi} = [\boldsymbol{\Xi}_1, \boldsymbol{\Xi}_2, ..., \boldsymbol{\Xi}_N]$ and the fixed power allocation policy $\mathbf{p} = [\mathbf{p}_1^T, \mathbf{p}_2^T, ..., \mathbf{p}_N^T]^T$, $\mathbf{p}_n = [p_{0,n}, p_{1,n}, ..., p_{Q-1,n}]^T$, $\forall n$ by [CV93], [TH98]

$$\mathcal{C}^{\text{MAC}}\Big(\boldsymbol{\Xi}, \mathbf{p}\Big) = \Bigg\{\mathbf{R}\Bigg| \sum_{n\in\mathcal{I}} R_n \leq Q^{-1} \log_2 \det\left(\mathbf{I} + \rho_{\text{SNR}} \sum_{n\in\mathcal{I}} \boldsymbol{\Xi}_n \mathbf{Q}_n(\mathbf{p}_n) \boldsymbol{\Xi}_n^H\right), \forall \mathcal{I} \subseteq \{1, 2, ..., N\}\Bigg\}, \tag{2.66}$$

where $\mathcal{I}$ is any subset of users in $\{1, 2, ..., N\}$ and $\mathbf{Q}_n(\mathbf{p}_n)$ is the covariance matrix of the nth user's transmit symbol vector $\mathbf{d}_n(k)$, defined by $\mathbf{Q}_n(\mathbf{p}_n) \equiv \mathbb{E}[\mathbf{d}_n(k)\mathbf{d}_n^H(k)] = \text{diag}(\mathbf{p}_n)$ with $\text{Trace}(\mathbf{p}_n) \leq P_n$ for all n. It is well known that the rate region in (2.66)

is convex and has precisely $N!$ boundary points, each achievable with Gaussian input distributions and a successive decoding strategy [TH98]. In the case of an $N = 2$ multiuser system, the rate region in (2.66) reduces to a simple pentagon which is constrained by the mutual information achieved by each user as well as the sum mutual information. When all transmitters know the current state of the channels, this knowledge can be used to find the optimal input distribution of each user to maximize the sum rate. For this scenario, the achievable rate region is given by the convex set [GT06]

$$\mathcal{C}^{\text{MAC}}\big(\boldsymbol{\Xi}\big) = \bigcup_{\mathbf{p}_n:\text{Trace}(\mathbf{p}_n)\leq P_n,\forall n} \mathcal{C}^{\text{MAC}}\big(\boldsymbol{\Xi},\mathbf{p}\big),$$

whose boundary points can be achieved by multiuser water-filling [YRBC04] in frequency-domain and successive decoding. In practice, the knowledge about the channel state at the transmitters is obtained from the receiver that estimates the channel and feds back the information to the N users. In this model, it is implicitly assumed that the channel is fixed or its variations can be accurately tracked and the amount of data required for the feedback link is negligible compared to the information transmitted from the N users to the receiver.

For the more general case where the frequency domain MIMO channel matrix $\boldsymbol{\Xi}$ is not fixed but random, the achievable rate region is not only a function of the SNR, but also of the channel statistics. For this scenario, we assume that the receiver has perfect knowledge about the state of the channel but the N transmitters have no such information. It means the input distributions at the transmitters can not be chosen with respect to state of the channel. Similar to the single-user case of Section 2.8.1, we distinguish for this setup two different types of rate regions. The term outage rate region is used to refer to the set of rate vectors that can be achieved with a probability of at least $1 - P_{\text{out}}$ as

$$\mathcal{C}^{\text{MAC}}_{\text{out}}(P_{\text{out}}) \equiv \Big\{\mathbf{R}\Big|\text{Prob}\Big(\mathbf{R} \notin \mathcal{C}^{\text{MAC}}\Big(\boldsymbol{\Xi},\mathbf{1}_{QN}\Big)\Big) \leq P_{\text{out}}\Big\}, \tag{2.67}$$

where $\text{Prob}\Big(\mathbf{R} \notin \mathcal{C}^{\text{MAC}}\Big(\boldsymbol{\Xi},\mathbf{1}_{QN}\Big)\Big)$ is the outage probability constraint for the rate vector $\mathbf{R}$.

Furthermore, the ergodic rate region is defined as the set of all rate vectors achieved with arbitrary small error probability, as the the number of fading blocks within each transmitted frame tends to infinity. This region with evenly allocated

transmit powers at each user can be concisely expressed as

$$\mathcal{C}_{\text{erg}}^{\text{MAC}} \equiv \Bigg\{\mathbf{R}\Big| \sum_{n\in\mathcal{I}} R_n \leq \lim_{Q\to\infty} Q^{-1}\mathbb{E}\Big[\log_2\det\Big(\mathbf{I}+\rho_{\text{SNR}}\sum_{n\in\mathcal{I}}\boldsymbol{\Xi}_n(q)\boldsymbol{\Xi}_n^H(q)\Big)\Big], \forall\mathcal{I}\subseteq\{1,...,N\}\Bigg\}. \tag{2.68}$$

Finally, we define the average information sum rate as a performance measure of the multiple access channel as

$$R_{\text{sum}}^{\text{MAC}} \equiv Q^{-1}\mathbb{E}\Bigg[\log_2\det\Bigg(\mathbf{I}+\rho_{\text{SNR}}\sum_{n=1}^{N}\boldsymbol{\Xi}_n\boldsymbol{\Xi}_n^H\Bigg)\Bigg]. \tag{2.69}$$

2.8.2. Mutual Information with Finite Constellation Size

In the previous section, we have analyzed the mutual information and capacity of single- and multiuser MIMO ISI channels employing unconstrained input symbols having Gaussian distributions. However, in practical applications, the signals to be transmitted are constrained to be from a finite constellation, such as e.g., BPSK or quaternary-PSK (QPSK) modulation. In practical applications, the mutual information and capacity with Gaussian signaling can therefore not be achieved, especially in the high SNR region. Hence, we evaluate in the following the mutual information under the constraint of input symbols taken from a finite constellation.

Consider first a transmission over a fixed single-user MIMO ISI channel with no precoding at the transmitter and independent and uniformly distributed input symbols. The input and output symbols of the channel are arranged into the vectors $\mathbf{d}(k)$ and $\mathbf{r}(k)$, $k = 1, ..., N_b$, respectively. Since the additive Gaussian noise and the input symbols are assumed to be independent, the average mutual information between the input and output sequence is given, as in (2.58), by

$$I(\mathbf{d},\mathbf{r}) = \lim_{k\to\infty}\frac{1}{kQ}\Big(h\Big(\mathbf{r}(1),\mathbf{r}(2),...,\mathbf{r}(k)\Big) - h\Big(\mathbf{n}(1),\mathbf{n}(2),...,\mathbf{n}(k)\Big)\Big) \tag{2.70}$$

As in (2.59), the differential entropy $h\Big(\mathbf{n}(1),\mathbf{n}(2),...,\mathbf{n}(k)\Big)$ of the noise can be computed in a closed-form since the covariance matrix $\mathbb{E}[\mathbf{n}(k)\mathbf{n}(k)^H]$ is known. Hence, the calculation of the mutual information reduces to the estimation of the differential entropy $h\Big(\mathbf{r}(1),\mathbf{r}(2),...,\mathbf{r}(k)\Big)$ that can be expressed as [CT91]

$$h\Big(\mathbf{r}(1),\mathbf{r}(2),...,\mathbf{r}(k)\Big) = -\mathbb{E}\Big[\log_2\Big(p(\mathbf{r})\Big)\Big], \tag{2.71}$$

where $p(\mathbf{r})$ is the joint probability of the output vector sequence $\{\mathbf{r}(1), \mathbf{r}(2), ..., \mathbf{r}(k)\}$, given by $p(\mathbf{r}) = \sum_{\mathbf{d}\in\mathcal{S}} p(\mathbf{r}|\mathbf{d})p(\mathbf{d})$ with $\mathcal{S}$ being the set of all possible values for the input vector sequence $\{\mathbf{d}(1), \mathbf{d}(2), ..., \mathbf{d}(k)\}$. Unfortunately, the differential entropy of the received vector can not be expressed in a closed-form and numerical methods have to be taken into account. In [PSS01] and [ZDK04] simulation-based techniques have been proposed to estimate $h\Big(\mathbf{r}(1), \mathbf{r}(2), ..., \mathbf{r}(k)\Big)$. The main idea is to generate a set of output received vectors $\mathbf{r}(k)$ by simulation, set up a trellis based on the MIMO channel $\mathbf{H}$ and the input vectors $\mathbf{d}(k)$, $k = 1, ..., N_b$ and then to employ the forward recursion of the BCJR algorithm [BCJR74] to estimate for the output sequence the joint probability $p(\mathbf{r})$. An estimate of $h\Big(\mathbf{r}(1), \mathbf{r}(2), ..., \mathbf{r}(k)\Big)$ is then obtained by calculating the logarithm of the joint probability estimate using a single simulation with a very large frame length [PSS01].

Instead of using the above BCJR-based estimation method, the differential entropy can also be estimated directly by Monte-Carlo integration. For this, a large number N_e of random input vectors $\mathbf{d}^{(i)}(k)$ and the corresponding output vectors $\mathbf{r}^{(i)}(k)$, $1 \le k \le N_b$, $1 \le i \le N_e$ are generated. The estimate of the differential entropy in (2.71) is then obtained as

$$h\Big(\mathbf{r}(1), \mathbf{r}(2), ..., \mathbf{r}(k)\Big) \approx -N_e^{-1} \sum_{i=1}^{N_e} \log_2 \Big(p(\mathbf{r}^{(i)})\Big). \tag{2.72}$$

We can also apply the above simulation-based techniques to the case of multiuser systems. For example, the rate region for the 2-user multiple access channel under the constraint of finite signal constellations is given by the closure of the convex hull of all rate pairs (R_1, R_2) [CT91]:

$$\mathcal{C}_{\text{con}}^{\text{MAC}} \equiv \left\{ (R_1, R_2) : \begin{array}{c} R_1 \le I(\mathbf{d}_1, \mathbf{r}|\mathbf{d}_2) \\ R_2 \le I(\mathbf{d}_2, \mathbf{r}|\mathbf{d}_1) \\ R_1 + R_2 \le I(\mathbf{d}_1, \mathbf{d}_2, \mathbf{r}) \end{array} \right\}, \tag{2.73}$$

where the mutual informations $I(\mathbf{d}_1, \mathbf{r}|\mathbf{d}_2)$, $I(\mathbf{d}_2, \mathbf{r}|\mathbf{d}_1)$ and $I(\mathbf{d}_1, \mathbf{d}_2, \mathbf{r})$ are computed by the same method as in the single-user case described above. Also, we can give expressions for the average sum rate and the outage rate region [HA04] for block-fading multiple access channels under the constraint of finite signal constellations, respectively, which are defined as

$$R_{\text{con}}^{\text{MAC}} \equiv \mathbb{E}\Big[I(\mathbf{d}_1, \mathbf{d}_2, \mathbf{r})\Big], \tag{2.74}$$

$$\mathcal{C}_{\text{con,out}}^{\text{MAC}}(P_{\text{out}}) \equiv \Big\{(R_1, R_2)\Big|\text{Prob}\Big((R_1, R_2) \notin \mathcal{C}_{\text{con}}^{\text{MAC}}\Big) \le P_{\text{out}}\Big\}. \tag{2.75}$$

2.9. Chapter Summary

We have introduced the models for coded single-user point-to-point and multiuser SIMO single-carrier signaling over the MIMO ISI channel. The considered radio channel is frequency selective due to multipath propagation. Therefore, the concept of block transmission is applied, as it allows channel equalization at the receiver employing the discrete Fourier transform. Several stochastic models for block-fading MIMO ISI channels have been discussed and the correlation properties of the frequency domain channel gains have been analyzed. The transmitter and receiver models based on turbo equalization for the coded single- and multiuser transmission setups have been introduced. We have also discussed some basic properties of LLRs constituting the basis of any iterative decoding scheme. Finally, several analytical expressions for the mutual information and capacity of single- and multiuser transmissions under several constraints have been derived.

3. Turbo Equalization for MIMO Systems

In this chapter, we discuss the design of several turbo receivers which are the core part of the investigated communication systems of this work. In the presence of ISI caused by channel multipath propagation, the main component of an iterative receiver is the soft-in soft-out channel equalizer that performs symbol estimation on the transmitted data by utilizing the received data and probabilistic information fed back from channel decoding. A great variety of soft-in soft-out channel equalization schemes exist in the literature for the application in iterative receivers. Among them are trellis-based equalization methods, soft-list soft-sphere decoding approaches and soft interference cancellation (SIC) and linear filtering concepts. The latter present an important class of low-complexity equalizers which can almost preserve the performance of the optimum MAP trellis-based equalizer in MIMO ISI channels. Due to the very good complexity/performance trade-offs of such equalizers, we set the main focus in this chapter on SIC-based channel equalization.

The remainder of this chapter is organized as follows. In Section 3.1, we review the optimum soft-in soft-out MAP equalization algorithm, originally employed in the context of trellis-based turbo equalization in [DJB+95]. Other suboptimal approaches of turbo equalization, offering much lower computational complexities than the optimal approach are summarized as well. In the following Section 3.2, we discuss channel equalization based on SIC combined with linear filtering. Thereby, we distinguish between three commonly used filter types: the time-domain MMSE filter, the channel matched filter (MF), and the combined MMSE/MF filter. Since these filters process the signals in time-domain, their computational complexities depend directly on the channel memory-length. Of course, this restricts their application in practical systems. A frequency-domain MMSE turbo equalizer is derived in Section 3.3. Compared to systems with time-domain equalization, this method drastically reduces the computational cost of channel equalization. In addition, the equalizer is robust to variations of the channel delay spread. In Section 3.4, we devise a novel turbo equalizer in the framework of nonlinear MMSE estimation. The SNR at the output of the equalizer is analyzed compared to the SNR of the standard SC-MMSE turbo equalizer. It is known that MMSE-based turbo equalizers

exhibit a serious performance degradation in spatially-correlated MIMO ISI fading channels. To overcome this drawback, we propose in Section 3.5 a novel frequency domain turbo technique that is robust against channel spatial correlation by combining groupwise SC-MMSE filtering [VMJ04], [GM07] with optimal MAP detection. The computational complexities and performances of the proposed schemes are evaluated in Section 3.6 and Section 3.7, respectively. Finally, Section 3.8 summarizes the main results of this chapter.

3.1. Maximum A Posteriori Equalization

In order to start with the description of equalization techniques, we review in the following the optimal symbol-wise SfISfO MAP equalizer, first proposed in the context of turbo equalization by Douillard *et. al.* in [DJB+95].

Let us consider a coded single-user MIMO or multiuser SIMO transmission scheme where a number of coded data symbols, arranged in a QN-length vector $\mathbf{b}$, are transmitted over N transmit antennas. At the receiver the data from M receive antennas is collected in a QM-length vector $\mathbf{r}$ and further processed by the equalizer. Note that for the following derivations in this chapter, we drop the block-index k from all data vectors for notational simplicity.

Choosing the symbol-wise SfISfO MAP estimator (the so-called *a posteriori* probability (APP) detector) as equalization algorithm, the LLR-valued *a posteriori* information of the coded BPSK-symbol $b_{q,n}$ from the n-th transmit antenna at the q-th signaling instant is given by (see also (2.38))

$$\theta\Big[b_{q,n}\Big] = \log\left(\frac{\mathrm{Prob}\Big(b_{q,n}=+1|\mathbf{r},\mathbf{H}_c\Big)}{\mathrm{Prob}\Big(b_{q,n}=-1|\mathbf{r},\mathbf{H}_c\Big)}\right), \tag{3.1}$$

where the conditional symbol probabilities are defined by

$$\mathrm{Prob}\Big(b_{q,n}=c|\mathbf{r},\mathbf{H}_c\Big) = \sum_{\mathbf{x}\in\mathcal{X}_{q,n}^{<c>}} \mathrm{Prob}\Big(\mathbf{b}=\mathbf{x}|\mathbf{r},\mathbf{H}_c\Big), c\in\{-1,+1\}. \tag{3.2}$$

Here, $\mathcal{X}_{q,n}^{<c>} = \{\mathbf{x}\,\big|\mathbf{x}=[x_{0,1},...,x_{q-1,n},c,x_{q+1,n},...,x_{Q-1,N}]^T\in\{+1,-1\}^{QN}\}$ denotes the set of 2^{QN} BPSK-symbols $\mathbf{x}\in\mathcal{X}_{n,q}^{<c>}$ for which $x_{q,n}=c$. Inserting (3.2) into (3.1) and applying Bayes' theorem, the *a-posterori* LLR on the coded BPSK-symbol reads as

$$\theta\Big[b_{q,n}\Big] = \log\left(\frac{\sum_{\mathbf{x}\in\mathcal{X}_{q,n}^{<+1>}} p\Big(\mathbf{r}|\mathbf{b}=\mathbf{x},\mathbf{H}_c\Big)\mathrm{Prob}(\mathbf{b}=\mathbf{x})}{\sum_{\mathbf{x}\in\mathcal{X}_{q,n}^{<-1>}} p\Big(\mathbf{r}|\mathbf{b}=\mathbf{x},\mathbf{H}_c\Big)\mathrm{Prob}(\mathbf{b}=\mathbf{x})}\right), \tag{3.3}$$

where the probability term $\text{Prob}(\mathbf{b} = \mathbf{x})$ represents an *a priori* knowledge on the vector $\mathbf{b}$, provided in the form of the bit-wise *extrinsic* LLRs on the coded bits from outer channel decoding. The probability density function of the received signal $\mathbf{r}$ conditioned on the transmitted symbol vector $\mathbf{b}$ and the overall MIMO channel matrix $\mathbf{H}_c$ (see Section 2.7) in (3.3) can be obtained from the multivariate complex-valued Gaussian distribution:

$$p\Big(\mathbf{r}|\mathbf{b} = \mathbf{x}, \mathbf{H}_c\Big) = \frac{1}{(\pi\sigma_0^2)^{MQ}} \exp\Big[-\frac{1}{\sigma_0^2}(\mathbf{r} - \mathbf{H}_c\mathbf{x})^H(\mathbf{r} - \mathbf{H}_c\mathbf{x})\Big]. \tag{3.4}$$

To simplify the calculation of the LLR in (3.3), we introduce the following assumption:

Assumption 3.1. All interleavers of the coded system ensure perfect statistical independence between the interleaved coded bits.

Assumption 3.1 implies infinite random interleaving and infinite codeword (frame) lengths. We remark that in practice, this is also well satisfied for finite, but large codeword lengths. Hence, the probability $\text{Prob}(\mathbf{b} = \mathbf{x})$ in (3.3) can be written as

$$\text{Prob}(\mathbf{b} = \mathbf{x}) = \prod_{q=0}^{Q-1} \prod_{n=1}^{N} \text{Prob}\Big(b_{q,n} = x_{q,n}\Big). \tag{3.5}$$

Substituting (3.5) and (3.4) into (3.3), and dividing the nominator and denominator by the term $\prod_{q=0}^{Q-1} \prod_{n=1}^{N} \text{Prob}\Big(b_{q,n} = -1\Big)$, we finally obtain

$$\theta\Big[b_{q,n}\Big] = \underbrace{\log\left(\frac{\sum_{\mathbf{x}\in\mathcal{X}_{q,n}^{<+1>}} \exp\Big[-\frac{1}{\sigma_0^2}\left\|\mathbf{r} - \mathbf{H}_c\mathbf{x}\right\|^2 + \sum_{(l,u)\in\mathcal{A}_{q,n}} \zeta[b_{l,u}]\Big]}{\sum_{\mathbf{x}\in\mathcal{X}_{q,n}^{<-1>}} \exp\Big[-\frac{1}{\sigma_0^2}\left\|\mathbf{r} - \mathbf{H}_c\mathbf{x}\right\|^2 + \sum_{(l,u)\in\mathcal{A}_{q,n}} \zeta[b_{l,u}]\Big]}\right)}_{\lambda_e[b_{q,n}]}$$
$$+ \underbrace{\log\left(\frac{\text{Prob}(b_{q,n} = +1)}{\text{Prob}(b_{q,n} = -1)}\right)}_{\zeta_e[b_{q,n}]}, \tag{3.6}$$

where the set $\mathcal{A}_{q,n}$ is defined by

$$\mathcal{A}_{q,n} \equiv \Big\{(l,u)|l = 0, ..., Q-1, u = 1, ..., N, x_{l,u} = +1, (l,u) \neq (q,n)\Big\},$$

and $\zeta_e[b_{q,n}]$ and $\lambda_e[b_{q,n}]$ again denote *a priori* and *extrinsic* LLRs on the code bit $b_{q,n}$, respectively. Equation (3.6) can be very efficiently calculated by the BCJR algorithm, exploiting the Markovian structure of the MIMO ISI channel. This algorithm works jointly on the trellis diagrams of the ISI channels of all users. Although this

equalization scheme is optimal with respect to the error performance of the receiver, its complexity which is directly related to the number of states of the channel and the system configuration, grows exponentially with the product of the number of transmit antennas N and the effective channel memory length L. The application of the optimum MAP estimation in practical transmissions systems is therefore strongly limited, even for systems having only a moderate number of transmit antennas and for channels with only a few multipath components.

Several SfISfO algorithms for equalization and detection have been proposed in recent years, all of them with the aim to approximately solve (3.6) at a reasonable complexity (however, at the cost of decreased performance). Some of the available schemes are trying to reduce the complexity by excluding possible transmitted symbol sequences from the search space of (3.6) that have a low likelihood. In this context, the soft-list sphere detector of [BGBF03] (see also [HtB03] and [SB10] for improvements and variations thereof), reduces the search space by considering only the transmit symbol vector candidates for which the corresponding (noiseless) receive signals lie in a hypersphere of given radius around the received signal. Although, as shown in [HtB03], the list sphere detector can achieve very close-to-optimal performance (provided that the search radius is large enough), its worst-case complexity is still exponential in $N \times L$. A semi definite relaxation-based detection principle that yields similar performance to that of the sphere detector with polynomial rather than exponential worst-case complexity has been presented in [SLW03]. Other works have attempted to tackle the detection problem by resorting to list-sequential algorithms [TR02], [BHW03], [HK07] or iterative tree search schemes [JW05], [KC09], or to algorithms employing massive trellis-state reduction techniques [EQ88], [VB03]. These methods have in common that soft-probabilistic information fed back from channel decoding is used to reduce the search space. Some other available works have concentrated on signal preprocessing methods to reshape the MIMO ISI channel with the aim to reduce its impulse response to a shorter length [AD01], [MDEJ03]. However, for MIMO systems with a large number of antennas/users and/or signal sets, the number of transitions per trellis state is still very large; reducing the length of the channel response alone is thus not sufficient to reduce complexity.

Another promising approach attractive for SfISfO equalization of MIMO ISI channels are iterative-based SIC schemes combined with linear filtering (see, e.g., [WP99a], [TSK02], [TH02], [GM08], [AM03], [KM07], [AJL07], [KSMT05], [WP99b], [LP04], [GM07], [YGWP08] and [JPSL04]). The main idea of these schemes is to decompose the optimum scheme (3.6) into several "smaller" detection problems with reduced dimension that can be solved independently. Compared to trellis-based approaches or to sphere decoding, the major advantage of turbo equalization employing SIC is that it can achieve in many cases a very close-to-optimal performance at polynomial

(at most cubic) complexity. Because of these merits, we restrict ourselves in the following sections to SIC-based turbo equalization concepts.

3.2. SC-MMSE Time Domain Equalization

In this section, we discuss the soft interference cancellation linear MMSE equalization schemes, which is one of the most popular concepts in the literature. The basic idea of this approach is to utilize the probabilistic information fed back from channel decoding to calculate a soft estimate of the interference components and to subtract it from the received signal. A successive linear MMSE filter is applied for filtering of the residual signal to further suppress the residual interference components. Here, the term "linear" means that the filtering itself is a linear operation with respect to the filter-input signal; the whole equalizer itself is nonlinear, though. Based on the filter output signal, a soft symbol de-mapper then calculates the bit-*extrinsic* LLR information on the code bits.

For the description of the algorithm, let us focus on the equalization of a single block $\mathbf{b}$ comprising QN BPSK symbols. In a first step the SC-MMSE algorithm uses the available *a priori* information $\boldsymbol{\zeta}_e[\mathbf{b}]$ on the code symbols provided by channel decoding to compute the first two moments of each transmitted symbol $b_{q,n}$. Let us denote by $\bar{\mathbf{b}} = \mathbb{E}\big[\mathbf{b}|\boldsymbol{\zeta}_e[\mathbf{b}]\big]$ and $\boldsymbol{\Lambda} \equiv \mathrm{Cov}\big[\mathbf{b},\mathbf{b}|\boldsymbol{\zeta}_e[\mathbf{b}]\big]$ the mean vector and the covariance matrix of $\mathbf{b}$, respectively. Under Assumption 3.1, the entries of vector $\bar{\mathbf{b}} = [\bar{b}_{0,1}, \bar{b}_{1,1}, ..., \bar{b}_{q,n}, ..., \bar{b}_{Q-1,N}]^T$ can be expressed by the conditional mean as

$$\bar{b}_{q,n} = \mathbb{E}\big[b_{q,n}|\zeta_e[b_{q,n}]\big] = \sum_{c\in\{+1,-1\}} \frac{c}{1+e^{-c\zeta_e[b_{q,n}]}} = \tanh\Big(\frac{1}{2}\zeta_e[b_{q,n}]\Big), \forall q,n. \tag{3.7}$$

Similarly to (3.7), the conditional covariance of the transmit symbols is given by

$$\mathrm{Cov}\big[b_{q,n}, b_{r,l}|\boldsymbol{\zeta}_e[\mathbf{b}]\big] = \begin{cases} 1-\bar{b}_{q,n}^2 \text{ for } (q,n)=(r,l) \\ 0 \text{ otherwise} \end{cases}. \tag{3.8}$$

Note that due to (3.8), $\boldsymbol{\Lambda}$ is a diagonal matrix, defined by

$$\begin{aligned} \boldsymbol{\Lambda} &\equiv \mathrm{diag}\Big(\mathrm{diag}(\boldsymbol{\Lambda}_1), ..., \mathrm{diag}(\boldsymbol{\Lambda}_n), ..., \mathrm{diag}(\boldsymbol{\Lambda}_N)\Big) \\ \boldsymbol{\Lambda}_n &\equiv \mathrm{diag}\Big(1-\bar{b}_{0,n}^2, ..., 1-\bar{b}_{q,n}^2, ..., 1-\bar{b}_{Q-1,n}^2\Big), \text{ for all } n=1,...,N. \end{aligned}$$

Further note when no *a priori* information about the code bits is available, which is typically in the first turbo iteration, the symbol mean vector $\bar{\mathbf{b}}$ and the covariance matrix $\boldsymbol{\Lambda}$ are given by the all-zero vector and the identity matrix, respectively. On

the other hand, when perfect *a priori* information about the code bits is available, then $|\zeta_e[b_{q,n}]| \to \infty$, $\forall q, n$, and $\bar{\mathbf{b}} \approx \mathbf{b}$ and $\mathbf{\Lambda} \approx 0 \cdot \mathbf{I}_{QN}$.

The first two moments on the transmit symbol vector $\mathbf{b}$ are used in the soft cancellation of the interference components from the received symbol vector $\mathbf{r}$, followed by a linear MMSE filtering stage removing residual interferences, to compute an estimate $z_{q,n}$ for each symbol $b_{q,n}$, as

$$z_{q,n} = \mathbf{w}_{q,n}^H \Big(\mathbf{r} - \bar{\mathbf{r}} + \mathbf{H}_c \mathbf{e}_{w(q,n)} \bar{b}_{q,n} \Big), \tag{3.9}$$

where $\mathbf{w}_{q,n}$ and $\bar{\mathbf{r}} = \mathbf{H}_c \bar{\mathbf{b}}$ designate the linear MMSE filter coefficient vector and the estimate of the received signal, respectively. The vector $\mathbf{e}_{w(q,n)}$ in (3.9) denotes the all-zero vector with entry $w(q,n) = (n-1)Q + q + 1$ being one. A typical choice for $\mathbf{w}_{q,n}$ is the linear conditional MMSE filter. This filtering approach has been presented originally by Wang *et. al.* in the context of multiuser detection for CDMA systems in [WP99a], and applied by Tüchler *et. al.* for channel equalization in [TSK02], and by Abe *et al.* for MIMO channel equalization in [AM03]. The linear filter is derived to minimize the conditional MSE between the symbol $b_{q,n}$ and the filter output symbol $z_{q,n}$,

$$\mathbb{E}\Big[\, |b_{q,n} - z_{q,n}|^2 \Big| \, \boldsymbol{\zeta}_e[\mathbf{b}] \Big], \tag{3.10}$$

and it is explicitly given by [WP99a], [AM03]

$$\mathbf{w}_{q,n} = \Big[\mathbf{H}_c \mathbf{\Lambda} \mathbf{H}_c^H + \sigma_0^2 \mathbf{I} - \bar{b}_{q,n}^2 \mathbf{H}_c \mathbf{e}_{w(q,n)} \mathbf{e}_{w(q,n)}^H \mathbf{H}_c^H \Big]^{-1} \mathbf{H}_c \mathbf{e}_{w(q,n)}. \tag{3.11}$$

The matrix $\Big[\mathbf{H}_c \mathbf{\Lambda} \mathbf{H}_c^H + \sigma_0^2 \mathbf{I} - \bar{b}_{q,n}^2 \mathbf{H}_c \mathbf{e}_{w(q,n)} \mathbf{e}_{w(q,n)}^H \mathbf{H}_c^H \Big]$ is positive definite, whose eigenvalues are upper bounded by σ_0^2. It is therefore invertible for all possible choices of the channel matrix $\mathbf{H}_c$, so far $\sigma_0^2 > 0$ which is typically satisfied in practical systems. Applying the matrix inversion lemma to (3.11), and writing the filter output signals corresponding to the transmitted symbol block from antenna n, $\mathbf{b}_n$ in matrix-vector notation, we obtain the well known result [SGT04], [Kan05]

$$\begin{aligned} \mathbf{z}_n &\equiv [z_{0,n}, z_{1,n}, ..., z_{Q-1,n}]^T, n = 1, ..., N \\ &= \mathbf{\Theta}_n^{\text{TD}} \mathbf{H}_{c,n}^H \mathbf{\Sigma}^{\text{TD}-1} (\mathbf{r} - \bar{\mathbf{r}}) + \mathbf{\Theta}_n^{\text{TD}} \mathbf{\Upsilon}_n^{\text{TD}} \bar{\mathbf{b}}_n, \end{aligned} \tag{3.12}$$

where $\bar{\mathbf{b}}_n = [\bar{b}_{0,n}, \bar{b}_{1,n}, ..., \bar{b}_{Q-1,n}]^T$, $\mathbf{\Upsilon}_n^{\text{TD}} \equiv \text{ddiag}\{\mathbf{H}_{c,n}^H \mathbf{\Sigma}^{\text{TD}-1} \mathbf{H}_{c,n}\}$ and

$$\mathbf{\Sigma}^{\text{TD}} \equiv \Big[\mathbf{H}_c \mathbf{\Lambda} \mathbf{H}_c^H + \sigma_0^2 \mathbf{I}_{QM} \Big], \tag{3.13}$$

$$\mathbf{\Theta}_n^{\text{TD}} \equiv \Big(\mathbf{I}_Q + \mathbf{\Upsilon}_n^{\text{TD}} (\mathbf{I}_Q - \mathbf{\Lambda}_n) \Big)^{-1}. \tag{3.14}$$

One readily verifies from (3.12) that for $\boldsymbol{\zeta}_e[\mathbf{b}] = \mathbf{0}$ (no *a priori* information) and $|\boldsymbol{\zeta}_e[\mathbf{b}]| = c \cdot \mathbf{1}$, where $c \to \infty$ (perfect *a priori* information), the above equalizer becomes equivalent to the classical block-based MMSE linear equalizer [Qur85] and to the ideal MMSE-based interference canceler [GL81], respectively. The SC-MMSE equalizer presents thus a flexible structure that adapts the equalization strategy with respect to the available *a priori* information about the code bits.

However, a serious drawback of the above scheme is the calculation of the conditional MMSE filter that has to be performed once per transmit block and turbo iteration. This calculation involves the inversion of the covariance matrix $\boldsymbol{\Sigma}^{\text{TD}}$ of the residual signal $\mathbf{r} - \bar{\mathbf{r}}$ in (3.13) with dimension $QM \times QM$. Due to the presence of matrix $\boldsymbol{\Lambda}$ in (3.13), $\boldsymbol{\Sigma}^{\text{TD}}$ is not block circulant despite the CP operations. The matrix inversion is therefore computationally demanding and requires at least $O(M^3Q^3)$ computations. One suitable method to reduce its complexity with only a marginal performance loss is to apply the so-called sliding window filtering approach [WP99a], [AM03]. That is, instead of using the whole received symbol vector $\mathbf{r}$ for detection of symbol $b_{q,n}$, only the L received samples from the M receive antennas directly affected by $b_{q,n}$ are used in the MMSE filtering. In this way, the number of filter coefficients is reduced from QM to LM per transmitted symbol. Moreover, due to the structured nature of the (sliding window) covariance matrix of the residual signal at the output of the soft canceler, one can also adopt recursive algorithms (see e.g., [TSK02], [KM03], [LP04], [JPSL04]) for the calculation of the matrix inverse. Such schemes utilize in most cases the Cholesky factorization and exploit the structural similarities between subsequent matrices. The complexity is predominantly of order $O(L^2M^2)$ and directly depends on the channel memory length L. Therefore, we refer to the sliding window SC-MMSE filtering methods as well as to the direct implemenation of (3.12) as SC-MMSE time domain equalizer (SC-MMSE TDE) .

3.2.1. Equivalent AWGN Channel Assumption and LLR Computation

To derive the *extrinsic* LLR at the output of the equalizer, we decompose (3.12) into two terms:

$$\mathbf{z}_n = \boldsymbol{\Theta}_n^{\text{TD}} \boldsymbol{\Upsilon}_n^{\text{TD}} \mathbf{b}_n + \boldsymbol{\nu}_n, \tag{3.15}$$

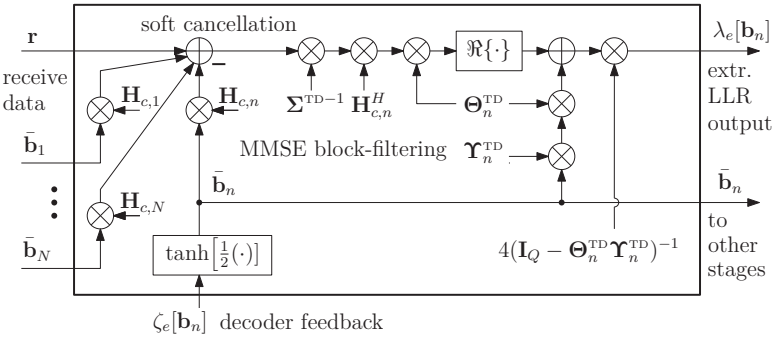

Figure 3.1.: Signal flow chart of the SC-MMSE TDE for the nth data stream.

where vector

$$\begin{aligned}\boldsymbol{\nu}_n &\equiv [\nu_{0,n}, \nu_{1,n}, ..., \nu_{Q-1,n}]^T \\ &= \boldsymbol{\Theta}_n^{\text{TD}}\Big(\Big(\mathbf{H}_{c,n}^H\boldsymbol{\Sigma}^{\text{TD}-1}\mathbf{H}_{c,n} - \boldsymbol{\Upsilon}_n^{\text{TD}}\Big)(\mathbf{b}_n - \bar{\mathbf{b}}_n) + \mathbf{H}_{c,n}^H\boldsymbol{\Sigma}^{\text{TD}-1}\Big(\sum_{l\neq n}\mathbf{H}_{c,l}(\mathbf{b}_l - \bar{\mathbf{b}}_l) + \mathbf{n}\Big)\Big)\end{aligned}$$

is the contribution of the filtered residual interference components and channel noise.

Assumption 3.2. The (q,n)-th component of the filter output (3.15) can be written in the form $z_{q,n} = \mu_{q,n}b_{q,n} + \nu_{q,n}$, where $\mu_{q,n}$ denotes an equivalent channel gain, and $\nu_{q,n}$, modeling the residual interference and channel noise, is circularly-symmetric Gaussian distributed with probability density function $\mathcal{CN}(0, \sigma_{\nu,q,n}^2)$.

Assumption 3.2 is widely known as the equivalent AWGN channel assumption (see, e.g., [PV97]) which approximates the residual interference signal and channel noise at the equalizer output as Gaussian distributed. It is straightforward to show that the equivalent channel gain $\mu_{q,n}$ and noise variance $\sigma_{\nu,q,n}^2$ can be solved to

$$\mu_{q,n} = \mathbf{e}_q^T\boldsymbol{\Theta}_n^{\text{TD}}\boldsymbol{\Upsilon}_n^{\text{TD}}\mathbf{e}_q, \tag{3.16}$$

$$\sigma_{\nu,q,n}^2 = \mathbf{e}_q^T\boldsymbol{\Theta}_n^{\text{TD}}\boldsymbol{\Upsilon}_n^{\text{TD}}\Big(\mathbf{I}_Q - \boldsymbol{\Theta}_n^{\text{TD}}\boldsymbol{\Upsilon}_n^{\text{TD}}\Big)\mathbf{e}_q. \tag{3.17}$$

Given the filter output signals (3.12), the *extrinsic* LLR for each code bit can now be expressed as

$$\lambda_e\Big[b_{q,n}\Big] = \log\Bigg(\frac{p\Big(z_{q,n}|b_{q,n}=+1\Big)}{p\Big(z_{q,n}|b_{q,n}=-1\Big)}\Bigg), \tag{3.18}$$

where the conditional PDFs $p\Big(z_{q,n}|b_{q,n}=c\Big)$, $c\in\{-1,+1\}$ are given under Assump-

tion 3.2 by $p\big(z_{q,n}|b_{q,n}=c\big) \sim \mathcal{CN}(\mu_{q,n}c, \sigma^2_{\nu,q,n})$. Using (3.16) and (3.17), the LLRs in Eqn. (3.18) can be written in vector-notation as

$$\lambda_e\Big[\mathbf{b}_n\Big] = 4(\mathbf{I}_Q - \mathbf{\Theta}_n^{\text{TD}}\mathbf{\Upsilon}_n^{\text{TD}})^{-1}\Re\{\mathbf{z}_n\}, \forall n. \tag{3.19}$$

The *extrinsic* LLR sequences $\lambda_e\Big[\mathbf{b}_n\Big]$ in (3.19) are forwarded via the bit-interleavers to the channel decoders and serve there in the next turbo iteration as *a priori* information about the code bits. The resulting SC-MMSE TDE implementing (3.19) is depicted in Fig. 3.1.

3.2.2. Matched Filter Approximation and Advanced Techniques

The computational complexity of the SC-MMSE approach is dominated by matrix inversions, whose dimensions directly depend on the channel memory length and the number of receive antennas. For channels with a large delay spread, or system setups with a large number of receive antennas, the calculation of these inverses is still computationally expensive. Therefore, several attempts have been made toward reducing the computational complexity of the SC-MMSE TDE by means of a simplified filtering [GLL97], [BDU06], [JLA08b], [JLA08a].

In [GLL97], a low complexity equalizer was proposed that replaces the MMSE filter (3.12) with the low-complexity channel matched filter MF, i.e., $\mathbf{w}_{q,n} = \mathbf{H}_c\mathbf{e}_{w(q,n)}$, $\forall q, n$, resulting in the following filter-output equation:

$$\mathbf{z}_n = \mathbf{H}_{c,n}^H(\mathbf{r} - \bar{\mathbf{r}}) + \mathbf{M}_n\bar{\mathbf{b}}_n, n = 1, ..., N, \tag{3.20}$$

where $\mathbf{M}_n \equiv \text{ddiag}\{\mathbf{H}_{c,n}^H\mathbf{H}_{c,n}\}$ denotes the equivalent channel matrix after the channel MF. Since no matrix inversion is involved, the complexity of (3.20) is mainly determined by simple matrix-vector multiplications and thus of order $O(NQL^2)$ per transmit block and turbo iteration. The MF-filtering idea proposed in [GLL97] has been combined with SC-MMSE filtering through switching in [OAM01] and [TH02]. The idea of these papers is to use the SC-MMSE filter, that provides a large gain for equalization in terms of reduced bit error rate, only in the first turbo iterations. It can be expected that when *a priori* information fed back from channel decoding is sufficient reliable, which is typically after few turbo iterations, the simple MF-filtering is satisfactory for equalization to improve performance. It was demonstrated that such a combined SC-MMSE/MF TDE utilizing a powerful error correcting code can nearly achieve the performance of the pure SC-MMSE TDE in channels with large multipath diversity.

Alternatively, approximate MMSE filtering solutions employing a finite sum of weighted matrix polynomials and a truncated Taylor series expansion to approxi-

mate the matrix inversion has been proposed in [BDU06] and [JLA08b], [JLA08a]. The coefficients of the finite series are chosen to optimize a system performance criterion. Depending on the number of terms involved in the series expansion, the resulting equalizer can be scaled from the simple MF equalizer to the complex SC-MMSE TDE with direct matrix inversion. In particular, by taking advantage of soft feedback from channel decoding, the authors showed that the performance loss due to the polynomial/Taylor-series approximation is negligible after few iterations.

3.3. SC-MMSE Frequency Domain Equalization

A further reduction in complexity of the SC-MMSE TDE is obtained by exploiting the circulant property of the channel matrix (see (2.14)) and performing the MMSE filtering part in the frequency domain. In particular, an SC-MMSE frequency domain equalizer (FDE) performs the fast Fourier transform (FFT), the soft interference cancellation and the single-tap filtering followed by an inverse FFT (IFFT) on the receive data. This solution has been first suggested for single-user SISO turbo equalization by Tüchler *et. al.* in [TSK02], and later extended to multi-user MIMO turbo equalization by Kansanen *et. al.* in [KM07]. In these papers, the algorithms were derived by transforming the time domain conditional MMSE filter output signal in (3.9) directly into the frequency domain. Moreover, the authors introduced a couple of approximations to reduce the complexity of matrix inversions, involved in the computation of the frequency domain MMSE filter. In this section, we present a new derivation by utilizing the unconditional filter approximation [CMT04], and by deriving the linear MMSE equation in the frequency domain. It will be shown that the resulting equalizer is equivalent to the SC-MMSE FDE from [KM07].

Let us start by writing the linear filter output in (3.9) in matrix-vector notation as

$$\mathbf{z}_n = \mathbf{O}_n^H\left(\mathbf{r} - \bar{\mathbf{r}}\right) + \mathbf{\Phi}_n\bar{\mathbf{b}}_n, n = 1, ..., N, \tag{3.21}$$

where $\mathbf{O}_n \equiv [\mathbf{O}_{n,1}^H, ..., \mathbf{O}_{n,m}^H, ..., \mathbf{O}_{n,M}^H]^H \in \mathbb{C}^{QM\times Q}$, $\mathbf{O}_{n,m} \in \mathcal{C}^{Q\times Q}$ is the block-filtering matrix for the nth transmit data stream, and $\mathbf{\Phi}_n \in \mathbb{C}^{Q\times Q}$ is an equivalent channel matrix after filtering, defined as

$$\mathbf{\Phi}_n \equiv \text{ddiag}\{\mathbf{O}_n^H\mathbf{H}_{c,n}\}. \tag{3.22}$$

Assumption 3.3. For an efficient frequency domain implementation of the linear filtering equation (3.21), the filtering matrices $\mathbf{O}_n$, $n = 1, ..., N$ are constrained to be block-circulant.

Under Assumption 3.3, the eigen-decomposition of the block-filtering matrix $\mathbf{O}_n$ can be written by $\mathbf{O}_n = \mathbf{F}_M^H \mathbf{\Gamma}_n \mathbf{F}$, where $\mathbf{\Gamma}_n \equiv [\mathbf{\Gamma}_{n,1}^H, ..., \mathbf{\Gamma}_{n,m}^H, ..., \mathbf{\Gamma}_{n,M}^H]^H \in \mathbb{C}^{QM \times Q}$, $\mathbf{\Gamma}_{n,m} \in \mathbb{C}^{Q \times Q}$ is the block-diagonal frequency domain filtering matrix. Here, the entry $[\mathbf{\Gamma}_{n,m}]_{q,q}$ of the diagonal matrix $\mathbf{\Gamma}_{n,m}$ denotes the filter coefficient at the qth frequency-bin for transmit/receive antenna pair (n, m). Applying the block-filter decomposition together with the channel matrix decomposition (2.14) to (3.22), the equivalent channel matrix $\mathbf{\Phi}_n$ can be rewritten as a diagonal matrix with constant entries $\bar{\mu}_n \equiv Q^{-1}\text{Trace}(\mathbf{\Gamma}_n^H \mathbf{\Xi}_{c,n})$, i.e.,

$$\begin{aligned} \mathbf{\Phi}_n &= \text{ddiag}(\mathbf{F}^H \mathbf{\Gamma}_n^H \mathbf{\Xi}_{c,n} \mathbf{F}) \\ &= \bar{\mu}_n \mathbf{I}_Q. \end{aligned} \tag{3.23}$$

As a consequence of (3.23), the frequency domain representation of the filter output signal in (3.21) is found to

$$\begin{aligned} \underline{\mathbf{z}}_n &\equiv \mathbf{F}\mathbf{z}_n \\ &= \mathbf{\Gamma}_n^H \left(\underline{\mathbf{r}} - \bar{\underline{\mathbf{r}}} \right) + \bar{\mu}_n \bar{\underline{\mathbf{b}}}_n, \end{aligned} \tag{3.24}$$

where we have used the following definitions: $\underline{\mathbf{r}} \equiv \mathbf{F}_M \mathbf{r}$, $\bar{\underline{\mathbf{r}}} \equiv \mathbf{F}_M \bar{\mathbf{r}}$ and $\bar{\underline{\mathbf{b}}}_n \equiv \mathbf{F}\bar{\mathbf{b}}_n$. In order to avoid the complexity impairments of the SC-MMSE TDE, we use the so-called unconditional MSE [CMT04], instead of the conditional MSE in (3.10), as a design criterion for the block-diagonal filtering matrix $\mathbf{\Gamma}_n$ in (3.24). The unconditional MSE between the frequency domain version of the transmit signal vector $\underline{\mathbf{b}}_n \equiv \mathbf{F}\mathbf{b}_n$ and the filter output signal $\underline{\mathbf{z}}_n$ can be expressed as

$$\text{MSE}_n^{\text{FD}} \equiv Q^{-1}\mathbb{E}\left[\|\underline{\mathbf{z}}_n - \bar{\mu}_n \underline{\mathbf{b}}_n\|^2 \right]. \tag{3.25}$$

Using the well known relations about expectations (see, e.g., [PP02]),

$$\begin{aligned} \mathbb{E}\left[\bar{\mathbf{b}}_n \mathbf{b}_n^T\right] &= \mathbb{E}\left[\mathbb{E}\left[\bar{\mathbf{b}}_n \mathbf{b}_n^T | \zeta_e[\mathbf{b}_n]\right]\right] \\ &= \mathbb{E}\left[\bar{\mathbf{b}}_n \bar{\mathbf{b}}_n^T\right], \end{aligned} \tag{3.26}$$

the MSE in (3.25) can be written with the help of Assumption 3.1 as

$$\begin{aligned} \text{MSE}_n^{\text{FD}} &= Q^{-1}\text{Trace}\Big(\mathbb{E}\left[(\underline{\mathbf{z}}_n - \bar{\mu}_n \underline{\mathbf{b}}_n)(\underline{\mathbf{z}}_n - \bar{\mu}_n \underline{\mathbf{b}}_n)^H \right] \Big) \\ &= Q^{-1}\text{Trace}\Big(\mathbf{\Gamma}_n^H \mathbf{\Psi}^{\text{FD}} \mathbf{\Gamma}_n - (1 - \bar{\varphi}_n) \mathbf{\Gamma}_n^H \mathbf{\Xi}_{c,n} \bar{\mu}_n^* \mathbf{I}_Q \\ &\quad - (1 - \bar{\varphi}_n) \mathbf{\Xi}_{c,n}^H \mathbf{\Gamma}_n \bar{\mu}_n \mathbf{I}_Q + (1 - \bar{\varphi}_n) |\bar{\mu}_n|^2 \mathbf{I}_Q \Big) \end{aligned} \tag{3.27}$$

$$= Q^{-1}\text{Trace}\Big(\mathbf{\Gamma}_n^H \mathbf{\Psi}^{\text{FD}} \mathbf{\Gamma}_n \Big) - (1 - \bar{\varphi}_n) |\bar{\mu}_n|^2, \tag{3.28}$$

where $\bar{\varphi}_n \equiv \mathbb{E}[\bar{b}_{q,n}^2]$, $\forall n$ designates the average power of the soft symbol estimates, and $\mathbf{\Psi}^{\text{FD}} \equiv \left[\mathbf{\Xi}_c \mathbf{\Lambda}' \mathbf{\Xi}_c^H + \sigma_0^2 \mathbf{I}_{QM}\right]$ is the frequency domain covariance matrix of the residual signal $\underline{\mathbf{r}} - \underline{\bar{\mathbf{r}}}$ after soft interference cancellation. Here, $\mathbf{\Lambda}'$ is the unconditional covariance matrix of the transmit symbol vector $\mathbf{b}$, given by

$$\begin{aligned}\mathbf{\Lambda}' &= \mathbb{E}\Big[\mathbb{E}\big[(\mathbf{b}-\bar{\mathbf{b}})(\mathbf{b}-\bar{\mathbf{b}})^T|\zeta_e[\mathbf{b}]\big]\Big] \\ &= \text{diag}\big(1-\bar{\varphi}_1, ..., 1-\bar{\varphi}_n, ..., 1-\bar{\varphi}_N\big) \otimes \mathbf{I}_Q. \end{aligned} \tag{3.29}$$

The power levels $\bar{\varphi}_n$, $n = 1, ..., N$ may be estimated, in practice, over the whole frame of symbol estimates $\bar{b}_{q,n}[k]$, $\forall k$ using the sample mean. This means for a multiuser system setup, where the channel coding at each user is performed over a frame of N_b transmit blocks, an estimate of the power levels can be obtained by

$$\bar{\varphi}_n \approx \frac{1}{QN_b} \sum_{q=0}^{Q-1} \sum_{k=1}^{N_b} \bar{b}_{q,n}^2[k], \forall n. \tag{3.30}$$

For the single-user transmission setup, the coding scheme is uniform over all transmit antennas. Consequently, the power levels are identical for all N data streams and a single parameter $\bar{\varphi}$ is sufficient in this case,

$$\bar{\varphi} \equiv \frac{1}{N} \sum_{n=1}^{N} \bar{\varphi}_n. \tag{3.31}$$

The problem of minimizing the MSE in (3.25) can now be formulated as a constrained optimization problem. In detail, the linear frequency domain MMSE filter can be found by solving the following optimization problem:

$$\text{minimize } Q^{-1}\text{Trace}\Big(\mathbf{\Gamma}_n^H \mathbf{\Psi}^{\text{FD}} \mathbf{\Gamma}_n\Big) - (1-\bar{\varphi}_n)|\bar{\mu}_n|^2 \text{ subject to: } \bar{\mu}_n = 1. \tag{3.32}$$

The constraint $\bar{\mu}_n = 1$ in (3.32) is introduced to avoid the trivial solution $\mathbf{\Gamma}_n = \mathbf{0}$. It also ensures that the block-filter output vector $\mathbf{z}_n$ is an unbiased estimate of the transmit signal vector $\mathbf{b}_n$. Using the method of Lagrange multipliers, it is shown in Appendix B that the solution to the above problem is given by

$$\mathbf{\Gamma}_n = \gamma_n^{-1} \mathbf{\Psi}^{\text{FD}-1} \mathbf{\Xi}_{c,n}, \tag{3.33}$$

where $\gamma_n \equiv Q^{-1}\text{Trace}(\mathbf{\Xi}_{c,n}^H \mathbf{\Psi}^{\text{FD}-1} \mathbf{\Xi}_{c,n})$ is a scalar. As a result, the symbol estimate of the whole transmit block corresponding to the nth transmit data stream can

efficiently be expressed with (3.33) as

$$\mathbf{z}_n = \gamma_n^{-1}\mathbf{F}^H\boldsymbol{\Xi}_{c,n}^H\boldsymbol{\Psi}^{\mathrm{FD}-1}\Big(\underline{\mathbf{r}} - \underline{\bar{\mathbf{r}}}\Big) + \bar{\mathbf{b}}_n. \tag{3.34}$$

We refer to (3.34) as the SC-MMSE FDE. The computational complexity of the unconditional filter depends on the calculation of the inverse of the covariance matrix $\boldsymbol{\Psi}^{\mathrm{FD}}$. In contrast to the conditional SC-MMSE TDE from (3.12), this matrix inversion has to be computed only once per turbo iteration and is valid for all transmit antennas and the whole data frame. The covariance matrix $\boldsymbol{\Psi}^{\mathrm{FD}}$ is a structured block-diagonal matrix and independent of the effective channel memory length L. Its inversion can be efficiently performed with $O(QM^3)$ operations which leads to a complexity reduction of factor Q^2 as compared to (3.12). The SC-MMSE FDE is thus also applicable for equalization of MIMO ISI channels with large channel delay spread.

3.3.1. Equivalent AWGN Channel Assumption and LLR Computation

As in Assumption 3.2 used in the derivation of the *extrinsic* LLRs of the SC-MMSE TDE, we introduce the following approximation on the filter output of the SC-MMSE FDE.

Assumption 3.4. The (q,n)-th component of the MMSE filter-output can be written in the form $z_{q,n} = b_{q,n} + \bar{\nu}_{q,n}$, where $\bar{\nu}_{q,n}$ is modeled as zero-mean circularly-symmetric Gaussian distributed, so that its statistics are completely described by the variance $\sigma^2_{\bar{\nu},q,n}$.

The above assumption implies identical variances for the real and imaginary parts of the interference and noise term $\bar{\nu}_{q,n}$. The block-filter output signals in (3.34) can then be equivalently expressed as output signals of a complex-valued memoryless AWGN channel with variance

$$\sigma^2_{\nu,q,n} \equiv \mathrm{Var}[z_{q,n}] = \gamma_n^{-1} - (1 - \bar{\varphi}_n), n = 1, .., N. \tag{3.35}$$

As observed from (3.35), in contrast to the time domain approach, the variance of the equivalent noise $\bar{\nu}_{q,n}$ does not depend on the symbol indices (q,k) and hence, it has to be computed only once per turbo iteration and transmit data stream. Accordingly, the *extrinsic* LLR sequences of the code bits are obtained by (3.18) as

$$\lambda_e\Big[\mathbf{b}_n\Big] = \frac{4\Re\{\mathbf{z}_n\}}{\gamma_n^{-1} - (1 - \bar{\varphi}_n)}, \forall n. \tag{3.36}$$

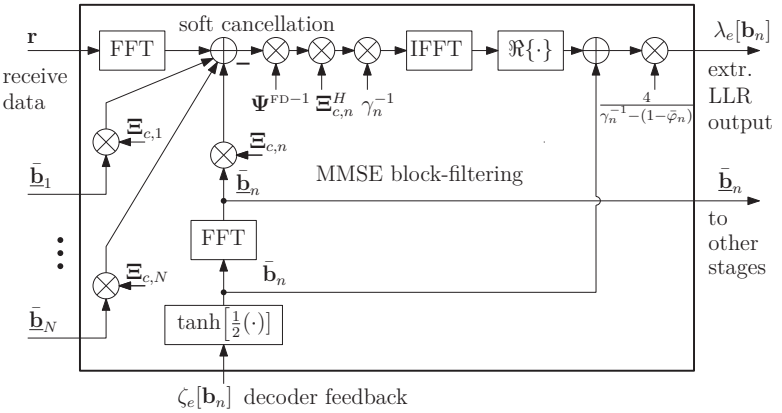

Figure 3.2.: Signal flow chart of the SC-MMSE FDE for the nth data stream.

Fig. 3.2 illustrates the block-diagram of the resulting SC-MMSE FDE implementing (3.36).

Proposition 3.5. The *extrinsic* LLR outputs (3.36) of the unbiased SC-MMSE FDE are identical to the LLR outputs of the biased SC-MMSE FDE derived in [KM07].

The proof of Proposition 3.5 is straightforward and skipped here for brevity.

3.3.2. SNR Analysis

Under Assumption 3.4 and the expression in (3.36), we find that the conditional PDFs of the *extrinsic* LLRs are given by real-valued Gaussian distributions

$$\mathcal{N}(\mu_{\lambda_e,n}c, \sigma^2_{\lambda_e,n}), c \in \{\pm 1\}, \tag{3.37}$$

where the mean $\mu_{\lambda_e,n} = 4(\gamma_n^{-1} - (1 - \bar{\varphi}_n))^{-1}$ and the variance $\sigma^2_{\lambda_e,n} = 8(\gamma_n^{-1} - (1 - \bar{\varphi}_n))^{-1}$ are related by a factor $\mu_{\lambda_e,n}/\sigma^2_{\lambda_e,n} = 1/2$, $\forall n$. The LLRs fulfill the exponential-symmetry condition (see Section 2.5.3), so that

$$p(\lambda_e[b_{q,n}]) = p(-\lambda_e[b_{q,n}]) \exp(\lambda_e[b_{q,n}]), \tag{3.38}$$

where $p(\lambda_e[b_{q,n}])$ is the PDF of the LLR message. The corresponding SNR ψ_n^{FD} of $\lambda_e[b_{q,n}]$ is found to

$$\psi_n^{\mathrm{FD}} \equiv \psi_n^{\mathrm{FD}}(\bar{\boldsymbol{\varphi}}) = \frac{2\gamma_n(\bar{\boldsymbol{\varphi}})}{1 - \gamma_n(\bar{\boldsymbol{\varphi}})(1 - \bar{\varphi}_n)}, \tag{3.39}$$

where $\bar{\boldsymbol{\varphi}} \equiv [\bar{\varphi}_1, \bar{\varphi}_2, ..., \bar{\varphi}_N]$ is the vector containing the sample averages from (3.30) and $\gamma_n = \gamma_n(\bar{\boldsymbol{\varphi}})$ is a function on the power levels and the channel gains.

Lemma 3.6. The SNR $\psi_n^{\text{FD}}(\bar{\boldsymbol{\varphi}})$ in (3.39) is component-wise monotonically increasing in $\bar{\boldsymbol{\varphi}}$.

Proof: See Appendix A.2. The maximum SNR at the LLR-output of the SC-MMSE FDE is obtained for the case of $\bar{\varphi}_n \to 1$, $\forall n$ (perfect *a priori* information) and bounded by

$$\psi_n^{\text{FD}}(\mathbf{1}_N) = 2Q^{-1}\sigma_0^{-2}\text{Trace}(\boldsymbol{\Xi}_{c,n}\boldsymbol{\Xi}_{c,n}^H). \tag{3.40}$$

The value $\psi_n^{\text{FD}}(\mathbf{1}_N)$ corresponds to the SNR of the matched filter bound (MFB) achieved when all interference has been removed in the system. The MFB serves as an upper bound on the performance and will be used in the numerical analysis presented in Section 3.7.

A compact expression for (3.39) is obtained for the case of a single-user single-antenna transmission system. The SNR then reads as

$$\begin{aligned}
\psi^{\text{FD}}(\bar{\varphi}) &\equiv \psi_1^{\text{FD}}(\bar{\varphi}, ..., \bar{\varphi}) \\
&= \frac{\gamma}{1-\gamma(1-\bar{\varphi})} \\
&= \left(\sum_{q=0}^{Q-1} \frac{\kappa(q)}{\sigma_0^2 + (1-\bar{\varphi})\kappa(q)}\right)\left(\sum_{q=0}^{Q-1} \frac{\sigma_0^2}{\sigma_0^2 + (1-\bar{\varphi})\kappa(q)}\right)^{-1} \\
&= \frac{1}{1-\bar{\varphi}}\left[Q\left(\sum_{q=0}^{Q-1} \frac{1}{1+\rho(\bar{\varphi})\kappa(q)}\right)^{-1} - 1\right],
\end{aligned} \tag{3.41}$$

where $\rho(\bar{\varphi}) \equiv (1-\bar{\varphi})\sigma_0^{-2}$. Note that the indices denoting the antennas/user have been skipped for notational simplicity from all the variables in (3.41). The SNR expression in (3.41) will extensively be utilized in Chapter 4.3 to analyze the convergence of MMSE-based turbo equalizers.

3.4. Nonlinear MMSE Frequency Domain Equalization

Next, we introduce a turbo scheme based on the framework of nonlinear MMSE (NMMSE) estimation [PP02]. The conceptual basis of this receiver is the PDA filtering [LPWH01], where the PDF of the composite ISI and CAI/MAI components is approximated by a multivariate Gaussian random process. Signal detection based on optimal NMMSE estimation has been first considered in the context of multiuser

CDMA by Gollamudi *et. al.* in [GH99]. It was shown that the calculation of the optimal NMMSE signal estimate, which requires the computation of a sum of terms that grows exponentially in the number of users, can be well approximated by iterative algorithms. This result was used to arrive at a receiver structure employing an iterative soft-decision interference cancellation scheme. In [PR06], Tan *et. al.* have related the optimal NMMSE multiuser detector to the PDA detector from [LPWH01], where a multivariate Gaussian approximation of the MAI was used to calculate the NMMSE estimate of the transmitted bits in coded multiuser CDMA. Similar to [GH99], the NMMSE estimation is performed by iterative interference cancelers. In this section, we extend the work from [PR06] to signal detection for MIMO ISI channels and derive a low-complexity frequency domain turbo MMSE equalizer that exploits the principle of PDA filtering. It is shown that this equalizer has a similar structure than the SC-MMSE FDE, but, in addition, it posses an internal feedback loop, by which the symbol estimates can be further improved.

3.4.1. Derivation of Nonlinear MMSE Filter Coefficients

Let $z_{q,n} \equiv f^*(\mathbf{r})$ denote the NMMSE estimate of the transmitted symbol $b_{q,n}$, where $f^*(\mathbf{r}) : \mathbb{C}^{MQ} \to \mathbb{R}$ is the nonlinear function that minimizes the MSE $\mathbb{E}\big[\,|b_{q,n} - f(\mathbf{r})|^2\,\big]$ over all $f(\mathbf{r}) : \mathbb{C}^{MQ} \to \mathbb{R}$. In order to find the optimal function $f^*(\cdot)$, we apply the expectation rule $\mathbb{E}\big[a\big(\mathbf{r}, b_{q,n}\big)\big] = \mathbb{E}\big[\mathbb{E}\big[\,a\big(\mathbf{r}, b_{q,n}\big)\big|\,\mathbf{r}\big]\big]$ [PP02], where $a(\mathbf{r}, b_{q,n}) \equiv |b_{q,n} - f(\mathbf{r})|^2$, and rewrite the MSE as

$$\int_{-\infty}^{\infty} \mathbb{E}\big[\,a\big(\mathbf{r}, b_{q,n}\big)\big|\,\mathbf{r}\big] p(\mathbf{r}) \mathrm{d}\mathbf{r}. \tag{3.42}$$

The integrand of (3.42) is always nonnegative. Minimizing the MSE is hence equivalent to the minimization of the conditional expected value $\mathbb{E}[h(\mathbf{r}, b_{q,n})|\,\mathbf{r}]$. Applying this result to the MSE leads to

$$f^*(\mathbf{r}) = \arg\min_{f}\ \mathbb{E}\Big[\,|b_{q,n} - f(\mathbf{r})|^2\Big|\,\mathbf{r}\Big]. \tag{3.43}$$

The solution to the above optimization problem is the well known conditional expectation, $z_{q,n} = \mathbb{E}\big[b_{q,n}|\mathbf{r}\big]$, which may be computed by invoking Bayes' theorem from the conditional probability function $\mathrm{Prob}(b_{q,n}|\mathbf{r})$ as

$$z_{q,n} = \sum_{b_{q,n}=\pm 1} b_{q,n} \mathrm{Prob}\big(b_{q,n}|\mathbf{r}\big) = \sum_{b_{q,n}=\pm 1} b_{q,n} \frac{p\big(\mathbf{r}|b_{q,n}\big)\mathrm{Prob}\big(b_{q,n}\big)}{\sum\limits_{b_{q,n}=\pm 1} p\big(\mathbf{r}|b_{q,n}\big)\mathrm{Prob}\big(b_{q,n}\big)}. \tag{3.44}$$

Here, $p(\mathbf{r}|b_{q,n})$ denotes the PDF of $\mathbf{r}$ conditioned on $b_{q,n}$, which is defined with (3.4) as

$$p\Big(\mathbf{r}|b_{q,n}\Big) = \sum_{\mathbf{x}\in\mathcal{X}_{q,n}^{<c>}} \text{Prob}(\mathbf{x}) \frac{\exp\Big[-\frac{1}{\sigma_0^2}\Big\|\mathbf{r}-\mathbf{H}_c\mathbf{e}_{w(q,n)}b_{q,n}-\boldsymbol{\Delta}_{q,n}(\mathbf{x})\Big\|^2\Big]}{(\pi\sigma_0^2)^{MQ}}, \tag{3.45}$$

where $\mathcal{X}_{q,n}^{<c>}$ is the binary set, as defined in (3.2), containing all possible combinations of the transmit symbol vector $\mathbf{b}$, and

$$\boldsymbol{\Delta}_{q,n}(\mathbf{x}) = \sum_{(r,l)\in\mathcal{S}_{q,n}} \mathbf{H}_c\mathbf{e}_{w(r,l)}x_{r,l}, \mathcal{S}_{q,n} \equiv \{r,l|0\le r\le Q-1, 1\le l\le N, (r,l)\ne(n,q)\} \tag{3.46}$$

is a interference vector containing the ISI and CAI/MAI contributions with respect to the qth signaling instant of the nth transmit data stream. As observed from (3.45), the computation of the conditional PDF $p\Big(\mathbf{r}|b_{q,n}\Big)$, required to obtain the NMMSE estimate (3.44), involves a summation over 2^{NQ-1} terms. The computation of this sum is intractable even for small number of transmit antennas N and block-sizes Q. In order to reduce the complexity, we adopt here the concept of PDA filtering [LPWH01], and make the following assumption (see also [PR06]).

Assumption 3.7. The interference vector $\boldsymbol{\Delta}_{q,n}$ can be modeled as a random process with multivariate circularly-symmetric Gaussian distribution with mean

$$\boldsymbol{\mu}_{q,n} \equiv \mathbb{E}[\boldsymbol{\Delta}_{q,n}|\mathbf{r}] = \sum_{(r,l)\in\mathcal{S}_{q,n}} \mathbf{H}_c\mathbf{e}_{w(r,l)}z_{r,l} \tag{3.47}$$

and covariance

$$\boldsymbol{\Omega}_{q,n} \equiv \text{Cov}[\boldsymbol{\Delta}_{q,n}\boldsymbol{\Delta}_{q,n}^H|\mathbf{r}] = \sum_{(r,l)\in\mathcal{S}_{q,n}}\sum_{(t,z)\in\mathcal{S}_{q,n}} \mathbf{H}_c\mathbf{e}_{w(r,l)}\text{Cov}(b_{r,l}b_{t,z}|\mathbf{r})\mathbf{e}_{w(t,z)}^H\mathbf{H}_c^H. \tag{3.48}$$

The Gaussian model of the interference term is a direct result from the application of the central limit theorem to (3.46), for $Q, N \to \infty$. We may then replace the summation in (3.45) by an integration over the space of $\boldsymbol{\Delta}_{q,n}$. This yields for the conditional probability density function $p\Big(\mathbf{r}|b_{q,n}\Big)$ the following expression:

$$p\Big(\mathbf{r}|b_{q,n}\Big) = \int_{-\infty}^{\infty} p(\mathbf{r}|\boldsymbol{\Delta}_{q,n}, b_{q,n})p(\boldsymbol{\Delta}_{q,n})\mathrm{d}\boldsymbol{\Delta}_{q,n}, \tag{3.49}$$

where $p(\boldsymbol{\Delta}_{q,n}) \sim \mathcal{CN}(\boldsymbol{\mu}_{q,n}, \boldsymbol{\Omega}_{q,n})$ denotes the Gaussian multivariate function of the interference vector $\boldsymbol{\Delta}_{q,n}$. Substituting the PDF $p(\mathbf{r}|\boldsymbol{\Delta}_{q,n}, b_{q,n})$ from (3.45) in (3.49),

and performing the integration, we obtain

$$p\big(\mathbf{r}|b_{q,n}\big) \propto \exp\Big[2\Re\Big\{\mathbf{e}_{w(q,n)}^H\mathbf{H}_c^H\Big[\mathbf{\Omega}_{q,n}+\sigma_0^2\mathbf{I}_{QM}\Big]^{-1}(\mathbf{r}-\boldsymbol{\mu}_{q,n})\Big\}b_{q,n}\Big]. \tag{3.50}$$

Now using the probablity-LLR relation $\text{Prob}(b_{q,n}) = (1+\exp\big(-b_{q,n}\zeta_e[b_{q,n}]\big)^{-1}$ (see Eqn. (2.35)), and plugging (3.50) into (3.44), the NMMSE estimate of $b_{q,n}$ is finally obtained as

$$z_{q,n} = \tanh\left(\tfrac{1}{2}\zeta_e[b_{q,n}] + 2\Re\Big\{\mathbf{e}_{w(q,n)}^H\mathbf{H}_c^H\Big[\mathbf{\Omega}_{q,n}+\sigma_0^2\mathbf{I}_{QM}\Big]^{-1}(\mathbf{r}-\boldsymbol{\mu}_{q,n})\Big\}\right). \tag{3.51}$$

3.4.2. Approximation of Covariance Matrix and Channel Decomposition

Considering (3.51), it becomes clear that the calculation of the NMMSE estimate for the code bit $b_{q,n}$ is dominated by the inversion of matrix $\big[\mathbf{\Omega}_{q,n}+\sigma_0^2\mathbf{I}_{QM}\big]$. This computation has a complexity of order $O(M^3Q^3)$ per BPSK-symbol, which is still prohibitive as the number of receive antennas M and the block-size Q increase. For a low-complexity implementation of an NMMSE-based turbo equalizer, we invoke an approximation of the covariance matrix $\mathbf{\Omega}_{q,n}$ by a structured matrix, and also exploit the decomposition property (2.14) of the circulant channel matrices $\mathbf{H}_{c,n}$, $n = 1,..,N$.

Assumption 3.8. The cross-correlation coefficients of the NMMSE symbol estimates are given by

$$\text{Cov}[b_{q,n}b_{q',n'}|\mathbf{r}] = \begin{cases} 1-|z_{q,n}|^2 \text{ for } q=q' \wedge n=n' \\ 0 \text{ others.} \end{cases} \tag{3.52}$$

In other words, it is supposed that the NMMSE estimates are uncorrelated to each other. This approximation becomes valid as N and Q grows large, since it is expected that $\mathbb{E}[b_{q,n}b_{q',n'}|\mathbf{r}] \to z_{q,n}z_{q',n'}$ (cf. [PR06].). Based on this simplification, the covariance matrix $\mathbf{\Omega}_{q,n}$ can be written as

$$\begin{aligned}\mathbf{\Omega}_{q,n} &= \sum_{l=1}^{N}\mathbf{H}_{c,l}\mathbf{\Lambda}^{''}{}_l\mathbf{H}_{c,l}^H - (1-|z_{q,n}|^2)\mathbf{H}_c\mathbf{e}_{w(q,n)}\mathbf{e}_{w(q,n)}^H\mathbf{H}_c^H, \\ &= \sum_{l=1}^{N}\mathbf{F}_M^H\mathbf{\Xi}_{c,l}\mathbf{F}^H\mathbf{\Lambda}^{''}{}_l\mathbf{F}\mathbf{\Xi}_{c,l}^H\mathbf{F}_M - (1-|z_{q,n}|^2)\mathbf{H}_c\mathbf{e}_{w(q,n)}\mathbf{e}_{w(q,n)}^H\mathbf{H}_c^H \end{aligned} \tag{3.53}$$

where $\mathbf{\Lambda}^{''}{}_n = \text{diag}\big(1-|z_{0,n}|^2,...,1-|z_{q,n}|^2,...,1-|z_{Q-1,n}|^2\big) \in \mathbb{R}^{Q\times Q}$, $n = 1,...,N$

is diagonal matrix containing the variances of the NMMSE symbol estimates. In (3.53), we have applied the eigen-decompositions of the compound channel matrices $\mathbf{H}_{c,n} = \mathbf{F}_M^H \mathbf{\Xi}_{c,n} \mathbf{F}$ $\forall n$ to replace the time domain matrices $\mathbf{H}_{c,n}$ by their frequency domain equivalents. For large block-sizes Q, the diagonal elements of $\mathbf{F}^H {\mathbf{\Lambda}''}_n \mathbf{F}$ in (3.53) are dominant, encouraging the approximation $\mathbf{F}^H {\mathbf{\Lambda}''}_n \mathbf{F} \approx (1 - \bar{\bar{\varphi}}_n)\mathbf{I}_Q$, $\forall n$ with $\bar{\bar{\varphi}}_n \equiv \frac{1}{QN_b} \sum_{q=0}^{Q-1} \sum_{k=1}^{N_b} |z_{q,n}[k]|^2$ for all $n = 1, ..., N$ being the average power of the NMMSE estimates. The covaricane matrix $\mathbf{\Omega}_{q,n}$ can then be further simplified to

$$\mathbf{\Omega}_{q,n} \approx \sum_{l=1}^{N} (1 - \bar{\bar{\varphi}}_l) \mathbf{H}_{c,l} \mathbf{H}_{c,l}^H - (1 - \bar{\bar{\varphi}}_n) \mathbf{H}_c \mathbf{e}_{w(q,n)} \mathbf{e}_{w(q,n)}^H \mathbf{H}_c^H. \tag{3.54}$$

For a compact notation of (3.54), we apply the matrix inversion lemma and stack the NMMSE estimates for the n-th data stream into a vector $\mathbf{z}_n$. This yields the following compact expression for (3.51):

$$\begin{aligned} \mathbf{z}_n &= [z_{0,n}, ..., z_{q,n}, ..., z_{Q-1,n}]^T \\ &= \tanh\left(\tfrac{1}{2} \boldsymbol{\zeta}_e[\mathbf{b}_n] + \mathbf{\Theta}_n^{\text{NL}} \Re\Big\{ \mathbf{H}_{c,n}^H \mathbf{\Sigma}^{\text{NL}-1} (\mathbf{r} - \textstyle\sum_{l=1}^{N} \mathbf{H}_{c,l} \mathbf{z}_l) \Big\} + \mathbf{\Theta}_n^{\text{NL}} \mathbf{\Upsilon}_n^{\text{NL}} \mathbf{z}_n \right), \forall n, \end{aligned} \tag{3.55}$$

where

$$\mathbf{\Sigma}^{\text{NL}} \equiv \sum_{l=1}^{N} (1 - \bar{\bar{\varphi}}_l) \mathbf{H}_{c,l} \mathbf{H}_{c,l}^H + \sigma_0^2 \mathbf{I}_{QM}, \tag{3.56}$$

$$\mathbf{\Theta}_n^{\text{NL}} \equiv 2\Big(\mathbf{I}_Q - \mathbf{\Upsilon}_n^{\text{NL}} (1 - \bar{\bar{\varphi}}_n) \Big)^{-1}, \tag{3.57}$$

$$\mathbf{\Upsilon}_n^{\text{NL}} \equiv \text{ddiag}(\mathbf{H}_{c,n}^H \mathbf{\Sigma}^{\text{NL-1}} \mathbf{H}_{c,n}). \tag{3.58}$$

Finally, we apply the eigen-decomposition of the compound channel matrix $\mathbf{H}_c$, and convert the matrices in (3.56)-(3.58) into the frequency domain. Hence, we arrive at $\mathbf{\Psi}^{\text{NL}} \equiv \mathbf{F}_M^H \mathbf{\Sigma}^{\text{NL}} \mathbf{F}_M$, $\mathbf{\Theta}_n^{\text{NL}} = \theta_n \mathbf{I}_Q$ and $\mathbf{\Upsilon}_n^{\text{NL}} = \bar{\gamma}_n \mathbf{I}_Q$, where the scalars θ_n and $\bar{\gamma}_n$ are given by $\theta_n = 2(1 - \bar{\gamma}_n(1 - \bar{\bar{\varphi}}_n))^{-1}$ and $\bar{\gamma}_n = Q^{-1} \text{Trace}(\mathbf{\Xi}_{c,n}^H \mathbf{\Psi}^{\text{NL}-1} \mathbf{\Xi}_{c,n})$, respectively. Using these notations, the NMMSE estimate in (3.55) can be further written as

$$\mathbf{z}_n = \tanh\left(\tfrac{1}{2} \boldsymbol{\zeta}_e[\mathbf{b}_n] + \theta_n \Re\left\{ \mathbf{F}^H \mathbf{\Xi}_{c,n}^H \mathbf{\Psi}^{\text{NL}-1} \Big(\underline{\mathbf{r}} - \textstyle\sum_{l=1}^{N} \mathbf{\Xi}_{c,l} \underline{\mathbf{z}}_l \Big) \right\} + \theta_n \bar{\gamma}_n \mathbf{z}_n \right). \tag{3.59}$$

with $\underline{\mathbf{z}}_l \equiv \mathbf{F}\mathbf{z}_l$. Eqn. (3.59) is a fixed-point problem which may be iteratively solved following the PDA principle. For this purpose, we introduce the iteration index τ.

The NMMSE vector of the code bits can be recursively obtained as

$$\mathbf{z}_n^{(\tau+1)} = \tanh\Bigg(\frac{1}{2}\boldsymbol{\zeta}_e[\mathbf{b}_n] + \theta_n^{(\tau)}\Re\left\{\mathbf{F}^H\boldsymbol{\Xi}_{c,n}^H(\boldsymbol{\Psi}^{\mathrm{NL}(\tau)})^{-1}\Big(\underline{\mathbf{r}} - \textstyle\sum_{l=1}^{N}\boldsymbol{\Xi}_{c,l}\underline{\mathbf{z}}_l^{(\tau)}\Big)\right\} + \theta_n^{(\tau)}\bar{\gamma}_n^{(\tau)}\mathbf{z}_n^{(\tau)}\Bigg) \quad (3.60)$$

for $\tau = 0, 1, ..., \tau_{\max}$. A typical choice of the initial solution $\mathbf{z}_n^{(0)}$ is the most recent *a priori* LLR sequence from channel decoding, i.e., $\mathbf{z}_n^{(0)} = \tanh\left(\frac{1}{2}\boldsymbol{\zeta}_e[\mathbf{b}_n]\right)$, for $n = 1, ..., N$ (see [PR06]). The aim of these iterations is to adjust the mean and the covariance of the multivariate Gaussian distribution of the interference vector $\boldsymbol{\Delta}_{q,n}$ by exploiting the knowledge of previous estimates on the code bits. The output of the iterative estimator provides after a sufficient number of iterations an approximate solution to the NMMSE estimates $\mathbf{z}_n$, for all n. Note that convergence of (3.60) relies on the Gaussian approximation (Assumption 3.7) and is not ensured, in general. Especially, when the parameters Q and N are small and/or the MIMO-ISI channel has only a small number of dominant paths or a high spatial correlation, we have found that the Gaussian approximation is less accurate. In such cases, Eqn. (3.60) may fail to converge. The convergence properties may then be improved by introducing iteration-depending weighting factors to previous NMMSE estimates (see cf. [GS01], [PR06]). This weighting factor approach might ensure convergence at the expense of a decreasing convergence rate to the steady state. The iterative estimator (3.60) is evaluated in Section 3.7 through a series of numerical examples in spatially uncorrelated MIMO channels, for which convergence always has been observed.

A low-complexity equalizer suited for the application in turbo receivers may now directly be derived from (3.59). Supposing a sufficient number of iterations so that (3.60) has converged to a steady state, the conditional PDF in (3.50) reads as

$$p\Big(\mathbf{r}|b_{q,n}\Big) \propto \exp\Bigg[\left(\theta_n\mathbf{e}_q^T\Re\Big\{\mathbf{F}^H\boldsymbol{\Xi}_{c,n}^H\boldsymbol{\Psi}^{\mathrm{NL}-1}\Big(\underline{\mathbf{r}} - \textstyle\sum_{l=1}^{N}\boldsymbol{\Xi}_{c,l}\underline{\mathbf{z}}_l\Big)\Big\} + \theta_n\bar{\gamma}_n z_{q,n}\right)b_{q,n}\Bigg]. \quad (3.61)$$

The corresponding *extrinsic* LLR vector at the equalizer output for the code bits of the transmit block $\mathbf{b}_n$ forwarded to the channel decoder(s) can immediately be determined with (3.61) as

$$\lambda_e\Big[\mathbf{b}_n\Big] = 2\theta_n\Re\Big\{\mathbf{F}^H\boldsymbol{\Xi}_{c,n}^H\boldsymbol{\Psi}^{\mathrm{NL}-1}\Big(\underline{\mathbf{r}} - \sum_{l=1}^{N}\boldsymbol{\Xi}_{c,l}\underline{\mathbf{z}}_l\Big)\Big\} + 2\theta_n\bar{\gamma}_n\mathbf{z}_n, \quad (3.62)$$

A block diagram of the resulting equalizer to (3.62) is depicted in Fig 3.3. We see that the structure of the above equalization scheme is similar to the SC-MMSE FDE

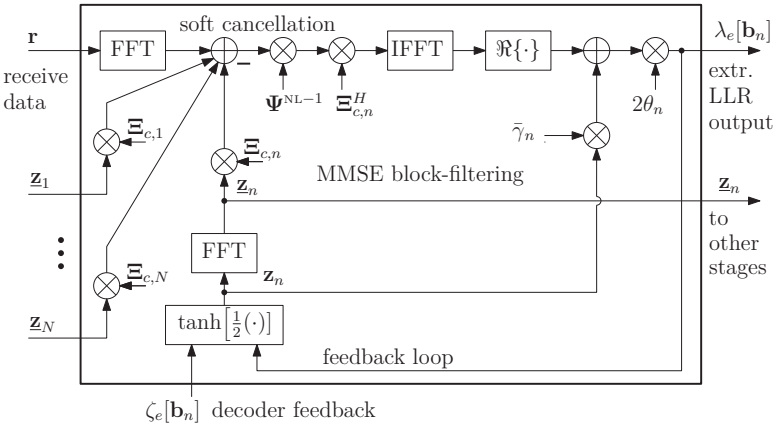

Figure 3.3.: Signal flow chart of the PDA SC-MMSE FDE for the nth transmit data stream.

introduced in Section 3.3. However, with the presented method, internal iterations within the equalizer following the PDA principle are used to improve the NMMSE estimates. The proposed equalization scheme is therefore denoted as PDA SC-MMSE FDE in what follows.

We remark that with the present turbo structure, we have three separate iterations: i) the overall turbo iteration, exchanging *extrinsic* LLRs between the PDA SC-MMSE FDE and the channel decoders; ii) the internal PDA SC-MMSE FDE iterations, improving the soft symbol NMMSE estimates; and iii) the iterations within the channel decoders.

3.4.3. SNR Analysis

In order to analyze the SNR of the *extrinsic* LLRs at the PDA SC-MMSE FDE output, we rewrite (3.62) in signal-plus-distortion form as $\lambda_e[b_{q,n}] = \bar{\bar{\mu}}_{q,n} b_{q,n} + \bar{\bar{\nu}}_{q,n}$ with $\bar{\bar{\mu}}_{q,n}$ being an equivalent gain at the equalizer output and $\bar{\bar{\nu}}_{q,n}$ modeling the residual interference and noise components. The corresponding SNR of the *extrinsic* LLRs is given by

$$\psi_{q,n}^{\mathrm{NL}} \equiv \frac{\bar{\bar{\mu}}_{q,n}^2}{\mathbb{E}[\bar{\bar{\nu}}_{q,n}^2]}. \tag{3.63}$$

To derive an exact closed-form expression to (3.63), it would be necessary to take into account the cross-correlations between different NMMSE estimates over the internal equalizer iterations. However, such a modeling is beyond analytical tractability for

large block-sizes Q and users/transmit antennas N. For the ease of analysis, it is assumed that the following holds true.

Assumption 3.9. The additive samples $\bar{\bar{\nu}}_{q,n}$ are zero-mean i.i.d. Gaussian distributed and independent of the code bit $b_{q,n}$. The corresponding PDF of the *extrinsic* LLR $\lambda_e[b_{q,n}]$ satisfies the exponential symmetry condition.

In other words, it is supposed that the NMMSE estimates at each internal equalizer iteration are uncorrelated with each other, and are independent of the channel noise. With this simplification, the equivalent gain and variance are solved as $\bar{\bar{\mu}}_{q,n} = 2\theta_n\bar{\gamma}_n$ and $\mathbb{E}[\bar{\bar{\nu}}^2_{q,n}] = 4\theta_n\bar{\gamma}_n$, respectively. The parameter $\bar{\gamma}_n$ is a function of vector $\bar{\bar{\boldsymbol{\varphi}}} \equiv [\bar{\bar{\varphi}}_1, ..., \bar{\bar{\varphi}}_n, ..., \bar{\bar{\varphi}}_N]^T$ containing the power values of the NMMSE estimates from all users/transmit antennas. To emphasize this, we write $\bar{\gamma}_n = \bar{\gamma}_n(\bar{\bar{\boldsymbol{\varphi}}})$. Using the above expressions for the mean and variance, the SNR in (3.63) is obtained as

$$\psi_n^{\mathrm{NL}} \equiv \psi_{q,n}^{\mathrm{NL}} = \frac{2\bar{\gamma}_n(\bar{\bar{\boldsymbol{\varphi}}})}{1 - \bar{\gamma}_n(\bar{\bar{\boldsymbol{\varphi}}})(1 - \bar{\bar{\varphi}}_n)}. \tag{3.64}$$

The parameter $\bar{\bar{\varphi}}_n$ in (3.64) can be obtained by invoking the sample mean and noting that for large number of blocks and frame length Q and N_b, respectively, the sample mean converges to the ensemble expectation, so that

$$\begin{aligned}\bar{\bar{\varphi}}_n &= \lim_{Q,N_b\to\infty} \frac{1}{QN_b} \sum_{q=0}^{Q-1} \sum_{k=1}^{N_b} |z_{q,n}[k]|^2 = \mathbb{E}[z^2_{q,n}] \\ &= \mathbb{E}[b_{q,n} z_{q,n}],\end{aligned} \tag{3.65}$$

where the equivalence between the first and second line in (3.65) follows from the expectation rule (3.26) (see also [PP02]). To proceed, we require the knowledge of the distribution of the input LLRs $\zeta_e[b_{q,n}]$ at the equalizer to express $\mathbb{E}[b_{q,n}z_{q,n}]$ in a closed form. We adopt the Gaussian model (2.48) from Section 2.5.2, and assume that the input LLRs $\zeta_e[b_{q,n}]$ are drawn from an exponential-symmetric Gaussian distribution. This model has been widely used in the convergence analysis of multiple concatenated codes and coded systems and is formalized in the following assumption[1].

Assumption 3.10. The LLRs $\zeta_e[b_{q,n}] \sim \mathcal{N}(2\varrho_n b_{q,n}, 4\varrho_n)$ are i.i.d. exponential-symmetric Gaussian distributed with channel SNR ϱ_n.

The input LLRs at the equalizer can now be treated as samples from a memoryless binary-input AWGN channel with SNR ϱ_n. Due to the symmetry constraint, the

[1] Examples of multiple concatenated codes are LDPC and turbo codes (see e.g., [PSU05], [RU01], [RSU01], [BGT93]).

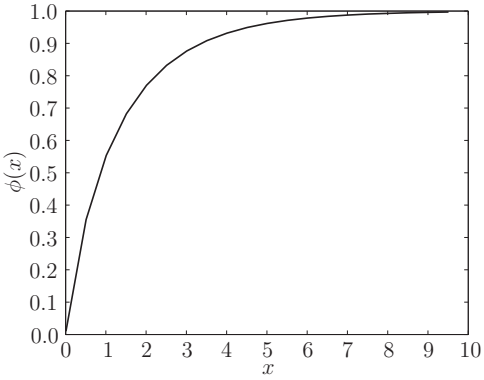

Figure 3.4.: Graph of function $\phi(x)$ responsible for mapping of SNR values to power levels for the NMMSE estimates.

single SNR parameter ϱ_n is sufficient to characterize the statistics of $\zeta_e[b_{q,n}]$. Based on Assumption 3.9 and 3.10, the power levels $\bar{\bar{\varphi}}_n$ of the NMMSE estimates can now be written with (3.62) by an integral equation as

$$\begin{aligned}\bar{\bar{\varphi}}_n &= \mathbb{E}[b_{q,n} z_{q,n}] \\ &= \frac{1}{\sqrt{2\pi}} \int \tanh\left(z\sqrt{\varrho_n + \psi_n^{\mathrm{NL}}} + \varrho_n + \psi_n^{\mathrm{NL}}\right) e^{-\frac{z^2}{2}} \mathrm{d}z \\ &= \phi(\varrho_n + \psi_n^{\mathrm{NL}}),\end{aligned} \tag{3.66}$$

where we have defined $\phi(x) \equiv \frac{1}{\sqrt{2\pi}} \int_{-\infty}^{\infty} \tanh\left(z\sqrt{x} + x\right) e^{\frac{-z^2}{2}} \mathrm{d}z$. As shown in Fig. 3.4, $\phi(x)$ is continuous, strictly monotonically increasing and bounded, $0 \leq \phi(x) \leq 1$. Therefore, it has a unique inverse $\phi^{-1}(\cdot)$. Both functions $\phi(x)$ and $\phi^{-1}(x)$ have no-closed form solution. However, good approximations of them can be obtained by numerical integration (c.f., [SBR06]) as

$$\begin{aligned}\phi(x) &\approx \left(1 - 2^{-H_1 (4x)^{H_2}}\right)^{H_3}, \\ \phi^{-1}(x) &\approx \frac{1}{4}\left(-\frac{1}{H_1} \log_2\left(1 - x^{\frac{1}{H_3}}\right)\right)^{\frac{1}{H_2}},\end{aligned} \tag{3.67}$$

where $H_1 = 0.4282$, $H_2 = 0.8130$ and $H_3 = 1.1699$. The function $\phi(\cdot)$ and its inverse $\phi^{-1}(\cdot)$ as well as their approximations in (3.67) will be exploited in the convergence analysis of turbo systems in the following Chapter 4.

With expression (3.66), Eqn. (3.64) can finally be rewritten as a fixed point

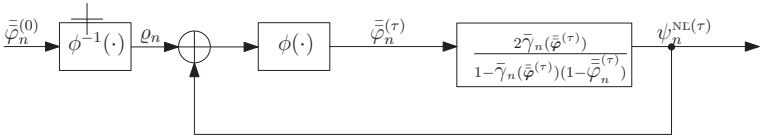

Figure 3.5.: Illustration of the recursive calculation of the SNR at the PDA SC-MMSE FDE output.

equation. In order to efficiently calculate a solution to this fixed point equation, we develop a recursive relationship describing the SNR improvement achieved by the internal iterations. By replacing each variable with the corresponding variable at internal iteration τ, and using (3.66) and (3.64) in a recursive fashion, the SNR at the equalizer output can be determined, for the input SNR values ϱ_n, $\forall n$ as (see Fig. 3.5)

$$\bar{\bar{\varphi}}_n^{(\tau)} = \phi\Big(\varrho_n + \psi_n^{\mathrm{NL}(\tau)}\Big), \psi_n^{\mathrm{NL}(0)} \equiv 0, \forall n, \tag{3.68}$$

$$\psi_n^{\mathrm{NL}(\tau+1)} = \frac{2\bar{\gamma}_n(\bar{\bar{\boldsymbol{\varphi}}}^{(\tau)})}{1-\bar{\gamma}_n(\bar{\bar{\boldsymbol{\varphi}}}^{(\tau)})(1-\bar{\bar{\varphi}}_n^{(\tau)})}, \forall n. \tag{3.69}$$

$$\varrho_n = \phi^{-1}(\bar{\bar{\varphi}}_n^{(0)}), \tag{3.70}$$

where $\bar{\bar{\varphi}}_n^{(0)} \in [0,1]$ denotes the initial power level of the NMMSE estimates. The above calculations are carried out for all N data streams and all iterations $\tau \in \{0, ..., \tau_{\max}\}$. With some effort, it is possible to verify that for all $j = 1, .., N$, the partial derivatives $\partial\psi_n^{\mathrm{NL}(\tau)}/\partial\bar{\bar{\varphi}}_j$ are non-negative with respect to $\bar{\bar{\varphi}}_j$. Together with the fact that $\phi(\cdot)$ is bounded and monotonically increasing, we deduce that the sequence generated by (3.68)-(3.70) is guaranteed to converge to a unique fixed-point $\psi_n^{\mathrm{NL}(\infty)}$ as $\tau \to \infty$, $\psi_n^{\mathrm{NL}(\infty)} \equiv \lim_{\tau\to\infty} \psi_n^{\mathrm{NL}(\tau)}$, $\forall n$.

With the above expressions, we can evaluate and compare the output SNRs of the PDA SC-MMSE FDE and the SC-MMSE FDE. For this purpose, we define the SNR gain of the nth LLR output achieved by the PDA SC-MMSE FDE over the SC-MMSE FDE as

$$\mathring{\psi}_n \equiv \frac{\psi_n^{\mathrm{NL}(\infty)}}{\psi_n^{\mathrm{NL}(1)}}, \forall n. \tag{3.71}$$

Obviously without the internal iterations, i.e., $\tau = 0$, we immediately see that the SNRs of the output LLRs of the PDA SC-MMSE FDE and the conventional SC-MMSE FDE are identical and hence $\psi_n^{\mathrm{NL}(1)} = \psi_n^{\mathrm{FD}}$ follows.

Fig 3.6 illustrates the SNR gains $\mathring{\psi}_n$, $n = 1, 2$ for a single-user $N = M = 2$

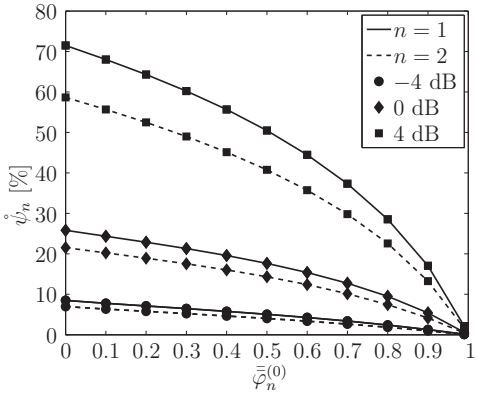

Figure 3.6.: SNR gain $\mathring{\psi}_n$, $n = 1, 2$ at the LLR output of the PDA SC-MMSE FDE at different receive SNRs $E_s/N_0 = -4$ dB, 0 dB and 4 dB for a turbo system with FFT-size $Q = 32$. Single $L = 32$-tap Rayleigh fading $N = M = 2$ MIMO channel realization with equal average path energy.

MIMO system at different receive SNRs E_s/N_0 and different initial values[2] of $\bar{\bar{\varphi}}^{(0)}$. We observe that significant gains are obtained for low to moderate values of $\bar{\bar{\varphi}}_n^{(0)}$, indicating that improvements in performance of turbo equalization can be expected through the internal iterations when probabilistic information fed back from channel decoding is unreliable (which is typically the case in the first turbo iterations). The combination of soft decision feedback within the equalizer and *a priori* knowledge from channel decoding thus leads to an improvement of convergence speed and threshold of the turbo receiver. We evaluate this feature of the PDA SC-MMSE FDE by numerical simulations in terms of BER and throughput (TP) in Section 3.7.

3.5. Hybrid SC-MMSE Frequency Domain Equalization

Unfortunately, due to its simplicity, the conventional SC-MMSE-based turbo receivers suffer from a considerable performance loss, e.g., as shown by the author in [GM07] when applied to the ISI multiple access spatially-correlated fading channel. To overcome this performance degradation, groupwise turbo equalization [VMJ04],

[2]For a single-user transmission system, the input LLRs of all data streams at the equalizer are assumed to have the same distribution, and therefore, we set $\bar{\bar{\varphi}}_1^{(0)} = \bar{\bar{\varphi}}_2^{(0)}$.

[GM07] can be employed that combines SC-MMSE filtering and optimal MAP detection.

The idea of groupwise multiuser detection was first introduced by Varanesi in [Var95] for uncoded CDMA channels. The group detector (GD) partitions the users' signals into a set of disjoint subgroups, and then employs the maximum likelihood detection (MLD) sequentially or in parallel to the signals in each subgroup. Compared to the optimal solution, the GD achieves near-optimal performance at a significantly reduced complexity. The concept from [Var95] was extended in [LHLF00] to group antenna detection (GAD) using linear subspace processing for inter-group interference (IGI) suppression of spatially-multiplexed MIMO channels with frequency-flat fading. Also, the authors of [LHLF00] presented a channel correlation-based group selection (GS) scheme that optimizes the grouping for each individual antenna with respect to optimum system performance. Among other contributions, Moon *et. al.* [MJLL10] has recently shown that the performance of the GAD scheme [LHLF00] can be further improved when taking into account the noise statistics at the receiver. Particularly, they proposed a groupwise detection strategy based on linear filtering maximizing the SINR in each subgroup. In addition, the authors derived an SINR-based GS method that maximizes the overall system's performance.

Several group detectors employing turbo processing for coded data transmission were presented in [EPP06], [VMJ04], [VBC06], [GM07]. Iterative soft interference cancellation combined with groupwise noise-whitening filtering, incorporating *a priori* information from channel decoding, was used in [EPP06] to group detection for MIMO flat-fading systems having more transmitter than receiver antennas. Note that due to presence of *a priori* information, the iterative receiver used the MAP instead of the ML algorithm. In [VMJ04], Veselinovic *et al.* considered a space-time trellis-coded (STTrC) system in multiple-access ISI fading channels and derived a time-domain groupwise SC-MMSE-based filtering technique for joint signal detection of multiple transmit antennas. The aim of jointly detecting symbols from different antennas was to preserve the effective degrees of freedom that can be used for suppression of unknown co-channel interfering signals. In [GM07], the author extended the groupwise SC-MMSE technique from [VMJ04] to OFDM systems with iterative detection. Group equalization combining frequency domain SC-MMSE filtering and MAP symbol detection has also been considered in [VBC06]. However, unlike to the groupwise filtering approach [VMJ04], [GM07], the MMSE block from [VBC06] performs the suppression of residual interferences on a user-by-user basis, similar to the standard MMSE filter [TSK02], to separate the transmitted signals. The MSE at the equalizer output can therefore not be used to evaluate the performance of each subgroup, which is needed for an adaptive GS at each turbo iteration.

The main goal of this section is to design a computationally efficient turbo re-

ceiver for multiuser systems that is robust against spatial channel correlation. To achieve this goal, we adapt the group detection strategy from [Var95] and extend the SC-MMSE FDE from Section 3.3 to an equalizer that performs frequency domain groupwise processing of the multiple users' transmitted symbols. In particular, the proposed algorithm divides the users' signals into several non-overlapping subgroups, and then it performs IGI equalization utilizing *a priori* information about the transmitted data obtained from channel decoding. The groupwise filter is designed to minimize the MSE in each subgroup. Similar to the derivation of the FDE in Section 3.3, we derive the groupwise filter in the frequency domain by introducing an additional design criterion in the optimization. More specifically, the structure of the filtering matrix is constrained to be block-circulant. This restriction significantly reduces the complexity for the covariance matrix inversions involved in SC-MMSE equalization.

Particular emphasis is also put on the grouping strategy, which mainly determines the overall performance of the system. Three greedy algorithms based on MSE and correlation criteria for grouping the users into several subgroups are proposed. The aim of these algorithms is to find groupings that reduce noise enhancement due to the SC-MMSE interference suppression of highly correlated user signals. The first scheme dynamically forms subgroups at each turbo iteration by computing among all possible group partitions the one that minimizes the maximum subgroup's MSE. The calculation of each partition involves a number of matrix inversions, which however, limits the application of the dynamic MSE-based algorithm to systems with a small number of users. The second and third schemes reduce complexity by providing a static grouping that is valid for all turbo iterations. It is shown that the simple static correlation-based algorithm outperforms the static MSE-based grouping scheme and achieves similar performance as the dynamic MSE-based algorithm at a significantly reduced complexity when applied to the proposed turbo receiver.

3.5.1. Modified System Model

The hybrid equalizer separates the transmitted signals into G disjoint subgroups, labeled by the sets $(\mathcal{A}_1, ..., \mathcal{A}_g, ..., \mathcal{A}_G)$, such that each subgroup $\mathcal{A}_g = \{a_1, ..., a_U\}$, $a_1 < .... < a_U$ contains U integers corresponding to indices of users that are jointly detected[3]. Without loss of generality, we assume identically sized subgroups, such that $N = GU$. Fig. 3.7 shows an example of a possible grouping of the users when $N = 6$, $G = 3$ and $U = 2$.

Consider equalization of the transmitted signals from the U users of the gth

[3]Note that the proposed scheme can easily be extended to group detection with overlapping subgroups.

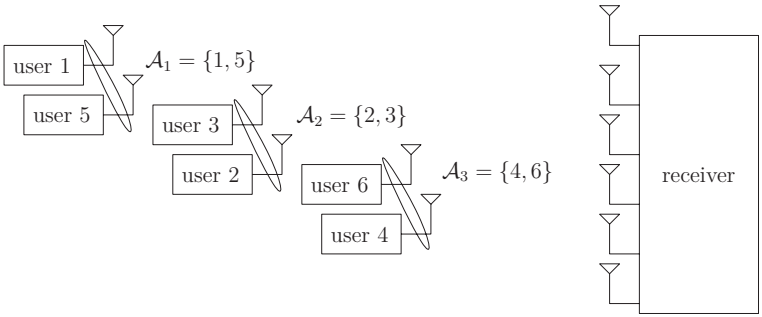

Figure 3.7.: Example for grouping 6 users into 3 subgroups. $G = 3$ and $U = 2$.

subgroup and kth data block. Correspondingly, the received signals can be split into two parts: the first part contains the transmitted signals from the users of the desired gth subgroup and the second part contains the interference components from the remaining $G-1$ subgroups and the additive Gaussian noise. By denoting $\mathbf{t}_g \equiv [\mathbf{b}_{a_1}^T, ..., \mathbf{b}_{a_u}^T, ..., \mathbf{b}_{a_U}^T]^T$, $\forall a_u \in \mathcal{A}_g$ as the vector containing the users' transmitted signals of the gth subgroup, we can rewrite (2.52) as

$$\mathbf{r} = \overline{\mathbf{H}}_g \mathbf{t}_g + \sum_{j=1, j\neq g}^{G} \overline{\mathbf{H}}_j \mathbf{t}_j + \mathbf{n}, \tag{3.72}$$

where $\overline{\mathbf{H}}_g \equiv [\mathbf{H}_{c,a_1}, ..., \mathbf{H}_{c,a_u}, ..., \mathbf{H}_{c,a_U}] \in \mathbb{C}^{QM \times QU}$, $a_u \in \mathcal{A}_g$ is the gth subgroup's channel matrix. Here, the term $\sum_{j=1,j\neq g}^{G} \overline{\mathbf{H}}_j \mathbf{t}_j$ denotes the interference components from the $G-1$ non-desired subgroups. For a compact notation of (3.72), we define

$$\overline{\overline{\mathbf{H}}}_g \equiv [\overline{\mathbf{H}}_1, ..., \overline{\mathbf{H}}_{g-1}, \overline{\mathbf{H}}_{g+1}, ..., \overline{\mathbf{H}}_G], 1 \leq g \leq G \tag{3.73}$$

and

$$\mathbf{f}_g \equiv [\mathbf{t}_1^T, ..., \mathbf{t}_{g-1}^T, \mathbf{t}_{g+1}^T, ..., \mathbf{t}_G^T]^T, 1 \leq g \leq G \tag{3.74}$$

as the matrix and the vector containing all users' channels and all users' transmitted signals, respectively, except those from the gth subgroup. Equipped with (3.73) and (3.74), Eqn. (3.72) can be compactly written as

$$\mathbf{r} = \overline{\mathbf{H}}_g \mathbf{t}_g + \overline{\overline{\mathbf{H}}}_g \mathbf{f}_g + \mathbf{n}. \tag{3.75}$$

3.5.2. Derivation of Frequency Domain Filter Coefficients

The hybrid equalizer performs soft interference cancellation and frequency domain MMSE filtering for groupwise separation of the users' transmitted signals. Specifically, following the standard SC-MMSE approach (see Section 3.2), it uses the available *a priori* LLR sequences $\boldsymbol{\zeta}_e[\mathbf{b}_n]$, $n = 1, ..., N$ to compute soft-estimates $\bar{b}_{q,n} = \mathbb{E}\big[b_{q,n}|\zeta_e[b_{q,n}]\big]$ for each transmitted symbol using the conditional mean estimator. As for the standard SC-MMSE FDE, the soft-estimates are used to construct a soft replica $\bar{\mathbf{r}}$ of the gth subgroup's desired signals and the interference components. It then performs soft interference cancellation and linear groupwise MMSE filtering of the received signal $\mathbf{r}$ to separate the transmitted signals into G independent subgroups. In contrast to the standard SC-MMSE approach from Section 3.2 that performs ISI/MAI cancellation on a user-by-user basis, the groupwise MMSE filter suppresses all residual interference components from non-desired subgroups as well as the desired subgroup's residual ISI components, while preserving the effective degrees of freedom of the desired subgroup's spatial components for joint signal MAP detection.

Let us define by $\mathbf{W}_g \equiv [\mathbf{W}_{g,1}, ..., \mathbf{W}_{g,u}, ..., \mathbf{W}_{g,U}] \in \mathbb{C}^{QM\times QU}$, $1 \leq g \leq G$ the filtering matrix for the gth subgroup, where each sub-matrix

$$\mathbf{W}_{g,u} \equiv [\mathbf{W}_{g,u,1}^H, ..., \mathbf{W}_{g,u,m}^H, ..., \mathbf{W}_{g,u,M}^H]^H \tag{3.76}$$

with $\mathbf{W}_{g,u,m} \in \mathbf{C}^{Q\times Q}$ defines the filter matrix corresponding to the uth user. Based on the modified system model in (3.75), the filter output signal at the gth subgroup, which is an estimate of $\mathbf{t}_g$, can be expressed as

$$\begin{aligned}\mathbf{z}_g &= \mathbf{W}_g^H\big(\mathbf{r} - \bar{\mathbf{r}}\big) + \mathbf{M}_g\bar{\mathbf{t}}_g \\ &= \mathbf{M}_g\mathbf{t}_g + (\mathbf{W}_g^H\overline{\mathbf{H}}_g - \mathbf{M}_g)\big(\mathbf{t}_g - \bar{\mathbf{t}}_g\big) + \mathbf{W}_g^H\overline{\overline{\mathbf{H}}}_g\big(\mathbf{f}_g - \bar{\mathbf{f}}_g\big) + \mathbf{W}_g^H\mathbf{n},\end{aligned} \tag{3.77}$$

where $\bar{\mathbf{t}}_g$ and $\bar{\mathbf{f}}_g$ are the conditional mean of $\mathbf{t}_g$ and $\mathbf{f}_g$, respectively, and $\mathbf{M}_g \in \mathbb{C}^{QU\times QU}$ is the equivalent channel matrix after groupwise MMSE filtering,

$$\mathbf{M}_g \equiv \begin{bmatrix} \mathbf{M}_{g,1,1} & \dots & \mathbf{M}_{g,1,U} \\ \vdots & \ddots & \vdots \\ \mathbf{M}_{g,U,1} & \dots & \mathbf{M}_{g,U,U} \end{bmatrix} \tag{3.78}$$

with $\mathbf{M}_{g,i,j} \in \mathbb{C}^{Q\times Q}$, $1 \leq i, j \leq U$ being diagonal sub-matrices, whose entries are given by

$$\mathbf{M}_{g,i,j} \equiv \mathrm{ddiag}(\mathbf{W}_{g,i}^H\mathbf{H}_{c,a_j}), a_j \in \mathcal{A}_g.$$

Note that in (3.77) the first term represents the received signal of the desired gth subgroup, the second term represents the residual self-interference components from all users within the gth subgroup, the third term represents the residual interference components from the users' signals of the remaining $G-1$ subgroups ($j \neq g$), and the last term represents filtered additive Gaussian noise.

Similar to Assumption 3.3, we restrict $\mathbf{W}_g$ to be block-circulant to efficiently implement (3.77) into the frequency domain. Using again the eigendecomposition property (2.14) of a circulant matrix, $\mathbf{W}_g$ can then be decomposed into

$$\mathbf{W}_g = \mathbf{F}_M^H \widehat{\mathbf{\Gamma}}_g \mathbf{F}_U, \tag{3.79}$$

where $\widehat{\mathbf{\Gamma}}_g \equiv [\widehat{\mathbf{\Gamma}}_{g,1}, ..., \widehat{\mathbf{\Gamma}}_{g,u}, ..., \widehat{\mathbf{\Gamma}}_{g,U}] \in \mathbb{C}^{QM \times QU}$ is the frequency domain filtering matrix, consisting of sub-matrices $\widehat{\mathbf{\Gamma}}_{g,u} \equiv [\widehat{\mathbf{\Gamma}}_{g,u,1}^H, ..., \widehat{\mathbf{\Gamma}}_{g,u,m}^H, ..., \widehat{\mathbf{\Gamma}}_{g,u,M}^H]^H$ with $\widehat{\mathbf{\Gamma}}_{g,u,m} \in \mathbb{C}^{Q \times Q}$ being a diagonal matrix. Here the entry $[\widehat{\mathbf{\Gamma}}_{g,u,m}]_{q,q}$ denotes the gth subgroup's filter coefficient at frequency-bin q for user/receive antenna pair (a_u, m), $a_u \in \mathcal{A}_g$. By applying the matrix decomposition (3.79) to (3.77), the linear filtering equation can be converted into the frequency domain,

$$\begin{aligned} \underline{\mathbf{z}}_g &\equiv \mathbf{F}_U \mathbf{z}_g \\ &= \mathbf{M}_g \underline{\mathbf{t}}_g + (\mathbf{\Gamma}_g^H \overline{\mathbf{\Xi}}_g - \mathbf{M}_g)(\underline{\mathbf{t}}_g - \bar{\underline{\mathbf{t}}}_g) + \mathbf{\Gamma}_g^H \overline{\overline{\mathbf{\Xi}}}_g (\underline{\mathbf{f}}_g - \bar{\underline{\mathbf{f}}}_g) + \mathbf{\Gamma}_g^H \underline{\mathbf{n}}, \end{aligned} \tag{3.80}$$

where $\overline{\mathbf{\Xi}}_g = [\mathbf{\Xi}_{c,a_1}, ..., \mathbf{\Xi}_{c,a_u}, ..., \mathbf{\Xi}_{c,a_U}]$, $a_u \in \mathcal{A}_g$, $1 \leq g \leq G$ is the gth subgroup's frequency domain channel matrix, $\overline{\overline{\mathbf{\Xi}}}_g = [\overline{\mathbf{\Xi}}_1, ..., \overline{\mathbf{\Xi}}_{g-1}, \overline{\mathbf{\Xi}}_{g+1}, ..., \overline{\mathbf{\Xi}}_G]$, and $\underline{\mathbf{t}}_g = \mathbf{F}_U \mathbf{t}_g$, $\bar{\underline{\mathbf{t}}}_g = \mathbf{F}_U \bar{\mathbf{t}}_g$, $\underline{\mathbf{f}}_g = \mathbf{F}_{N-U} \mathbf{f}_g$, $\bar{\underline{\mathbf{f}}}_g = \mathbf{F}_{N-U} \bar{\mathbf{f}}_g$, and $\underline{\mathbf{n}} = \mathbf{F}_M \mathbf{n}$. Moreover, using (3.79), we can also write (3.78) as

$$\mathbf{M}_g = \mathbf{F}_U^H \mathbf{M}_g \mathbf{F}_U = \mathbf{U}_g \otimes \mathbf{I}_Q,$$

where $\mathbf{U}_g \in \mathbb{C}^{U \times U}$ with the (i,j)th element being given as

$$[\mathbf{U}_g]_{i,j} = Q^{-1} \mathrm{Trace}\Big(\widehat{\mathbf{\Gamma}}_{g,i}^H \mathbf{\Xi}_{c,a_j}\Big), 1 \leq i,j \leq U, a_j \in \mathcal{A}_g. \tag{3.81}$$

The average unconditional linear MSE between the gth subgroup's transmitted signals and the filter output (3.80) is used as a design criterion for the groupwise MMSE filter $\widehat{\mathbf{\Gamma}}_g$,

$$\mathrm{MSE}_g^{\mathrm{GrFD}} \equiv Q^{-1} \mathbb{E}\Big[\Big\| \underline{\mathbf{z}}_g - \mathbf{M}_g \underline{\mathbf{t}}_g \Big\|^2 \Big]. \tag{3.82}$$

By rewriting the frequency domain covariance matrix of the residual signal $\underline{\mathbf{r}} - \bar{\underline{\mathbf{r}}}$ in

(3.28) as

$$\mathbf{\Psi}^{\text{FD}} = \overline{\mathbf{\Xi}}_g \mathbf{\Lambda}_g^{(1)} \overline{\mathbf{\Xi}}_g^H + \overline{\overline{\mathbf{\Xi}}}_g \mathbf{\Lambda}_g^{(2)} \overline{\overline{\mathbf{\Xi}}}_g^H + \sigma_0^2 \mathbf{I} \tag{3.83}$$

with $\mathbf{\Lambda}_g^{(1)}$ and $\mathbf{\Lambda}_g^{(2)}$ being the covariance matrices of the vectors $\underline{\mathbf{t}}_g$ and $\underline{\mathbf{f}}_g$, respectively,

$$\begin{aligned}
\mathbf{\Lambda}_g^{(1)} &\equiv \mathbb{E}\Big[\mathbb{E}\Big[\Big(\underline{\mathbf{t}}_g - \bar{\underline{\mathbf{t}}}_g\Big)\Big(\underline{\mathbf{t}}_g - \bar{\underline{\mathbf{t}}}_g\Big)^H \Big| \boldsymbol{\zeta}_e[\mathbf{t}_g]\Big]\Big] \\
&= \hat{\mathbf{\Lambda}}_g \otimes \mathbf{I}_Q, \qquad (3.84) \\
\mathbf{\Lambda}_g^{(2)} &\equiv \mathbb{E}\Big[\mathbb{E}\Big[\Big(\underline{\mathbf{f}}_g - \bar{\underline{\mathbf{f}}}_g\Big)\Big(\underline{\mathbf{f}}_g - \bar{\underline{\mathbf{f}}}_g\Big)^H \Big| \boldsymbol{\zeta}_e[\mathbf{f}_g]\Big]\Big] \\
&= \text{diag}\Big(\text{diag}(\mathbf{\Lambda}_1^{(1)}), ..., \text{diag}(\mathbf{\Lambda}_{g-1}^{(1)}), \text{diag}(\mathbf{\Lambda}_{g+1}^{(1)}), ..., \text{diag}(\mathbf{\Lambda}_G^{(1)})\Big) \qquad (3.85)
\end{aligned}$$

with $\hat{\mathbf{\Lambda}}_g \equiv \text{diag}\Big(1 - \bar{\varphi}_{a_1}, ..., 1 - \bar{\varphi}_{a_u}, ..., 1 - \bar{\varphi}_{a_U}\Big)$, $a_u \in \mathcal{A}_g$, the MSE in (3.82) can be expressed as

$$\begin{aligned}
\text{MSE}_g^{\text{GrFD}} &= Q^{-1}\text{Trace}\left(\hat{\mathbf{\Gamma}}_g^H \mathbf{\Psi}^{\text{FD}} \hat{\mathbf{\Gamma}}_g - \hat{\mathbf{\Gamma}}_g^H \overline{\mathbf{\Xi}}_g \mathbf{\Lambda}_g^{(1)} \mathbf{M}_g^H - \mathbf{M}_g \mathbf{\Lambda}_g^{(1)} \overline{\mathbf{\Xi}}_g^H \hat{\mathbf{\Gamma}}_g + \mathbf{M}_g \mathbf{\Lambda}_g^{(1)} \mathbf{M}_g^H\right) \\
&= Q^{-1}\text{Trace}\left(\hat{\mathbf{\Gamma}}_g^H \mathbf{\Psi}^{\text{FD}} \hat{\mathbf{\Gamma}}_g - \mathbf{M}_g \mathbf{\Lambda}_g^{(1)} \mathbf{M}_g^H\right). \qquad (3.86)
\end{aligned}$$

With the MSE in (3.86) as our cost function, the linear filtering problem reads as

$$\begin{aligned}
\tilde{\mathbf{\Gamma}}_g = \arg \min_{\hat{\mathbf{\Gamma}}_g \in \mathbb{C}^{MQ \times UQ}} & Q^{-1}\text{Trace}\Big(\hat{\mathbf{\Gamma}}_g^H \mathbf{\Psi}^{\text{FD}} \hat{\mathbf{\Gamma}}_g - \mathbf{M}_g \mathbf{\Lambda}_g^{(1)} \mathbf{M}_g^H\Big) \\
\text{s.t. } & \text{diag}(\mathbf{M}_g) = \mathbf{1}_{UQ}, \qquad (3.87)
\end{aligned}$$

where the constraint on matrix $\mathbf{M}_g$ is imposed to avoid the trivial solution $\tilde{\mathbf{\Gamma}}_g = \mathbf{0}$. To express (3.87) in a more convenient form, we define by $\check{\mathbf{\Gamma}}_g \equiv \hat{\mathbf{\Gamma}}_g(\mathbf{I}_U \otimes \mathbf{1}_Q) \in \mathbb{C}^{QM \times U}$ and $\mathbf{\Upsilon}_g \equiv \overline{\mathbf{\Xi}}_g(\mathbf{I}_U \otimes \mathbf{1}_Q) \in \mathbb{C}^{QM \times U}$ the subgroup's filtering and channel matrix, respectively. Using these notations, the MSE in (3.86) can be written as

$$\begin{aligned}
\text{MSE}_g^{\text{GrFD}} &= Q^{-1}\text{Trace}\Big(\hat{\mathbf{\Gamma}}_g^H \mathbf{\Psi}^{\text{FD}} \hat{\mathbf{\Gamma}}_g - (\mathbf{U}_g \otimes \mathbf{I}_U)(\hat{\mathbf{\Lambda}}_g \otimes \mathbf{I}_U)(\mathbf{U}_g^H \otimes \mathbf{I}_H)\Big) \\
&= Q^{-1}\text{Trace}\Big(\check{\mathbf{\Gamma}}_g^H \mathbf{\Psi}^{\text{FD}} \check{\mathbf{\Gamma}}_g - Q\mathbf{U}_g \hat{\mathbf{\Lambda}}_g \mathbf{U}_g^H\Big) \\
&= Q^{-1}\text{Trace}\Big(\check{\mathbf{\Gamma}}_g^H \mathbf{\Psi}^{\text{FD}} \check{\mathbf{\Gamma}}_g - Q^{-1}\check{\mathbf{\Gamma}}_g^H \mathbf{\Upsilon}_g \hat{\mathbf{\Lambda}}_g \mathbf{\Upsilon}_g^H \check{\mathbf{\Gamma}}_g\Big) \\
&= Q^{-1}\text{Trace}\Big(\check{\mathbf{\Gamma}}_g^H \mathbf{\Psi}_0^{\text{FD}} \check{\mathbf{\Gamma}}_g\Big) \qquad (3.88)
\end{aligned}$$

where $\mathbf{\Psi}_0^{\text{FD}} \equiv \mathbf{\Psi}^{\text{FD}} - Q^{-1}\mathbf{\Upsilon}_g \hat{\mathbf{\Lambda}}_g \mathbf{\Upsilon}_g^H$. Based on (3.88), we can rewrite the optimization

problem (3.87) as

$$\begin{aligned}\breve{\mathbf{\Gamma}}_g \equiv \arg \min_{\breve{\mathbf{\Gamma}}_g \in \mathbb{C}^{MQ\times U}} & Q^{-1}\mathrm{Trace}\big(\breve{\mathbf{\Gamma}}_g^H \mathbf{\Psi}_0^{\mathrm{FD}} \breve{\mathbf{\Gamma}}_g\big) \\ \text{s.t. } & Q^{-1}\mathrm{diag}(\breve{\mathbf{\Gamma}}_g^H \mathbf{\Upsilon}_g) = \mathbf{1}_U. \end{aligned} \tag{3.89}$$

In Appendix B, it is shown that $\breve{\mathbf{\Gamma}}_g$ under the constraint in (3.89) can be derived as

$$\breve{\mathbf{\Gamma}}_g = \mathbf{\Psi}^{\mathrm{FD}-1}\mathbf{\Upsilon}_g \mathbf{\Theta}_g^{-1}\mathbf{\Omega}_g^{-1}, \tag{3.90}$$

where

$$\begin{aligned}\mathbf{\Omega}_g &\equiv Q^{-1}\mathrm{ddiag}\big(\mathbf{\Upsilon}_g^H \mathbf{\Psi}^{\mathrm{FD}-1}\mathbf{\Upsilon}_g \mathbf{\Theta}_g^{-1}\big), \\ \mathbf{\Theta}_g &\equiv \mathbf{I}_U - Q^{-1}\hat{\mathbf{\Lambda}}_g \mathbf{\Upsilon}_g^H \mathbf{\Psi}^{\mathrm{FD}-1}\mathbf{\Upsilon}_g.\end{aligned}$$

Rewriting (3.90) in the diagonal-block form (3.79), the optimal groupwise frequency domain MMSE filter $\tilde{\mathbf{\Gamma}}_g$ is obtained as

$$\tilde{\mathbf{\Gamma}}_g = \mathbf{\Psi}^{\mathrm{FD}-1}\overline{\mathbf{\Xi}}_g\big(\mathbf{\Theta}_g^{-1}\mathbf{\Omega}_g^{-1} \otimes \mathbf{I}_Q\big). \tag{3.91}$$

Lemma 3.11. By setting $U = 1$, the proposed hybrid equalizer is equivalent to the conventional biased SC-MMSE FDE.

For the special case of $U = 1$, i.e., the gth set $\mathcal{A}_g$ contains only the index of one user, Eqn. (3.91) reduces to the unbiased frequency domain MMSE filter

$$\tilde{\mathbf{\Gamma}}_g = \frac{\mathbf{\Psi}^{\mathrm{FD}-1}\overline{\mathbf{\Xi}}_g}{Q^{-1}\mathrm{Trace}(\overline{\mathbf{\Xi}}_g^H \mathbf{\Psi}^{\mathrm{FD}-1}\overline{\mathbf{\Xi}}_g)}. \tag{3.92}$$

The equalizer structure based on (3.92) and the conventional biased SC-MMSE FDE [KM07], [AJL07], [TH02], [YGWP08] have an identical LLR decision metric. Therefore, both schemes have equal performance in terms of BER.

Using (3.91) and (3.77), we may finally express the groupwise time-domain filter output at the equalizer as

$$\mathbf{z}_g = \tilde{\mathbf{M}}_g \mathbf{t}_g + \mathbf{v}_g, \tag{3.93}$$

where $\tilde{\mathbf{M}}_g = \breve{\mathbf{U}}_g \otimes \mathbf{I}_Q$ with $\breve{\mathbf{U}}_g = Q^{-1}\breve{\mathbf{\Gamma}}_g^H \mathbf{\Upsilon}_g$, and $\mathbf{v}_g$ is the residual interference plus noise term.

3.5.3. Joint Detection

After groupwise filtering of the received signals, joint detection of the users' signals within one subgroup is performed. The symbol estimates corresponding to the users' signals of the gth subgroup to be jointly detected are first grouped together into vectors $\mathbf{z}_{g,q} \equiv [z_{q,a_1}, ..., z_{q,a_u}, ..., z_{q,a_U}]^T \in \mathbb{C}^{U\times 1}$, $a_u \in \mathcal{A}_g$, for all $q = 1, ..., Q$. These vectors are given by

$$\begin{aligned}\mathbf{z}_{g,q} &= \mathbf{S}_q \mathbf{z}_g \\ &= \breve{\mathbf{U}}_g \mathbf{t}_{g,q} + \mathbf{v}_{g,q},\end{aligned} \tag{3.94}$$

where $\mathbf{c}_{g,q} = \mathbf{S}_q \mathbf{t}_g$ and $\mathbf{v}_{g,q} = \mathbf{S}_q \mathbf{v}_g$ are the gth subgroup's transmitted signal vector and the residual interference and noise vector during the qth transmission period, respectively, obtained from $\mathbf{t}_g$ and $\mathbf{v}_g$ by multiplication with selection matrix $\mathbf{S}_q \equiv \mathbf{I}_U \otimes \mathbf{e}_q^T$. The equivalent channel matrix $\breve{\mathbf{U}}_g$ in (3.94) is found with (3.90) as

$$\breve{\mathbf{U}}_g = Q^{-1} \mathbf{\Omega}_g^{-1} \mathbf{\Theta}_g^{-1} \mathbf{\Upsilon}_g^H \mathbf{\Psi}^{\text{FD}-1} \mathbf{\Upsilon}_g.$$

In order to compute LLR messages for the filtered signal components $\mathbf{z}_{g,q}$ in (3.94), we resort to the Gaussian approximation of the residual interference plus noise term at the filter output.

Assumption 3.12. The distribution of the residual interference plus noise vector $\mathbf{v}_{g,q}$ can be modeled as a multivariate circularly-symmetric Gaussian distributed random vector with zero-mean and covariance matrix

$$\begin{aligned}\mathbf{R}_g &= \mathbb{E}[\mathbf{v}_{g,q} \mathbf{v}_{g,q}^H] \\ &= Q^{-1} \mathbf{\Omega}_g^{-1} \mathbf{\Theta}_g^{-1} \mathbf{\Upsilon}_g^H \mathbf{\Psi}^{\text{FD}-1} \mathbf{\Upsilon}_g \mathbf{\Omega}_g^{-1}.\end{aligned} \tag{3.95}$$

We remark that $\breve{\mathbf{U}}_g$ and $\mathbf{R}_g$ are identical for all (q, k) and have to be computed only once for each subgroup and turbo iteration. Therefore, the *extrinsic* LLR for each b_{q,a_u} is obtained as [CMT04]

$$\lambda_e[b_{q,a_u}] = \log \frac{\sum\limits_{\mathbf{x}\in\mathcal{X}_u^{<+1>}} \exp\left[\rho_{g,q} + \sum\limits_{\forall j: j\neq u, x_j=+1} \zeta_e[b_{q,a_j}]\right]}{\sum\limits_{\mathbf{x}\in\mathcal{X}_u^{<-1>}} \exp\left[\rho_{g,q} + \sum\limits_{\forall j: j\neq u, x_j=+1} \zeta_e[b_{q,a_j}]\right]}, \tag{3.96}$$

where $\rho_{g,q}$ is the MAP-decision metric, defined as

$$\rho_{g,q} \equiv -\left(\mathbf{z}_{g,q} - \breve{\mathbf{U}}_g \mathbf{x}\right)^H \mathbf{R}_g^{-1} \left(\mathbf{z}_{g,q} - \breve{\mathbf{U}}_g \mathbf{x}\right), \tag{3.97}$$

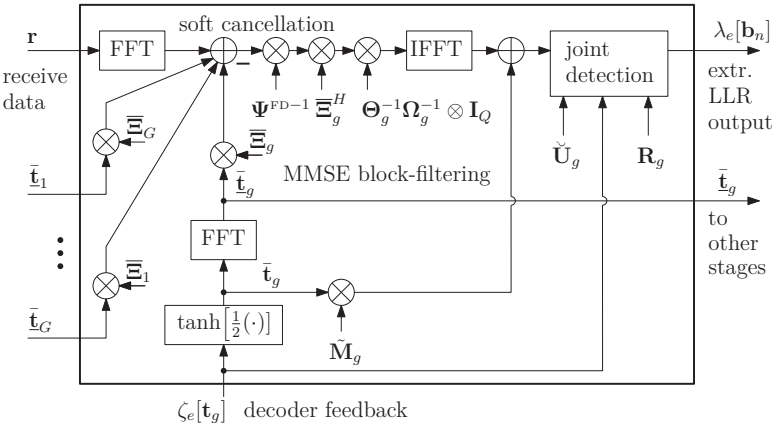

Figure 3.8.: Signal flow chart of the hybrid SC-MMSE FDE for the gth subgroup.

and $\mathcal{X}_u^{<\pm 1>}$ is the set of 2^U BPSK data symbols $\mathbf{x} \in \mathcal{X}_u^{<\pm 1>}$ for which the uth component $x_u = \pm 1$.

Fig. 3.8 depicts the corresponding signal flow chart to the hybrid scheme based on (3.96).

3.5.4. Comparison with other Criteria

Different alternative choices of optimization criteria can be used for cancellation of interference components between subgroups. In [VBC06], equalization is performed by linear filtering minimizing the unconditional MSE

$$\text{minimize } Q^{-1}\mathbb{E}\left[\left\|\mathbf{K}_g\left(\mathbf{r}-\overline{\overline{\mathbf{H}}}_g\bar{\mathbf{f}}_g\right)-\mathbf{t}_g\right\|^2\right], \tag{3.98}$$

where $\mathbf{K}_g \in \mathbb{C}^{QU\times QM}$ is the time domain MMSE block-filtering matrix. Also, as shown in [VBC06], a frequency domain equivalent can be derived from $\mathbf{K}_g$ by utilizing the eigenvalue decomposition of the circulant channel matrices. We note that the criterion in (3.98) in the absence of *a priori* information is simply a block-wise notation of the symbol-wise (unconditional) MSE formulation from [TH02]. The SC-MMSE filtering block resulting from (3.98) is therefore during the first turbo iteration equivalent to the standard SC-MMSE filtering that removes interference user-by-user from the received signal to separate the transmitted signals. Unlike to the above MSE criterion, the objective of our criterion (3.87) is to obtain a frequency domain groupwise MMSE filter that jointly suppresses residual interferences

for the users' signals in each subgroup. Besides, more important, only the MSE in (3.82) can be used to evaluate the performance of each subgroup, which is needed for adaptive user grouping incorporating *a priori* information from channel decoding, as considered in Section 3.5.5.

Recently, the authors of [MJLL10] proposed a groupwise filtering technique maximizing the SINR in each subgroup for non-iterative joint detection of multi-antenna signals in flat-fading MIMO channels. Here, we extend the approach from [MJLL10] to iterative frequency domain soft interference cancellation equalization employing groupwise maximum-SINR filtering. Using the notations in (3.72)-(3.77), the filtering matrix maximizing the SINR for the gth subgroup can be obtained as

$$\mathring{\mathbf{\Gamma}}_g \equiv \arg \max_{\{\widehat{\mathbf{\Gamma}}_g \in \mathbb{C}^{QM \times QU}\}} \text{SINR}_g, \tag{3.99}$$

where SINR_g is defined as

$$\text{SINR}_g \equiv \frac{\mathbb{E}\Big[\|\mathbf{M}_g \mathbf{t}_g\|^2 \Big]}{\mathbb{E}\Big[\|\mathbf{z}_g - \mathbf{M}_g \mathbf{t}_g\|^2 \Big]}.$$

As shown in Appendix B, the optimal value of $\mathring{\mathbf{\Gamma}}_g$ can be found as a solution of a generalized eigenvalue problem.

We now present a theorem that compares the proposed MSE and SINR criteria.

Theorem 3.13. The groupwise hybrid equalizers based on MSE and SINR criteria in (3.87) and (3.99), respectively, have an identical MAP decision metric.

Proof. The proof is given in Appendix A.3. □

The groupwise MMSE and SINR-based filter designs in (3.87) and (3.99), respectively, thus lead to turbo equalizer structures having identical complexities and *extrinsic* output LLRs.

3.5.5. Group Selection Methods

The performance of the hybrid turbo equalizer is largely determined by the assignment of the users' signals to subgroups. In [MJLL10], a GS method based on a capacity criterion was proposed that maximizes the achievable information rate of MIMO systems employing non-iterative group detection. The same authors presented in [JLML08] a grouping scheme using a min-max subgroup SINR formulation. The algorithms in [MJLL10] and [JLML08] compute the GS metric for all possible group partitions, and then select the optimum one. Since calculating the GS metric for each partition involves a number of complex matrix calculations, these schemes

are restricted to systems having a small number of users or groupings which generate large subgroups. Other GS methods exploiting the channel correlation matrix $\mathbf{S}$ have been presented in [LHLF00] and [GM07]. The algorithm in [LHLF00] optimizes the grouping for each individual antenna of the MIMO system by allowing overlapping subgroups. Although such an antenna-by-antenna optimized scheme maximizes performance, it requires very high complexity cost in practical system configurations. The GS approach from [GM07] reduces complexity by adopting only max/min operations to successively form disjoint subgroups maximizing the pairwise correlation sum.

In this subsection, several new GS criteria for groupwise MMSE turbo equalization are proposed. Particularly, an algorithm is presented that computes an MSE criterion using the available *a priori* knowledge about the code bits to find, among all possible combinations of G subgroups, the group partition guaranteeing optimum performance at each turbo iteration. Also, different schemes providing a static grouping valid for all turbo iterations are discussed. In this regard, a very simple channel correlation-based algorithm is proposed which does not need max/min or compare operations. The performance of these methods will be compared in Section 3.7.

3.5.5.1. Grouping based on Min-Max-MSE

First, we propose a GS criterion based on minimization of the MSE at the groupwise filter output. The MSE for the gth subgroup is obtained by substituting (3.90) into (3.86), which results in the following expression:

$$\mathrm{MSE}_g^{\mathrm{GrFD}} = \mathrm{Trace}(\mathbf{\Omega}_g^{-1}). \tag{3.100}$$

The overall performance of the hybrid equalizer is mainly dominated by the subgroup, whose MSE is the highest among all subgroups. In order to maximize performance, we select among all possible group partitions the one that minimizes the worst subgroup's MSE. A convenient criterion for grouping N users into G subgroups is therefore given by

$$\hat{s} = \arg \min_{1 \le s \le S} \max_{1 \le g \le G} \mathrm{Trace}(\mathbf{\Omega}_g^{(s)-1}), \tag{3.101}$$

where S denotes the total number of possible combinations of pairs, and $\mathrm{Trace}(\mathbf{\Omega}_g^{(s)-1})$ is the MSE of the gth subgroup corresponding to the sth ($1 \le s \le S$) combination. Based on (3.101), we devise a simple method, which is summarized in Algorithm 3.1, that dynamically forms G subgroups at each turbo iteration.

Algorithm 3.1 requires the calculation of $T = \binom{N}{U}$ inverses of $U \times U$ matrices, and it

Algorithm 3.1 Dynamic MSE-based grouping

1: Calculate at each turbo iteration the MSE in (3.100) for all subgroups and possible pairings.
2: Solve (3.101).

needs to perform the minimum operation $S = \binom{N}{U}\binom{N-U}{U}\cdots\binom{U}{U}/(G\cdot(G-1)\cdot\ldots\cdot 2)$ times. This leads to a high complexity if the numbers of users or subgroups are large. For example, for $N = 16$ and $G = 4$, we obtain $T = 1820$ and $S = 2627625$. To reduce complexity, instead of dynamically forming the subgroups at each turbo iteration, a static set can be used for all turbo iterations. This is the motivation behind the second grouping method, which is summarized in Algorithm 3.2, that performs the allocation in (3.101) only once at the first turbo iteration.

Algorithm 3.2 Static MSE-based grouping

1: Calculate at the first turbo iteration the MSE in (3.100) for all subgroups and possible pairings.
2: Solve (3.101).

The MSE in (3.100) could also be replaced by the subgroup SINR (B.18). However, calculating the SINR requires for each possible partition the Cholesky factorization and the eigenvalue decomposition of the large $QM \times QM$ matrices (B.15) and (B.16), respectively, which may be impractical for large FFT-sizes and number of receive antennas.

3.5.5.2. Grouping based on Channel Correlation

Next, we propose a correlation-based method to assign users into subgroups. For this purpose, let us define by

$$\bar{\rho}_{n,l} = \frac{\mathrm{Trace}\left(\boldsymbol{\Xi}_{c,n}^{H}\boldsymbol{\Xi}_{c,l}\right)}{\sqrt{\mathrm{Trace}\left(\boldsymbol{\Xi}_{c,n}\boldsymbol{\Xi}_{c,n}^{H}\right)}\cdot\sqrt{\mathrm{Trace}\left(\boldsymbol{\Xi}_{c,l}\boldsymbol{\Xi}_{c,l}^{H}\right)}}$$

the pairwise normalized correlation coefficient between user channel n and l. Further, let $\mathbf{L}$ be the upper triangular correlation matrix with entries

$$[\mathbf{L}]_{n,l} = \begin{cases} \bar{\rho}_{n,l}, n < l \\ 0, \text{ otherwise.} \end{cases}$$

At high SNR, the performance of the equalizer is largely influenced by the minimum euclidean distance between the users' channels of the G subgroups. It is therefore

desirable to find a group partition that minimizes the maximum pairwise channel correlation between members of different subgroups. Given the normalized correlation matrix $\mathbf{L}$, this problem can formally be expressed as

$$\min \max_{n\in\mathcal{A}_{g_1}, l\in\mathcal{A}_{g_2}, g_1\neq g_2, 1\leq g_1, g_2\leq G} \bar{\rho}_{n,l}. \tag{3.102}$$

Solving (3.102) is a combinatorial problem that requires an exhaustive search over all possible partitions. Obviously, this is prohibitively expensive in terms of complexity for large N and G. Instead, we propose a greedy approach, which yields a suboptimal solution, but reduces drastically the computational load. The proposed method is listed in Algorithm 3.3.

Algorithm 3.3 Static correlation-based grouping

1: Initialize the subgroup sets $\mathcal{A}_n = \{n\}$, $n = 1, ..., N$.
2: Initialize the set containing the user indices $\mathcal{N} = \{1, ..., N\}$.
3: Sort the normalized cross-correlation values of matrix $\mathbf{L}$ in descending order in a vector $\mathbf{l}$, and keep the information of the user indices i, j in $\mathbf{L}$.
4: Set $l = 1$.
5: **if** $|\mathcal{N}| > G$ **then**
6: Select the lth position in vector $\mathbf{l}$. Let i, j be the corresponding indexes to that position.
7: **if** $i \in \mathcal{A}_{n_1}$ and $j \in \mathcal{A}_{n_2}$, $n_1 \neq n_2$, $n_1, n_2 \in \mathcal{N}$ **then**
8: **if** $|\mathcal{A}_{n_1}| + |\mathcal{A}_{n_2}| \leq U$ **then**
9: $\mathcal{A}_{n_1} = \mathcal{A}_{n_1} \cup \mathcal{A}_{n_2}$
10: Remove index n_2 from set $\mathcal{N}$.
11: **end if**
12: **end if**
13: **end if**
14: Increment l, and repeat step 5 until the last element of vector $\mathbf{l}$, or if G subgroups are filled, i.e., $|\mathcal{N}| = G$.

Algorithm 3.3 first allocates the N users into N subgroups, and sorts the correlation values of matrix $\mathbf{L}$ in descending order in a vector $\mathbf{l}$. The algorithm then iteratively allocates two users corresponding to the lth position (iteration index l) of vector $\mathbf{l}$ into one subgroup (lines 5-13). At each iteration, the two groups having the maximum pairwise channel correlation are merged. As a result, highly spatially correlated users are allocated to the same subgroup. This selection may not be optimal with respect to (3.102), however, it reduces the noise enhancement due to the MMSE interference suppression of highly correlated user signals. The advantage of Algorithm 3.3 over the other two methods is that search complexity is significantly reduced and computation of matrix inverses is not required.

Table 3.1.: Number of complex multiplications/divisions per symbol and per iteration of different equalizers.

Algorithm	Multiplications/Divisions
SC-MMSE TDE	$2/3M^3L^3 + 5M^2L^2$
	$+ ML((2+ML)N(2L-1)+7/3)+6$
SC-MMSE FDE	$2/3M^3 + 5M^2 + NM(2M+N+3) + 1/3M + 8$
FFT/IFFT operations	$(M(N+1)+2N)\log_2 Q$
HY SC-MMSE FDE	$GMU(2M+2U+1) + 2/3(GU^3+M^3)$
	$+6GU^2 + 5M^2 + 1/3(UG+M) + 6G + 4$
Group detection	$2^U U(2U+1)+1$
FFT/IFFT operations	$(M(N+1)+2N)\log_2 Q$

3.6. Complexity Comparison

An approximate operation count in terms of complex multiplications required by the SC-MMSE TDE, SC-MMSE FDE and HY SC-MMSE FDE per turbo iteration is shown in Table 3.1. For the complexity analysis, the calculation of the expected values of soft estimates requiring the $\tanh(\cdot)$ function as well as the calculation of channel estimates are not taken into account. It is assumed that the channel matrix is perfectly available in time domain, and has to be converted to the frequency domain for the use in the FDEs. Moreover, it is assumed that matrix inversions are performed by inversion of the Cholesky factorization [Kre05]. Note that the complexity of the PDA SC-MMSE FDE has not explicitly been listed in Table 3.1, as it is of the same order than that of the SC-MMSE FDE. Observing Table 3.1, we find that the time domain SC-MMSE algorithm essentially has an complexity order of $O(M^3L^3)$. The SC-MMSE and HY SC-MMSE FDEs both need $M(N+1)+2N$ Q-point FFT-operations per transmitted block, which is due to the frequency domain conversion of the received signal, the soft feedback from channel decoding and the channel estimates. However, as opposed to time domain filtering, the overall complexities for the quite realistic case of $M \geq N$ and $MN\log_2(Q) > M^3$, are of order $O\Big(MN\log_2 Q)\Big)$ and $O\Big(2^U U^2 + M(M^2 + N\log_2 Q)\Big)$, respectively, and thus independent of the channel memory length L due to the frequency domain processing. We remark that when the number of users per subgroup is high, i.e., for large values of U, the exact calculation of the LLRs (3.96) of the HY SC-MMSE FDE becomes computational expensive. In such cases, the complexity can be reduced by applying the list soft-output sphere detection [BGBF03].

3.7. Simulation Results

In this section, numerical results of BER, frame error rate (FER) and TP simulations conducted to evaluate the performances achieved by the turbo equalizers introduced above. We consider a single carrier cyclic prefix assisted block-based transmission with FFT-size $Q = 128$ or $Q = 512$. The length of the cyclic prefix is always set to the maximum channel delay. The channels gains are perfectly known at the receiver and remain static over a fixed number of transmitted blocks, but change independently from frame to frame. As channel encoding, we employ either the rate-compatible memory-3 SCC from [Pro01] with code rates $r_c = 1/2, 2/3$ and $7/8$ or the rate-compatible punctured, memory-4 SCCC proposed in [Tüc04] with code rates $r_c = 1/4, 1/2$, $3/4$ and $9/10$. The inner and outer encoders of the SCCC are the recursive rate-1 inner encoder with polynomials $(g_r, g_0) = (3, 2)$ and the recursive, systematic, rate-$1/2$ convolutional code with polynomials $(g_r, g_1) = (23, 35)$, respectively. Here, g_r denotes the feedback polynomial in octal notation. The overall rate of the SCCC is controlled through puncturing or by adding more generators and using puncturing, as specified in [Tüc04].

Three different system and channel setups are investigated for the simulations:

- First, we consider a single-user transmission over the $L = 10$-tap Rayleigh block-fading channel with uncorrelated receive and transmit antennas (i.e., $\mathbf{S} = \mathbf{R} = \mathbf{I}$) and equal average tap-energy. The number of transmit and receive antennas is set to $N = 2$ and $M = 2$, respectively. The SC-MMSE and PDA SC-MMSE FDEs with FFT-size $Q = 128$ are considered for equalization of the MIMO ISI channel. Both turbo receivers perform $T_e = 10$ iterations between the equalizer and the channel decoder. In addition, the PDA SC-MMSE FDE performs five internal iterations in each turbo iteration. The numbers of iterations are in general chosen to be large enough to ensure convergence of both turbo receivers.

- Second, we consider two multiuser transmission setups with $N = M = 4$ and $N = M = 8$ over the simple stochastic $L = 32$-tap Rayleigh block-fading MIMO channel employing the conventional SC-MMSE FDE and the proposed HY SC-MMSE FDEs with FFT size $Q = 512$. The delay power profile of the channel is uniform and the spatial channel correlation follows the Kronecker model from Section 2.3. The receive antennas are spatially uncorrelated, such that $\mathbf{R} = \mathbf{I}$. The number of turbo iterations of both receivers is identically set to $T_e = 10$.

- The third transmission setup is identical to the second one, except that the channel is an $L = 22$-tap measurement data-based MIMO channel. This sim-

Table 3.2.: Simulation Parameters.

Tx antennas N	$2, 4$ or 8
Rx antennas M	$2, 4$ or 8
FFT-length Q	128 or 512
Frame-length N_bQ	4096 symbols
Channel coding	
SCC	Code rates $r_c = 1/2$, $2/3$ or $7/8$
SCCC	Code rates $r_c = 1/4$, $1/2$, $3/4$ or $9/10$
Outer (mother) SCCC encoder	Recursive, memory-4, rate-1/2 SCC
Inner SCCC encoder	Rate-1 recursive conv. code
Channel model	
Stochastic channel model	$L = 10$ or 32-tap Rayleigh fading
Delay power profile	Equal average power per tap
Spatial correlation model	Kronecker model
Measurement data-based channel model	$L = 22$ tap channel
Interleaving	Random at each user
Turbo iterations	$T_e = 10$
Decoder iterations	$T_d = 10$
Channel estimation	Perfect

ulation setup is used to assess the performance of the proposed turbo receivers in real fields.

Table 3.2 summarizes the major simulation parameters.

3.7.1. Numerical Results for Setup 1

Fig 3.9 (a) and (b) depict the average BER performance versus E_b/N_0 achieved by the SC-MMSE and PDA SC-MMSE FDEs over Rayleigh fading MIMO ISI channels employing rate-compatible SCCs and SCCCs, respectively. Note that for the chosen number of internal iterations of the PDA SC-MMSE FDE we have observed that for all channel code configurations a steady state of the NMMSE estimation (3.60) is achieved.

Comparing the presented curves, it is found that the PDA SC-MMSE FDE offers improved BER performance compared to the conventional SC-MMSE FDE for both code classes at medium-to-large E_b/N_0. In detail, we see that the higher the rate of the channel code the larger the gain achieved by the PDA SC-MMSE FDE. This can be explained by the superiority of the NMMSE estimation over the MMSE estimation as it is used by the simple SC-MMSE filtering. The application of the internal equalizer iterations within the PDA SC-MMSE FDE leads to a better sup-

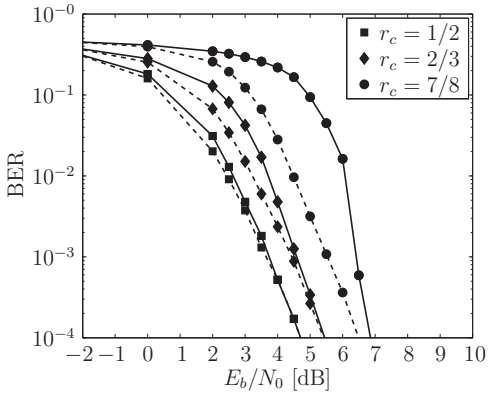

(a) Rate-compatible SCCs

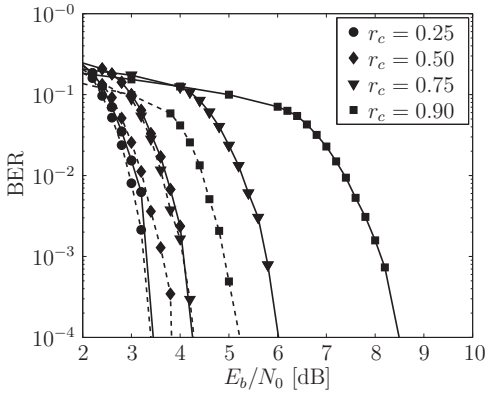

(b) Rate-compatible SCCCs

Figure 3.9.: Average BER performance of the SC-MMSE FDE (solid curves) and the PDA SC-MMSE FDE (dashed curves) utilizing channel codes with different rates.

pression of the residual interference components. Consequently, the reliability of the probabilistic information is increased at the equalizer output which results in an additional SNR gain of the *extrinsic* LLRs $\lambda_e[b_{q,n}]$. This additional SNR gain can be used by channel decoders of high rate codes to improve their error correcting capabilities. In addition, we see that strong error control codes, such as the SCCCs can achieve substantially higher gains than the weaker SCCs. This behavior will be explained in Chapter 4 when analyzing the convergence properties of both turbo

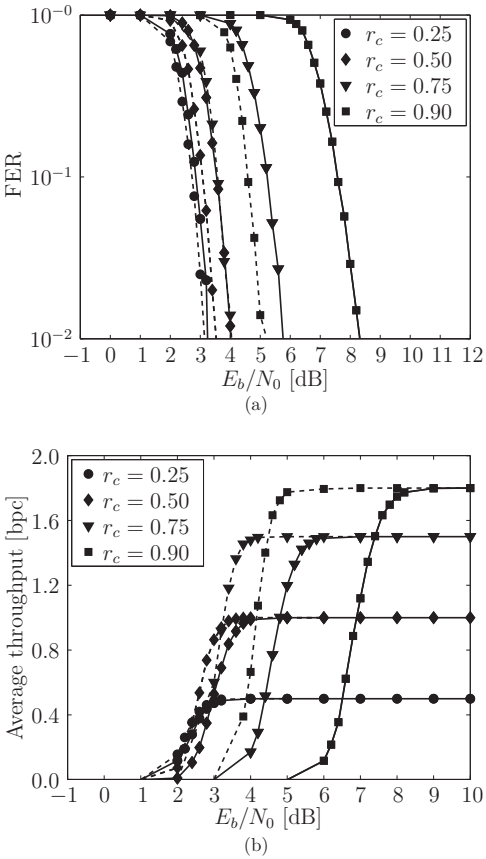

Figure 3.10.: Average FER performance (a) and TP performance (b) of the SC-MMSE FDE (solid curves) and the PDA SC-MMSE FDE (dashed curves) employing rate-compatible SCCCs.

receivers using correlation charts [Cho07].

The average FER and TP performances versus E_b/N_0 for both turbo systems are depicted in Fig. 3.10 (a) and (b), respectively. The throughput efficiency in bits per channel use (bpc) has been evaluated by assuming a selective-repeat automatic repeat-request (ARQ) system with infinite buffer size [LC98]. As it is evident from these figures, significant gains in FER as well as in throughput efficiency are obtained by the proposed PDA SC-MMSE scheme over the conventional SC-MMSE FDE.

This again justifies the usage of the PDA SC-MMSE FDE in spatially-uncorrelated MIMO ISI channels.

3.7.2. Numerical Results for Setup 2

Fig. 3.11 depicts the average BER performance versus E_s/N_0 achieved at each turbo iteration by the SC-MMSE FDE and HY SC-MMSE FDE for an $N = M = 4$ multiuser system in a scenario where all four users' channels are identically spatially correlated with parameter $\alpha = 0.0$ or $\alpha = 0.9$. The correlation factor α corresponds to the off-diagonal elements of the transmit correlation matrix $\mathbf{S}$, such that $[\mathbf{S}]_{i,j} = \alpha$ for $1 \leq i, j \leq N$, $i \neq j$. The groupsize of the hybrid turbo equalizer is set to $U = N$ ($G = 1$) such that all users are allocated into a single group. In this setup, all ISI components of the received signals from the M antennas are suppressed by groupwise SC-MMSE frequency domain filtering, while the separation of the transmitted signals from the N users is performed by MAP symbol detection. This solution is especially preferable in spatially-correlated MIMO channels with a large number of multipath components. As a reference curve, Fig. 3.11 also shows the simulation result of the corresponding MFB, achieved when all interference has been removed in the system. Again, the MFB serves as a lower bound on the BER of both turbo receivers here, obtained when the LLR feedback from the N channel decoders is perfect. According to Fig. 3.11, the two systems achieve identical BER performances at each turbo iteration. Both schemes offer the same signal separation capabilities when the users' channels are spatially uncorrelated ($\alpha = 0.0$). In addition, we also find that the gap to the MFB vanishes at medium-to-large SNRs E_s/N_0 ($E_s/N_0 > 0.8$ dB). In the presence of high spatial correlation ($\alpha = 0.9$), however, the numerical results impressively show that the HY SC-MMSE FDE outperforms the conventional turbo receiver. The SC-MMSE FDE looses 2.2 dB compared to the HY SC-MMSE FDE at a BER=10^{-4}. This phenomenon is caused by the fact that the hybrid scheme preserves the degrees of freedom of jointly detected user signals using the groupwise filtering approach and uses the optimal MAP algorithm for signal separation. Furthermore, it is interesting to note that the iteration gain of the two different receivers is almost identical and about 4 dB at a BER of 10^{-4} for both channels.

Next, we consider the $N = M = 8$ multiuser scenario with $[\mathbf{S}]_{i,j} = \alpha$ for $1 \leq i, j \leq 4$, $i \neq j$ and $[\mathbf{S}]_{i,j} = 0$ for $5 \leq i, j \leq 8$, $i \neq j$. We chose a groupsize of $U = 4$ ($G = 2$) and allocate the four correlated user signals into the first subgroup. Fig 3.12 (a) and (b) depict the resulting BER and FER curves, respectively, for the two subgroups and turbo receivers of this system setup with the correlation value α as a parameter. As it can be seen, the performance of users in the first subgroup

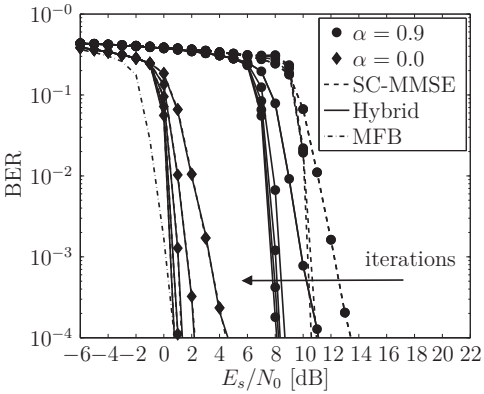

Figure 3.11.: Average BER performance of the proposed HY SC-MMSE FDE and the SC-MMSE FDE at each turbo iteration for an $N = M = 4$ multiuser transmission over Rayleigh block-fading channels with a spatial transmit correlation coefficient of $\alpha = 0.0$ and $\alpha = 0.9$.

significantly degrades for both turbo schemes with increasing values of α. Clearly, the larger the spatial correlation the larger the gain achieved by the HY SC-MMSE scheme over the conventional equalizer. On the other hand, we observe that the performances of users in the second subgroup are nearly identical for all values of α, indicating that both turbo schemes can perfectly separate the users' signals between both subgroups.

More importantly, we observe that the slope of the FER curves remains identical when increasing the value of α, implying that the achievable diversity order is maintained, regardless of the users' spatial channel correlation. Similar to the results obtained in [KKHN09] for linear MMSE detectors, we notice that spatial channel correlation does not have any impact on the diversity order of MMSE-based turbo systems.

3.7.3. Numerical Results for Setup 3

In the previous subsections, the performance of the turbo receivers was analyzed utilizing a stochastic MIMO channel model with predefined fixed spatial correlations. In realistic scenarios, however, the spatial-temporal properties of the radio channel depend on the propagation environment and the location of the mobile users and the receiver. Since these channel properties are strongly time-varying, the spatial transmit and receive correlation matrices constructed from the MIMO channel matrix, are time-varying as well. The two extreme cases leading to relatively high and

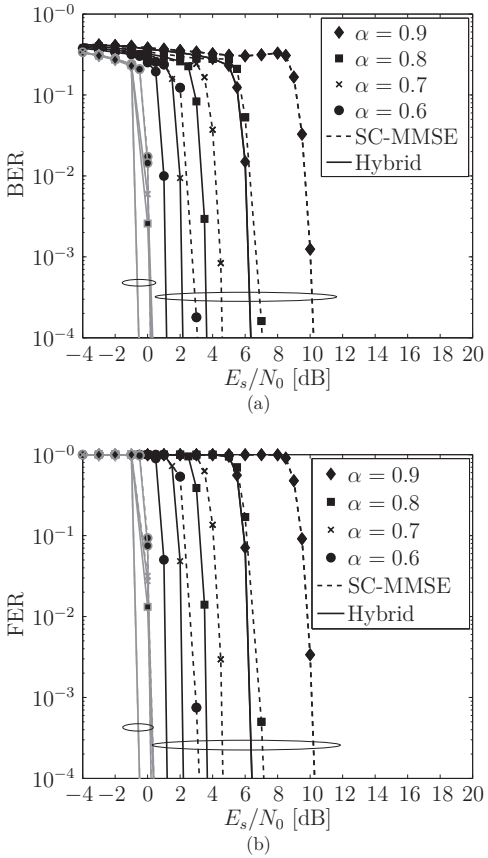

Figure 3.12.: Average BER performance (a) and FER performance (b) for the two subgroups (black curves: first subgroup (user 1 to 4)), gray curves: second subgroup (user 5 to 8)) of the hybrid scheme and the conventional SC-MMSE FDE for an $N = M = 8$ multiuser system over Rayleigh block-fading channels with varying spatial transmit correlation values α.

low spatial correlation coefficients between the users' channels are the line-of-sight (LOS) and the non-line-of-sight (NLOS) propagation scenario, respectively.

In order to assess the practicality of the proposed hybrid equalizer in real fields, the performance is evaluated in this subsection by a series of simulations using channel-sounding field measurement data. For this purpose, a measurement campaign was

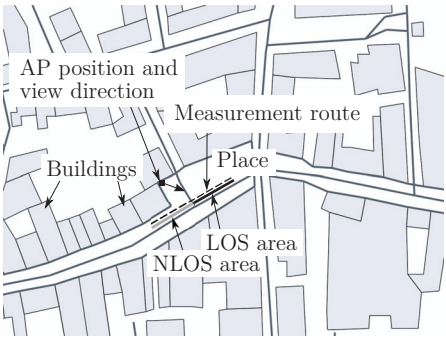

Figure 3.13.: Overview of measurement route and position of AP.

conducted in the city center of Ilmenau, Germany. A top view of the considered urban micro-cell scenario is shown in Fig. 3.13. The measurement route has a length of approximately 60 m and was sampled with 2000 snapshots, corresponding to a distance of about 0.03 m between neighboring snapshots. An 16-element uniform circular array (UCA) with minimum element spacing of half the wavelength was used at the transmitter side as a mobile terminal (MT). The MT was moved at walking speed along the route marked by the dashed line shown in Fig. 3.13. At the receiver side, an 8-element uniform linear array (ULA) with element spacing of 0.4 times wavelength was used as an access point (AP). The receiver position was fixed and the height of the ULA was about 4 m above ground. The measurement route can roughly be divided into two regions; the first part in front of the large open place is mainly dominated by LOS propagation between MT and AP; the second part at half of the route, the MT moves from the open place into the pedestrian street, is mainly characterized by NLOS propagation. The area was surrounded by buildings with a height of approximately 10 to 15 m. In order to highlight the LOS and NLOS propagation conditions along the measurement route, the normalized total receive power (P_r) at the AP is depicted in Fig. 3.14. The major specifications of the measurement campaign and the antenna setup are summarized in Table 3.3.

Preprocessing of Channel-Sounding Data The measured CIRs are preprocessed to be applicable in system simulations. Following [TST05], the noise power estimation and cut method is applied to each measured CIR to remove the influence of the measurement noise. Moreover, a subband of 20 MHz, corresponding to the channel bandwidth used in the system simulations, is extracted from the measurement data at the center frequency. The channel matrices for the multiuser setup are

Table 3.3.: Measurement Campaign Setup.

Scenario	Urban micro-cell
Environment	Open place with LOS cond. and pedestrain street with NLOS cond.
Track length	60 m
Channel Sounder	RUSK ATM, Medav GmbH
Transmit array	UCA, 16 elements
Receive array	ULA, 8 elements
Transmitter height/tilt	1.5 m/0°
Receiver height/tilt	4 m/2°-3° down
Transmit power	33 dBm at power amplifier output
Center frequency	5.2 GHz
Bandwidth	120 MHz
AGC switching	between MIMO snapshots
Maximal velocity	6 km/h

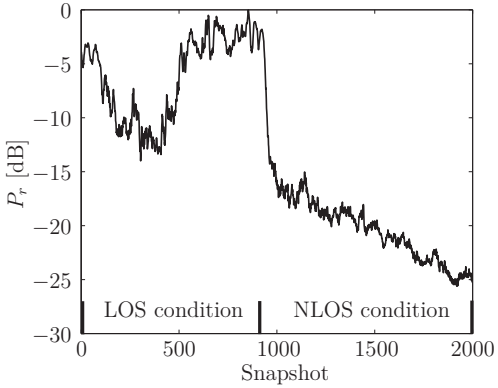

Figure 3.14.: Normalized total receive power along measurement route

generated by combining the CIRs at eight randomly chosen mobile positions along the measurement route. At each position, one element of the antenna array at the transmitter side is randomly selected. This results in $N = M = 8$ MIMO channels.

Three different multiuser scenarios are considered for system simulations.

S1) In the first scenario, the eight users are randomly distributed into two subgroups. The four users of the first and second subgroup are placed in the subarea with LOS and NLOS propagation condition, respectively. The two subgroups are well separated by 1000 snapshots, which corresponds to a distance of approximately 30 m between the MTs. Furthermore, the distance

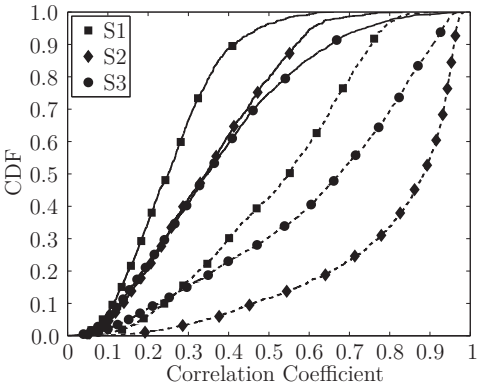

Figure 3.15.: CDF of pairwise users' channel correlation coefficient for each subgroup (dashed curves: first subgroup; solid curves: second subgroup) of the three multiuser scenarios.

between users within each subgroup is fixed and set to 100 snapshots, resulting in a spatial separation of around 3 m. The two subgroups are moved along the measurement route until the end of the LOS/NLOS subarea is reached. This multiuser scenario reflects the behavior of moving, spatially, spacious, located users.

S2) The second multiuser scenario is identical to the first scenario, except that the spatial separation between the users in each subgroup is reduced to 5 snapshots (≈ 0.15 m). This scenario reflects the behavior of moving, spatially, very dense, located users.

S3) The third multiuser scenario models a random drop-based approach. Each drop is defined over 10 subsequent snapshots (≈ 0.30 m) by randomly allocating the eight users into two subgroups that are placed in the subareas with LOS/NLOS propagation condition. The radius of the two subgroups is fixed and set to 15 snapshots (≈ 0.45 m). Moreover, the users' positions within each subgroup and the subgroups' center positions on the measurement route are randomly chosen for each drop. Similar to the spatial channel modeling (SCM) or WINNER channel model [WIN08], the drops are independent and represent randomly selected multiuser setups, where the MIMO channel undergoes fast fading according to the mobile movement of the users.

Fig. 3.15 depicts the cumulative density function (CDF) of the pairwise users' channel correlation coefficient for the three multiuser scenarios S1, S2 and S3. In

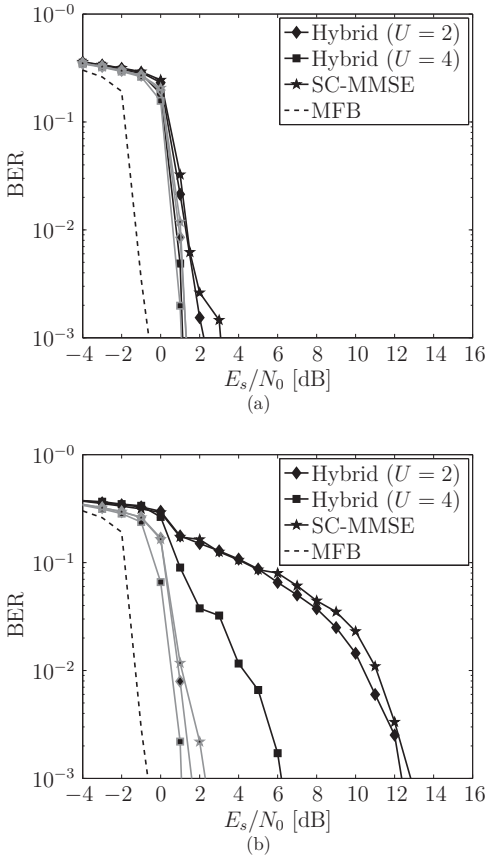

Figure 3.16.: Average BER performance for the two subgroups (black curves: first subgroup (user 1 to 4)), gray curves: second subgroup (user 5 to 8)) of the HY SC-MMSE FDE and the conventional SC-MMSE FDE for an $N = M = 8$ multiuser system for scenario S1 (a) and scenario S2 (b).

all three scenarios, as expected, we observe that users (from the first subgroup) placed in the LOS subarea experience higher spatial correlations than users (from the second subgroup) placed in the NLOS subarea. Furthermore, we find that the largest correlation coefficients are obtained for the spatially, closely, located users from scenario S2.

Fig. 3.16 (a) and (b) depict the BER performance for the two subgroups achieved

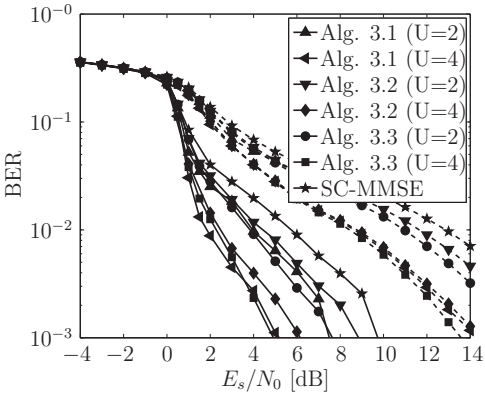

Figure 3.17.: Average BER performance for three different grouping algorithms of scenario S3.

by the HY SC-MMSE FDE (with groupsizes $U = 2$ and $U = 4$) and the SC-MMSE FDE for scenario S1 and S2, respectively. As can be seen, similar performances are obtained by both turbo receivers for both subgroups when all users are spatially well separated (scenario S1). On the contrary, when users are spatially, closely, located and experience LOS propagation, as in scenario S2, the proposed hybrid scheme clearly outperforms the conventional receiver and achieves 1 dB and 6 dB gains at BER=10^{-2} for the groupsizes $U = 2$ and $U = 4$, respectively.

Fig. 3.17 illustrates the BER comparison for the hybrid receiver with MSE and correlation-based group selection for scenario S3. Similar to Fig. 3.16, we observe a performance gain with increasing groupsize. Interestingly, we also see that both groupings perform similar at the first iteration of the hybrid turbo receiver, whereas the simple static correlation-based grouping scheme (Algorithm 3.3) yields a significant gain over the static MSE-based scheme (Algorithm 3.2) at the last turbo iteration. This indicates that group selection based on the MSE criterion at the first iteration may not be optimal for the overall iterative process. The results in Fig. 3.17 further show that the simple correlation-based grouping (Algorithm 3.3) achieves similar performance than the dynamic MSE-based scheme (Algorithm 3.1) at a reduced complexity.

3.8. Chapter Summary

In this chapter several low-complexity turbo equalizers relying on the principle of SC-MMSE filtering have been discussed. The proposed turbo equalizers can be applied

in single- or multiuser single-carrier block-data coded transmissions over MIMO ISI channels. After reviewing the optimum MIMO MAP equalizer, the standard SC-MMSE TDE introduced by Wang and Poor [WP99a], and extensions thereof, have been presented as low-complexity alternatives with only cubic computational complexities in all system parameters. The complexity of the SC-MMSE TDE can further be reduced when resorting to a cyclic prefix-based transmission scheme, and performing the MMSE filtering in the frequency domain. It has been shown that the necessary approximations used in the derivations in [KM07] and [YGWP08] of the SC-MMSE filter coefficients can be avoided by utilizing the unconditional filter approximation [CMT04].

As a main contribution of this chapter, a novel frequency domain turbo equalization scheme for single-carrier block transmission based on the PDA concept has been derived. The SNR at both equalizer outputs has been analyzed and compared. It has been illustrated that significant improvements in terms of SNR can be achieved through the internal equalizer iterations. This additional SNR gain can be used by channel decoders for high rate codes in turbo equalization schemes to improve their error correcting capabilities. Numerical results obtained by simulations in spatially uncorrelated MIMO channels reveal that PDA SC-MMSE FDE offers improved performance compared to standard SC-MMSE FDE.

Furthermore, a novel turbo equalization scheme based on a groupwise soft interference cancellation and linear filtering approach has been presented as a framework for multiple access uplink single-carrier block transmission. Numerical results of BER and FER performances confirm that the novel scheme achieves for moderately chosen group sizes considerable performance gains over the standard SC-MMSE FDE in channels with high spatial correlation. In addition, three new algorithms based on MSE and correlation criteria for group selection have been developed.

4. Convergence Analysis of Turbo Equalization

A general approach to analyze the convergence behavior of iterative systems, including iterative decoding, iterative detection and turbo equalization, is to treat the LLRs of the binary messages exchanged between the SfISfO components as statistical random variables, and to track the evolution of their PDFs by means of numerical simulations. An example of this approach is the density evolution technique, initially proposed by Richardson and Urbanke in [RU01], see also [RSU01], for the performance analysis of iterative decoding of low density parity check (LDPC) codes. Results obtained from density evolution can be used to predict the error performance and convergence threshold of the system, or to optimize the parameters of a channel code for a fixed convergence threshold.

Although the density evolution technique is a powerful mathematical tool, its application is pretty limited in practice, as the complexity of tracking the densities becomes quite severe in large decoding systems. Other simpler methods for analyzing iterative decoding and iterative detection/equalization are EXIT charts [tB01], fidelity [TtBH02], [Hag04] or also called correlation charts [Cho07], variance transfer charts [AGR98], [SS01], SNR-variance charts [YGWP08], and MSE-transfer charts [BN07]. As opposed to density evolution, these methods characterize the true densities involved in iterative decoding only by a unique statistical parameter. Consequently, the input-to-output relationship of each SfISfO component can be expressed by a single function in terms of the used metric. Depending on the applied analysis technique, the metric can be the noise variance of the LLRs, the MSE, the correlation, or the mutual information between LLRs and information/code bits. With the knowledge of these functions, the convergence point (convergence limit) representing the transmission reliability in terms of the bit error rate achieved after convergence of the iterative system, and the convergence threshold representing the receive SNR at the convergence limit, can easily be predicted without performing extensive Monte-Carlo bit error rate simulations. Moreover, the evolution of the LLR densities between the SfISfO blocks can be visualized by decoding trajectories in two or multidimensional figures.

A very popular approach for analyzing the convergence properties of iterative

decoding schemes are EXIT charts, introduced by ten-Brink in [tB01], which trace the evolution of the mutual information between LLRs and code bits over a number of iterations. Several authors have utilized EXIT charts to analyze iterative decoding of serially or parallel concatenated codes [Tüc04], [BRG05], [tB01], and iterative joint decoding and detection for BICM [LR97], [tBSY98a], [tBSY98b], [SGHB03].

The EXIT chart analysis has been applied to turbo equalization [DV02], [LS03], [TH02] in selected fixed channels, where the EXIT functions for the equalizer and decoder(s) are determined by histogram-based measurements on the LLRs. Although such histogram measurements are very accurate, the high computational effort prevents their application for convergence analysis of turbo equalization in block-fading channels, where the equalizer and decoder EXIT functions are evaluated over an ensemble of channel realizations. Hereby, the majority of the simulation effort is the calculation of the equalizer EXIT functions, as they depend on the channel coefficients. Note that unlike to the equalizer EXIT function, the decoder EXIT function is independent of the channel realization, and may therefore be precomputed and stored in a look up table (LUT) for any given code. In order to avoid the complexity impairments of histogram measurements, analytic computations of EXIT functions for time and frequency domain MMSE-filtering based equalizers have been proposed in [HS05], [NWY05], [KM07] and [RHV07]. As shown in these papers, under the assumption of Gaussian distributed LLRs at the input/output of the equalizer, the equalizer EXIT functions can be described by simple analytical expressions which are parametrized by the channel coefficients and receive SNR. Hence, if the EXIT function of the decoder is determined in advance, the EXIT chart may semi-analytically be computed at low computational cost. This approach allows to evaluate the convergence properties and to estimate the average bit error rate performance of MMSE-based turbo equalizers in block-fading channels without the need of requiring extensive Monte-Carlo simulations.

The EXIT chart provides not only a mathematical tool to analyze the convergence properties, it also provides a method to optimize the transmission parameters in turbo equalization systems such as the channel coding scheme [WNYH06], [TWN$^+$08], [WKTM05].

The purpose of this chapter is to gain insights into the working principles of the proposed turbo equalizers in Chapter 3. The framework of correlation charts [TtBH02], [Hag04], [Cho07] is adapted for the convergence analysis of the iterative receivers. The correlation chart analysis is similar to the well known EXIT chart analysis, except that the evolution of densities is described by the correlation instead of the mutual information between information/code bits and the corresponding LLRs. The main difference between both approaches is, hence, only the metric used to characterize the densities involved in the iterative decoding. Moreover, as found

by the authors of [TtBH02], both metrics essentially provide similar results in terms of modeling accuracy.

The reminder of this chapter is organized as follows: In Section 4.1, we define the correlation functions of the equalizer and channel decoder for single- and multiuser systems. In detail, we use the SNR expressions for the SC-MMSE FDE and PDA SC-MMSE FDE, derived in Chapter 3, to compute analytically the correlation function of the equalizer. The accuracy of the proposed expressions are verified by numerical simulations. In Section 4.2, we briefly introduce the EXIT chart analysis for turbo equalization. In particular, we show that EXIT and correlation charts have a very close relationship in terms of the considered metric. Moreover, the area theorem of EXIT functions is reviewed. Finally, a closed-form approximation and a lower bound on the outage probability of the turbo system is derived in Section 4.3. Numerical results for various channel setups are demonstrated to show the approximation accuracy of the proposed method on the outage performance of turbo equalization.

The results obtained in this chapter provide a basis for analytically verifying the impact of system and channel parameters on the convergence properties of MMSE-based turbo receivers. Moreover, they will be used for developing new transmission rate and power allocation schemes, as shown in Chapter 5, which explicitly take into account the convergence properties of the turbo equalizer.

4.1. Correlation Chart Analysis

As previously stated, the framework of correlation charts is adopted in this section to analyze the convergence behavior of the turbo receiver in single- and multiuser system setups. Similar to the EXIT chart, the correlation chart analysis relies on the fundamental assumption that the LLR messages exchanged between the SfISfO blocks within the turbo receiver are discrete-time ergodic random processes. Together with Assumption 3.1, the *a priori* and *extrinsic* LLRs $\zeta_{(\cdot)}\Big[x_n[k]\Big]$ and $\lambda_{(\cdot)}\Big[x_n[k]\Big]$, $n = 1, ..., N$ can therefore be modeled as output samples of independent random variables $\zeta^n_{(\cdot)}$ and $\lambda^n_{(\cdot)}$, respectively. Here, the variable $x_n[k]$ is a placeholder for the binary signals $a_{n,i}$, $c_{n,i}$, $e_{n,i}$, $c'_{n,i}$, $e'_{n,i}$ or $b_{q,n}[k]$, and the subscript notation $(\cdot)$ is used to distinguish between the different SfISfO modules. The statistics of the random variables $\zeta^n_{(\cdot)}$ and $\lambda^n_{(\cdot)}$ are thus fully defined by the conditional PDFs $p\Big(\zeta^n_{(\cdot)}|e\Big)$ and $p\Big(\lambda^n_{(\cdot)}|e\Big)$, $e \in \{0, 1\}$, respectively. To facilitate a simple tracking of these densities over a number of turbo iterations by a single unique statistical parameter, we follow [DDP01], [GH01], [AGR98], [BC02], [CRU01], and introduce the following assumption.

Assumption 4.1. The *a priori* LLRs $\zeta_{(\cdot)}[x_n(k)]$, $\forall n$ at each SfISfO block can be modeled as output signals of an equivalent binary-input AWGN channel, $\zeta_{(\cdot)}\big[x_n[k]\big] = \mu_{\zeta,n} x_n[k] + n_n[k]$, $n = 1, ..., N$, where the effective channel SNR ϱ_n, the effective channel gain $\mu_{\zeta,n}$, and the noise variance $\sigma^2_{\zeta,n}$ satisfies the relation $\varrho_n = \frac{\mu_{\zeta,n}}{2} = \frac{\sigma^2_{\zeta,n}}{4}$ for all n.

The evolution of the densities $p\big(\zeta^n_{(\cdot)}|e\big)$ and $p\big(\lambda^n_{(\cdot)}|e\big)$ may then also be observed by tracking the correlation between the transmitted code bits and the corresponding soft-symbol estimates, conditioned on the LLR messages [Cho07]. For this purpose, let us define by $\alpha_{(\cdot),n} \equiv \mathbb{E}\big[x_n[k]\bar{x}_n[k]\big]$, $n = 1, ..., N$ the correlation between the true binary transmit signal $x_n[k]$ and its conditional estimate

$$\bar{x}_n[k] \equiv E\Big[x_n[k]\,\Big|\zeta_{(\cdot)}\big[x_n[k]\big]\,\Big] = \tanh\Big((1/2)\zeta_{(\cdot)}\big[x_n[k]\big]\Big), \tag{4.1}$$

given the *a priori* LLR $\zeta_{(\cdot)}\big[x_n[k]\big]$. With the Gaussian model of Assumption 4.1, the correlation parameter $\alpha_{(\cdot),n}$ can be written as a function of the input channel SNR ϱ_n, and hence as a particular function of the conditional PDF $p(\zeta^n_{(\cdot)}|e)$, as

$$\begin{aligned}
\alpha_{(\cdot),n} &= \mathbb{E}\big[x_n[k]\bar{x}_n[k]\big] \\
&= \mathbb{E}\Big[\tanh\Big(r_a\big[x_n[k]\big]\Big)\Big] \\
&= \frac{1}{\sqrt{2\pi}}\int_{-\infty}^{\infty}\tanh\Big(z\sqrt{\varrho_n}+\varrho_n\Big)\,e^{\frac{-z^2}{2}}\mathrm{d}z \\
&= \phi(\varrho_n).
\end{aligned} \tag{4.2}$$

Here, $r_a\big[x_n[k]\big] \equiv (1/2)x_n[k]\zeta_{(\cdot)}\big[x_n[k]\big] \sim \mathcal{N}(\varrho_n, \varrho_n)$ is a Gaussian random variable with identical mean and variance. Similarly, we define by $\varphi_{(\cdot),n} \equiv \mathbb{E}\Big[\tanh\Big(r_e\big[x_n[k]\big]\Big)\Big]$, where $r_e\big[x_n[k]\big] \equiv (1/2)x_n[k]\lambda_{(\cdot)}\big[x_n[k]\big]$, the correlation between the true transmit signal $x_n[k]$ and its conditional estimate $\mathbb{E}\big[x_n[k]|\lambda_{(\cdot)}\big[x_n[k]\big]\big]$, given the *extrinsic* LLR $\lambda_{(\cdot)}\big[x_n[k]\big]$. With these definitions, the convergence behavior of the turbo system can be evaluated independently component-by-component, by defining several multidimensional functions that describe the correlation characteristics of the equalizer and the multiple channel decoders.

Let us first focus on the equalizer. It processes the received data $\mathbf{r}$ and the *a priori* LLR sequences $\boldsymbol{\zeta}_e$, and outputs the *extrinsic* LLR messages $\boldsymbol{\lambda}_e$. As shown in Fig. 4.1 (a), its convergence characteristic can be expressed by an N-dimensional mapping of the input correlation parameter vector $\boldsymbol{\alpha}_e \equiv [\alpha_{e,1}, \alpha_{e,2}, ..., \alpha_{e,N}]^T$ to the output correlation parameter vector $\boldsymbol{\varphi}_e \equiv [\varphi_{e,1}, \varphi_{e,2}, ..., \varphi_{e,N}]^T$, conditioned on the specific channel realization $\mathbf{H}$, the transmit strategy $\mathbf{T}$, and the receiver noise power

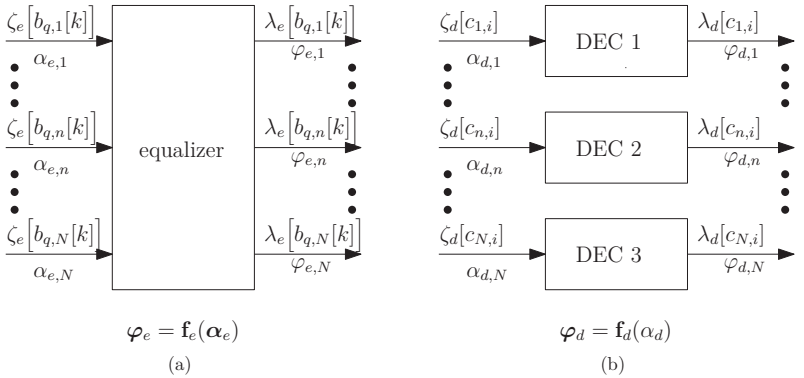

Figure 4.1.: Correlation characteristics and input/output LLRs of the equalizer (a) and the decoders (b).

σ_0^2. This means

$$\boldsymbol{\varphi}_e = \mathbf{f}_e : \boldsymbol{\alpha}_e \in \mathbb{D}^N \rightarrow \mathbf{f}_e \equiv \Big(f_{e,1}(\boldsymbol{\alpha}_e), ..., f_{e,n}(\boldsymbol{\alpha}_e), ..., f_{e,N}(\boldsymbol{\alpha}_e)\Big) \in \mathbb{D}^N, \tag{4.3}$$

with $\mathbb{D}^N \equiv \{\mathbf{x}|\mathbf{x} \in [0,1]^N\}$ being the set of correlation values. For the notational simplicity, we have omitted the conditioning on the channel matrix and receiver noise in (4.3).

Similarly, as shown in Fig. 4.1 (b), the convergence characteristic of the N channel decoders, that use the *a priori* LLR sequence $\boldsymbol{\zeta}_d$ as inputs and yield the LLR information $\boldsymbol{\lambda}_d$ as outputs, can be expressed by N independent correlation functions:

$$\boldsymbol{\varphi}_d = \mathbf{f}_d : \boldsymbol{\alpha}_d \in \mathbb{D}^N \rightarrow \mathbf{f}_d \equiv \Big(f_{d,1}(\alpha_{d,1}), ..., f_{d,1}(\alpha_{d,n}), ..., f_{d,N}(\alpha_{d,N})\Big) \in \mathbb{D}^N. \tag{4.4}$$

Note that if SCCC encoding is performed at the N transmitters, the decoder functions in (4.4) designate the combined correlation functions of the inner and outer channel decoders.

Assumption 4.2. The correlation functions $f_{(\cdot),n}(\cdot)$, $n = 1, ..., N$ are continuous and strictly monotonically increasing in all arguments.

The above assumption on the correlation functions, which is supposed to be valid for any iterative decoding algorithm, guarantees that all correlation values of the turbo system approach unique fixed values, for an unlimited number of turbo iterations [BRG05]. The corresponding limiting values define the convergence point and threshold of the turbo system. In addition, each decoder function $f_{d,n}(\cdot)$ is assumed to have a unique inverse $f_{d,1}^{-1}(\cdot)$.

We remark that in the case of single-user transmission, as shown in the sequel, the equalizer characteristic and channel decoder characteristic in (4.3) and (4.4), respectively, reduce to simple one-dimensional functions

$$\varphi_e = f_e(\alpha_e) \text{ and } \varphi_d = f_d(\alpha_d), \tag{4.5}$$

where the antenna index has been skipped in the variable and function notations.

4.1.1. Equalizer Correlation Characteristic

The equalizer correlation characteristic in (4.3) is usually obtained via Monte-Carlo simulation. The correlation functions are determined by artificially generating i.i.d. random binary-input sequences $\Big\{b_{q,n}[k]\Big\}$ and LLR sequences $\boldsymbol{\zeta}_e$ for arbitrary values $\boldsymbol{\alpha}_e \in \mathbb{D}^N$, according to the Gaussian model in Assumption 4.1. The conditional PDFs $p(\zeta_e^n|b_{q,n}[k])$, $n = 1, ..., N$ follow exponential-symmetric Gaussian distributions with mean $2\varrho_n b_{q,n}[k]$ and variance $4\varrho_n$. The quality of the input LLRs $\zeta_e\Big[b_{q,n}[k]\Big]$ is quantified by the channel SNRs ϱ_n via the input correlation parameter vector $\boldsymbol{\alpha}_e$ as $\varrho_n = \phi^{-1}(\alpha_{e,n})$, $\forall n$. For each value $\boldsymbol{\alpha}_e \in \mathbb{D}^N$, the equalizer uses the artificially generated *a priori* LLRs $\boldsymbol{\zeta}_e$ and the received data $\{\mathbf{r}(k)\}$ to produce *extrinsic* LLR sequences $\boldsymbol{\lambda}_e$. Based on the obtained LLR output vectors $\boldsymbol{\lambda}_e$, the corresponding correlation parameter vector $\boldsymbol{\varphi}_e$ can be numerically calculated by histogram-based measurements using the conditional PDFs $p(\lambda_e^n| - 1)$ and $p(\lambda_e^n| + 1)$, $\forall n$,

$$\varphi_{e,n} = \frac{1}{2}\int_{-\infty}^{+\infty} \tanh\left(\frac{\lambda_e^n}{2}\right) p(\lambda_e^n| + 1)\mathrm{d}\lambda_e^n - \frac{1}{2}\int_{-\infty}^{+\infty} \tanh\left(\frac{\lambda_e^n}{2}\right) p(\lambda_e^n| - 1)\mathrm{d}\lambda_e^n. \tag{4.6}$$

Alternatively, by invoking the ergodicity property and assuming a sufficient long transmit frame, the output correlations $\varphi_{e,n}$ at the equalizer may also be computed via the conditional mean estimator as

$$\begin{aligned}\varphi_{e,n} &= \mathbb{E}\Big[b_{q,n}(k)\bar{b}_{q,n}(k)\Big] \\ &\approx \frac{1}{QN_b}\sum_{q=0}^{Q-1}\sum_{k=1}^{N_b} b_{q,n}[k]\tanh\left(\frac{\lambda_e\Big[b_{q,n}[k]\Big]}{2}\right), n = 1, ..., N.\end{aligned} \tag{4.7}$$

The calculation of (4.7) requires perfect knowledge of the binary-input sequences $\Big\{b_{q,n}[k]\Big\}$. A simple method for estimating $\varphi_{e,n}$ without knowing these sequences is obtained using the relation in (3.26), so that $\varphi_{e,n} = \mathbb{E}\Big[b_{q,n}[k]\bar{b}_{q,n}[k]\Big] = \mathbb{E}\Big[\bar{b}_{q,n}^2[k]\Big]$.

Therefore, $\varphi_{e,n}$ may be estimated by

$$\varphi_{e,n} \approx \frac{1}{QN_b} \sum_{q=0}^{Q-1} \sum_{k=1}^{N_b} \tanh^2\left(\frac{\lambda_e\left[b_{q,n}[k]\right]}{2}\right). \tag{4.8}$$

Equation (4.8) may be used in applications requiring an on-line tracking of the convergence at the turbo receiver, such as dynamic scheduling of the iteration loops in multiple concatenated systems [BRG05].

Similar to the EXIT chart approach, in general, long binary-input sequences are needed to accurately compute the output correlation parameter vector $\boldsymbol{\varphi}_e$ [tB01]. The above simulation-based method is hence impractical due to the increased computational complexity for the evaluation of the equalizer correlation characteristic in large system configurations. Furthermore, the problem of estimating the correlation parameter vectors becomes more intricate for non-ergodic fading channels, since the equalizer correlation function $\mathbf{f}_e$ depends always on the particular channel realization.

4.1.1.1. Analytical Computation of Equalizer Correlation Function for SC-MMSE FDE

In [Gro09], [Gro11], the author proposed a method to analytically compute the correlation function $\mathbf{f}_e$ of the SC-MMSE FDE. It relies on a characterization of the instantaneous SNR ψ_n^{FD} (see (3.39)) of the *extrinsic* LLR sequences $\boldsymbol{\lambda}_e$ at the FDE output as a function of the input correlation parameter vector $\boldsymbol{\alpha}_e$. The SNR ψ_n^{FD} can be considered as a multidimensional function of the combined frequency domain channel matrix $\boldsymbol{\Xi}_c$, the receiver noise variance σ_0^2, and the power levels $\bar{\varphi}_n$, $n = 1, .., N$ of the soft-symbol estimates computed from the decoder feedback LLR sequences $\boldsymbol{\zeta}_e$. By invoking (3.26) again, we immediately see the equivalence between $\bar{\varphi}_n$ and the input correlation parameter $\alpha_{e,n}$ of the prior messages $\zeta_e\left[b_{q,n}[k]\right]$, so that $\bar{\varphi}_n = \alpha_{e,n}$, $\forall n$ follows. Using this identity, the input correlation parameter vector $\boldsymbol{\alpha}_e$ can directly be used in the computation of the instantaneous SNRs as

$$\psi_n^{\mathrm{FD}}(\boldsymbol{\alpha}_e) = \frac{2\gamma_n(\boldsymbol{\alpha}_e)}{1 - \gamma_n(\boldsymbol{\alpha}_e)(1 - \alpha_{e,n})}, \forall n. \tag{4.9}$$

As argued in Section 3.3.2, the *extrinsic* LLR messages $\lambda_e\left[b_{q,n}[k]\right]$ can be equivalently expressed by discrete-time binary-input parallel AWGN channels of the form $\lambda_e\left[b_{q,n}[k]\right] = \mu_{\lambda_e,n} b_{q,n}(k) + n_{q,n}(k)$, $n_{q,n}(k) \sim \mathcal{N}(0, \sigma^2_{\lambda_e,n})$, where the channel gain $\mu_{\lambda_e,n}$ and the noise variance $\sigma^2_{\lambda_e,n}$ are defined via their SNR ψ_n^{FD}, and are given by $\mu_{\lambda_e,n} = 2\psi_n^{\mathrm{FD}}(\boldsymbol{\alpha}_e)$ and $\sigma^2_{\lambda_e,n} = 4\psi_n^{\mathrm{FD}}(\boldsymbol{\alpha}_e)$, respectively. The equalizer's output signals

$r_e[b_{q,n}(k)]$ are thus Gaussian distributed, so that the N components of the output correlation parameter vector $\boldsymbol{\varphi}_e$ are found to

$$\varphi_{e,n} = \mathbb{E}\Big[b_{q,n}[k]\bar{b}_{q,n}[k]\Big] = \mathbb{E}\Big[\tanh\Big(r_e\Big[b_{q,n}[k]\Big]\Big)\Big]. \tag{4.10}$$

Hence, we can summarize the result as follows.

Lemma 4.3. The output correlation parameter of the SC-MMSE FDE is given by

$$\begin{aligned}\varphi_{e,n} &= \phi\Big(\psi_n^{\mathrm{FD}}(\boldsymbol{\alpha}_e)\Big)\\ &= f_{e,n}(\boldsymbol{\alpha}_e), \forall n.\end{aligned} \tag{4.11}$$

We remark that (4.11) requires, unlike to the Monte-Carlo simulation, the output LLRs of the equalizer to be Gaussian distributed, which is in general true as shown in [KM07], [NWY05] for spatially-uncorrelated MIMO channels. The computational complexity of (4.11) is very low, since the matrices/vectors involved in the computation are independent of the transmit frame length N_b. The equalizer correlation characteristic may therefore be totally predicted analytically for a given particular channel realization, transmit precoding strategy and value of the receiver noise variance.

Special Case of Single-User Transmission For a single-user transmission system, the channel encoding at the transmitter is performed over a single data frame that is uniformly spread over all N transmit antennas. Hence, it is sufficient to characterize the distribution of the decoder feedback LLRs $\boldsymbol{\zeta}_e$ by a single correlation value α_e, instead of the correlation parameter vector $\boldsymbol{\alpha}_e$. However, as in the multiuser case discussed above, the transmitted signals from the different antennas can undergo different channel fading conditions. Therefore, we still need N SNR values to describe the N equivalent AWGN channels of the *extrinsic* LLR sequences $\boldsymbol{\lambda}_e$. These SNR values are given with (3.39) as

$$\psi_n^{\mathrm{FD}}(\alpha_e) = \frac{2\gamma_n(\alpha_e)}{1-\gamma_n(\alpha_e)(1-\alpha_e)}, \forall n, \tag{4.12}$$

where the notation $\gamma_n(\alpha_e)$ stands for $\gamma_n(\boldsymbol{\alpha}_e)$ with $\boldsymbol{\alpha}_e = [\alpha_e, \alpha_e, ..., \alpha_e]^T$ being an $N \times 1$ correlation parameter vector. Based on (4.12), the FDE output vector $\boldsymbol{\varphi}_e = [\varphi_{e,1}, ..., \varphi_{e,n}, ..., \varphi_{e,N}]^T$ can be obtained, as in (4.11), by a mapping of the individual SNR values to the correlation parameters $\varphi_{e,n}$ via the function $\phi(\cdot)$. The N correlation parameter outputs of the equalizer presuppose that the correlation characteristic of the channel decoder is defined by a function having as argument an $N \times 1$ input correlation parameter vector. In general, such a decoder characteristic

could be obtained by a Monte-Carlo simulation and stored in a LUT by assuming that the input LLRs are generated by N independent AWGN channels with SNRs defined by the inverse of (4.2). For large values of N, however, such a LUT would be very large for all possible combinations of input correlation parameters. To reduce the decoder and equalizer correlation characteristics to simple one-to-one relations, as given by (4.5), we map the FDE output correlation parameter vector $\boldsymbol{\varphi}_e$ to a scalar value φ_e by an average operation, i.e.,

$$\begin{aligned}\varphi_e &= \frac{1}{N}\sum_{n=1}^{N}\phi\Big(\psi_n^{\mathrm{FD}}(\alpha_e)\Big)\\ &= f_e(\alpha_e).\end{aligned} \tag{4.13}$$

Obviously, (4.13) is equivalent to the statistical expectation $\mathbb{E}\Big[\tanh\Big(r_e\Big[b_{q,n}[k]\Big]\Big)\Big]$ taken over all n, q, k. The idea behind this averaging relies, similar to the EXIT chart analysis, on the fundamental principle that in the single-user case the conditional PDFs $p(\lambda_e^n|e)$, $n = 1, ..., N$, $e \in \{\pm 1\}$ can be replaced by a single conditional distribution $p(\lambda_e|e)$, with matched mean and variance, which is identical for all *extrinsic* LLRs $\lambda_e\Big[b_{q,n}[k]\Big]$.

4.1.1.2. Analytical Computation of Equalizer Correlation Function for PDA SC-MMSE FDE

Like for the SC-MMSE FDE, the analytical approximation of the correlation characteristic (see also [GM08]) of the PDA SC-MMSE FDE is derived by adopting the Gaussian model of (2.48) for the equalizer's *a priori* and *extrinsic* LLRs $\zeta_e\Big[b_{q,n}[k]\Big]$ and $\lambda_e\Big[b_{q,n}[k]\Big]$, respectively. Moreover, for the analytical tractability of the internal iterations of the PDA SC-MMSE FDE, we suppose, as in Assumption 3.8 of Section 3.4, uncorrelated NMMSE soft-symbol estimates which are initialized as $\mathbf{z}_n^{(0)} = \tanh\Big(\frac{1}{2}\boldsymbol{\zeta}_e[\mathbf{b}_n]\Big)$, $\forall n$. Based on these assumptions, the SNRs of the *extrinsic* output LLRs $\lambda_e\Big[b_{q,n}[k]\Big]$, conditioned on the frequency domain compound channel matrix $\boldsymbol{\Xi}_e$ and receiver noise variance σ_0^2, at internal iteration $\tau + 1$ are given by (see Eq. (3.69))

$$\psi_n^{\mathrm{NL}(\tau+1)} = \frac{2\bar{\gamma}_n(\bar{\bar{\boldsymbol{\varphi}}}^{(\tau)})}{1 - \bar{\gamma}_n(\bar{\bar{\boldsymbol{\varphi}}}^{(\tau)})\Big(1 - \bar{\bar{\varphi}}_n^{(\tau)}\Big)}, \forall n, \tag{4.14}$$

Equipped with the SNR expressions (4.14) and the Gaussian assumption on the equalizer's input and output messages (see also Assumption 4.1 and 3.10),

$$r_a\Big[b_{q,n}[k]\Big] \sim \mathcal{N}(\phi^{-1}(\alpha_{e,n}), \phi^{-1}(\alpha_{e,n})) \tag{4.15}$$

$$r_e\Big[b_{q,n}[k]\Big] \sim \mathcal{N}(\psi_n^{\mathrm{NL}(\tau)}, \psi_n^{\mathrm{NL}(\tau)}), \tag{4.16}$$

the value of the power levels $\bar{\varphi}_n^{(\tau)}$ of the NMMSE symbol estimates at internal iteration τ can be solved for suppositionally uncorrelated decisions with respect to the initialization $\mathbf{z}_n^{(0)} = \tanh\left(\frac{1}{2}\boldsymbol{\zeta}_e[\mathbf{b}_n]\right)$, $\forall n$ as

$$\begin{aligned}\bar{\varphi}_n^{(\tau)} &= \mathbb{E}\Big[b_{q,n}[k] z_{q,n}^{(\tau)}[k]\Big] \\ &= \mathbb{E}\Big[\tanh\Big(r_a\Big[b_{q,n}[k]\Big] + r_e\Big[b_{q,n}[k]\Big]\Big)\Big] \\ &= \phi\Big(\phi^{-1}(\alpha_{e,n}) + \psi_n^{\mathrm{NL}(\tau)}\Big), \psi_n^{\mathrm{NL}(0)} \equiv 0, \forall n. \end{aligned} \tag{4.17}$$

Equations (4.14) and (4.17) are carried out successively for each realization of the input correlation parameter vector $\boldsymbol{\alpha}_e \in \mathbb{D}^N$ and for all users/transmit antennas and all internal equalizer iterations. The SNR sequence $\{\psi_n^{\mathrm{NL}(\tau)}\}_{\tau=0}^{\infty}$, $\forall n$ converges, for any input $\boldsymbol{\alpha}_e \in \mathbb{D}^N$, monotonically to a limit point $\psi_n^{\mathrm{NL}(\infty)} = \lim_{\tau\to\infty} \psi_n^{\mathrm{NL}(\tau)}$, $\forall n$, as $\tau \to \infty$. Having obtained the SNRs $\psi_n^{\mathrm{NL}(\infty)}$ in the asymptotic limit, the N output correlation parameters of the PDA SC-MMSE FDE with respect to the *extrinsic* LLRs $\lambda_e\Big[b_{q,n}[k]\Big]$ can finally be solved as $\varphi_{e,n} = \mathbb{E}\Big[\tanh\Big(r_e\Big[b_{q,n}[k]\Big]\Big)\Big]$. We summarize this result in the following lemma.

Lemma 4.4. The output correlation parameter of the PDA SC-MMSE FDE is given by

$$\begin{aligned}\varphi_{e,n} &= \phi\Big(\psi_n^{\mathrm{NL}(\infty)}\Big) \\ &= f_{e,n}(\boldsymbol{\alpha}_e), \forall n. \end{aligned} \tag{4.18}$$

Taking into account that the asymptotic SNRs $\psi_n^{\mathrm{NL}(\infty)}$ are always larger or at least equal than the SNRs $\psi_n^{\mathrm{NL}(1)}$ at internal iteration $\tau = 0$, it follows from the monotonicity of the function $\phi(\cdot)$, that

$$\begin{aligned}\phi\Big(\psi_n^{\mathrm{NL}(\infty)}\Big) &\geq \phi\Big(\psi_n^{\mathrm{NL}(1)}\Big) \\ &= \phi\Big(\psi_n^{\mathrm{FD}}\Big) \end{aligned} \tag{4.19}$$

holds for all $\boldsymbol{\alpha}_e \in \mathbb{D}^N$. This means, the output correlation parameters of the PDA SC-MMSE FDE are always larger or at least equal than the output correlation parameters of the SC-MMSE FDE, supposing the same single channel realization,

transmit precoding matrix, receiver noise variance and a sufficiently large number of internal iterations. Moreover, as will be shown by the numerical results presented in Section 4.1.3, this correlation gain leads to more reliable *extrinsic* LLR estimates of the equalizer and to an enhanced performance with respect to the bit error rate of the overall turbo system.

Before proceeding with the analytical approximation of the correlation characteristic of the PDA SC-MMSE FDE in the single-user case, we summarize the calculation of the correlation function $\mathbf{f}_e$ for a multiuser system in the following flowchart:

For each realization of the input correlation parameter vector $\boldsymbol{\alpha}_e \in \mathbb{D}^N$

- Initialize the SNR variables $\psi_n^{(0)}$ to zero for all $n \in \{1, ..., N\}$.

  For user $n = 1 : N$

    For internal iteration $\tau = 0 : \tau_{max}$

    · Calculate the power level $\bar{\bar{\varphi}}_n^{(\tau)}$ of the NMMSE estimates.

    · Calculate the SNR $\psi_n^{\mathrm{NL}(\tau+1)}$ of the extrinsic LLRs $\lambda_e\Big[b_{q,n}[k]\Big]$.

    end

  end

– Calculate the output correlation parameters $\varphi_{e,n}$ for all $n \in \{1, ..., N\}$.

end

Special Case of Single-User Transmission In the single-user case the input correlation parameter of the PDA SC-MMSE FDE can be represented by a single scalar value α_e. This scalar input correlation parameter is mapped via the individual SNRs in (4.14) and the function $\phi(\cdot)$ to an output correlation parameter vector $\boldsymbol{\varphi}_e$, by running the above algorithm with the initialization $\alpha_{e,1} = ... = \alpha_{e,N} = \alpha_e$, for a number of iterations. Similar to the SC-MMSE FDE of Section 4.1.1.1, the *extrinsic* LLRs $\lambda_e\Big[b_{q,n}[k]\Big]$ of the equalizer can be characterized by a single distribution, such that the components of the output correlation parameter vector $\boldsymbol{\varphi}_e$ can be averaged to a single scalar value φ_e,

$$\varphi_e = \frac{1}{N}\sum_{n=1}^{N}\varphi_{e,n} = f_e(\alpha_e). \tag{4.20}$$

Equation (4.20) yields the analytical approximation of the correlation characteristic of the PDA SC-MMSE FDE.

4.1.1.3. Numerical and Analytical Results

In order to show the usefulness of the analytical approximation of the equalizer correlation characteristic for the SC-MMSE and PDA SC-MMSE FDEs, numerical results obtained from Monte Carlo-based histogram measurements are presented and compared to the corresponding results of the analytical approximation. Furthermore, we present some results for the HY SC-MMSE FDE and compare them with those obtained from the SC-MMSE FDE. For the simulation experiments the following three scenarios are considered.

The first scenario covers a two-by-two multiuser transmission over an spatially-uncorrelated Rayleigh block-fading channel with uniform power delay profile. The corresponding correlation functions $f_{e,1}(\cdot)$ and $f_{e,2}(\cdot)$ for the SC-MMSE and the PDA SC-MMSE FDEs at different receive SNRs E_s/N_0 are depicted in Fig. 4.2 (a) and (b), respectively. The correlation values are obtained by computing (4.6) for a single $L = 10$-tap channel realization over a frame of 65536 BPSK symbols per user. Inspecting these figures, we see that the simulated correlation surfaces almost coincide completely with those estimates from the analysis. In particular, the displayed results indicate that the assumptions made in analysis of both receiver algorithms are well justified for the given system and channel setup. Moreover, from the tight accordance of both surfaces for the PDA SC-MMSE FDE over all E_s/N_0 values, it can be concluded that omitting possible correlations between different NMMSE data estimates over the internal equalizer iterations (see Assumption 3.6) has no influence on the accuracy of the analytical approximation on the equalizer correlation characteristics.

Besides this, we see that the PDA SC-MMSE FDE attains significantly higher output correlation values than the SC-MMSE FDE for rising E_s/N_0. As explained in Section 3.4, this is a consequence of the exploitation of the internal equalizer iterations that successively improve the NMMSE data estimates what finally leads to more reliable *extrinsic* LLRs at the equalizer output.

The mean absolute and relative errors between the simulated and analytical surfaces, found by averaging the output correlation values over 30 random channel realizations, are listed in Table 4.1. Regarding this table, it turns out that the maximum approximation error is less than 1.67% for the given receive SNRs. A similar result is obtained for the equalizer correlation curves of the second scenario, depicted in Fig 4.3, that covers a single-user transmission over a single random two-by-two $L = 32$-tap spatially-uncorrelated Rayleigh fading channel. Also here, it is noteworthy that the PDA SC-MMSE FDE provides higher output correlations than the SC-MMSE FDE for the same channel realization and receiver noise variance.

From the plots of Fig. 4.2 and 4.3 and Table 4.1, we can conclude that the

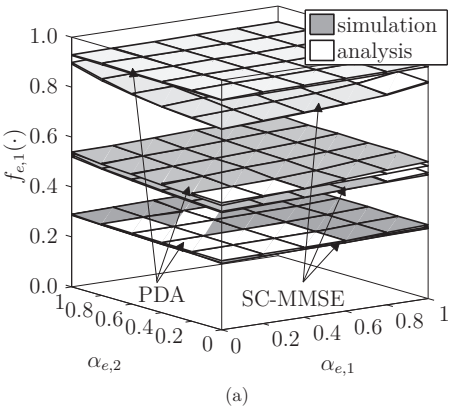

(a)

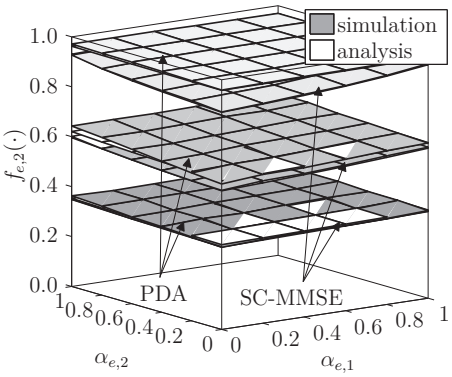

(b)

Figure 4.2.: Analytical and simulated equalizer correlation characteristics $f_{e,1}(\cdot)$ (a) and $f_{e,2}(\cdot)$ (b) of the SC-MMSE FDE and PDA SC-MMSE FDE (denoted as 'PDA') for a two-by-two multiuser system at receive SNRs $E_s/N_0 = -6$ dB, -2 dB and 4 dB (from bottom to top).

proposed analysis method is sufficiently accurate to predict well the equalizer correlation characteristics over a large range of E_s/N_0 values and different system and channel setups.

Finally, the third scenario covers a four-by-four multiuser transmission where the channel matrix is generated according to a spatially correlated Rayleigh fading distribution with uniform power delay profile. The transmit and receive channel correlation matrices follow the Kronecker model in (2.22) of Section 2.3.1, and they

Table 4.1.: Mean absolute errors (and relative errors in [%]) between simulation and analysis at different receive SNRs.

Algorithm	−6 dB	2 dB	4 dB
SC-MMSE FDE	0.19 (0.57)	0.30 (0.54)	0.48 (0.56)
PDA SC-MMSE FDE	0.51 (1.60)	0.97 (1.67)	0.45 (0.47)

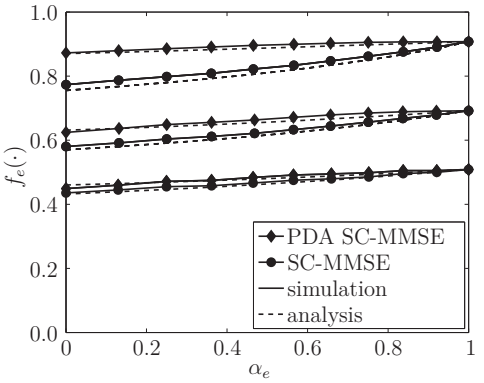

Figure 4.3.: Comparison of analytical and simulated correlation characteristics of the SC-MMSE FDE and PDA SC-MMSE FDE for a single-user two-by-two MIMO system at $E_s/N_0 = -3$ dB, -0.5 dB and 3 dB (from bottom to top).

are given, respectively, by

$$\mathbf{R} = \begin{bmatrix} 1.0 & 0.0 & 0.0 & 0.0 \\ 0.0 & 1.0 & 0.0 & 0.0 \\ 0.0 & 0.0 & 1.0 & 0.0 \\ 0.0 & 0.0 & 0.0 & 1.0 \end{bmatrix} \text{ and } \mathbf{S} = \begin{bmatrix} 1.0 & 0.9 & 0.9 & 0.9 \\ 0.9 & 1.0 & 0.9 & 0.9 \\ 0.9 & 0.9 & 1.0 & 0.9 \\ 0.9 & 0.9 & 0.9 & 1.0 \end{bmatrix}. \tag{4.21}$$

Thus, this scenario models a highly spatially-correlated multiuser setup. Note that visualizing the corresponding equalizer correlation characteristics for such a system is not easy because all functions $f_{e,n}(\cdot)$, $n = 1, ..., 4$ are expressed by four-dimensional mappings. This difficulty in the visualization can be avoided by projecting each function $f_{e,n}(\cdot)$ to a three-dimensional surface by setting $\alpha_{e,3}$ and $\alpha_{e,4}$ to zero. These projections provide lower bounds on the equalizer's correlation characteristics. As an example, we depict the projections of $f_{e,1}(\cdot)$ and $f_{e,2}(\cdot)$ for the HY SC-MMSE FDE in Fig. 4.4 (a) and (b), respectively. These surfaces are obtained by Monte Carlo simulation and histogram measurements for different E_s/N_0 values by setting

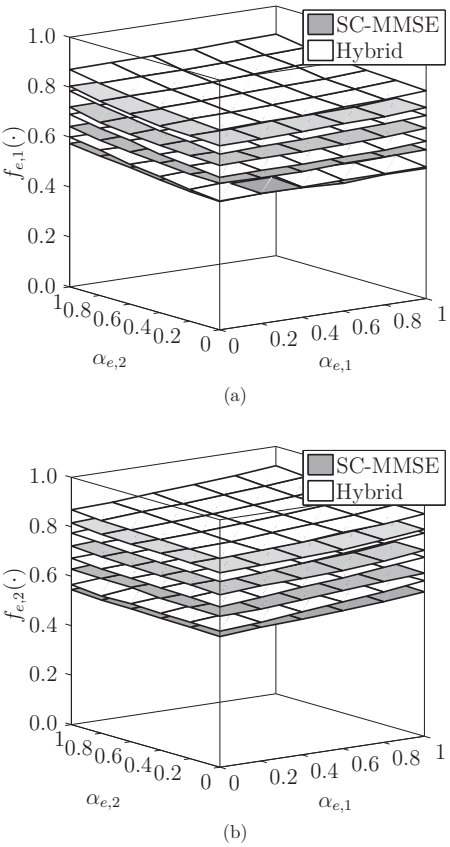

Figure 4.4.: Comparison of equalizer correlation characteristics $f_{e,1}(\cdot)$ (a) and $f_{e,2}(\cdot)$ (b) of the SC-MMSE FDE and HY SC-MMSE FDE for a 4-user transmission at $E_s/N_0 = 6$ dB, 8 dB, 10 dB and 12 dB (from bottom to top).

$G = 1$, so that all users' signals are grouped together into a single subgroup. In addition, the projected correlation surfaces for the SC-MMSE FDE are shown as well for comparison. As seen in these figures, the SC-MMSE FDE provides considerably "lower" correlation characteristics than the HY SC-MMSE FDE for rising E_s/N_0. These surfaces evidence the limited interference cancellation abilities of the simple standard MMSE filtering used in the SC-MMSE FDE when the users' signals are highly correlated. More explicitly, it justifies the considerable performance loss over

the HY SC-MMSE FDE shown in Fig. 3.11, 3.16 and 3.17. It can be concluded that the application of the MAP algorithm for the detection of the users' signals may be preferred over the standard SC-MMSE FDE in channels with high spatial correlation.

4.1.2. Decoder Correlation Characteristic

Let us now consider the correlation characteristic of the channel decoders. In general, for a single-convolutional coded system the correlation function $f_d(\cdot)$, can be determined by Monte-Carlo simulations[1]. Unlike to the equalizer characteristic, the decoder function $f_d(\cdot)$ is specific to the channel code and the decoding algorithm used at the receiver, and does not depend on the particular channel state and receiver noise variance. It can therefore be computed off-line and stored in an one-dimensional LUT. To determine $f_d(\cdot)$, the input LLRs $\zeta_d[c_i]$ to the channel decoder are artificially generated from an encoded sequence $\mathbf{c}$ via the Gaussian model (2.48). Here, the channel SNR $\varrho = \phi^{-1}(\alpha_d)$ of each LLR is defined by the current value of the input correlation parameter α_d. The conditional PDFs $p(\lambda_d|-1)$ and $p(\lambda_d|+1)$ of the produced *extrinsic* LLRs $\lambda_d[c_i]$ at the decoder output are mostly non-Gaussian due to the non-linearity operation of the channel decoding. These PDFs are appropriately determined by histogram-based measurements and then used to calculate the corresponding output correlation parameter φ_d, similar to (4.6). In this way, we evaluate the decoder function $f_d(\cdot)$ for each value of $\alpha_d \in [0, 1)$.

Fig. 4.5 shows examples of decoder correlation functions for the rate-compatible SCCs from [Tüc04] with coding rates from $r_c = 0.1$ to 0.9. The codes are generated from a rate-1/2, memory-4 recursive systematic convolutional (RSC) mother code defined by the generator $(g_r, g_0) = (23, 35)$, where g_r denotes the feedback polynomial in octal notation. The axis are flipped in Fig 4.5, so that the curves represent the inverse functions $f_d^{-1}(\cdot)$ of $f_d(\cdot)$. From the figure, we also see that the shape of the inverse correlation function is related to the rate of code. Although, there exists no analytical relationship between shape and code rate, it reveals that, in principle, the higher the rate of the SCC the larger is the area under the corresponding decoder function $f_d^{-1}(\cdot)$.

We remark that in a multiuser case, the correlation functions $f_{d,n}(\cdot)$, $n = 1, ..., N$ may be specific to each user. Then, they have to be determined in an user-by-user manner by the procedure described above.

[1] As shown in [StB06], [AKtB04], [tBKA04], [tBK03] for certain codes and simple channel models the decoder function can also be expressed analytically in a closed form.

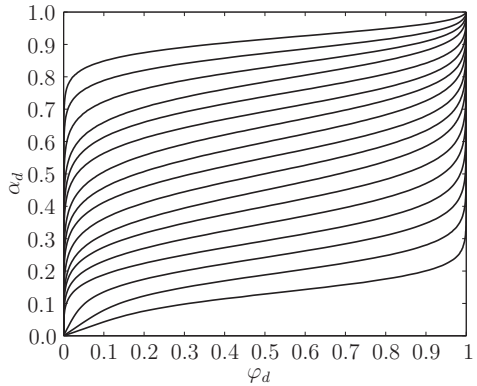

Figure 4.5.: Inverse decoder correlation functions $f_d^{-1}(\cdot)$ for coding rates from $r_c =$ 0.1, 0.15, 0.2 to 0.9 (from bottom to top).

4.1.2.1. Decoder Correlation Function for a Serial Concatenated Code

When an SCCC is employed for channel coding, the iterative decoding scheme from Fig. 2.9 can be applied at the receiver. As shown in this figure, the inner decoder II has the two *extrinsic* LLR outputs $\lambda_{d2}[e'_i]$ and $\lambda_d[c_i]$, and the two *a priori* LLR inputs $\zeta_{d2}[e'_i]$ and $\zeta_d[c_i]$. The inner decoder has therefore two correlation parameter outputs, namely φ_{d2} and φ_d, both of which are functions of the two correlation parameter inputs α_{d2} and α_d. The corresponding two correlation functions are defined as

$$\varphi_{d2} = f_{d2}(\alpha_d, \alpha_{d2}), \tag{4.22}$$

$$\varphi_d = h_{d2}(\alpha_d, \alpha_{d2}). \tag{4.23}$$

Unlike to the inner decoder, the correlation characteristic of the outer decoder is given by a one-to-one relation,

$$\varphi_{d1} = f_{d1}(\alpha_{d1}). \tag{4.24}$$

The functions $f_{d2}(\cdot,\cdot)$, $h_{d2}(\cdot,\cdot)$, and $f_{d1}(\cdot)$ are obtained by Monte-Carlo simulations of the individual component codes. With the definitions in (4.22)-(4.24), the convergence of the serial concatenated code can be analyzed by evaluating the correlation parameter sequences $\left\{(\varphi_{d2}^{(t)}, \varphi_{d1}^{(t)})\right\}_{t=0}^{T_d}$, $t = 0, .., T_d$ over T_d iterations between the inner and the outer decoder[2]. This is done by assuming that the output correlation

[2]For the ease of analysis, we assume that in the multi-user case the number of iterations T_d is identical at all users.

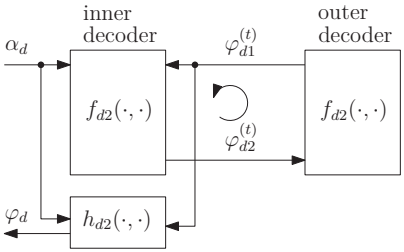

Figure 4.6.: Illustration of the recursive calculation of $f_d(\cdot)$.

parameter of the inner (outer) decoder is equal to the input correlation parameter of the outer (inner) decoder. As a consequence, we obtain the identities $\varphi_{d2} = \alpha_{d1}$, $\varphi_{d1} = \alpha_{d2}$. The sequence $\left\{(\varphi_{d2}^{(t)}, \varphi_{d1}^{(t)})\right\}_{t=0}^{T_d}$, representing the correlation exchange between the two decoders for any given value of the input correlation parameter $\alpha_d \in [0, 1]$ of the inner decoder, is then defined by

$$\varphi_{d2}^{(t)} = f_{d2}(\alpha_d, \varphi_{d1}^{(t)}) \text{ with } \varphi_{d1}^{(0)} = 0, \tag{4.25}$$

$$\varphi_{d1}^{(t+1)} = f_{d1}(\varphi_{d2}^{(t)}). \tag{4.26}$$

The functions $f_{d2}(\cdot,\cdot)$ and $f_{d1}(\cdot)$ are monotonically increasing, which implies that for a fixed value of α_d, $\varphi_{d2}^{(t+1)} \geq \varphi_{d2}^{(t)}$ and $\varphi_{d1}^{(t+1)} \geq \varphi_{d1}^{(t)}$ follows for all t. Thus, the values of (4.25) and (4.26) converge monotonically to $(\varphi_{d2}^{(T_d)}, \varphi_{d1}^{(T_d)})$. After performing T_d iterations between the inner and the outer decoder, the correlation parameter φ_d at the inner decoder output (directed to the equalizer) is calculated with (4.23) as

$$\varphi_d = h_{d2}(\alpha_d, \varphi_{d1}^{(T_d)}). \tag{4.27}$$

To simplify the analysis in the sequel of the overall turbo equalization system, we use the result of (4.25)-(4.27) to define a joint decoder correlation function $f_d(\cdot)$,

$$\varphi_d = f_d(\alpha_d) \equiv h_{d2}(\alpha_d, \varphi_{d1}^{(T_d)}) \text{ with } f_d(0) = 0 \text{ and } f_d(1) = 1, \tag{4.28}$$

which combines the operations of the two decoders into a single decoder component. The recursive calculations of (4.25), (4.26) and (4.28) to characterize the joint decoder correlation characteristic $f_d(\cdot)$ are summarized in the block diagram of Fig. 4.6.

The convergence behavior of the inner and the outer decoder may be visualized by plotting the functions (4.22) and (4.24) in one chart, as shown in Fig. 4.7 (a). Also shown in Fig. 4.7 (a) are two trajectories that visualize the correlation exchange

between the two decoders and represent the sequence $\left\{(\varphi_{d2}^{(t)}, \varphi_{d1}^{(t)})\right\}_{t=0}^{T_d}$ obtained for $T_d = 10$ iterations. Specifically, the two correlation functions of the inner decoder and the two trajectories are depicted for the inner decoder input correlation values $\alpha_d^{(0)} = 0.65$ and $\alpha_d^{(1)} = 0.67$, respectively. The correlation characteristics related to the two decoders are obtained when the outer encoder I is a rate-1/2 RSC code and the inner encoder II is a simple rate-1 code having the polynomials $(g_r, g_0) = (3, 2)$. The corresponding joint decoder correlation characteristic of this rate-1/2 SCCC is shown in Fig 4.7 (b). Note that, as in Fig 4.5, both axes are flipped in Fig 4.7 (b) so that the output correlation parameter φ_d is depicted on the abscissa.

4.1.2.2. Bit Error Probability

The correlation chart analysis may not only be used to visualize the iterative decoding behavior and to predict the convergence threshold, but also to provide an estimate of the bit error probability P_b of the turbo system. For this purpose, we define by $\hat{\varphi}_d$ the correlation between the information bit a_i and the *a posteriori* LLR $\theta_d[a_i]$ at the decoder output. A simple expression on P_b was derived in [Cho07] by supposing that the *a posteriori* LLR $\theta_d[a_i]$ is Gaussian distributed with mean value $2\hat{\varrho}$ and variance $4\hat{\varrho}$, where $\hat{\varrho}$ denotes the equivalent SNR. Then, the bit error probability after a hard decision on the *a posteriori* LLRs $\theta_d[a_i]$ depends solely on $\hat{\varrho}$, and is found to

$$P_b = \frac{1}{2}\mathrm{erfc}\left(\sqrt{\frac{\hat{\varrho}}{2}}\right) = \frac{1}{2}\mathrm{erfc}\left(\sqrt{\frac{\phi^{-1}(\hat{\varphi}_d)}{2}}\right), \tag{4.29}$$

where $\mathrm{erfc}(x) = \frac{2}{\sqrt{\pi}}\int_x^\infty e^{-t^2}\mathrm{d}t$ is the complementary Gaussian error function. For systematic codes, Eqn. (4.29) can further be simplified by assuming that both the *a priori* input and the *extrinsic* output LLRs are independent Gaussian distributed. Then, the bit error probability can be estimated as

$$P_b = \frac{1}{2}\mathrm{erfc}\left(\sqrt{\frac{\phi^{-1}(\alpha_d) + \phi^{-1}(\varphi_d)}{2}}\right). \tag{4.30}$$

It has been found that (4.29) and (4.30) provide reliable BER estimates down to 10^{-3}. A closer approximation is obtained by directly evaluating the BER via the Monte Carlo method and storing the estimates in a one-dimensional LUT. The BER is then given by a function

$$P_b = f_{\mathrm{BER}}(\alpha_d) \tag{4.31}$$

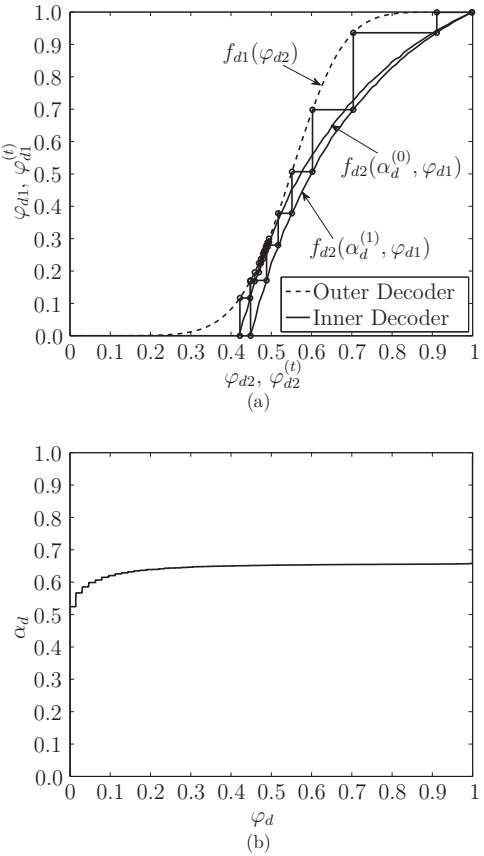

Figure 4.7.: Correlation functions for the inner and the outer decoder for a rate-1/2 outer RSC code (a) and the corresponding joint decoder correlation characteristic (b). The two correlation characteristics of the inner decoder are shown for the inner decoder input correlation values $\alpha_d^{(0)} = 0.65$ and $\alpha_d^{(1)} = 0.67$, respectively.

that is specific to the channel code. Unless otherwise specified, we use in the sequel the direct method in (4.31) to estimate the BER performance of the turbo system.

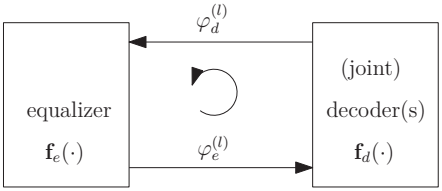

Figure 4.8.: Illustration of correlation exchange between equalizer and channel decoders.

4.1.3. The Correlation Chart

Having determined the vector-functions (4.3) and (4.4) of the equalizer and the channel decoders, it remains to describe the evolution of the correlation values over the turbo iterations. As in the previous section, we assume that any turbo iteration l ($l = 0, ..., T_e$), the correlation of the *extrinsic* soft information at the equalizer output is equal to the correlation of the corresponding *a priori* soft information at the decoder input. Therefore, we can write $\alpha_{d,n} = \varphi_{e,n}$ and $\alpha_{e,n} = \varphi_{d,n}$ for all $n = 1, ..., N$. The convergence behavior of the overall turbo system can then be fully evaluated as shown in Fig 4.8 by the vector-sequence $\left\{(\boldsymbol{\varphi}_d^{(l)}, \boldsymbol{\varphi}_e^{(l)})\right\}_{l=0}^{T_e}$ with $\boldsymbol{\varphi}_d^{(l)} = [\varphi_{d,1}^{(l)}, ..., \varphi_{d,N}^{(l)}]^T$ and $\boldsymbol{\varphi}_e^{(l)} = [\varphi_{e,1}^{(l)}, ..., \varphi_{e,N}^{(l)}]^T$ being the input and the output correlations at the equalizer at iteration l, respectively. The corresponding values of this vector-sequence depend obviously on the schedule of activations of the SfISfO components of the turbo system. For example, $\left\{(\boldsymbol{\varphi}_d^{(l)}, \boldsymbol{\varphi}_e^{(l)})\right\}_{l=0}^{T_e}$ is defined for a system with parallel activations, i.e., a parallel schedule of the turbo iterations, by

$$\begin{aligned} \boldsymbol{\varphi}_e^{(l)} &= \mathbf{f}_e(\boldsymbol{\varphi}_d^{(l)}) \text{ with } \boldsymbol{\varphi}_d^{(0)} = \mathbf{0}, \\ \boldsymbol{\varphi}_d^{(l+1)} &= \mathbf{f}_d(\boldsymbol{\varphi}_e^{(l)}), \forall l. \end{aligned} \tag{4.32}$$

Subject to Assumption 4.2, $\boldsymbol{\varphi}_d^{(l)}$ and $\boldsymbol{\varphi}_e^{(l)}$ convergence asymptotically to a limit point, $(\tilde{\boldsymbol{\varphi}}_d, \tilde{\boldsymbol{\varphi}}_e)$ with $\tilde{\varphi}_{e,n} = \lim_{l\to\infty} \varphi_{e,n}^{(l)}$ and $\tilde{\varphi}_{d,n} = \lim_{l\to\infty} \varphi_{d,n}^{(l)}$, $\forall n$, for $T_e \to \infty$. As shown in [BRG05, Theorem 1], this limit point is unique and independent of the actual activation ordering. Convergence of turbo equalization is achieved, and hence an infinitesimally small BER after channel decoding may be attained, when all components of the vector $\boldsymbol{\varphi}_d^{(l)}$ attain its maximum value $\tilde{\varphi}_{d,n} = 1$. The receive SNR E_s/N_0, for which $\tilde{\varphi}_{d,n} \approx 1$, $\forall n$ holds, defines the convergence threshold of the turbo system.

We can use the functions in (4.3)-(4.4) with the corresponding decoding trajectories, obtained in (4.32), to visualize the correlation exchange between the equalizer and the channel decoders. However, as indicated by (4.3), in the multi-user case,

each $f_{e,n}(\cdot)$ depends on N input correlation values. Thus, the corresponding surface is $(N+1)$-dimensional. The convergence property of the iterative receiver could therefore, in principle, be described by several interconnected multi-dimensional correlation charts. In order to avoid such a cumbersome visualization, Braennstroem *et. al.* introduced in [BRG05] the so-called projection technique to reduce the dimensionality of each surface to two dimensions (2D). We apply this technique in the multi-user case to the vector-function $\mathbf{f}_e$ and calculate for each user a projected equalizer correlation function $g_{e,n}(\alpha_{e,n})$, $n = 1, ..., N$. These functions are independent of the decoding schedule and can be found, for a specific frequency domain compound channel matrix $\mathbf{\Xi}_c$ and receiver noise variance σ_0^2, using (4.3)-(4.4), by

$$g_{e,n}(\alpha_{e,n}) \equiv \lim_{T_e \to \infty} f_{e,n}(\varphi_{d,1}^{(T_e)}, ..., \varphi_{d,n-1}^{(T_e)}, \alpha_{e,n}, \varphi_{d,n+1}^{(T_e)}, ..., \varphi_{e,N}^{(T_e)}), \alpha_{e,n} \in [0,1], \forall n, \quad (4.33)$$

where for each index n, the $N-1$ equalizer's input correlations $\varphi_{d,r}^{(T_e)}$, $r = 1, ..., N$, $r \neq n$ are the result of the following recursions:

$$\begin{aligned} \varphi_{e,r}^{(l)} &= f_{e,r}(\varphi_{d,1}^{(l)}, ..., \varphi_{d,n-1}^{(l)}, \alpha_{e,n}, \varphi_{d,n+1}^{(l)}, ..., \varphi_{d,N}^{(l)}), \\ \varphi_{d,n}^{(l+1)} &= f_{d,n}(\varphi_{e,n}^{(l)}), \forall n, \text{ for } l = 0, ..., T_e \text{ with } \varphi_{d,n}^{(0)} = 0, \forall n. \end{aligned} \quad (4.34)$$

With the 2D-projections in (4.33), the convergence behavior of the turbo system can be assessed by N equalizer and decoder correlation functions, one for each user, that can be plotted with the decoding trajectories in a single two-dimensional chart. The projections are visualized by drawing $g_{e,n}(\cdot)$ and $f_{d,n}(\cdot)$ versus $\varphi_{d,n}$ and $\varphi_{e,n}$, respectively, in the same chart. Note that a vertical step between the 2D-projected equalizer curve and the channel decoder curve in the correlation chart corresponds then with respect to (4.34) to a large number of iterations between the equalizer and all N channel decoders (except the nth one), until the equalizer output correlation $\varphi_{e,n}^{(l)}$ has converged to a fixed value. Correspondingly, a horizontal step between both curves represents a single activation of the channel decoder of user n.

4.1.3.1. Examples and Numerical Results

In this subsection, we present some examples to illustrate the correlation chart analysis for the turbo receivers discussed in Chapter 3. We also present numerical results of BER simulations to verify the accuracy of the analytical expressions in (4.13), (4.20) and (4.31).

Fig. 4.9 shows the equalizer and the decoder correlation curves for the SC-MMSE and PDA SC-MMSE FDEs for a single-user $N = M = 2$ and $L = 10$ Rayleigh fading random channel realization with uniform delay-power profile at different E_s/N_0.

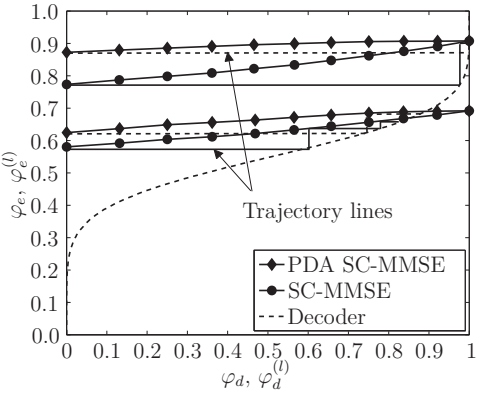

Figure 4.9.: Correlation chart for the SC-MMSE and PDA SC-MMSE FDEs employing rate-1/2 SCCs. Equalizer correlation curves are shown for a random channel realization ($N = M = 2$, $Q = 128$ and $L = 10$) at $E_s/N_0 = 3$ dB and -0.5 dB (from top to bottom).

The corresponding trajectories show the information exchange between both SfISfO components of the turbo receiver over a number of iterations which is defined by the vector sequence in (4.32). From the correlation chart in Fig. 4.9, we observe the improvement of the convergence threshold and convergence rate of the PDA SC-MMSE FDE over the standard SC-MMSE FDE. This property justifies the BER performance enhancement of the PDA-based turbo receiver shown in Fig. 3.10 of Section 3.7.

Next, we compare the analytical BER performance prediction with the simulated results for both receivers in Fig 4.10 (a) and (b). The curves are obtained by averaging over a large number of random channel realizations. It can be seen that for both receivers the analytical results coincide perfectly with the simulated curves for the considered channel codes and SNR value range. Similar results are obtained for turbo systems employing SCCCs and larger antenna configurations ($N = M > 2$). We conclude that the proposed analytical method for calculating the equalizer correlation functions and the corresponding BER estimates allows to accurately predict the convergence behavior and BER performance of both turbo receivers.

Finally, we present results for an $N = M = 8$ multiuser turbo system and compare the convergence behavior of the HY SC-MMSE FDE with the standard SC-MMSE FDE. We consider a scenario where four of the eight users' channels are highly spatially correlated at the transmit side and the remaining users' channels are close to orthogonal. The off-diagonal elements of the transmit correlation matrix $\mathbf{S}$ are

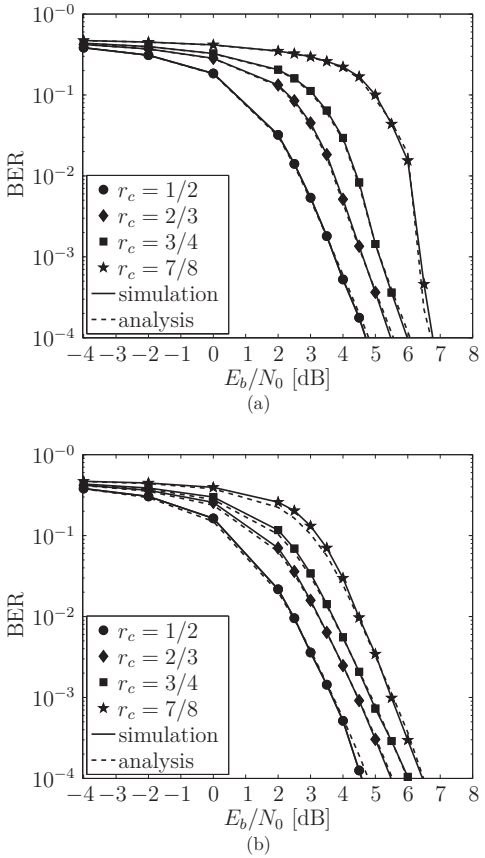

Figure 4.10.: Comparison of average analytical and simulated BER performance obtained for the SC-MMSE FDE (a) and the PDA SC-MMSE FDE (b) for simple SCCs. Single-user MIMO transmission with $N = M = 2$, $Q = 128$ and $L = 10$.

set to $[\mathbf{S}]_{ij} = 0.9$, for $1 \leq i, j \leq 4$, $i \neq j$, and $[\mathbf{S}]_{ij} = 0$ otherwise. The groupsize of the hybrid SC-MMSE FDE is chosen to $U = 4$, such that the four highly correlated users' signals are allocated into one subgroup.

Fig. 4.11 (a) and (b) illustrate the corresponding projected correlation curves and trajectories for both receivers at SNR $E_s/N_0 = 2$ dB and $E_s/N_0 = 6$ dB, respectively. The correlation functions are identical for all users and obtained when an rate-1/2 SCCC is employed at each user. As observed from Fig. 4.11 (a), for the low SNR

value of 2 dB, both turbo equalization techniques have similar performances for all users. Moreover, we find that only for the users' signals with low spatial transmit correlation, the convergence tunnels between the equalizer and decoder curves are existent and thus convergence of turbo equalization may be achieved, whereas for the remaining four highly correlated users' signals, the two turbo equalizers fail to convergence and thus to decode these users' messages. In contrast, as shown in Fig. 4.11 (b) , when increasing the SNR value to 6 dB, we see that only the HY SC-MMSE FDE is able to form an open convergence tunnel for the four highly spatially correlated user signals and thus to successfully decode all users' messages. It indicates that the proposed hybrid scheme enhances the convergence properties of the turbo receiver which may finally result in an improved BER over the standard SC-MMSE FDE. These findings justify the performance results of the error rate performances of both receivers from Section 3.7.

4.2. EXIT Chart Analysis

The EXIT chart was introduced by ten Brink in [tB01] to analyze and design concatenated coding schemes with iterative decoding. As for the correlation chart, the EXIT chart uses a single parameter to describe the PDFs of the LLR messages within the turbo system. While the correlation chart visualizes the density evolution by expressing the correlation between the transmitted binary data and the corresponding LLRs, the EXIT chart uses the average mutual information. Both analysis methods have a close relationship, and are shown to be similar in terms of prediction accuracy of the modeling parameter [TtBH02]. However, as opposed to the correlation chart, the EXIT chart has an information-theoretic meaning, given by the area property theorem [AKtB04]. This theorem relates the area of EXIT functions to the rate of a channel code or to the capacity of a channel.

In this section, we briefly review the EXIT chart analysis and define the mutual information as well as the EXIT functions for the equalizer and channel decoder. We then focus on the area property theorem of EXIT functions, and discuss some important implications. We restrict our self to a single-user MIMO BICM transmission system. The extension to multiuser communication will be discussed in Chapter 5.

4.2.1. Mutual Information

Let I_e denote the average mutual information between the transmitted code bits $b_{q,n}[k]$ and the *extrinsic* LLRs $\lambda_e\left[b_{q,n}[k]\right]$ provided by the equalizer, expressed as

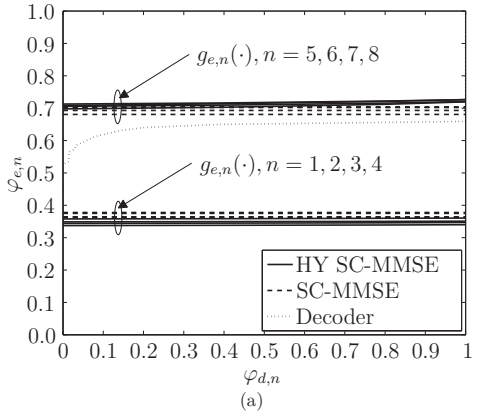

(a)

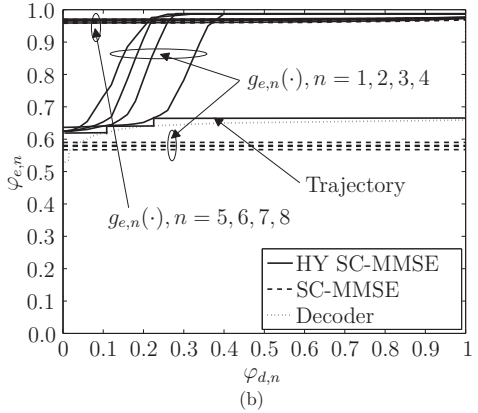

(b)

Figure 4.11.: Correlation functions (projection) of the HY SC-MMSE FDE ($U = 4$) and the standard SC-MMSE FDE ($U = 1$) for each user for a single random $L = 32$-tap Rayleigh fading channel realization at $E_s/N_0 = 2$ dB (a) and $E_s/N_0 = 6$ dB (b). $N = M = 8$ and $Q = 512$.

[AKtB04]:

$$I_e = \frac{1}{NQN_b} \sum_{k=1}^{N_b} \sum_{q=0}^{Q-1} \sum_{n=1}^{N} I\Big(b_{q,n}[k], \lambda_e\big[b_{q,n}[k]\big]\Big) \in \mathbb{D}. \tag{4.35}$$

Further, let I_d be the mutual information between $b_{q,n}[k]$ and the equalizer *a priori* LLRs $\zeta_e\Big[b_{q,n}[k]\Big]$ provided by the channel decoder in the form of the *extrinsic* LLRs. The mutual information I_d can be expressed as

$$I_d = \frac{1}{NQN_b}\sum_{k=1}^{N_b}\sum_{q=0}^{Q-1}\sum_{n=1}^{N} I\Big(b_{q,n}[k], \zeta_e\Big[b_{q,n}[k]\Big]\Big) \in \mathbb{D}. \tag{4.36}$$

To characterize the convergence behavior of the turbo equalizer, similar to (4.5), we define two functions $I_e = \hat{f}_e(I_d)$ and $I_d = \hat{f}_d(I_e)$, that describe the input-to-output mutual information characteristic of the equalizer and channel decoder, respectively. The values of the mutual information in (4.35) and (4.36) can be estimated by histogram-based measurements on the conditional PDFs of the LLRs $\lambda_e\Big[b_{q,n}[k]\Big]$ and $\zeta_e\Big[b_{q,n}[k]\Big]$. Assuming uniformly distributed coded bits $b_{q,n}[k]$, the mutual information I then reads as [tB01]

$$\begin{aligned} I(b_{q,n}[k], l) &= \frac{1}{2}\sum_{b_{q,n}[k]=\pm 1}\int_{-\infty}^{\infty} p(l|b_{q,n}[k]) \\ &\qquad \times \log_2\left(\frac{2p(l|b_{q,n}[k])}{p(l|b_{q,n}[k]=+1)+p(l|b_{q,n}[k]=-1)}\right)\mathrm{d}l \\ &= 1 - \frac{1}{NQN_b}\sum_{k=1}^{N_b}\sum_{q=0}^{Q-1}\sum_{n=1}^{N}\log_2\left(1+e^{b_{q,n}[k]l}\right), \end{aligned} \tag{4.37}$$

where $p(l|b_{q,n}[k])$ is the PDF of the LLRs $l \equiv L\Big[b_{q,n}[k]\Big]$ conditioned on the coded bit $b_{q,n}[k] \in \{-1,+1\}$. We remark that the second line of (4.37) has been derived based on the ergodic property and the exponential-symmetry condition on the LLRs l. Besides this, as the LLRs at the input and output of the channel equalizer are Gaussian distributed, the well known relationship between the channel SNR ϱ on the LLRs l and the mutual information is obtained, by using the so-called J-function [tB01], as

$$\begin{aligned} I &= J(2\sqrt{\varrho}) = 1 - \frac{1}{\sqrt{2\pi}}\int_{-\infty}^{+\infty}\log_2\left(1+e^{-2\varrho-2\sqrt{\varrho}x}\right)e^{-\frac{x^2}{2}}\mathrm{d}x \\ &\equiv \phi_J(\varrho). \end{aligned} \tag{4.38}$$

Similar to the function $\phi(\cdot)$ in (3.66) and (4.2), $\phi_J(\cdot)$ is strictly monotonically increasing and hence, it has a unique inverse, expressed by $\varrho = \phi_J^{-1}(I)$.

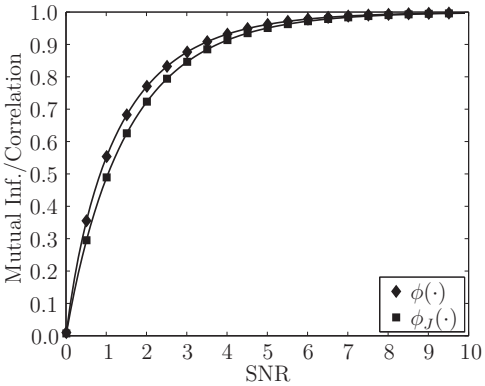

Figure 4.12.: Functions $\phi_J(\cdot)$ and $\phi(\cdot)$ over the equivalent SNR of the LLRs.

4.2.2. Relationship to Correlation Measure

The EXIT chart and the correlation chart are closely related. Supposing exponential-symmetric Gaussian distributed LLRs, the mutual information and the correlation are formally described by the functions $\phi_J(\cdot)$ and $\phi(\cdot)$ over the SNR of the LLRs, respectively. Although both functions can not be calculated in closed form, they can be closely approximated by analytical expressions obtained using numerical integration techniques. The close relationship between the EXIT chart and the correlation chart is emphasized when comparing $\phi_J(\cdot)$ and $\phi(\cdot)$ in one chart, as shown in Fig. 4.12. It can be seen that both functions are similar, which is also supported by equations (4.37) and (4.7), that can be written as [Hag04]

$$1 - \mathbb{E}\Big[\log_2\left(1+e^{-x}\right)\Big] = \mathbb{E}\Big[\log_2\left(1+\tanh\left(\frac{x}{2}\right)\right)\Big] \approx \frac{1}{\ln 2}\mathbb{E}\Big[\tanh\left(\frac{x}{2}\right)\Big]. \quad (4.39)$$

Based on this similarity result, Shephard *et. al.* [SBR06] showed that mutual information and correlation can also be combined by a function $\phi_T(\cdot)$, $I \equiv \phi_T(\varphi) = \phi_J\Big(\phi^{-1}(\varphi)\Big)$, used to translate the mutual information I into the correlation φ and vice versa.

4.2.3. Area Property of EXIT Functions

One of the most important properties of EXIT charts is the so-called area property theorem, that relates the area under the EXIT function to the rate of a channel code or to the capacity of a channel. Let us consider a serial concatenated system with linear channel coding (i.e., an encoder with an one-to-one (invertible) mapping

[AKtB04]) and an i.i.d. information data source. For such a system, it was proven by Ashikhmin *et. al.* [AKtB04] that the area $A_c = \int_0^1 \hat{f}_d^{-1}(I_d)\mathrm{d}I_d$ under the inverse decoder EXIT function $\hat{f}_d^{-1}(\cdot)$ equals to the rate r_c of the channel code, i.e., $A_c = r_c$, for MAP decoding if the *a priori* LLR information is from a binary erasure channel (BEC). Moreover, it was shown that for an optimal MAP equalizer the area $A_e = \int_0^1 \hat{f}_e(I_d)\mathrm{d}I_d$ under the EXIT function $\hat{f}_e(\cdot)$ satisfies the equality $A_e = I(\mathbf{b}, \mathbf{r})$ in the case of a non-precoded BPSK signal transmission, where the value of the mutual information $I(\mathbf{b}, \mathbf{r})$ defines the constellation constraint capacity C_{con} of the channel. Therefore, we obtain the remarkable property that the area under the equalizer EXIT characteristic is equal to the capacity C_{con} of the channel. Although the above area property has only been proven for the case when the *a priori* LLRs is assumed to be the output from a BEC, it also appears to work well for Gaussian distributed LLRs [Tüc04]. Note that both the area A_e and the capacity C_{con} are constrained by the modulation scheme used for the transmit signal generation, but are independent (for higher order signal constellations) of the applied mapping method. Further, if we apply non-optimal equalization algorithms, such as MMSE-based turbo receivers, we have $A_e < C_{\text{con}}$ [AKtB04]. This means the use of sub-optimal equalizers already incurs a loss in rate. The area A_e then corresponds to the maximum achievable rate of the turbo system, constrained by the receiver algorithm.

Some important conclusions of the area property theorem are as follows:

- For successful convergence of turbo equalization, the (inverse) decoder EXIT function must lie under the equalizer EXIT function, implying that $A_c < A_e$. Supposing optimal channel decoding and equalization, this relation leads to the fundamental coding theorem [CT91], revealing that the overall transmission rate should be smaller than the capacity, i.e., $r_c < C_{\text{con}}$.

- The difference $A_e - A_c$ between the both areas corresponds to the rate loss $C_{\text{con}} - r_c$ of the turbo system. A direct consequence of this result is that to approach capacity, the EXIT functions of the equalizer and the decoder should be as closely as possible without crossing each other, to guarantee an open convergence tunnel for an error-free transmission. In other words, the two EXIT curves are not allowed to intersect, until the mutual information I_d at the decoder output approximately achieves the value one.

Based on the above results, the design of capacity-approaching turbo systems can obviously be reduced, in principle, to a curve-fitting problem of the EXIT functions of the equalizer and channel decoder [AKtB04], [tBKA04], [tBK03]. In this regard, one approach is to optimize the parameters of the channel code such that both EXIT functions are well matched to each other. In [tBKA04], ten Brink *et*

al. applied the curve-fitting technique to design powerful capacity-achieving LDPC codes for flat-fading MIMO BICM systems with iterative decoding and detection. A similar idea based on repeat-accumulate codes was investigated by the authors of [tBK03]. In a related work, Tüchler [Tüc04] used rate-compatible irregular convolutional codes to optimize the decoder EXIT function in non-fading SISO channels. Similarly, Schreckenbach *et al.* [SGHB03], [SB06] employed irregular (hybrid) signal constellations and mappings to shape the EXIT function of the detector to match both EXIT curves to each other.

Further applications of the curve-fitting approach are the adaptation of the equalizer EXIT function through optimization of transmission power with respect to a QoS constraint, while keeping the channel code fixed, or the adjustment of the code rate at the transmitter by rate allocation with a set of fixed rate-compatible channel codes [GOM10], [GM09]. Both approaches will be investigated more in detail in the following Chapter 5.

4.3. Outage Probability Analysis

The outage performance of the turbo receiver equipped with the standard SC-MMSE FDE can be assessed, in principle, by performing the correlation chart analysis for a sufficiently large number of random channel realizations. However, as for each channel realization the correlation function of the equalizer has to be computed, this approach may be time-consuming. This motivates the need for simpler methods for calculating the outage probability of the turbo equalizer. In this section, we propose a novel method that avoids the necessity of recalculating the equalizer correlation function. The case of single-user single antenna transmission over Rayleigh fading ISI channels with exponential delay-power profile is considered. In particular, by using a union bounding technique and a specific central limit theorem, it is shown that an error bound for the outage probability can be derived. In addition, a lower bound on the system's outage performance is found by assuming a transmission with perfect ISI cancellation at the receiver. Analytical and simulation results that demonstrate the tightness of the proposed error bound for various channel setups are shown. As we consider in the following a single-user single antenna transmission system, the antenna indices are skipped from all antenna-dependent variables.

4.3.1. Derivation of Closed-form Expression on Outage Performance

For the following analysis, the equalizer correlation characteristic $f_e(\cdot)$ is considered as a random process, as it depends on the frequency domain channel matrix $\mathbf{\Xi}_c$,

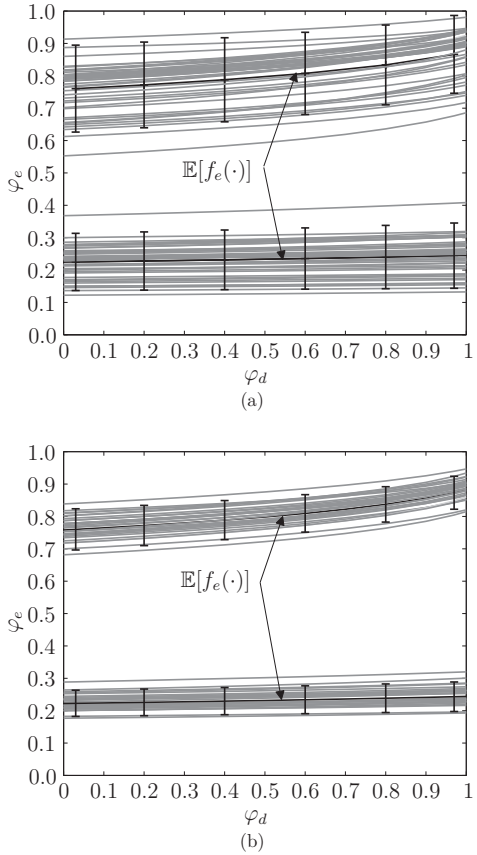

Figure 4.13.: Example of equalizer functions $f_e(\cdot)$ (gray curves) and resulting averaged output correlations (black curves) for different random realizations of a Rayleigh fading channel with exponential delay-power profile at receive SNRs $E_s/N_0 = 2$ dB (top curves) and $E_s/N_0 = -8$ dB (bottom curves). (a) $\tau_d = 8$, $Q = 128$. (b) $\tau_d = 32$, $Q = 512$.

whose entries change independently frame-by-frame. The turbo equalizer fails to converge to the maximum value $\tilde{\varphi}_d = 1$ and thus to decode a message, if for a specific realization of $\boldsymbol{\Xi}_c$ the correlation curves of the equalizer and the decoder intersect, such that $\tilde{\varphi}_d < 1$ follows. An outage event occurs when $f_e(\varphi_d) \leq f_d^{-1}(\varphi_d)$ for at least one value of $\varphi_d \in [0, 1)$. We can therefore evaluate the outage probability

of the SC-MMSE FDE as

$$P_o \equiv \text{Prob}\left(f_e(\varphi_d) \leq f_d^{-1}(\varphi_d),\ \exists \varphi_d \in [0,1)\right). \tag{4.40}$$

Examples of the correlation function $f_e(\cdot)$ for various randomly generated realizations of a Rayleigh fading channel with two different exponential delay-power profiles are depicted in Fig. 4.13 (a) and (b). The mean $\mathbb{E}[f_e(\varphi_d)]$ and the variance $\text{Var}[f_e(\varphi_d)]$ of the correlation is shown as well. The half band width is restricted to $2\sqrt{\text{Var}[f_e(\varphi_d)]}$. As observed from these figures, the delay-power profile of the channel and the receive SNR have a direct influence on the slope and spread of the correlation function values around their means $\mathbb{E}[f_e(\varphi_d]$. The outage performance of the turbo system thus does not alone depend on the channel code used at the transmitter, but also on the channel fading distribution as well as on the SNR at the receiver.

In order to derive a closed-form expression on the outage probability in (4.40), we plug the SNR expression from (3.41) into (4.13), exploit the monotonicity property of the function $\phi(\cdot)$ (see Fig. 3.4), and write

$$P_o = \text{Prob}\left(S(\boldsymbol{\kappa}, \varphi_d) > A(\varphi_d),\ \exists \varphi_d \in [0,1)\right), \tag{4.41}$$

where

$$S(\boldsymbol{\kappa}, \varphi_d) \equiv \frac{1}{Q} \sum_{q=0}^{Q-1} \frac{1}{1 + \rho(\varphi_d)\kappa(q)}, \tag{4.42}$$

$$\boldsymbol{\kappa} \equiv [\kappa(0), ..., \kappa(q), ..., \kappa(Q-1)]^T, \tag{4.43}$$

$$A(\varphi_d) \equiv \frac{2}{(1-\varphi_d)\phi^{-1}(f_d^{-1}(\varphi_d)) + 2}. \tag{4.44}$$

A direct evaluation of the inequality $S(\boldsymbol{\kappa}, \varphi_d) > A(\varphi_d)$ in the probability term (4.41) on the continuous interval $\varphi_d \in [0,1)$ is analytically intractable. In order to proceed, we impose the inequality condition on a discrete set $\mathcal{J}$ of D values, $\mathcal{J} \equiv \{\varphi_d^{(1)}, ..., \varphi_d^{(k)}, ..., \varphi_d^{(D)}\} \subset [0,1)$, so that the probability can be approximated as

$$P_o \approx \text{Prob}\left(S(\boldsymbol{\kappa}, \varphi_d^{(k)}) > A(\varphi_d^{(k)}),\ \exists \varphi_d^{(k)} \in \mathcal{J}\right). \tag{4.45}$$

Then, by applying the union bound [Kre05] on (4.45), we obtain

$$P_o \leq \sum_{k=1}^{D} \text{Prob}\left(S(\boldsymbol{\kappa}, \varphi_d^{(k)}) > A(\varphi_d^{(k)})\right). \tag{4.46}$$

The calculation of the probability terms in (4.46) requires knowledge of the distri-

bution of the random variable $S(\boldsymbol{\kappa}, \varphi_d^{(k)})$ for each value $\varphi_d^{(k)} \in \mathcal{J}$. However, an exact derivation of this distribution is not easy, since due to the exponential delay-power profile of the channel the frequency domain gains $\kappa(q)$ are correlated with order $1/(\Delta q)^2$, $\Delta q = q_1 - q_2$, as shown in Section 2.3. Therefore, we study in the following the asymptotic behavior of the random variable $S(\boldsymbol{\kappa}, \varphi_d^{(k)})$ for the case of $Q \to \infty$. In particular, using a theorem from Arcones [Arc94], it can be shown that $S(\boldsymbol{\kappa}, \varphi_d^{(k)})$ is asymptotically Gaussian distributed. We remark that Arcones' theorem has also been adopted in [CST07] to calculate the capacity of OFDM systems. We state this theorem below. A proof of it can be found in [Arc94].

Theorem 4.5. Let $\{\mathbf{X}_j\}$, $\mathbf{X}_j \equiv \left[X_j^{(1)}, X_j^{(2)}, ..., X_j^{(d)}\right]^T$, $0 \leq j < \infty$ be a stationary zero-mean sequence of Gaussian random vectors in $\mathbb{R}^d$ with covariance function

$$r^{(i,l)}(k) = \mathbb{E}\left[X_m^{(i)} X_{m+k}^{(l)}\right] \tag{4.47}$$

for $k \in \mathbb{Z}$, $0 \leq m < \infty$ and $m + k \geq 0$. Let $f : \mathbb{R}^d \to \mathbb{R}$ be a real-valued function with Hermite rank $\omega(f)$ such that $1 \leq \omega(f) < \infty$. Suppose that

$$\sum_{k=-\infty}^{\infty} \left| r^{(i,l)}(k) \right|^{\omega(f)} < \infty \tag{4.48}$$

for $1 \leq i, l \leq d$. Then, as Q tends to infinity

$$\frac{1}{\sqrt{Q}} \sum_{j=0}^{Q-1} \Big(f(\mathbf{X}_j) - \mathbb{E}[f(\mathbf{X}_j)] \Big) \xrightarrow{d} \mathcal{N}\Big(0, \sigma_T^2\Big), \tag{4.49}$$

where $\xrightarrow{d}$ denotes convergence in distribution, and

$$\sigma_T^2 = \mathbb{E}\Big[\Big(f(\mathbf{X}_0) - \mathbb{E}[f(\mathbf{X}_0)]\Big)^2\Big] + 2\sum_{j=0}^{\infty} \mathbb{E}\Big[\Big(f(\mathbf{X}_0) - \mathbb{E}[f(\mathbf{X}_0)]\Big)\Big(f(\mathbf{X}_k) - \mathbb{E}[f(\mathbf{X}_k)]\Big)\Big]. \tag{4.50}$$

We apply Theorem 4.5 to the sequence of complex channel coefficients $\{\tau(q)\}$, $\tau(q) = \Re\{\tau(q)\} + \sqrt{-1}\Im\{\tau(q)\}$, $0 \leq q \leq Q-1$. We set $\mathbf{X}_q = [\Re\{\tau(q)\}, \Im\{\tau(q)\}]^T$, $0 \leq q \leq Q-1$, $d = 2$, and let

$$\begin{aligned} f(\mathbf{X}_q) &= h_k\Big(\Re\{\tau(q)\}, \Im\{\tau(q)\}\Big) \\ &= c_k(\kappa(q)) \equiv \frac{1}{1 + \rho(\varphi_d^{(k)})(\Re\{\tau(q)\}^2 + \Im\{\tau(q)\}^2)}. \end{aligned} \tag{4.51}$$

Using the channel correlation properties in (2.27), it can easily be shown that the

covariance function in (4.47) satisfies condition (4.48) if the Hermite rank of $h_k(\cdot)$ is at least two [CST07]. We present the definition of the Hermite rank of a function in the following, and show that $h_k(\cdot)$ has Hermite rank $\omega(h_k) \geq 2$. We basically follow the same derivation as in [CST07], where the Hermite rank of the sub-channel capacity as a function of the channel gains for an OFDM system has been calculated.

Hermite Rank Let $\mathbf{X}$ be a Gaussian vector with zero-mean and unit-variance. Further, let $f : \mathbb{R}^d \to \mathbb{R}$ be a real-valued function with $\mathbb{E}[f(\mathbf{X})^2] < \infty$. The Hermite rank $\omega(f)$ of $f(\cdot)$ with respect to $\mathbf{X}$ is defined in [Arc94] as

$$\omega(f) \equiv \inf\Big\{\tau : \exists \text{ polynomial Pol of degree } \tau \text{ with } \mathbb{E}\Big[\Big(f(\mathbf{X}) - \mathbb{E}[f(\mathbf{X})]\Big)\mathrm{Pol}(\mathbf{X})\Big] \neq 0\Big\}. \quad (4.52)$$

First, consider a zero-order polynomial $\mathrm{Pol}(\mathbf{X}) = A_0$ with $\mathbf{X} = (X_1, X_2)$, for which the condition in (4.52) becomes

$$\begin{aligned}\mathbb{E}\Big[\Big(h_k(\mathbf{X}) - \mathbb{E}[h_k(\mathbf{X})]\Big)\mathrm{Pol}(\mathbf{X})\Big] &= A_0\mathbb{E}\Big[h_k(\mathbf{X})\Big] - A_0\mathbb{E}\Big[h_k(\mathbf{X})\Big] \\ &= 0, \end{aligned} \quad (4.53)$$

for all $A_0 \in \mathbb{R}$. Thus, $\omega(h_k) \neq 0$. Next, consider a first-order polynomial $\mathrm{Pol}(\mathbf{X}) = A_0X_1 + A_1X_2 + A_3$. Then, we have

$$\begin{aligned}&\mathbb{E}\Big[\Big(h_k(\mathbf{X}) - \mathbb{E}[h_k(\mathbf{X})]\Big)\mathrm{Pol}(\mathbf{X})\Big] \\ &= A_0\mathbb{E}\Big[X_1h_k(\mathbf{X})\Big] + A_1\mathbb{E}\Big[X_2h_k(\mathbf{X})\Big], \end{aligned} \quad (4.54)$$

where we have used the property $\mathbb{E}[X_1] = \mathbb{E}[X_2] = 0$. The random variables X_1 and X_2 are identically Gaussian distributed. $\mathbb{E}\Big[X_1h_k(\mathbf{X})\Big]$ can then be expressed as

$$\begin{aligned}\mathbb{E}\Big[X_1h_k(\mathbf{X})\Big] &= \mathbb{E}\Big[X_2h_k(\mathbf{X})\Big] \\ &= \int_{-\infty}^{\infty}\int_{-\infty}^{\infty} x_1h_k(x_1, x_2)p(x_1, x_2)\mathrm{d}x_1\mathrm{d}x_2, \end{aligned} \quad (4.55)$$

where $p(x_1, x_2)$ is the joint PDF of the two correlated Gaussian random variables X_1 and X_2. We remark that both functions $p(x_1, x_2)$ and $h_k(x_1, x_2)$ are even in (X_1, X_2). The integral in (4.55) is therefore zero and $\mathbb{E}\Big[X_1h_k(\mathbf{X})\Big] = \mathbb{E}\Big[X_2h_k(\mathbf{X})\Big] = 0$. We conclude that $\omega(h_k)$ is at least 2.

With the fact that $\omega(h_k) \geq 2$, requirement (4.48) is satisfied, so that for $Q \to \infty$

$$\frac{1}{\sqrt{Q}} \sum_{q=0}^{Q-1} \Big(h_k\Big(\Re\{\tau(q)\}, \Im\{\tau(q)\}\Big) - \mathbb{E}\Big[h_k\Big(\Re\{\tau(q)\}, \Im\{\tau(q)\}\Big)\Big]\Big) \xrightarrow{d} \mathcal{N}\Big(0, \sigma_T^2\Big). \tag{4.56}$$

Equation (4.56) states that the probability $\text{Prob}\Big(S(\boldsymbol{\kappa}, \varphi_d^{(k)}) > A(\varphi_d^{(k)})\Big)$ in (4.46) approaches a Gaussian probability function for sufficiently large values of Q. For large finite Q, $S(\boldsymbol{\kappa}, \varphi_d^{(k)})$ may thus be approximated by a Gaussian random variable having mean $\mathring{\mu}_k \equiv \mathbb{E}\Big[S(\boldsymbol{\kappa}, \varphi_d^{(k)})\Big] = \mathbb{E}\Big[c_k(\kappa(q))\Big]$ and variance

$$\begin{aligned}\mathring{\sigma}_k^2 &\equiv \text{Var}\Big[S(\boldsymbol{\kappa}, \varphi_d^{(k)})\Big] \\ &= \frac{1}{Q}\mathbb{E}\Big[c_k^2(\kappa(q))\Big] - \Big(\mathbb{E}\Big[c_k(\kappa(q))\Big]\Big)^2 + \frac{2}{Q^2}\sum_{j=1}^{Q-1}(Q-j)\mathbb{E}\Big[c_k(\kappa(0))c_k(\kappa(j))\Big], \forall k,\end{aligned} \tag{4.57}$$

where the quantities $\mathbb{E}\Big[c_k(\kappa(q))\Big]$, $\mathbb{E}\Big[c_k^2(\kappa(q))\Big]$ and $\mathbb{E}\Big[c_k(\kappa(0))c_k(\kappa(q))\Big]$ are calculated as

$$\mathbb{E}\Big[c_k(\kappa(q))\Big] = \int_0^\infty \frac{1}{1+\rho(\varphi_d^{(k)})x} p(x)\mathrm{d}x, \tag{4.58}$$

$$\mathbb{E}\Big[c_k^2(\kappa(q))\Big] = \int_0^\infty \frac{1}{\Big(1+\rho(\varphi_d^{(k)})x\Big)^2} p(x)\mathrm{d}x, \tag{4.59}$$

$$\mathbb{E}[c_k(\kappa(0))c_k(\kappa(j))\Big] = \int_0^\infty \int_0^\infty \frac{1}{\Big(1+\rho(\varphi_d^{(k)})x\Big)\Big(1+\rho(\varphi_d^{(k)})y\Big)} p(x,y)\mathrm{d}x\mathrm{d}y. \tag{4.60}$$

The functions $p(x)$ and $p(x,y)$ in (4.58)-(4.60) are the PDF and joint PDF of $\kappa(q)$ and $(\kappa(0), \kappa(j))$, respectively. Since $\kappa(q)$ is exponentially distributed, we have $p(x) = \exp(-x)$. Therefore, Eqn. (4.58) and (4.59) may be written as

$$\mathbb{E}\Big[c_k(\kappa(q))\Big] = \frac{\exp\left(\frac{1}{\rho(\varphi_d^{(k)})}\right)}{\rho(\varphi_d^{(k)})} E_1\left(\frac{1}{\rho(\varphi_d^{(k)})}\right), \tag{4.61}$$

$$\mathbb{E}\Big[c_k^2(\kappa(q))\Big] = \frac{1}{\rho(\varphi_d^{(k)})}\Big[1 - \mathbb{E}\Big[c_k(\kappa(q))\Big]\Big], \tag{4.62}$$

where $E_1(x) = \int_x^\infty e^{-t}t^{-1}\mathrm{d}t$ denotes the exponential integral function. The joint PDF $p(x,y)$ in (4.60) follows a bivariate exponential distribution, and has the fol-

lowing form [Mal03, eqn. (119)]:

$$p(x,y) = \chi_j \exp\Big[-\beta_j(x+y)\Big] \mathrm{I}_0\Big(\vartheta_j\sqrt{xy}\Big), \tag{4.63}$$

where $\chi_j = \frac{1}{(1-\delta_j)}$, $\beta_j = \chi_j$, $\vartheta_j = 2\chi_j\sqrt{\delta_j}$, $j = 1, ..., Q-1$, $\delta_j = \mathrm{Corr}[\kappa(0), \kappa(j)]$, and $\mathrm{I}_0(.)$ denotes the modified zero-order Bessel function of the first kind. Substituting (4.63) into (4.60), the term $\mathbb{E}\big[c_k(\kappa(0))c_k(\kappa(j))\big]$ can be expressed as

$$\begin{aligned}\mathbb{E}\big[c_k(\kappa(0))c_k(\kappa(j))\big] &= \chi_j \int_0^\infty \int_0^\infty \frac{1}{1+\rho(\varphi_d^{(k)})x} \frac{1}{1+\rho(\varphi_d^{(k)})y} \\ &\qquad \exp\Big[-\beta_j(x+y)\Big] \mathrm{I}_0(\vartheta_j\sqrt{xy})\mathrm{d}x\mathrm{d}y \\ &= \chi_j \sum_{n=0}^{\infty} \left(\frac{\vartheta_j^{2n}}{4^n (n!)^2} \Big[\int_0^\infty \frac{x^n}{1+\rho(\varphi_d^{(k)})x} \exp(-\beta_j x)\mathrm{d}x \Big]^2 \right). \end{aligned} \tag{4.64}$$

Note that (4.64) is obtained by using the series expansion of $\mathrm{I}_0(\cdot)$ [GR07]. Using the substitution from [GR07, Eqn. (3.353.2)], we may write the integral expression in (4.64) as

$$\begin{aligned}&\int_0^\infty \frac{x^n}{1+\rho(\varphi_d^{(k)})x} \exp(-\beta_j x)\mathrm{d}x = \\ &\qquad \frac{(-1)^n}{\rho(\varphi_d^{(k)})^{n+1}} \left[\exp\left(\frac{\beta_j}{\rho(\varphi_d^{(k)})}\right) \mathrm{E}_1\left(\frac{\beta_j}{\rho(\varphi_d^{(k)})}\right) + \sum_{s=1}^{n} (s-1)! \left(-\frac{\rho(\varphi_d^{(k)})}{\beta_j} \right)^s \right]. \end{aligned} \tag{4.65}$$

Now, substituting (4.65) into (4.64), we finally obtain

$$\begin{aligned}\mathbb{E}\big[c_k(\kappa(0))c_k(\kappa(j))\big] = \frac{\chi_j}{\rho(\varphi_d^{(k)})^2} \sum_{n=0}^{\infty} \left(\frac{\left(\frac{\vartheta_j}{2\rho(\varphi_d^{(k)})}\right)^{2n}}{(n!)^2} \left[\exp\left(\frac{\beta_j}{\rho(\varphi_d^{(k)})}\right) \mathrm{E}_1\left(\frac{\beta_j}{\rho(\varphi_d^{(k)})}\right) \right.\right. \\ \left.\left. + \sum_{s=1}^{n} (s-1)! \left(-\frac{\rho(\varphi_d^{(k)})}{\beta_j} \right)^s \right]^2 \right). \end{aligned} \tag{4.66}$$

Numerical calculations show that the series in (4.66) is rapidly convergent and can be used to efficiently calculate the integral in (4.60).

The outage performance of the turbo equalizer is fully determined by the means and variances of the approximately Gaussian distributed random variables $S(\boldsymbol{\kappa}, \varphi_d^{(k)})$, $k = 1.., D$. Using the derived results (4.57)-(4.66), we finally may express the outage

probability (4.46) as

$$P_o \leq \sum_{k=1}^{D} \frac{1}{\sqrt{2\pi}\mathring{\sigma}_k} \int_{A(\varphi_d^{(k)})}^{\infty} \exp\Big[\frac{-\big(x-\mathring{\mu}_k\big)^2}{2\mathring{\sigma}_k^2}\Big]\mathrm{d}x$$
$$= \frac{1}{2}\sum_{k=1}^{D} \mathrm{erfc}\Big(\frac{A(\varphi_d^{(k)})-\mathring{\mu}_k}{\sqrt{2}\mathring{\sigma}_k}\Big). \tag{4.67}$$

Simulations in Section 4.3.3 confirm that (4.67) is a good approximation on the outage performance of the SC-MMSE FDE for a large range of receive SNR values and different RMS channel delays τ_d. As observed from (4.57), (4.61), (4.62) and (4.66), only the variance $\mathring{\sigma}_k^2$ of $S(\boldsymbol{\kappa}, \varphi_d^{(k)})$ depends (through the covariance terms $\mathbb{E}[c_k(\kappa(0))c_k(\kappa(j))\big]$) on the correlation values δ_j, $j = 1, ..., Q-1$ of the frequency domain channel gains. By numerically evaluating (4.66), we find that the covariance $\mathbb{E}[c_k(\kappa(0))c_k(\kappa(j))\big]$ decreases, and thus also the variance $\mathring{\sigma}_k^2$, as the value of δ_j decreases. The minimum variance $\mathring{\sigma}_{k|min}^2 = \frac{1}{Q}\Big(\mathbb{E}\big[c_k^2(\kappa(q))\big] - \Big(\mathbb{E}\big[c_k(\kappa(q))\big]\Big)^2\Big) = \frac{1}{Q}\mathrm{Var}[c_k(\kappa(q))]$ is obtained for $\delta_j = 0$, $j = 1, ..., Q-1$, that means for uncorrelated gains $\kappa(q)$. Moreover, the function $\frac{1}{2}\mathrm{erfc}(x)$ is monotonically decreasing and bounded in $[0, \frac{1}{2}]$ for $x \geq 0$. As expected, we find that the outage probability P_o in (4.67) decreases with decreasing correlation between the frequency domain channel gains and attains its minimum when the gains are uncorrelated.

4.3.2. Derivation of Lower Bound

A lower bound on the outage performance of the SC-MMSE FDE can be derived when perfect ISI cancellation and optimal (i.e., capacity achieving) binary coding is assumed. The outage probability of such an ideal system can be evaluated as

$$P_o^{\star}(R) = \mathrm{Prob}\Big(C_{\mathrm{BPSK}}(\psi^{\mathrm{FD}}(1)) < R\Big), \tag{4.68}$$

where $C_{\mathrm{BPSK}}\Big(\psi^{\mathrm{FD}}(1)\Big)$ the BPSK-input capacity of an AWGN channel, as a function of the SNR $\psi^{\mathrm{FD}}(1)$ at the output of the equalizer for the case of perfect *a priori* information, i.e., $\alpha_e = 1$, and R is the rate of the code. Inspecting (4.68), we immediately see that $C_{\mathrm{BPSK}}(\psi^{\mathrm{FD}}(1))$ is nothing else than the J-function in (4.38), so that we can write $C_{\mathrm{BPSK}}\Big(\psi^{\mathrm{FD}}(1)\Big) = \phi_J\Big(\psi^{\mathrm{FD}}(1)\Big)$. It should be remarked that we assume here binary codes optimized for the AWGN channel, whose achieved rate-threshold pairs are very close to $R = C_{\mathrm{BPSK}}(\cdot)$ at vanishing BER[3].

To express (4.68) in an analytical form, we first write the SNR $\psi^{\mathrm{FD}}(1)$ (3.41) at

[3]Examples of such codes are turbo codes, repeat-accumulate codes and LDPC codes [BGT93], [RU01], [PSU05].

the output of the SC-MMSE FDE (for the case of perfect *a priori* information) as

$$\psi^{\mathrm{FD}}(1) = \frac{2}{Q\sigma_0^2} \sum_{q=0}^{Q-1} \kappa(q). \tag{4.69}$$

Using the fact that $\phi_J(\cdot)$ is strictly monotonically increasing and positive, we rewrite (4.68) as

$$P_o^{\star}(R) = \mathrm{Prob}\left(Z < \frac{Q\sigma_0^2}{2} \phi_J^{-1}(R) \right), \tag{4.70}$$

where $Z \equiv \sum_{q=0}^{Q-1} \kappa(q)$ is the sum of the correlated frequency domain channel gains. The random variables $\{\kappa(q)\}_{q=0}^{Q-1}$ are identical exponentially distributed. Using a result from [AAK01], the PDF of Z can be expressed as

$$p(z) = \prod_{n=1}^{Q} \left(\frac{\delta_1}{\delta_n} \right) \sum_{k=0}^{\infty} \frac{o_k z^{Q+k-1} e^{-z/\delta_1}}{\delta_1^{Q+k} \Gamma(Q+k)} U(z), \tag{4.71}$$

where $U(\cdot)$ is the unit step function, $\Gamma(\cdot)$ is the gamma function [GR07], $\delta_1 = \min_n\{\delta_n\}$, $\{\delta_n\}_{n=1}^{Q}$ are the eigenvalues of the $Q \times Q$ positive definite matrix $\mathbf{W}$, defined by

$$\mathbf{W} = \begin{bmatrix} 1 & \sqrt{\delta_1} & \cdots & \sqrt{\delta_{Q-1}} \\ \sqrt{\delta_1} & 1 & \cdots & \sqrt{\delta_{Q-2}} \\ \vdots & \vdots & \ddots & \vdots \\ \sqrt{\delta_{Q-1}} & \cdots & \cdots & 1 \end{bmatrix}, \tag{4.72}$$

and o_k are coefficients, whose values are obtained recursively by the formula

$$\begin{cases} o_0 & = 1 \\ o_{k+1} & = \frac{1}{k+1} \sum_{i=1}^{k+1} \left[\sum_{j=1}^{Q} \left(1 - \frac{\delta_1}{\delta_j} \right)^i \right] o_{k+1-i} \\ & \quad k = 0, 1, 2, \ldots \end{cases} \tag{4.73}$$

With the expression in (4.71), it can be shown with the help of [GR07, Eqn. (8.35.2)] that the outage probability in (4.70) can finally be expressed as

$$P_o^{\star}(R) = \prod_{n=1}^{Q} \left(\frac{\delta_1}{\delta_n} \right) \sum_{k=0}^{\infty} o_k \frac{\Gamma\left(Q+k, \frac{Q\sigma_0^2}{2\delta_1} \phi_J^{-1}(R) \right)}{\Gamma(Q+k)}, \tag{4.74}$$

where $\Gamma(\cdot,\cdot)$ is the incomplete gamma function [GR07].

4.3.3. Numerical Results

Next, we provide some numerical and analytical results for the outage performance evaluation of the SC-MMSE FDE and the error bounds (4.67) and (4.74). We consider a single-user single-antenna system using an SCCC as FEC. The two FFT-sizes $Q = 128$ and $Q = 512$ are considered. The outage performance is evaluated for $L = 32$ and $L = 128$-tap Rayleigh block-fading channels having exponential delay-power profiles with RMS delays $\tau_d = 8$ and $\tau_d = 32$. The length of a frame is fixed to 32768 BPSK symbols and assumed to be constant during the transmission of one frame. The turbo equalizer performs $T_e = 10$ iterations between the equalizer and the inner decoder, and $T_d = 10$ iterations between the inner and the outer decoder. The number of iterations are chosen to be large enough to ensure convergence. For the calculation of the error bound in (4.67), the inequality constraint in (4.41) is computed on a grid of $D = 4$ points, where $\varphi_d^{(k)} \in \mathcal{J} = \{0.05, 0.3, 0.6, 0.95\}$. Note that, in general, the values $\varphi_d^{(k)} \in \mathcal{J}$ have to be chosen appropriately depending on the shape of the correlation function of the channel decoder. Optimizing these values to increase the approximation accuracy of the error bound is an interesting further research topic, but beyond the scope of this thesis.

The outage performances of the SC-MMSE FDE for the first equalizer and decoder iteration and after convergence for the transmission with regular $r_c = 1/2$ and $r_c = 3/4$ outer RSC codes [Tüc04] over $\tau_d = 8$ and $\tau_d = 32$ Rayleigh fading channels are shown in Fig. 4.14 (a) and Fig. 4.14 (b), respectively. Further, the two error bounds (4.67) and (4.74) are shown as well. The value of $\Delta f \tau_d$ has been kept fixed at 0.0625. The outage probability P_{out} has been computed by averaging over 20000 random channel realizations. We observe that the performance improves with increasing values of the RMS delay τ_d due to increasing channel diversity. Also, observe that we obtain a reasonable analytical approximation of the outage probability for all the system configurations. Moreover, it is found that the approximation gets tight for higher values of τ_d.

The simulations performed are extremely time-consuming, especially due to the large frame length (interleaver size) used. In contrast, the proposed error bound (4.67) provides a simple, less time-consuming, tool to predict well the outage performance of the SC-MMSE FDE over a large range of SNR values and different delay-power profiles.

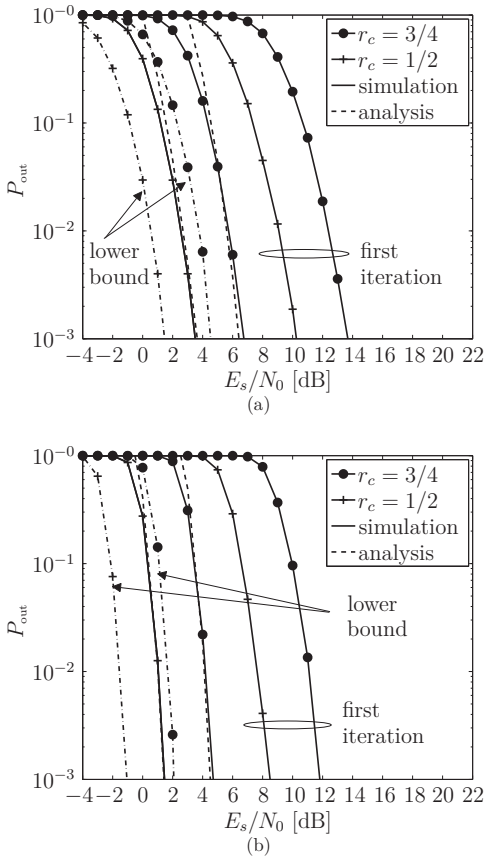

Figure 4.14.: Simulated outage probability and the error bounds (4.67) and (4.74) for regular SCCCs with rates $r = 1/2$ and $3/4$ over Rayleigh fading channel with RMS delay $\tau_d = 8$ ($Q = 128$, $L = 32$) (a) and $\tau_d = 32$ ($Q = 512$, $L = 128$) (b).

4.4. Chapter Summary

In this chapter, the convergence properties of the SC-MMSE, PDA SC-MMSE and HY SC-MMSE FDEs have been analyzed with the aid of a correlation chart analysis. Using the expressions of the SNR at the equalizer outputs, it has been found that the correlation functions for the SC-MMSE and PDA SC-MMSE FDEs may be represented by simple analytical expressions which are sufficient to accurately predict

the output correlation parameters of the equalizer. The impact of the internal equalizer iterations on the output correlation parameter values of the PDA SC-MMSE FDE has been evaluated. As a main result, it is found that the PDA SC-MMSE FDE provides significantly higher output correlation values than the standard SC-MMSE FDE for the same channel realization and receive SNR. The exploitation of the internal equalizer feedback leads to more reliable soft estimates at the equalizer output which improves the convergence properties of the turbo equalizer.

In addition, the correlation characteristic of the channel decoder has been analyzed for single-convolutionally and serially concatenated coded systems. To simplify the analysis of iterative SCCC channel decoding, the operations of the inner and the outer decoder have been combined into a single decoder component. The multidimensional surfaces of the iterative decoder may equivalently be expressed by a single correlation function which considerably simplifies the analysis of the overall iterative decoding process.

Furthermore, the convergence properties of the SC-MMSE and the HY SC-MMSE FDEs have been verified in several spatially-correlated multiuser channel configurations. Based on the projected equalizer and decoder correlation curves, the exchange of soft information in terms of the correlation parameters between the equalizer and the bank of single-user channel decoders has been visualized for both systems in 2D correlation charts. The corresponding decoding trajectories justify the considerable BER performance loss of the SC-MMSE FDE over the hybrid scheme in channels with high spatial correlation. The hybrid turbo scheme may thus be the preferred equalizer in spatially-correlated multiuser ISI channels.

Finally, the outage performance of the SC-MMSE FDE has been verified for a single-user single-antenna transmission over Rayleigh ISI fading channels with exponential delay-power profile. A closed form approximation on the outage probability at the last turbo iteration has been derived. The proposed error bound provides a simple analytical tool to accurately predict the outage performance of the SC-MMSE turbo equalizer. Naturally, this invokes the idea to exploit the error bound to designing channel coding schemes that guarantee a specific outage probability of the receiver. Clearly, the design of such channel coding schemes is an interesting research topic that will be discussed more in detail in the following chapter.

5. Rate and Power Allocation

When the time-variation or fading of the MIMO ISI channel is "slow" such that the transmitter may be able to acquire CSI, the available resources such as rate and transmission power can be allocated adaptively to enhance the system performance and to compensate for the fading of the channel. Therefore, there is a great interest to develop adaptive transmission techniques for single-carrier signaling schemes employing turbo equalization, which efficiently exploit the available resources at the transmitter based upon the channel conditions. One challenging issue to be addressed in this context is how the convergence properties of the iterative equalizer can be taken into account to meet a specific QoS requirement (e.g., a specific target bit error probability, throughput, etc.) of the system. The purpose of this chapter is therefore to address the problem of rate and power allocation for single and multiuser systems with turbo equalization by especially focusing on the convergence properties of the iterative receiver.

The remainder is organized as follows. In Section 5.1, we consider the problem of transmission rate allocation for the two-user Gaussian uplink multiple access ISI fading channel employing the SC-MMSE FDE at the receiver and a fixed power allocation at each transmitter. A variational optimization framework for maximizing the sum rate based on the EXIT chart analysis of the iterative system is presented. A simple code selection algorithm is proposed which aims to optimize the code parameters at each transmitter to improve the overall system throughput. For this scenario assumption, it is supposed that each transmitter can adapt its transmission strategy relative to the instantaneous state of the channel. In the following Section 5.2, we consider fixed-rate transmission strategies optimized with respect to the long-term channel statistics. In this case, the rate control is performed subject to an outage probability constraint of the iterative receiver. The outage probability specifies the convergence failure of the turbo system given a single random channel realization. By a Monte Carlo-based simulation method, the outage rate region of a two-user uplink multiple access system with rate-compatible channel coding at each user is derived. Thereby, we find all code rate pairs at both users satisfying a specific outage probability of the turbo equalizer. Using the outage region, an algorithm capable to allocate the optimal rate pairs to both users maximizing the total sum rate is proposed. Furthermore, an outage-based code design method is

derived for the single-user single-antenna transmission case. The code design method optimizes the parameters of the channel code with respect to the outage behavior of the turbo equalizer. Finally, we focus in Section 5.3 on transmission power allocation based on linear SVD channel precoding and SC-MMSE FDE in single-user MIMO ISI channels. Throughout this section, perfect CSI is assumed to be available both at the transmitter and the receiver. Several criteria for optimizing the transmit power levels are discussed.

5.1. Rate Allocation for Multiuser Systems

In this section we focus on the question how to optimize the rate allocation in a two-user setting with SC-MMSE frequency domain turbo equalization. Especially, we address the problem of maximizing the total sum rate of the system using the framework of EXIT charts. The EXIT chart analysis method has also been applied to transmission rate allocation in multiple access channels in [RD07], [SPS05] and [SSB06]. In [RD07], the authors optimize LDPC codes under the assumption of equal rates at the users for a 2-user non-fading AWGN multiple access channel employing iterative decoding. They show that equal rate allocation remarkably simplifies the LDPC code optimization. Similar to the single-user case, the code design is reduced to a simple 2D curve-fitting problem of EXIT functions [tBKA04], [tBK03]. Similar results with LDPC codes and iterative decoding are obtained in [ADU02] where it was shown that by properly choosing the multiuser code, any point on the boundary of the capacity region can be closely approached without requiring time-sharing [CT91] or rate-splitting [RU96]. In [SPS05], an EXIT chart framework for optimizing LDPC codes under a large-system perspective (i.e., the number of users and antennas are taken to infinity, while their ratio remains fixed) for the multiple access flat-fading MIMO channel is considered. Results from the asymptotic analysis of CDMA systems with random spreading are used to design equal-rate codes at the users by conventional 2D curve fitting of EXIT functions. The results of [SPS05] reveal that near capacity performance can be asymptotically achieved. Asymptotic techniques for rate allocation have also been applied in [SSB06] to design repetition codes in the context of equal-rate CDMA systems with iterative detection and decoding.

Unlike to the previous work [RD07], [SPS05], [SSB06], we consider in the following a transmission strategy for the 2-user Gaussian multiple access ISI fading channel with SC-MMSE turbo equalization. The rates at both users are not restricted to be equal. The equalizer EXIT characteristics are given by two three-dimensional surfaces, and the problem of rate allocation is no longer a simple 2D matching of EXIT curves as in the single-user case. Based on the area property of EXIT functions (see

also Section 4.2.3), an upper bound on the achievable instantaneous rate region of the two-user multiple access channel is derived given a particular channel realization and receiver noise variance. Using the rate region upper bound, the problem of maximizing the sum rate at both users subject to a convergence constraint of the turbo equalizer is discussed. A polynomial approximation on the equalizer EXIT functions is shown to be the key for solving this optimization problem. The obtained analytical results are used to come up with a practical code selection method for rate allocation at both users. Additionally, the case of EXIT chart-based rate adaption for single-user systems is addressed as well. Finally, some numerical results to verify the bit error rate and throughput performance of the turbo system are presented.

For following considerations, it is assumed that both users are notified of the codes selected by the receiver through separated feedback links. These feedback links have zero-delay and are error free.

5.1.1. Derivation of an Approximate Bound on the Sum Rate for Multiple Access Channels

Consider a 2-user multiple access system employing the SC-MMSE FDE. Let the mutual information between the transmitted bits $b_{q,n}[k]$ and the *extrinsic* LLRs $\lambda_e\big[b_{q,n}[k]\big]$ of the equalizer be denoted as

$$I_{e,n} = \frac{1}{N_b Q} \sum_{k=1}^{N_b} \sum_{q=0}^{Q-1} I\Big(b_{q,n}[k], \lambda_e\big[b_{q,n}[k]\big]\Big) \in \mathbb{D}, n = 1, 2,$$

and let the mutual information between $b_{q,n}[k]$ and the *a priori* LLR $\zeta_e\big[b_{q,n}[k]\big]$ of the equalizer be denoted as

$$I_{d,n} = \frac{1}{N_b Q} \sum_{k=1}^{N_b} \sum_{q=0}^{Q-1} I\Big(b_{q,n}[k], \zeta_e\big[b_{q,n}[k]\big]\Big) \in \mathbb{D}, n = 1, 2.$$

In the two-user case the convergence characteristic of the equalizer is defined by the two EXIT functions,

$$\hat{\mathbf{f}}_e : \mathbf{I}_d \in \mathbb{D}^2 \rightarrow \hat{\mathbf{f}}_e \equiv \Big(\hat{f}_{e,1}(\mathbf{I}_d), \hat{f}_{e,2}(\mathbf{I}_d)\Big) \in \mathbb{D}^2,$$

which have the mutual information $\mathbf{I}_d \equiv (I_{d,1}, I_{d,2}) \in \mathbb{D}^2$ in its argument. Using the relationship between the SNR $\psi_n^{\mathrm{FD}}(\boldsymbol{\varphi}_e)$ at the equalizer output in (3.39) and the mutual information defined by the J-function in (4.38), the two equalizer functions

are given by (see also [KM07])

$$I_{e,n} = \hat{f}_{e,n}(\mathbf{I}_d) = \phi_J(\psi_n^{\mathrm{FD}}(\boldsymbol{\varphi}_e)), n = 1, 2, \tag{5.1}$$

where the components of vector $\boldsymbol{\varphi}_e$ are given by $\varphi_{e,n} = \phi_T^{-1}(I_{d,n})$ for $n = 1, 2$.

Similarly, the convergence characteristic of both decoders is defined by two EXIT functions[1] $\hat{f}_{d,n} : I_{d,n} \in \mathbb{D} \rightarrow \hat{f}_{d,n}(I_{d,n}) \in \mathbb{D}$. In addition, these two functions have the extreme values $\hat{f}_{d,n}(0) = 0$ and $\hat{f}_{d,n}(1) = 1$ for $n = 1, 2$.

Assumption 5.1. All EXIT functions of the turbo system are monotonically increasing, continuous and differentiable.

An example of the two equalizer EXIT functions $\hat{\mathbf{f}}_e$ and the decoder EXIT function $\hat{f}_{d,1}$ is shown in Fig. 5.1. Also shown is a possible decoding trajectory of the mutual information exchange, which is plotted as a projection onto the plane region $\mathcal{U} \equiv \{\mathbf{I}_d \,|\mathbf{I}_d \in \mathbb{D}^2\}$. The four boundary points of this region are denoted as $a_0 = (0, 0)$, $a_1 = (0, 1)$, $a_2 = (1, 1)$ and $a_3 = (1, 0)$. Note that the decoder EXIT function $\hat{f}_{d,2}$ (which is not shown) would be drawn in the $I_{d,2}$-coordinate. For the computation of the trajectory, the codes of both users were in this case assumed to be identical and hence the shapes of their EXIT functions would be exactly the same.

Let $\mathcal{D}$ be a region defined by

$$\mathcal{D} \equiv \left\{ \mathbf{I}_d \,\middle|\, \hat{f}_{e,n}(\mathbf{I}_d) \geq \hat{f}_{d,n}(I_{d,n}), n = 1, 2 \right\}. \tag{5.2}$$

The region in (5.2) is shown in Fig. 5.1 as well, and is referred to as the feasible region of the EXIT characteristics $\hat{\mathbf{f}}_e$ and $\hat{f}_{d,n}$, $n = 1, 2$. We remark that due Assumption 5.1 $a_0 \in \mathcal{D}$, since $\hat{f}_{e,n}(a_0) \geq \hat{f}_{d,n}(0) = 0$ for $n = 1, 2$.

Let $\{\mathbf{v}^{(p)}\}$, $\mathbf{v}^{(p)} \in \mathcal{D}$, $\mathbf{v}^{(0)} = a_0$, $p = 0, ..., T$ be a sequence of $\mathbf{I}_d$-tuples that models the decoding trajectory (projected onto the plane region $\mathcal{U}$) according to a specific activation ordering of the equalizer and the two decoders over a number of iterations. The monotonicity of all EXIT functions together with the definition in (5.2) imply that $\mathbf{v}^{(p+1)} \geq \mathbf{v}^{(p)}$ for all p, and thus, the sequence $\{\mathbf{v}^{(p)}\}$ converges monotonically to a limit point $\mathbf{I}_d^* = \lim_{p\rightarrow\infty} \mathbf{v}^{(p)}$. As shown in Theorem 1 of [BRG05], this limit point is unique and independent of the actual activation ordering. Convergence of turbo equalization is achieved, when the decoding trajectory approximately attains the maximum point $\mathbf{I}_d^* = a_2$. This is possible for T being sufficiently large, if the following constraint holds:

$$\mathcal{D} \text{ is pathwise connected}^2 \text{ and } a_2 \in \mathcal{D}. \tag{5.3}$$

[1] Unlike to Section 4.2, for notational simplicity $\hat{f}_{d,n}$ denotes here the inverse decoder EXIT function.

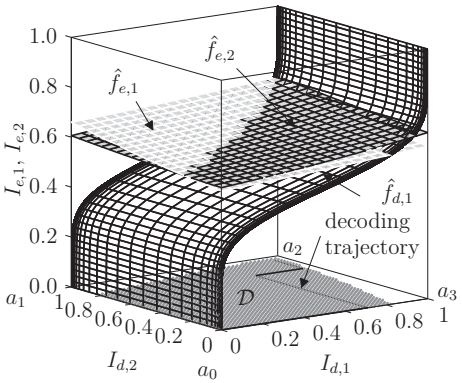

Figure 5.1.: Equalizer EXIT functions $\hat{f}_{e,1}$ and $\hat{f}_{e,2}$ for a single random channel realization and decoder EXIT function $\hat{f}_{d,1}$ for a constraint length 5 rate-1/2 SCC. A possible decoding trajectory visualizing the mutual information exchange over the iterations is plotted as projection onto the plane region $\mathcal{U}$. $Q = 128$, $L = 10$ and $E_s/N_0 = 0$ dB.

Assumption 5.2. Let $A_{\mathcal{D}} \equiv \iint_{\mathcal{D}} \mathrm{d}\mathbf{I}_d$ be the area of region $\mathcal{D}$. Each decoder EXIT function $\hat{f}_{d,n}$, $n = 1, 2$ is matched to the corresponding equalizer EXIT function $\hat{f}_{e,n}$, so that only an infinitesimally small open tube between the four surfaces remains, where the trajectory can go from $\mathbf{v}^{(0)} = a_0$ to $\mathbf{I}_d^* = a_2$.

The corresponding decoder EXIT functions to Assumption 5.2 imply 1) an ideally designed channel code at each user of infinite block length to achieve a nearly zero bit error probability and 2) an infinite number of iterations between the equalizer and the two decoders[3]. Under Assumption 5.2, the size of the area $A_{\mathcal{D}}$ is close to zero and the region $\mathcal{D}$ can be characterized by a curve $\mathcal{S}$, which is referred to as convergence curve in what follows. The convergence curve $\mathcal{S}$ is parametrized by a vector-function

$$\mathbf{u}(t) \equiv \Big(u_1(t), u_2(t)\Big) : \mathbb{D} \to \mathcal{S}, u_n \in \mathcal{F}^1[0,1], n = 1, 2, \tag{5.4}$$

where each $u_n(t)$, $t \in \mathbb{D}$ is monotonically increasing in the parameter t and has the prescribed boundary values $u_n(0) = 0$ and $u_n(1) = 1$. In (5.4), $\mathcal{F}^1[a, b]$ denotes the

[2]A set $\mathcal{A}$ is said to be pathwise-connected if for every $p, q \in \mathcal{A}$ there are two real numbers a, b with $a \leq b$ and a continuous mapping f such that $f(a) = p$, $f(b) = q$, and $f([a, b]) \subseteq \mathcal{A}$ [Kre05].

[3]Note that, however, this does not imply that the whole transmission chain can achieve a performance close to channel capacity, since the use of the sub-optimal equalizer such as the SC-MMSE FDE already incurs a loss in rate [AKtB04].

space of monotonically increasing, continuous and piecewise differentiable functions on the interval $[a, b]$.

Let $\mathbf{w}_n(\mathbf{u})$ be a three-dimensional space curve, obtained by projection of $\mathbf{u}$ on $\hat{f}_{e,n}$,

$$\mathbf{w}_n(\mathbf{u}) \equiv \Big(u_1(t), u_2(t), \hat{f}_{e,n}(\mathbf{u}(t))\Big) \in \mathbb{D}^3, \tag{5.5}$$

and let $\hat{f}_{p,n}^{(\mathbf{u})} : I_{d,n} \to \hat{f}_{p,n}^{(\mathbf{u})}(I_{d,n}) \in \mathbb{D}$ be a function obtained by projection of $\mathbf{w}_n$ onto the $I_{d,n}$-$I_{e,n}$-plane. The convergence curve $\mathbf{u} \subseteq \mathcal{D}$ satisfies the constraints in (5.3), which implies that

$$\hat{f}_{d,n}(I_{d,n}) < \hat{f}_{p,n}^{(\mathbf{u})}(I_{d,n}), \forall I_{d,n} \in [0, 1), \text{ for } n = 1, 2. \tag{5.6}$$

From (5.6), we easily obtain the following bound:

$$A_n < A_n^{(\mathbf{u})}, \tag{5.7}$$

where A_n and $A_n^{(\mathbf{u})}$ denote the areas under $\hat{f}_{d,n}(I_{d,n})$ and $\hat{f}_{p,n}^{(\mathbf{u})}(I_{d,n})$, respectively,

$$A_n \equiv \int_0^1 \hat{f}_{d,n}(I_{d,n}) \mathrm{d}I_{d,n}, \tag{5.8}$$

$$A_n^{(\mathbf{u})} \equiv \int_0^1 \hat{f}_{p,n}^{(\mathbf{u})}(I_{d,n}) \mathrm{d}I_{d,n}. \tag{5.9}$$

As shown in Section 4.2.3, the area under the EXIT function $\hat{f}_{d,n}$ of an MAP-based channel decoder for a rate-R_n channel code satisfies the property $R_n = A_n$. Combining this result with (5.7) yields an upper bound for the rate R_n of user n with respect to the convergence curve $\mathbf{u}$ as $R_n < A_n^{(\mathbf{u})}$. Equivalently, the area $A_n^{(\mathbf{u})}$ in (5.9) can be expressed as line integral of $\hat{\mathbf{f}}_{e,n}$ along $\mathcal{S}$ in $I_{d,n}$-direction, $A_n^{(\mathbf{u})} = \int_{\mathcal{S}} \hat{f}_{e,n}(\mathbf{I}_d) \mathrm{d}I_{d,n}$. Hence, we can also express the rate R_n as

$$R_n < \int_{\mathcal{S}} \hat{f}_{e,n}(\mathbf{I}_d) \mathrm{d}I_{d,n} \tag{5.10a}$$

$$= \int_0^1 \hat{f}_{e,n}\Big(\mathbf{u}(t)\Big) u_n'(t) \mathrm{d}t, \tag{5.10b}$$

where $u_n'(t)$ denotes the first derivative of $u_n(t)$. The equality in (5.10b) follows directly from the curve parametrization in (5.4). An example of the convergence curve with the two corresponding equalizer EXIT space curves and the related areas defining the achievable rates of both users is shown in Fig. 5.2.

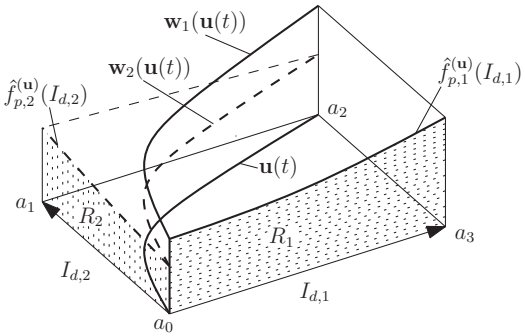

Figure 5.2.: Example of the parametric convergence curve $\mathbf{u}(t)$ with the two corresponding EXIT space curves and the two areas defining the achievable rates.

Let $\mathcal{V}$ be the set of admissible parametric curves in the plane region $\mathcal{U}$,

$$\mathcal{V} \equiv \Big\{ \mathbf{v} \Big| v_n \in \mathcal{F}^1[0,1], v_n'(t) \geq 0, \forall t, n = 1,2, \mathbf{v}(0) = a_0, \mathbf{v}(1) = a_2 \Big\}. \tag{5.11}$$

From the inequality in (5.10) and with the definition in (5.11), we finally obtain an upper bound for the rate region of both users as

$$\mathcal{R}^{\text{MAC}} \equiv \bigcup_{\mathbf{v} \in \mathcal{V}} \Big\{ (R_1, R_2) \Big| R_n < \int_{\mathbf{v}} \hat{f}_{e,n}(\mathbf{I}_d) \mathrm{d}I_{d,n}, n = 1,2 \Big\}. \tag{5.12}$$

Fig. 5.3 illustrates an example of the rate region in (5.12), where $\hat{f}_{e,1}$ and $\hat{f}_{e,2}$ have been computed using (5.1) for a single random channel realization. The rates at the corner point V_1 can be achieved by successive equalization and decoding techniques, where the signal from user 1 is detected first through iterations only between the equalizer and decoder of user 1, such that only the mutual information $I_{d,1}$ increases with the iterations, while the mutual information $I_{d,2}$ stays zero. After decoding the signal from user 1, the signal from user 2 is iteratively detected, while $I_{d,1} = 1$. Thus, for achieving the corner point V_1, the convergence curve $\mathcal{S}$ must be given by a path on the boundary $\partial\mathcal{U}$, which connects the points a_0, a_3 and a_2, $\mathcal{S} = \mathcal{L}(a_0, a_3, a_2)$, where $\mathcal{L}(q_0, q_1, ..., q_v)$ is defined as the union of v straight line segments, connecting

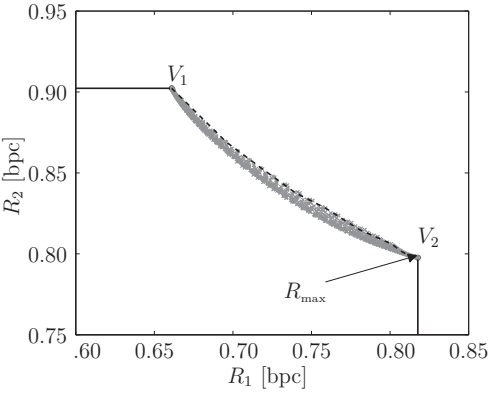

Figure 5.3.: Rate region of two-user multiple access channel with SC-MMSE frequency domain turbo equalization for a random channel realization at $E_s/N_0 = 5$ dB, numerically computed by generating a large number of different admissible convergence curves (a gray dot corresponds to one curve). $Q = 32$, $L = 10$.

the points $q_i \in \mathbb{D}^2$, $i = 0, ..., v$:

$$\mathcal{L}(q_0, q_1, ..., q_v) \equiv \bigcup_{i=0}^{v-1} \Big\{ q_i + \lambda(q_{i+1} - q_i) \Big| \lambda \in [0, 1] \Big\}. \tag{5.13}$$

The rate tuple at V_2 can similarly be achieved by first iteratively detecting the signal from user 2, followed by user 1's signal detection. In this case the convergence curve must be given by $\mathcal{S} = \mathcal{L}(a_0, a_1, a_2)$. Note that the rate region in (5.12) is non-convex, in general, where the dominant face of this region strongly depends on the particular realization of the equalizer EXIT functions $\hat{\mathbf{f}}_e$.

5.1.2. Maximization of Sum Rate

To identify the rates of both users and the corresponding convergence curve that maximize the sum rate, we are interested to solve the following variational optimization problem:

$$R_{\max} \equiv \max_{\mathbf{v} \in \mathcal{V}} \sum_{n=1}^{2} \int_{\mathbf{v}} \hat{f}_{e,n}(\mathbf{I}_d) \mathrm{d}I_{d,n}. \tag{5.14}$$

Using (5.10), the functional in (5.14) can also be expressed as

$$R[\mathbf{v}(t)] \equiv \int_0^1 Y\Big(\mathbf{v}(t)\Big)\,\mathrm{d}t, \tag{5.15}$$

where

$$Y(\mathbf{v}) = \sum_{n=1}^{2} \hat{f}_{e,n}\Big(\mathbf{v}(t)\Big) v_n'(t). \tag{5.16}$$

A first-order necessary condition of optimality to the variational problem is given by the Euler-Lagrange differential equations [JLJ98]:

$$\frac{\partial Y(\mathbf{v})}{\partial v_n} - \frac{\mathrm{d}}{\mathrm{d}t}\frac{\partial Y(\mathbf{v})}{\partial v_n'} \stackrel{!}{=} 0, n = 1, 2. \tag{5.17}$$

Using (5.16), one can easily check, that the differential equations in (5.17) reduce to one algebraic equation,

$$\frac{\partial \hat{f}_{e,2}(\mathbf{v})}{\partial v_1} - \frac{\partial \hat{f}_{e,1}(\mathbf{v})}{\partial v_2} \stackrel{!}{=} 0. \tag{5.18}$$

The solutions of (5.18), if they exist, are the candidates satisfying the optimality requirement. However, a direct computation of (5.18) is not possible, since $\hat{f}_{e,1}$ and $\hat{f}_{e,2}$ are not given in closed form. Moreover, the candidate curves of (5.18) are stationary paths, which generally do not satisfy the monotonicity and boundary conditions of (5.11). Hence, the extremal cannot be directly obtained from (5.18).

5.1.3. Analytical Solution based on EXIT Function Approximation

Since a closed-form solution to (5.14) is difficult to derive, we present in the following an approximate analytical solution to the above variational problem by approximating each equalizer EXIT characteristic by a polynomial function. We therefore introduce the following assumption.

Assumption 5.3. Each equalizer EXIT function $\hat{f}_{e,n}$ can be closely approximated by a two-dimensional quadratic form $\hat{f}_{e,n}(\mathbf{I}_d) \approx \beta_{n,0} + \beta_{n,1} I_{d,1} + \beta_{n,2} I_{d,2} + \beta_{n,3} I_{d,1} I_{d,2} + \beta_{n,4} I_{d,1}^2 + \beta_{n,5} I_{d,2}^2$ with the coefficients $\beta_{n,i}$ can be obtained from a standard regression method [Kre05].

Under the above assumption, Eqn. (5.17) reduces to a *linear algebraic* equation,

$$T(\mathbf{I}_d) \equiv \frac{\partial \hat{f}_{e,2}(\mathbf{I}_d)}{\partial I_{d,1}} - \frac{\partial \hat{f}_{e,1}(\mathbf{I}_d)}{\partial I_{d,2}} \stackrel{!}{=} 0. \tag{5.19}$$

Eqn. (5.19) has three possible outcomes: (i) no solution, (ii) infinite number of solutions, or (iii) a unique solution.

(i) If (5.19) has no solution, the partial derivatives $\partial \hat{f}_{e,2}(\mathbf{I}_d)/\partial I_{d,1}$ and $\partial \hat{f}_{e,1}(\mathbf{I}_d)/\partial I_{d,2}$ are non-equal constants in $\mathbb{R}$. In this case, we can state the following lemma.

Lemma 5.4. If (5.19) has no solution one of the boundary curves $\mathcal{L}(a_0, a_3, a_2)$ and $\mathcal{L}(a_0, a_1, a_2)$ solves the variational problem, and thus the achievable sum rate is maximized at the rate region corner point of either V_1 or V_2.

Proof: See Appendix A.4.

(ii) If (5.19) has an infinite number of solutions, i.e., curl $\hat{\mathbf{f}}_e = 0$ for all $\mathbf{I}_d \in \mathbb{D}^2$, the functional in (5.15) is path-independent [Kre05]. Thus, $R[\mathbf{v}]$ is identical for all $\mathbf{v} \in \mathcal{V}$ and the two corner points V_1 and V_2 are connected by a straight line segment having a decay of -1.

(iii) If (5.19) has a unique solution, the solution curve $\mathcal{E} \equiv \{\mathbf{I}_d \,|T(\mathbf{I}_d) = 0\}$ can be parameterized by a continuous vector-function $\mathbf{g} : \mathbb{D} \to \mathcal{E}$, where the first derivative of $\mathbf{g}$ satisfies $g_n'(t) \geq 0$ or $g_n'(t) \leq 0$ for all $t \in \mathbb{D}$. This property allows us to formulate the following theorem.

Theorem 5.5. Let $\mathcal{E} \subset \mathcal{U}$ be parametrized by a vector-function $\mathbf{g} : \mathbb{D} \to \mathcal{E}$. Let the following two conditions be satisfied:

$$g_n'(t) \geq 0, n = 1, 2 \text{ for all } t \in \mathbb{D}, \tag{5.20a}$$

$$T(\mathbf{I}_d) \begin{cases} \geq 0 \text{ for } \mathbf{I}_d \in \mathcal{G}_1, \\ \leq 0 \text{ for } \mathbf{I}_d \in \mathcal{G}_2, \end{cases} \tag{5.20b}$$

where the regions $\mathcal{G}_n$ are defined as $\mathcal{G}_1 \equiv \Big\{\mathbf{I}_d \,|I_{d,1} \leq g_1(t), I_{d,2} \geq g_2(t), \forall t \in \mathbb{D}\Big\}$ and $\mathcal{G}_2 \equiv \Big\{\mathbf{I}_d \,|I_{d,1} \geq g_1(t), I_{d,2} \leq g_2(t), \forall t \in \mathbb{D}\Big\}$. Then, the convergence curve

$$\mathcal{S} = \mathcal{E} \cup \mathcal{L}\Big(a_0, \mathbf{g}(0)\Big) \cup \mathcal{L}\Big(\mathbf{g}(1), a_2\Big) \tag{5.21}$$

comprised of the curve $\mathcal{E}$ and the two straight line segments (all shown in Fig. 5.4) is optimal with respect to (5.14).

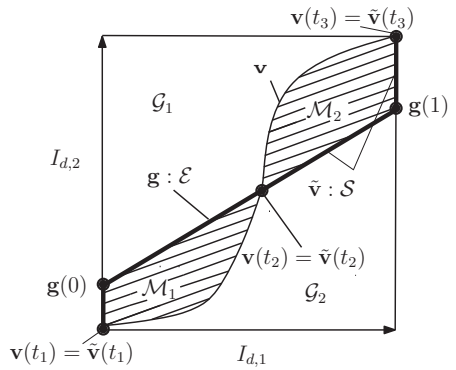

Figure 5.4.: Visualization of the curve $\mathcal{E}$ with parametrization $\mathbf{g}$, the corresponding convergence curve $\mathcal{S}$ with parametrization $\tilde{\mathbf{v}}$, and the partition of the curve $\tilde{\mathbf{v}}$ for an arbitrary parametric curve $\mathbf{v} \in \mathcal{V}$ in the plane region $\mathcal{U}$.

Proof: See Appendix A.5.

The optimality of the convergence curve (5.21) is given only when both conditions in (5.20) are satisfied. In cases when at least one of these conditions is violated, we can use Green's theorem [Kre05] (see also Appendix A.5) to show that candidate solutions to the variational problem are the convergence curves $\mathcal{H}_0(u) \equiv \mathcal{L}(a_0, r_{0,1}, r_{0,2}, a_2)$ and $\mathcal{H}_1(u) \equiv \mathcal{L}(a_0, r_{1,1}, r_{1,2}, a_2)$, comprised of the union of three straight-line segments connecting the points $r_{0,1} = (u, 0)$, $r_{0,2} = (u, 1)$ and $r_{1,1} = (0, u)$, $r_{1,2} = (1, u)$ with $u \in [0, 1]$.

Lemma 5.6. Based on the candidate solutions, the variational problem can be rewritten as a quadratic extremal problem which may be solved with standard methods of the classical calculus.

Proof: See Appendix A.6.

The approximate closed-form solution with respect to (5.14) presented above can now be summarized in Algorithm 5.1. We also present a second graph-based algorithm to solve the above sum rate problem in Appendix C. Note that this algorithm also extends the above sum rate allocation scheme to the N-user ($N > 2$) channel case.

5.1.4. Practical Method for Rate Allocation

With the algorithm presented above, the convergence curve $\bar{\mathbf{v}}$, $\bar{\mathbf{v}} \in \mathcal{V}$ that approximately solves (5.14) for a single random channel realization can be calculated. The

Algorithm 5.1 Algorithm for computing the convergence curve that maximizes sum rate

1: Calculate the polynomial coefficients $\beta_{n,i}$ for each equalizer EXIT function $\hat{f}_{e,n}$ using a standard regression method [Kre05].
2: **if** (A.19) is satisfied **then**
3: Output the boundary curve that solves (A.20).
4: **else if** (A.19a) is satisfied and (A.19b) is violated **then**
5: Output an arbitrary convergence curve $\mathbf{v} \in \mathcal{V}$.
6: **else if** (5.20) is satisfied **then**
7: Output the convergence curve in (5.21).
8: **else**
9: Output the convergence curve $\mathcal{H}_l(u)$, $l = 1, 2$, $u \in \mathbb{D}$ with (l, u) being the solution to (A.27).
10: **end if**

maximum rate at each user, corresponding to curve $\bar{\mathbf{v}}$, is then given by the area under the projected equalizer EXIT function $\hat{f}_{p,n}^{(\bar{\mathbf{v}})}$, as illustrated in Fig. 5.2. To closely approach this rate, the n-th user should have its decoder EXIT function $\hat{f}_{d,n}$ as close to $\hat{f}_{p,n}^{(\bar{\mathbf{v}})}$ as possible, while satisfying the constraints (5.3) for convergence of the turbo equalizer.

In practice, however, optimizing $\hat{f}_{d,n}$ by adjusting the available code parameters such that code optimality in a strict sense is always guaranteed is not possible as the code parameters may presumably be limited. Thus, a practical approach for rate allocation is to select for each user the code $\mathcal{C}_u \in \mathcal{C}$ with the highest possible rate from a finite code set $\mathcal{C} = \{C_1, C_2, ..., C_m\}$ for which convergence is achieved, while its decoder EXIT function $\hat{f}_{d,n}^{(C_u)}$ best fits to $\hat{f}_{p,n}^{(\bar{\mathbf{v}})}$. Here, m denotes the number of codes in the set $\mathcal{C}$.

Based on this idea a simple scheme for rate allocation can be derived, which is summarized as follows.

1. For each realization of the frequency domain channel matrix, calculate the equalizer EXIT functions $\hat{f}_{e,1}$ and $\hat{f}_{e,2}$ using (5.1).

2. Calculate the convergence curve $\bar{\mathbf{v}} \in \mathcal{V}$ that solves (5.14) using Algorithm 5.1.

3. Calculate $\hat{f}_{p,n}^{(\bar{\mathbf{v}})}$ by projecting the space curve $\mathbf{w}_n(\bar{\mathbf{v}})$ onto the $I_{e,n}$-$I_{d,n}$-plane.

4. To obtain high information rate, select the channel code for each user n satisfying

$$r_{c,n} = \max_{C_u \in \mathcal{C}} \left\{ r(C_u) \middle| \hat{f}_{p,n}^{(\bar{\mathbf{v}})}(I_{d,n}) \geq \hat{f}_{d,n}^{(C_u)}(I_{d,n}) + u(I_{d,n}), \forall I_{d,n} \in [0, 1) \right\}, \quad (5.22)$$

where $r(C_u)$ designates the rate of channel code C_u, and $u(I_{d,n})$ is a function to control the speed of convergence of the decoding trajectory to the maximum point $\mathbf{I}_d^* = a_2$.

5. If $r_{c,n}$ is NULL, select the code with the lowest possible rate in $\mathcal{C}$, $r_{c,n} = \min_{C_u \in \mathcal{C}} r(C_u)$.

6. Output the selected coding rates $r_{c,1}$ and $r_{c,2}$.

We remark that with (5.22) the selected codes of both users satisfy the constraint in (5.3). Therefore, the turbo equalizer can achieve asymptotically the convergence point $\mathbf{I}_d^* = a_2$ when the number of turbo and decoder iterations are sufficiently large.

Special Case of Single-User System: Obviously, in the single-user case the calculation of an optimal convergence is not necessary due to the dimensionality constraint of the EXIT chart. As the EXIT functions $\hat{f}_e$ and $\hat{f}_d$ are defined by two-dimensional mappings, the above approach simplifies to the following scheme.

1. Calculate the equalizer EXIT function $\hat{f}_e$ using (5.1).

2. Select the channel code satisfying

$$r_c = \max_{C_u \in \mathcal{C}} \left\{ r(C_u) \middle| \hat{f}_e(I_d) \geq \hat{f}_d^{(C_u)}(I_d) + u(I_d), \forall I_d \in [0,1) \right\}. \tag{5.23}$$

3. If r_c is NULL, select the code with the lowest possible rate in $\mathcal{C}$.

4. Output the selected coding rate r_c.

5.1.5. Numerical Results

Results of capacity evaluations and simulations to assess the throughput efficiency of the proposed rate allocation scheme are presented in this subsection. We consider a two-user single-carrier transmission over Rayleigh fading ISI channels employing the SC-MMSE FDE. Typical values for the channel memory L (3, 5 and 32) are assumed. The power delay profile of the channel is uniform.

5.1.5.1. Spectral Efficiency

Fig. 5.5 shows the spectral efficiency $\frac{Q}{Q+P}\bar{R}$ of the two-user turbo system when 'optimally' designed user codes are assumed, whose decoder EXIT functions satisfy: $\hat{f}_{d,n} = \hat{f}_{p,n}^{(\bar{\mathbf{v}})}$, for both users. Here, $\bar{\mathbf{v}}$ is the solution to problem (5.14) for the channel realizations given. The information rate $\bar{R}$ has been calculated by averaging the sum

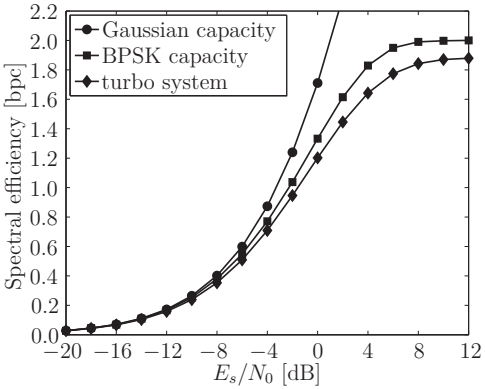

Figure 5.5.: Spectral efficiency of a two-user turbo system employing the SC-MMSE FDE with 'optimally' designed user codes for the transmission and ergodic sum capacity with Gaussian and BPSK input signals. $N = M = 2$, $Q = 32$ and $L = 3$.

rate $\sum_{n=1}^{2} \int_0^1 \hat{f}_{p,n}^{(\tilde{\mathbf{v}})}(I_{d,n})\mathrm{d}I_{d,n}$ over a large number of random channel realizations. For comparison, the ergodic i.i.d. Gaussian-input sum capacity $R_{\text{sum}}^{\text{MAC}}$ and the ergodic BPSK-input sum capacity $R_{\text{con}}^{\text{MAC}}$ of the frequency-selective Rayleigh fading channel with evenly allocated transmit power levels are also shown. The BPSK-input capacity result has been obtained by the Monte Carlo method described in Section 2.8.2. The CSI is assumed to be known only at the receiver. Comparing the numerical results in Fig. 5.5, we find that the loss incurred by the use of the SC-MMSE FDE with respect to the BPSK-input capacity slightly increases for large values of E_s/N_0. We also observe that there is almost no difference between the three curves up to $E_s/N_0 = -8$ dB, indicating that a two-user turbo system with BPSK-inputs and SC-MMSE FDE is nearly optimal in the low E_s/N_0 region.

5.1.5.2. Rate Allocation

The rate-compatible punctured SCCCs proposed in [Tüc04], consisting of a rate-r_c outer encoder and a recursive rate-1 inner encoder with polynomials $(g_r, g_0) = (3, 2)$ (g_r denotes the feedback polynomial) in octal notation, are assumed for channel encoding at both users. The outer encoder of the concatenated code is selected from a set of 17 subcodes having rates $r_c = 0.05 \cdot (2+p)$, $p = 1, .., P-1$. The length of a frame is fixed to 16384 symbols and the function $u(x)$ in (5.22) is defined as $u(x) = 0.025 - 0.025x$, $x \in [0, 1]$. The turbo equalizer performs $T_e = 15$ iterations between the equalizer and both SCCC decoders and $T_d = 20$ iterations between

Table 5.1.: Selected code rate pairs and information rate pairs at both users for the 'Max-Sum-Rate' and 'Min-Sum-Rate' code design.

	$r_{c,1}$	$r_{c,2}$	r_c	R_1	R_2	R
Max-Sum-Rate	0.75	0.85	1.60	0.84	0.90	1.74
Min-Sum-Rate	0.90	0.45	1.35	0.98	0.58	1.56

the inner and outer decoder. Note that $u(x)$ has been preliminarily optimized by computer simulations to find an acceptable trade-off between performance of the turbo equalizer and the number of iterations needed to ensure convergence.

Table 5.1 shows the selected code rate pairs at $E_s/N_0 = 4.75$ dB with respect to (5.22) and the information rate pairs satisfying (5.14) for a single random channel realization. For comparison, the selected code rate pairs $r_{c,n}$ and information rate pairs $R_n = \int_{\check{\mathbf{v}}} f_{e,n}(\mathbf{I}_d)\mathrm{d}I_{d,n}$, computed for the convergence curve satisfying $\check{\mathbf{v}} \equiv \arg\min_{\mathbf{v}\in\mathcal{V}} \sum_{n=1}^{2} \int_{\mathbf{v}} f_{e,n}(\mathbf{I}_d)\mathrm{d}I_{d,n}$, are also shown and referred to as 'Min-Sum-Rate,'. The results in Table 5.1 indicate that the selected code rate pairs and the total achievable sum rate of the turbo system strongly depend on the convergence curve chosen for the particular channel realization.

Fig. 5.6 shows the BER performance of the turbo receiver for a single channel realization. The channel code at each user is selected with respect to (5.22) at an SNR $E_s/N_0 = 4.75$ dB. Also shown is the SNR $E_s/N_0|_{\min}$ at which the instantaneous BPSK-input sum capacity (for the given channel realization) is equal to the sum rate $\sum_{n=1}^{2} r_{c,n} = 1.60$ bit per channel use (bpc) of the turbo system. It is observed that the turbo equalizer shows convergence starting at SNRS of 3.6 dB and 4.1 dB for user 1 and user 2, respectively. The SC-MMSE FDE indeed satisfies the convergence constraints (5.3) for the desired SNR $E_s/N_0|_{\mathrm{des}}$. Moreover, we find that the SC-MMSE FDE operates within about 2 dB E_s/N_0 to its respective capacity limit at a BER of 10^{-6}.

Fig. 5.7 shows the average total throughput of the 2-user turbo system versus the receive SNR for a transmission over $L = 32$ Rayleigh fading ISI channels. A selective-repeat ARQ is assumed. The spectral efficiency for 'optimally' designed user codes is shown as a reference. Also shown is the average total throughput for ARQ with fixed and identical codes at both users with rates $r_{c,1/2} = 0.1 \cdot n$, $n = 1, .., 9$. As observed in Fig. 5.7, substantial throughput gain is obtained by the adaptive rate allocation scheme over fixed rate ARQ. Further, we find that the throughput performance is only 1.5 dB away in the high SNR region from the throughput achieved with 'optimally' designed user codes. Notably, however, there is still a gap of almost 2.5 dB between both curves in the low SNR region. It should be noted though, that by using more flexible coding techniques, such as irregular

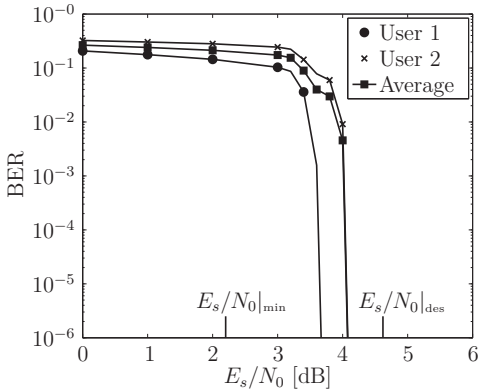

Figure 5.6.: Average BER performance of the SC-MMSE FDE for a fixed $L = 3$ random channel realization with coding rates $r_{c,1} = 0.75$ and $r_{c,2} = 0.85$ of both users. FFT-size $Q = 32$.

SCCCs or irregular LDPC codes (e.g., see [Tüc04], [tBKA04]), the performance loss can be further reduced.

5.2. Outage-based Rate Allocation and Code Design

In contrast to the previous section, let us now assume that the transmitters have only knowledge about the statistics of the channel condition (i.e., the fading distribution), but not of the instantaneous channel gains. A commonly used measure to characterize the receiver performance is then the probability of convergence failure of the turbo equalizer, which is also known as the outage probability. As for such transmission systems, the adaptive allocation of resources at the transmitter to the instantaneous channel state is not possible, outage-based allocation schemes may be preferred.

In this section, we firstly discuss the extension of the code selection algorithm from Section 5.1.4 to two-user transmission systems. In detail, we determine the achievable outage rate region, that specifies the set of all code rate pairs satisfying a specific outage probability of the turbo equalizer, for a specific channel fading distribution and set of rate-compatible codes. Having knowledge of this region, the objective is to determine the optimal code rate pairs of both users that maximize the total sum rate. The results obtained by this approach are compared to the outage capacity region of the two user multiple access channel.

Furthermore, an outage-based code design method for single-user single-antenna

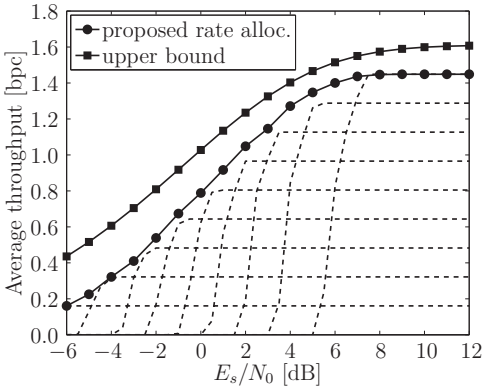

Figure 5.7.: Average total throughput of the turbo system achieved by rate allocation at each user (solid curves with marker 'o') and by fixed coding rate ARQ at both users with $r_{c,1/2} = 0.1 \cdot n$ with $n = 1, .., 9$ (dashed curves, from bottom to top). $Q = 128$ and $L = 32$.

turbo systems employing irregular recursive convolutional (IRC) codes is proposed. The analytical expressions for the outage probability of the SC-MMSE FDE from Section 4.3 are used to optimize the parameters of the IRC code. It is demonstrated that optimized IRC-coded turbo equalizer improves the outage performance over the turbo equalizer employing regular RSC codes.

5.2.1. Outage-based Code Selection for Multiple Access Channels

In the context of turbo equalization, the code rate $r_{c,n}$ of the n-th user should be no greater than $r^*_{c,n}(\bar{\mathbf{v}}) \equiv \max_{\mathcal{C}_u \in \mathcal{C}} \left\{ r(C_u) | f^{(\bar{\mathbf{v}})}_{p,n}(I_{d,n}) > f^{(C_u)}_{d,n}(I_{d,n}), \forall I_{d,n} \in [0,1) \right\}$ with $\bar{\mathbf{v}} \in \mathcal{V}$ being the solution to (5.14), so that the constraints in (5.3) for convergence are satisfied. Assume that for each code $C_u \in \mathcal{C}$ we have $f^{(C_u)}_d(I_d) \geq f^{(C_m)}_d(I_d)$, $\forall I_d \in [0,1)$ if $r(C_u) \geq r(C_m)$ with $C_m \in \mathcal{C}$. Then, the set of code rate pairs at which convergence of turbo equalization is achieved for a specific channel realization, is given by

$$\mathcal{T}(\bar{\mathbf{v}}) \equiv \left\{ (r_{c,1}, r_{c,2}) \left| r_{c,1} = r(C_u) \leq r^*_{c,1}(\bar{\mathbf{v}}), r_{c,2} = r(C_m) \leq r^*_{c,2}(\bar{\mathbf{v}}), C_u, C_m \in \mathcal{C} \right. \right\}. \tag{5.24}$$

For an outage-based rate allocation, we view the rate pair $(r^*_{c,1}(\bar{\mathbf{v}}), r^*_{c,2}(\bar{\mathbf{v}}))$ as a random process as the convergence curve $\bar{\mathbf{v}}$ depends on the channel matrix whose

particular realization changes independently, frame-by-frame. If the two users are transmitting with rates $(r_{c,1}, r_{c,2})$, an outage event occurs if either $r_{c,1} > r^*_{c,1}(\bar{\mathbf{v}})$ or $r_{c,2} > r^*_{c,2}(\bar{\mathbf{v}})$. Thus, we can define the outage rate region of turbo equalization as

$$\mathcal{R}^{\text{out}}_{\text{MAC}} = \Big\{(r_{c,1}, r_{c,2})\Big|\text{Prob}\Big((r_{c,1}, r_{c,2}) \notin \mathcal{T}(\bar{\mathbf{v}}) \leq P_o\Big\}, \tag{5.25}$$

where P_o denotes the outage probability. The maximum sum rate at which arbitrarily reliable transmission for the two users is possible for $(1 - P_o) \times 100\%$ of the channel realizations, is then given by

$$R^{\text{out}}_{\text{MAC}} = \max_{(r_{c,1}, r_{c,2})} \Big\{r_{c,1} + r_{c,2}\Big|(r_{c,1}, r_{c,2}) \in \mathcal{R}^{\text{out}}_{\text{MAC}}\Big\}. \tag{5.26}$$

The code rates obtained by (5.26) are the largest rates that can be achieved over the two-user multiple access channel for the codes in the set $\mathcal{C}$. The region in (5.25) is determined through Monte Carlo simulations, as described in the following section.

5.2.1.1. Numerical Results

Simulations were performed for the two-user frequency selective $L = 5$ Rayleigh fading ISI channel. The same code set as in Section 5.1.5 was assumed for outage-based rate allocation at both users.

Fig 5.8 shows the code rate pairs $(r_{c,1}, r_{c,2})$ that maximize the sum rate among those combinations of the codes in $\mathcal{C}$ for $P_o = 0.01$, 0.1, and 0.5. In all cases, the SNR E_s/N_0 was set at 4 dB. To obtain the outage rate region $\mathcal{R}^{\text{out}}_{\text{MAC}}$, the outage constraint in (5.25) was calculated by evaluating the convergence of the turbo equalizer over V independent random channel realizations. Specifically, the set of code rate pairs $\mathcal{T}(\bar{\mathbf{v}})$ is determined for each of the V channel realizations according to the definition in (5.24), and the total number U of outage events $((r_{c,1}, r_{c,2}) \notin \mathcal{T}(\bar{\mathbf{v}}))$ for a given code rate pair $(r_{c,1}, r_{c,2})$ is recorded. According to (5.25), the outage rate region is then given by all code rate pairs satisfying the condition $\frac{U}{V} \leq P_o$. Also shown in Fig 5.8 are the binary-input outage capacity regions $\mathcal{C}^{\text{MAC}}_{\text{con,out}}(P_{\text{out}})$ for the three outage probabilities and the achievable information rate pairs on the region boundaries maximizing the outage capacity, i.e., $(\mathring{R}_1, \mathring{R}_2) = \max_{(R_1,R_2)} \Big\{R_1 + R_2\Big|(R_1, R_2) \in \mathcal{C}^{\text{MAC}}_{\text{con,out}}(P_{\text{out}})\Big\}$. As evident from this figure, the larger the desired outage probability, the larger is the area of the outage capacity region. Further, as expected, the code rate pairs satisfying (5.26) are contained by their respective outage capacity region. We observe that these rate pairs are symmetric with respect to the line $R_1 = R_2 = R^{\text{out}}_{\text{MAC}}/2$. This is apparently obvious as we expect the two rates obtained by (5.14) to be equal. Note that, due to a finite number of Monte Carlo trials, the

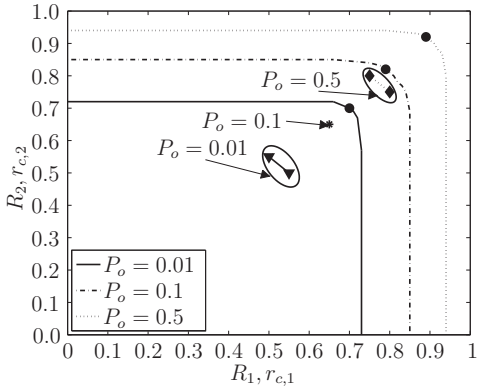

Figure 5.8.: Achievable code rate pairs (markers with '+', '$*$' and '$\diamond$') maximizing the sum rate of the turbo system and the respective binary-input outage capacity regions for $P_o = 0.01$, 0.1, 0.5 at $E_s/N_0 = 4$ dB. The points on the capacity region, indicated by the 'o' markers, show the achievable rates maximizing the outage capacity.

Table 5.2.: Code rate pairs and achievable information rates for a two-user turbo system with $P_o = 0.1$.

E_s/N_0 [dB]	$r_{c,1}$	$r_{c,2}$	$\sum_i r_{c,i}$	$\mathring{R}_1$	$\mathring{R}_2$	$\sum_i \mathring{R}_i$
0	0.35	0.35	0.70	0.47	0.53	1.00
1	0.40	0.40	0.80	0.55	0.61	1.16
2	0.50	0.50	1.00	0.64	0.67	1.31
3	0.55	0.60	1.15	0.70	0.76	1.46
	0.60	0.55				
4	0.65	0.65	1.30	0.79	0.82	1.61

rate pairs are not exactly symmetric.

The code rate pairs and maximal achievable information rates for a given outage probability of $P_o = 0.1$ at different E_s/N_0-values are listed in Table 5.2. As observed from this table, there is still a performance loss of about 0.3 bpc in sum rate over the considered SNR range of the outage-based rate allocation scheme compared to the outage capacity results. This loss can be reduced by using more appropriate coding techniques such as LDPC or turbo codes.

5.2.2. Outage-based Code Design for Single-User Setups

Unlike to the preceding algorithm where the channel code at each user is selected from a finite code set, we focus now on the design of a channel coding scheme that guarantees a specific outage probability of the turbo equalizer. Inspired by the results of the correlation chart analysis in Section 4.3, we exploit the analytical bound in (4.67) to design a channel encoder that optimizes the outage behavior. Specifically, the concept of IRC codes is invoked to shape the correlation function of the channel decoder with respect to the convergence properties of the equalizer. The corresponding channel code design problem can be formulated as a nonlinear optimization problem. It is shown that standard numerical tools can efficiently solve this optimization problem.

5.2.2.1. Channel Code Design

The IRC coding scheme from [Tüc04], constituted by a set of $P = 17$ outer convolutional subcodes having the rates $r_c^{(p)} = 0.05 \cdot (2+p)$, $p = 0, .., P-1$, and an inner rate-1 memory-1 convolutional code is used for the outage optimization. Each outer subcode encodes a specific fraction of the information bit sequence determined by the weighting coefficient $\epsilon_p \in [0, 1]$, $p = 0, .., P-1$. Given the overall coding rate r_c, the weighting coefficients satisfy:

$$\sum_{p=0}^{P-1} \epsilon_p = 1 \text{ and } \sum_{p=0}^{P-1} \epsilon_p r_c^{(p)} = r_c. \tag{5.27}$$

Similar to [Tüc04], we assume that for decoding the trellis fractions of the individual subcodes do not interfere with each other. The correlation function $f_{d1}(\alpha_{d1})$ of the outer IRC decoder is thus given by a weighted superposition of the correlation functions $f_{d1,p}(\alpha_{d1})$ of the individual subcodes, i.e.,

$$f_{d1}(\alpha_{d1}) = \sum_{p=0}^{P-1} \epsilon_p f_{d1,p}(\alpha_{d1}). \tag{5.28}$$

Using (5.28) together with (4.22)-(4.27), the *joint* IRC decoder correlation function (4.28), combining the iterative decoding of the inner and outer decoder, can be expressed for arbitrary values of $\alpha_d \in [0, 1]$ by

$$\varphi_d = f_d(\alpha_d) = f_{d2,2}\Big(\alpha_d, \sum_{p=0}^{P-1} \epsilon_p f_{d1,p}(\tilde{\nu})\Big), \tag{5.29}$$

$$\sum_{p=0}^{P-1} \epsilon_p f_{d1,p}(\nu) > f_{d2,1}^{-1}(\varphi_e, \nu) \text{ for all } \nu \in [0, \tilde{\nu}], 0 \leq \tilde{\nu} < 1, \tag{5.30}$$

where the function $f_{d2,1}^{-1}(\cdot,\cdot)$ denotes the inverse of $f_{d2,1}(\cdot,\cdot)$ with respect to its second argument. Note that (5.30) is equivalent to the recurrence relations (4.25) and (4.26) for the case of $T_d \to \infty$. Given a finite set of output correlation values $\{\varphi_d^{(1)},...,\varphi_d^{(k)},...,\varphi_d^{(D)}\}$, $\varphi_d^{(k)} \in \mathcal{J}$ and the weighting coefficients $\{\epsilon_p\}_{p=0}^{P-1}$ of the *joint* IRC decoder, we can use (5.29) and (5.30) to determine the corresponding set of input correlation values $\{\alpha_d^{(1)},...,\alpha_d^{(k)},...,\alpha_d^{(D)}\}$ with $\alpha_d^{(k)}$ satisfying $\alpha_d^{(k)} = f_d^{-1}(\varphi_d^{(k)})$, $k = 1,..,D$.

The goal of the optimization of the weighting coefficients $\{\epsilon_p\}$ is to minimize the system's outage probability. Therefore, using (4.44) and (4.67), we define the objective function to be minimized as

$$F_{\text{out}}(\varphi_e^{(1)},...,\varphi_e^{(D)}) \equiv \frac{1}{2}\sum_{k=1}^{D} \text{erfc}\left(\frac{\sqrt{2}}{\left((1-\varphi_d^{(k)})\phi^{-1}(\varphi_e^{(k)})+2\right)\mathring{\sigma}_k} - \frac{\mathring{\mu}_k}{\sqrt{2}\mathring{\sigma}_k}\right), \tag{5.31}$$

where $\varphi_e^{(k)} = f_d^{-1}(\varphi_d^{(k)})$, $k = 1,..,D$. With the definitions in (5.27)-(5.31), the problem of optimizing the weighting coefficients $\{\epsilon_p\}$ can then be formulated as

$$\underset{\{\epsilon_p\},\{\varphi_e^{(k)}\},\{\tilde{\nu}_k\}}{\text{minimize}} \; F_{\text{out}}(\varphi_e^{(1)},...,\varphi_e^{(D)}) \tag{5.32}$$

subject to

$$\varphi_d^{(k)} = f_{d2,2}\left(\varphi_e^{(k)}, \sum_{p=0}^{P-1}\epsilon_p f_{d1,p}(\tilde{\nu}_k)\right), k = 1..,D \tag{5.33}$$

$$\sum_{p=0}^{P-1}\epsilon_p f_{d1,p}(\nu_k) > f_{d2,1}^{-1}(\varphi_e^{(k)},\nu_k), \forall \nu_k \in [0,\tilde{\nu}_k], \forall k \tag{5.34}$$

$$\tilde{\nu}_k \in [0,1), \varphi_e^{(k)} \in [0,1), \forall k \tag{5.35}$$

$$\sum_{p=0}^{P-1}\epsilon_p = 1, \; \epsilon_p \in [0,1], \forall p \tag{5.36}$$

$$\sum_{p=0}^{P-1}\epsilon_p r_c^{(p)} = r_c. \tag{5.37}$$

Note that (5.33) and (5.34) are non-convex constraints, since the functions $f_{d2,2}(\cdot)$, $f_p(\cdot)$, $p = 1,..,P-1$ and $f_{d2,1}^{-1}(\cdot,\cdot)$ are non-convex for the specified IRC coding scheme. Moreover, by numerically evaluating (5.31), we also find that the objective F_{out} is non-convex. The above optimization problem is thereby a non-convex programming problem, whose global minimum solution can only be obtained through an exhaustive (brute-force) search. As a consequence, we only aim at the computation of a local minimizer to the above problem by using an algorithm based on the interior-reflective Newton method [CL94]. For a detailed discussion on the computational complexity, the convergence behavior and parameter choices of the

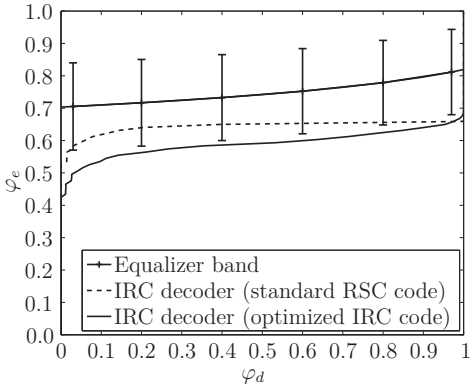

Figure 5.9.: Correlation characteristic of the joint IRC decoder for the optimized rate-1/2 IRC code and the regular rate-1/2 RSC code, and equalizer band for $L = 32$-tap Rayleigh fading channels with exponential decay and RMS delay $\tau_d = 8$.

interior-reflective Newton method, please refer to [CL94], [CL96].

Fig. 5.9 shows the correlation characteristic of the *joint* IRC decoder for a rate $r_c = 1/2$ outer code, whose weighting coefficients are optimized with respect to the outage behavior of the SC-MMSE FDE for transmissions over $L = 32$-tap Rayleigh fading channels with exponential decay and RMS delay $\tau_d = 8$ at an average SNR E_s/N_0 of 1.0 dB. The optimized weighting coefficients were obtained by computing (5.32)-(5.37) on a grid of $D = 4$ points, where $\varphi_d^{(k)} \in \mathcal{D} = \{0.05, 0.3, 0.6, 0.99\}$. They are given as follows:

$$\Big[\epsilon_1, .., \epsilon_{17}\Big] = \Big[0, 0, 0, 0, 0, 0.4612, 0.1195, 0, 0, 0, 0.2258, 0, 0.0196, 0.0995, 0, 0, 0.0744\Big]. \tag{5.38}$$

For comparison, Fig. 5.9 also shows the correlation characteristic of the *joint* IRC decoder for a regular RSC rate-1/2 outer code (defined by the generator $[23, 35]$) having the weighting coefficients: $\epsilon_8 = 1$, and $\epsilon_p = 0$, otherwise. Further, a band of the equalizer correlation curves, obtained by numerically computing the mean $\mathrm{E}[f_e(\varphi_d)]$ and the variance $\mathrm{Var}[f_e(\varphi_d)]$ of the correlation at the equalizer output for a large number of random channel realizations, is shown as well. As observed in Fig. 5.9, the band of the correlation curves of the equalizer and the correlation curve of the *joint* IRC decoder largely overlap when the regular RSC code is employed, so that for the majority of the channel realizations the turbo equalizer fails to converge and outage events occur. In contrast, it is easy to see that for the optimized IRC

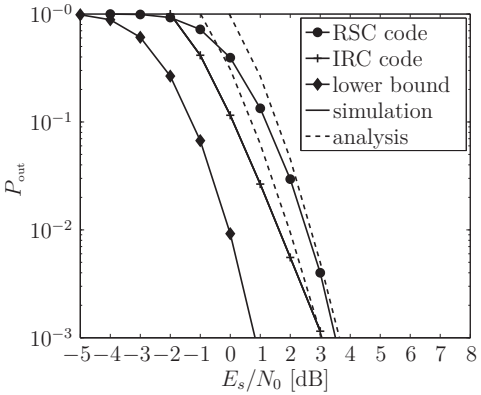

Figure 5.10.: Outage performance of the SC-MMSE FDE employing the regular rate-1/2 RSC code and the optimized rate-1/2 IRC code.

Table 5.3.: Optimized weighting coefficients of the rate-1/2 IRC code at different E_s/N_0 in dB.

E_s/N_0	$\epsilon_1,\epsilon_2,...,\epsilon_{17}$ in percent																
-1	00	00	00	00	22	38	00	00	00	00	00	02	28	00	00	00	10
0	00	00	00	00	10	50	00	00	00	00	00	11	19	00	00	00	10
1	00	00	00	00	00	46	12	00	00	00	23	00	02	10	00	00	07
2	00	00	00	00	00	24	37	00	00	03	18	00	00	11	00	00	07
3	00	00	00	00	00	18	45	00	00	00	19	01	00	10	00	00	07

code the convergence tunnel between the equalizer curves and the *joint* IRC decoder curve is greatly enlarged, indicating that for most of the channel realizations the turbo equalizer is able to successfully converge. Thus the probability of convergence failure of the turbo equalizer can be reduced greatly when employing the optimized IRC code for the transmission.

5.2.2.2. Numerical Results

Fig. 5.10 compares the outage performance of the SC-MMSE FDE turbo scheme employing the regular rate-1/2 outer RSC code and the optimized rate-1/2 outer IRC code for Rayleigh fading channels with exponential decay and RMS delay $\tau_d = 8$. The weighting coefficients $\{\epsilon_p\}_{p=0}^{P-1}$ of the optimized IRC codes for several SNR values E_s/N_0 are listed in Table 5.3. As a reference, the outage probability of a single-carrier system assuming perfect ISI cancellation and optimal (i.e., capacity achieving) binary coding is shown as well in Fig. 5.10. Note that outage probability

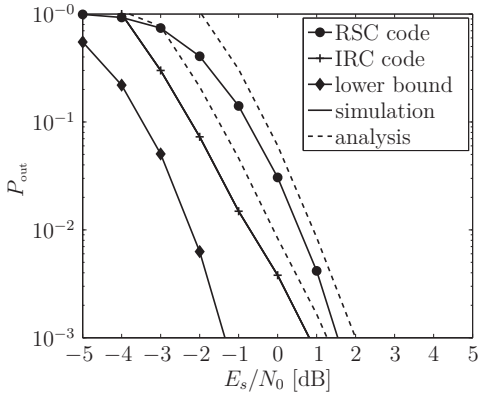

Figure 5.11.: Outage performance of the SC-MMSE FDE employing the regular rate-7/20 RSC code and the optimized rate-7/20 IRC code.

Table 5.4.: Optimized weighting coefficients of IRC codes with different rates at different E_s/N_0 in dB.

E_s/N_0	$\epsilon_1,\epsilon_2,...,\epsilon_{17}$ in percent																
-6	86	00	00	00	00	00	00	03	06	00	05	00	00	00	00	00	00
-2	00	05	53	04	00	00	01	22	00	00	01	04	03	03	00	00	04
2	00	00	00	00	00	18	45	00	00	00	19	01	00	10	00	00	07
6	00	00	00	00	00	00	00	00	00	00	00	00	00	54	00	00	46
10	00	00	00	00	00	00	00	00	00	00	00	00	00	00	00	00	100

of such a system is given by (4.68). As observed in Fig. 5.10, the optimized IRC-coded turbo scheme outperforms the RSC-coded turbo system over the considered E_s/N_0 value range, which is consistent with the result in Section 4.3. Specifically, it was found that a coding advantage of about 1.2 dB at outage probability $P_{\text{out}} = 10^{-1}$ can be achieved by the optimized code over the regular code. Additionally, we find that the performance gap to the lower bound is only 1.2 dB at $P_{\text{out}} = 10^{-1}$ for the optimized IRC-coded turbo system, while for the regular RSC-coded turbo system it is more than 2.3 dB. Similar results obtained for the SC-MMSE FDE employing rate-7/20 codes are shown in Fig. 5.11.

Fig. 5.12 shows the average TP for a selective-repeat ARQ system with turbo equalization utilizing optimized outer IRC codes over Rayleigh fading channels with RMS delay $\tau_d = 8$. The weighting coefficients $\{\epsilon_p\}_{p=0}^{P-1}$ are optimized to improve the throughput efficiency of the turbo equalizer. In order to maximize the throughput

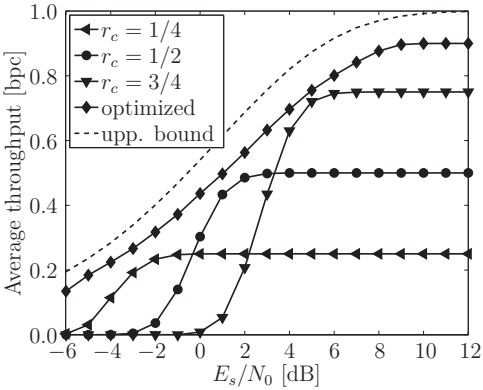

Figure 5.12.: Average throughput performance of the SC-MMSE turbo equalizer with optimized IRC and regular RSC codes having the rates $r_c = 1/4$, 1/2 and 3/4.

efficiency, $\{\epsilon_p\}$ should be found by solving the following optimization problem:

$$\underset{\{\epsilon_p\},\{\varphi_e^{(k)}\},\{\tilde{\nu}_k\}}{\text{maximize}} \Big(1 - F_{\text{out}}\Big) \sum_{p=0}^{P-1} \epsilon_p r_c^{(p)} \tag{5.39}$$

$$\text{subject to (5.33)-(5.36).} \tag{5.40}$$

Note that, similar to problem (5.32)-(5.37), the above problem is a non-convex one that can be approximately solved by the iterative interior-reflective Newton method [CL94], [CL96]. Table 5.4 presents some examples of optimized weighting coefficients for several E_s/N_0 values.

The throughput performance of the optimized IRC-coded turbo equalizer is compared in Fig. 5.12 with the performance of an ARQ scheme with regular RSC codes with coding rates $r_c = 1/4$, 1/2 and 3/4. For comparison, the upper bound on the throughput efficiency of the turbo system, given by $\text{TP}^\star = \arg\max_R \Big(1 - P_o^\star(R)\Big)R$, is shown as well. As it is evident from this figure, substantial throughput gain is obtained by the optimized IRC-coded turbo scheme over the RSC-coded turbo system. Further, we find that the performance gap to the upper bound of the IRC-coded turbo scheme diminishes at low E_s/N_0 values; the performance gap between both curves is smaller than 1.5 dB at TP = 0.2 bpc. This indicates that optimized IRC-coded SC-MMSE frequency domain turbo equalization can almost achieve the performance of a single-carrier system with perfect ISI cancellation and capacity achieving binary coding in the low E_s/N_0 region.

5.3. Power Allocation for Linearly Precoded Signals

When channel state information is available at the transmitter and receiver side, linear transmit precoding can be used to improve power efficiency of single-user MIMO wireless transmission systems. Most of the available precoding schemes assume a perfect knowledge of the channel state at the transmitter which is a reasonable assumption in low mobility full-duplex communication applications. The channel estimates are obtained at the receiver during the transmission of a frame of information bits, and are typically reused in subsequent transmissions as long as the channel varies slowly over time. The transmitter can acquire CSI using the channel estimates at the receiver, by either invoking the reciprocity or by using a dedicated feedback link [MP07]. Note that both reciprocity and feedback methods are applied widely in practical communication systems, including time-division-duplex (TDD) and frequency-division-duplex (FDD) systems.

When designing a linear precoder, various design criteria based on information theoretic and practical measures can be used to optimize the transmission power allocation. The information theoretic measures mostly include the error exponent, the instantaneous and ergodic capacity, while the practical measures include the bit error rate, symbol error rate, the pairwise error probability, the MSE, and the received SNR [MP07]. The choice of the design criteria mainly depend on the system structure, the system parameters and the detection principle used at the receiver. For example, a system employing strong channel coding with non-iterative detection over a flat-fading MIMO channel may operate very close to the capacity limit, and hence, a precoding design based on the error exponent may be the preferred choice. In contrast, for a system assuming infinite codeword length and Gaussian codebooks, the ergodic capacity may be a more suitable measure, e.g., see [CT91], [Tel99]. Other designs based on practical measures often jointly optimize both a linear precoder and a linear non-iterative detector based on the MSE, the BER, or the SNR (see [SSP01], [OSV03], [PCL03] and references therein). In these papers, optimizing a linear precoding and a linear detection matrix is formulated as a constrained optimization problem with the solution being given by a classical waterfilling expression.

Most of the existing work limits the application of linear precoding to communication systems employing non-iterative detection. In this section, we present a novel SVD-based precoding scheme applicable for single-carrier single-user block transmissions over MIMO ISI channels assuming SC-MMSE turbo equalization. Especially, we consider the problem of minimizing the transmission power with respect to the convergence behavior of the iterative receiver. Several criteria for transmission power allocation are discussed. To guarantee convergence of turbo equalization, we also invoke the correlation characteristics of the equalizer and channel decoder,

and formulate the power allocation problem as a curve fitting problem. More specifically, the transmission power is optimized so that the equalizer correlation curve lies above the decoder correlation curve up to a specific correlation point that specifies the target bit error rate of the system. It is shown that this problem is a convex one that can be efficiently solved by convex programming techniques. As a result of utilizing the power optimized precoding technique, the convergence properties of the SC-MMSE FDE can further be improved over the SC-MMSE FDE without precoding.

5.3.1. System Model of Linear Precoding

Consider a single-user single-carrier cyclic prefix assisted spatially multiplexing system employing N transmit and M receive antennas, as illustrated in Fig. 2.5. We assume that the number of receive antennas is equal or larger than the number of transmit antennas. After channel encoding and bit-interleaving, each transmit data stream $\mathbf{b}(k)$ is linearly precoded with a precoding matrix $\mathbf{T} \in \mathbb{C}^{NQ\times NQ}$ and then transmitted by the multiple transmit antennas.

As the precoder matrix $\mathbf{T}$ is block-circulant, i.e., $\mathbf{T} = \mathbf{F}_N^H \boldsymbol{\Xi}_T \mathbf{F}_N$, the vector of received symbols (see Eqn. (2.52)) at the equalizer can be expressed with the frequency domain compound channel matrix $\boldsymbol{\Xi}_c = \boldsymbol{\Xi}\boldsymbol{\Xi}_T$ as

$$\begin{aligned}\mathbf{r}(k) &= \mathbf{F}_M^H \boldsymbol{\Xi}_c \mathbf{F}_N \mathbf{b}(k) + \mathbf{n}(k) \\ &= \mathbf{F}_M^H \boldsymbol{\Xi}\boldsymbol{\Xi}_T \mathbf{F}_N \mathbf{b}(k) + \mathbf{n}(k). \end{aligned} \tag{5.41}$$

As shown in Section 2.8, the SVD of the frequency domain channel matrix $\boldsymbol{\Xi}$ is given by $\boldsymbol{\Xi} = \mathbf{U}\mathbf{G}\mathbf{V}^H$ where $\mathbf{G} = \mathrm{diag}\Big(\mathrm{diag}(\mathbf{G}_1), \mathrm{diag}(\mathbf{G}_2), ..., \mathrm{diag}(\mathbf{G}_N)\Big) \in \mathbb{C}^{MQ\times NQ}$ is a diagonal matrix with $\mathbf{G}_n = \mathrm{diag}(\sqrt{g_{n,0}}, \sqrt{g_{n,1}}, ..., \sqrt{g_{n,Q-1}}) \in \mathbb{C}^{Q\times Q}$, $\forall n$. Here, the variables $g_{n,q}$ are the eigenvalues of $\boldsymbol{\Xi}\boldsymbol{\Xi}^H$. Assume that the frequency domain precoding matrix $\boldsymbol{\Xi}_T$ can be decomposed into the matrix product $\boldsymbol{\Xi}_T = \mathbf{V}\mathbf{P}$ with $\mathbf{P} = \mathrm{diag}\Big(\mathrm{diag}(\mathbf{P}_1), \mathrm{diag}((\mathbf{P}_2), ..., \mathrm{diag}((\mathbf{P}_N)\Big)$, $\mathbf{P}_n = \mathrm{diag}\Big(\sqrt{p_{n,0}}, \sqrt{p_{n,1}}, ..., \sqrt{p_{n,Q-1}}\Big)$ being the diagonal power loading matrix. Here, the vector $\mathbf{p} = [\mathbf{p}_1^T, \mathbf{p}_2^T, ..., \mathbf{p}_N^T]^T$, $\mathbf{p}_n = [p_{n,0}, p_{n,1}, ..., p_{n,Q-1}]^T$, $n = 1, ..., N$ contains the values of the power allocation. With the SVD of $\boldsymbol{\Xi}$, the system model (5.41) can then be rewritten as

$$\mathbf{r}(k) = \mathbf{F}_M^H \mathbf{U}\mathbf{G}\mathbf{V}^H \mathbf{V}\mathbf{P}\mathbf{F}_N \mathbf{b}(k) + \mathbf{n}(k) \tag{5.42}$$

$$= \mathbf{F}_M^H \mathbf{U}\mathbf{G}\mathbf{P}\mathbf{F}_N \mathbf{b}(k) + \mathbf{n}(k). \tag{5.43}$$

Multiplying Eqn. (5.43) with matrix $\mathbf{F}_M^H \mathbf{U}^H \mathbf{F}_M$ does not change the statistics of the channel noise, as $\mathbf{U}$ and $\mathbf{F}_M$ are unitary. Therefore, the received signal can be

written as

$$\begin{aligned}\acute{\mathbf{r}}(k) &= \mathbf{F}_M^H \mathbf{U}^H \mathbf{F}_M \mathbf{r}(k) \\ &= \mathbf{F}_M^H \mathbf{G}\mathbf{P}\mathbf{F}_N \mathbf{b}(k) + \acute{\mathbf{n}}(k)\end{aligned} \tag{5.44}$$

with $\acute{\mathbf{n}}(k) \sim \mathcal{CN}(\mathbf{0}, \sigma_0^2\mathbf{I})$. Observing that the matrix product $\mathbf{GP}$ gives a diagonal matrix, we obtain as a result that SVD-based precoded single-carrier transmission perfectly decouples the MIMO ISI channel in the spatial domain into a set of N parallel channels. Eqn. (5.44) can hence equivalently be expressed as

$$\acute{\mathbf{r}}_n(k) = \mathbf{F}^H \mathbf{G}_n \mathbf{P}_n \mathbf{F} \mathbf{b}_n(k) + \acute{\mathbf{n}}_n(k) \text{ for } n = 1..., N, \tag{5.45}$$

where $\acute{\mathbf{r}}_n(k) = \hat{\mathbf{S}}\acute{\mathbf{r}}(k)$ and $\acute{\mathbf{n}}_n(k) = \hat{\mathbf{S}}_n\acute{\mathbf{n}}(k)$ with $\hat{\mathbf{S}}_n = [\mathbf{0}_{(Q,(n-1)Q)}, \mathbf{I}_Q, \mathbf{0}_{(Q,(M-n)Q)}] \in \mathbb{C}^{Q\times MQ}$ being a selection matrix. Owing to the circulant structure of the equivalent channel matrices $\mathbf{F}^H\mathbf{G}_n\mathbf{P}_n\mathbf{F}$ in (5.45), each of the N parallel channels is characterized by ISI and Gaussian noise.

5.3.2. SC-MMSE Frequency Domain Equalization of Linearly Precoded Signals

Next, a derivation of the SC-MMSE FDE to deal with linearly-precoded transmit signals is presented. The block diagram of the corresponding equalizer is shown in Fig. 5.13. After frequency domain conversion and multiplication by the unitary matrix $\mathbf{U}$, the received signal given by (5.43) is processed by the equalizer. The soft cancellation block cancels the interference components from the received signal. The residual interference is then further suppressed by the linear frequency domain MMSE filter $\dot{\mathbf{\Gamma}}_n$. The MMSE filter outputs the soft symbol estimates $\mathbf{z}_n$ of the transmitted symbols $\mathbf{b}_n$. With the aid of the MSE-formulation (3.28), the optimal MMSE filtering matrix $\dot{\mathbf{\Gamma}}_n$ can be found by solving the MSE optimization problem:

$$\begin{aligned}&\text{minimize } Q^{-1}\text{Trace}\Big(\dot{\mathbf{\Gamma}}_n^H \mathbf{\Psi}^{\text{FDPr}} \dot{\mathbf{\Gamma}}_n\Big) - (1-\bar{\varphi})Q^{-2}\text{Trace}\Big(\dot{\mathbf{\Gamma}}_n^H \mathbf{G}_n \mathbf{P}_n\Big)^2 \\ &\text{subject to: } Q^{-1}\text{Trace}\Big(\dot{\mathbf{\Gamma}}_n^H \mathbf{G}_n \mathbf{P}_n\Big) = 1,\end{aligned} \tag{5.46}$$

where $\mathbf{\Psi}^{\text{FDPr}} = [(1-\bar{\varphi})\mathbf{G}^2\mathbf{P}^2 + \sigma_0^2\mathbf{I}_{QM}]$ is the covariance matrix of the residual signal after MMSE filtering. The solution to the above optimization problem can be derived similarly to the SC-MMSE FDE without precoding, as shown in Section 3.3. We skip the full derivation for the MMSE filtering matrix $\dot{\mathbf{\Gamma}}_n$ here and present

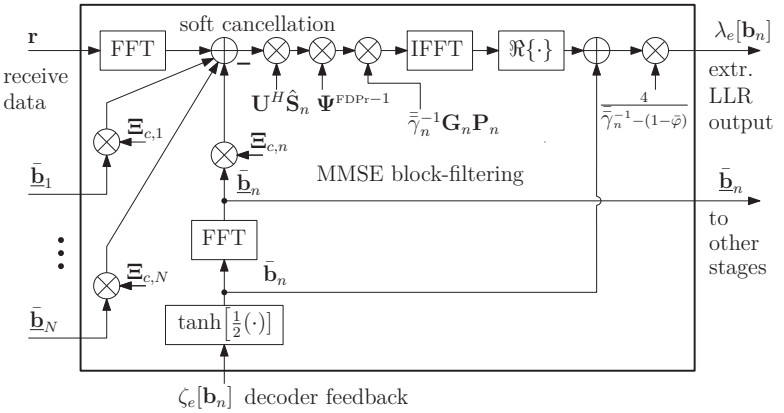

Figure 5.13.: Signal flow chart of the SC-MMSE FDE for precoded transmit signals.

only the expression for the optimal output vector $\mathbf{z}_n$,

$$\mathbf{z}_n = \bar{\bar{\gamma}}_n^{-1}\mathbf{F}^H\mathbf{G}_n\mathbf{P}_n\mathbf{\Psi}_n^{\mathrm{FDPr}-1}\hat{\mathbf{S}}_n\mathbf{U}^H\left(\underline{\mathbf{r}} - \underline{\bar{\mathbf{r}}}\right) + \bar{\mathbf{b}}_n. \tag{5.47}$$

where $\mathbf{\Psi}_n^{\mathrm{FDPr}} \equiv \left[(1-\bar{\varphi})\mathbf{G}_n^2\mathbf{P}_n^2 + \sigma_0^2\mathbf{I}_Q\right]$ and $\bar{\bar{\gamma}}_n = Q^{-1}\mathrm{Trace}(\mathbf{G}_n\mathbf{P}_n\mathbf{\Psi}_n^{\mathrm{FDPr}-1}\mathbf{G}_n\mathbf{P}_n)$. Based on (5.47), the *extrinsic* LLRs at the output of the equalizer are given by

$$\lambda_e\left[\mathbf{b}_n\right] = \frac{4\Re\{\mathbf{z}_n\}}{\bar{\bar{\gamma}}_n^{-1} - (1-\bar{\varphi})}, \forall n. \tag{5.48}$$

5.3.2.1. SNR Analysis and Correlation Function

The effective SNR of the *extrinsic* LLRs $\lambda_e\left[\mathbf{b}_n\right]$ at the equalizer output can be derived in closed form as a function of the power allocation vector $\mathbf{p}_n$ and the average energy level $\bar{\varphi}$ of the soft estimates calculated from the *extrinsic* feedback LLRs of the channel decoder. Supposing that Assumption 3.4 remains valid for the SVD-based precoded single-carrier transmission as well, the effective SNR $\psi_n^{\mathrm{FDPr}}(\mathbf{p}_n, \bar{\varphi})$

reads as (see also Eqn. (3.39))

$$\begin{aligned}\psi_n^{\mathrm{FDPr}}(\mathbf{p}_n,\bar{\varphi}) &= \frac{2\bar{\bar{\gamma}}_n(\mathbf{p}_n,\bar{\varphi})}{1-\bar{\bar{\gamma}}_n(\mathbf{p}_n,\bar{\varphi})(1-\bar{\varphi})} \\ &= \frac{2Q^{-1}\mathrm{Trace}(\mathbf{G}_n\mathbf{P}_n\boldsymbol{\Psi}_n^{\mathrm{FDPr}-1}\mathbf{G}_n\mathbf{P}_n)}{1-Q^{-1}\mathrm{Trace}(\mathbf{G}_n\mathbf{P}_n\boldsymbol{\Psi}_n^{\mathrm{FDPr}-1}\mathbf{G}_n\mathbf{P}_n)(1-\bar{\varphi})} \\ &= \frac{2\sum_{q=0}^{Q-1}\frac{g_{n,q}p_{n,q}}{\sigma_0^2+(1-\bar{\varphi})g_{n,q}p_{n,q}}}{Q-\left(\sum_{q=0}^{Q-1}\frac{g_{n,q}p_{n,q}}{\sigma_0^2+(1-\bar{\varphi})g_{n,q}p_{n,q}}\right)(1-\bar{\varphi})} \\ &= 2Q\Big(\sum_{q=0}^{Q-1} l_{n,q}(p_{n,q})^{-1}\Big)^{-1} - \frac{2}{1-\bar{\varphi}}, \end{aligned} \tag{5.49}$$

where $l_{n,q}(p_{n,q}) \equiv \frac{1}{1-\bar{\varphi}} + \frac{g_{n,q}p_{n,q}}{\sigma_0^2}$ and $\bar{\bar{\gamma}}_n = \bar{\bar{\gamma}}_n(\mathbf{p}_n,\bar{\varphi})$. It can easily be shown that the effective SNR $\psi_n^{\mathrm{FDPr}}(\mathbf{p}_n,\bar{\varphi})$ is a monotonically increasing function of its arguments. The above expression for the SNR can now be used to derive efficient allocation schemes that optimize the transmission power levels.

Moreover, the correlation function of the equalizer can now be expressed with (5.49) and (4.13) as

$$f_e(\mathbf{p},\alpha_e) = \frac{1}{N}\sum_{n=1}^{N}\phi\Big(\psi_n^{\mathrm{FDPr}}(\mathbf{p}_n,\alpha_e)\Big). \tag{5.50}$$

We note that the correlation function $f_e(\mathbf{p},\alpha_e)$ is monotonically increasing in all arguments, since

$$\frac{\partial f_e(\mathbf{p}_n,\alpha_e)}{\partial\alpha_e} \geq 0 \text{ and } \frac{\partial f_e(\mathbf{p}_n,\alpha_e)}{\partial p_{n,q}} \geq 0, \forall n,q. \tag{5.51}$$

5.3.3. Power Allocation Strategies

Having the analytical expressions for both the effective SNR $\psi_n^{\mathrm{FDPr}}(\mathbf{p}_n,\bar{\varphi})$ and the equalizer correlation function $f_e(\mathbf{p},\alpha_e)$, we can now consider the optimization of the power allocation over the frequency domain channel eigenmodes $g_{n,q}$. In this subsection, several approaches with respect to performance measures such as mean square error, capacity or correlation are introduced. Specifically, we consider several approaches that minimize the total power at the first iteration of the turbo equalizer. We also consider transmission power optimization based on the correlation chart analysis presented in Chapter 4. In detail, the goal of the correlation chart-based power optimization is to minimize the total transmitted power, subject to maintaining an acceptable bit error performance at the last iteration of the turbo equalizer.

1. *MinSumMSE Criterion.* The first method allocates the power levels with respect to the minimum total biased MSE [TSK02] at the output of the SC-MMSE FDE at the first iteration. Since no knowledge about the code bits is available at the first iteration, the total biased MSE is given by

$$\mathrm{MSE}^{\mathrm{FDPr}} = \sum_{n=1}^{N} \sum_{q=0}^{Q-1} \frac{\sigma_0^2}{\sigma_0^2 + g_{n,q} p_{n,q}} \tag{5.52}$$

Using (5.52), the problem of minimizing the total sum MSE can be expressed as

$$\begin{aligned} &\min_{\mathbf{p}} \sum_{n=1}^{N} \sum_{q=0}^{Q-1} \frac{\sigma_0^2}{\sigma_0^2 + g_{n,q} p_{n,q}} \\ &\text{subject to } \mathbf{1}^T \mathbf{p} \leq P_0, \mathbf{p} \geq \mathbf{0}, \end{aligned} \tag{5.53}$$

where P_0 is the total power over the frequency domain channel eigenmodes. We observe that the objective function and the constraint of (5.53) are convex and linear, respectively, with respect to the power levels $p_{n,q}$. The above optimization problem is hence a convex problem, whose solution is given by the following waterfilling expression [PF05]:

$$p_{n,q} = (c_{\mathrm{MinMSE}} g_{n,q}^{-1/2} - \sigma_0^2 g_{n,q}^{-1})^+, \forall n, \forall q \tag{5.54}$$

with c_{MinMSE} being a parameter chosen such that $\mathbf{1}^T \mathbf{p} = P_0$[4].

2. *MaxInfoRate Criterion.* The second approach maximizes the achievable mutual information $I(\mathbf{b}, \mathbf{r})$ of the turbo system by assuming Gaussian distributed input signals. As shown in Section 2.8, the classical waterfilling solution [Tel99], [XP03] over the frequency domain channel eigenmodes provides the maximum mutual information,

$$p_{n,q} = \left(c_{\mathrm{MaxRate}} - \sigma_0^2 g_{n,q}^{-1}\right)^+, \forall n, \forall q, \tag{5.55}$$

where c_{MaxRate} is the "water level" chosen to satisfy the power constraint $\mathbf{1}^T \mathbf{p} \leq P_0$. We observe from (5.55) that for the high SNR range ($\sigma_0^2 \to 0$) the transmission power is evenly allocated over the $g_{n,q}$'s, whereas in the low SNR range the main power is only allocated to the frequency domain subchannels having a strong eigenmode.

[4]Note that the expression in (5.54) has been numerically evaluated with the iterative algorithm proposed in [PF05] that terminates with an exact numerical solution in $O(NQ)$ arithmetic operations.

3. *MaxCorr Criterion.* The third approach employs a power allocation scheme that maximizes the output correlation $f_e(\mathbf{p}, 0)$ of the equalizer at the first iteration ($\alpha_e = 0$), i.e.,

$$\begin{aligned} &\max_{\mathbf{p}} \frac{1}{N} \sum_{n=1}^{N} \phi\Big(\psi_n^{\mathrm{FDPr}}(\mathbf{p}_n, 0)\Big) \\ &\text{subject to } \mathbf{1}^T\mathbf{p} \leq P_0, \mathbf{p} \geq \mathbf{0}. \end{aligned} \tag{5.56}$$

It is shown in the sequel that the optimization problem (5.56) is convex and can be efficiently solved by standard convex optimization tools [BV04].

4. *CorrChart Criterion.* The last approach considers the optimization of the power levels with respect to the convergence behavior of the iterative receiver. This approach adjusts the total transmission power to guarantee an open convergence tunnel between the equalizer and the decoder correlation curves up to a target correlation value $\varphi_d^{\mathrm{Target}}$. Consequently, this optimization problem can be formulated as follows:

$$\begin{aligned} &\min_{\mathbf{p}} \mathbf{1}^T\mathbf{p} \\ &\text{subject to } f_e(\mathbf{p}, \varphi_d) \geq f_d^{-1}(\varphi_d) + u(\varphi_d) \\ &\varphi_d \in [0, \varphi_d^{\mathrm{target}}], \mathbf{p} \geq \mathbf{0}, \end{aligned} \tag{5.57}$$

where $\varphi_d^{\mathrm{target}}$ denotes the channel decoder output correlation after convergence of the turbo equalizer required to achieve a target BER, and $u(\varphi_d)$, $u(\varphi_d) \geq 0$ is a function to control the speed of convergence to the fixed point.

Lemma 5.7. The optimization problem (5.57) is a convex one that can be efficiently solved by convex programming techniques.

Proof: See Appendix A.7.

5.3.3.1. Equalizer Correlation Characteristics for Different Power Allocation Schemes

Fig. 5.14 (a)-(d) show the correlation characteristics of the equalizer obtained by the analytical expression (5.50) and the numerical simulation for the four power-optimized SVD-based precoded transmission employing the four power allocation schemes discussed above. For comparison, we also show results of the non-precoded SC-MMSE FDE for the case when channel state information is not available at the transmitter. The equalizer correlation curves are obtained for the two SNRs $E_b/N_0 = 4.5$ dB and $E_b/N_0 = 2.4$ dB. The simulations are carried for a single-user

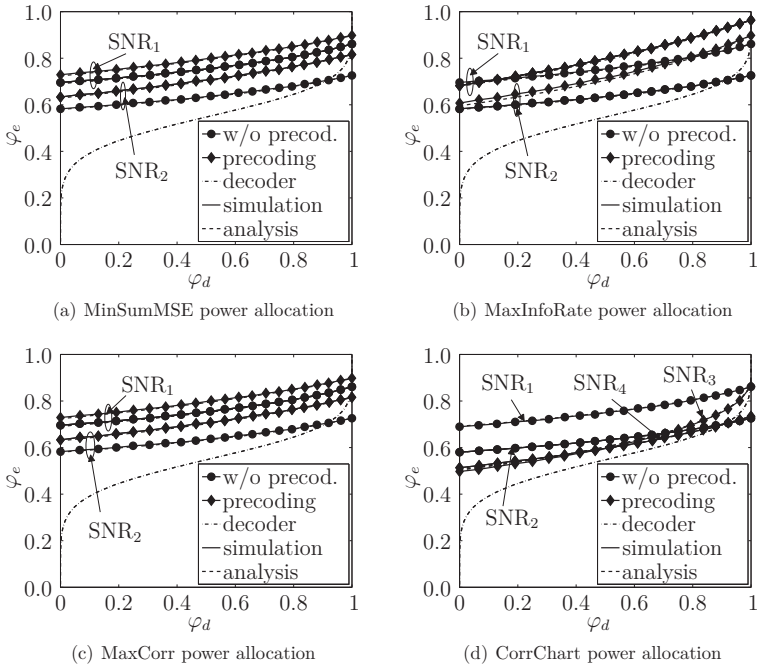

(a) MinSumMSE power allocation

(b) MaxInfoRate power allocation

(c) MaxCorr power allocation

(d) CorrChart power allocation

Figure 5.14.: Correlation characteristics of the equalizer and decoder for the 'MinSumMSE', 'MaxInfoRate', 'MaxCorr' and 'CorrChart' based power allocation schemes at different SNRs. $\mathrm{SNR}_1 = 4.5$ dB, $\mathrm{SNR}_1 = 2.4$ dB, $\mathrm{SNR}_3 = 0.7$ dB and $\mathrm{SNR}_4 = 0.1$ dB.

single-carrier $N = M = 2$ MIMO system. The $L = 32$-tap frequency selective fading Rayleigh channel with uniform delay power profile is assumed. The FFT-size at the receiver is set to $Q = 128$.

As observed from all four figures, the simulated curves coincide with the estimates from the analysis for all four power allocation schemes. In addition, we see that the equalizer correlation curves with SVD-based precoding are located at higher levels compared to the equalizer correlation curves without precoding. In fact, the results reflect that for both SNR values the equalizer correlation curves with the 'MinSumMSE', 'MaxInfoRate' and the 'MaxCorr' power allocation schemes intersect with the decoder correlation curve at significantly higher correlation values φ_e. We also find that the 'MinSumMSE' and 'MaxCorr' power allocations result in similar correlation curves of the equalizer. It is also interesting to see that the four power allocation schemes differently effect the convergence behavior of the equal-

izer. As can be seen, the equalizer curve at the correlation value $\varphi_d = 1$ with the 'MaxInfoRate' power allocation is significantly higher as compared to the equalizer curves with the 'MinSumMSE' or 'MaxCorr' power allocations. The reason for this can be found when analyzing the effective SNR ψ_n^{FDPr} at the equalizer output for the case of perfect ISI cancellation. The effective SNR ψ_n^{FDPr} with 'MaxInfoRate' power allocation is then given by

$$\psi_n^{\mathrm{FDPr}(1)}(\mathbf{p}_n, 1) = Q^{-1} \sum_{q=0}^{Q-1} \left(c_{\mathrm{MaxRate}} g_{n,q} - \sigma_0^2 \right)^+. \tag{5.58}$$

Similarly, the expression with 'MinSumMSE' power allocation is found to

$$\psi_n^{\mathrm{FDPr}(2)}(\mathbf{p}_n, 1) = Q^{-1} \sum_{q=0}^{Q-1} \left(c_{\mathrm{MinMSE}} \sqrt{g_{n,q}} - \sigma_0^2 \right)^+. \tag{5.59}$$

As the power levels of both criteria satisfy the constraint $\mathbf{1}^T\mathbf{p} \leq P_0$, the coefficients c_{MaxRate} and c_{MinMSE} in (5.58) and (5.59), respectively, must follow the relation $c_{\mathrm{MaxRate}} \geq c_{\mathrm{MinMSE}}$. Consequently, the largest effective SNR ψ_n^{FDPr} and correlation value φ_e at the equalizer output are achieved for perfect *a priori* information with the 'MaxInfoRate' power allocation scheme.

The equalizer curves with the 'MaxCorr' and 'CorrChart' power allocations shown in Fig. 5.14 (c) and (d), respectively, are obtained by convex programming [BV04]. Specifically, for the 'CorrChart' power allocation the constraint in (5.57) has been computed on a finite grid of points in the interval $[0, \varphi_d^{\mathrm{target}}]$, equally spaced by 0.01. The function $u(x)$ in (5.57) has been defined as $u(x) = 0.1(1 - \varphi_d^{\mathrm{target}-1} x)$. In order to asses the performance gain achieved with the power allocation given by (5.57) over the non-precoded transmission, the intersection point between the equalizer and decoder correlation curves has been set to an identical target correlation value $\varphi_d^{\mathrm{target}}$. Therefore, as illustrated in Fig. 5.14 (d) for both SNR values, the SC-MMSE FDE with precoding converges to the same fixed point as the equalizer without precoding. However, the equalizer without precoding achieves the target correlation value at significantly lower E_b/N_0 values.

In summary, the correlation curves presented in Fig. 5.14 (a)-(d) illustrate impressively that transmit precoding with optimized power allocation significantly enhances the convergence threshold of the turbo receiver. As a result, the turbo equalizer can achieve better performance than without precoding. Naturally, this performance improvement comes at the cost of increased complexity at the transmitter due to the computation of the precoding matrix.

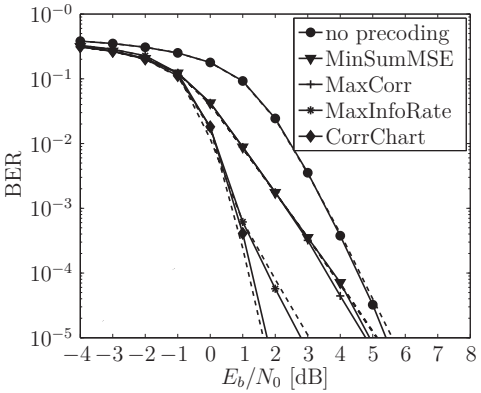

Figure 5.15.: BER performance of the SC-MMSE FDE (simulation results: black curves; analytical results: dashed curves) for different precoding schemes utilizing a memory-3, $r_c = 1/2$ convolutional code over Rayleigh fading channels. $N = M = 2$, $Q = 128$ and $L = 32$.

5.3.4. Numerical Results

Fig. 5.15 shows the BER performances achieved by the SC-MMSE FDE after $T_e = 20$ iterations with SVD-based transmit precoding and the four criteria used for transmission power allocation. For comparison, the performance of a turbo equalizer without precoding is shown as well. It can be seen that all four precoding schemes perform better than the non-precoded transmission over the considered E_b/N_0 value range, which is consistent with the analysis of Section 5.3.3. Moreover, we clearly observe that the 'CorrChart'-based power allocation approach outperforms the other three methods at moderate to high E_b/N_0 values.

Complexity: The four precoding schemes, discussed above require the computation of the SVD of the diagonal-block frequency MIMO channel matrix in (5.41). This can efficiently be performed in $O(QNM^2)$ (assuming $N \leq M$) arithmetic operations. The waterfilling expressions (5.54) and (5.54) of the 'MinSumMSE' and 'MaxInfoRate' power allocations, respectively, can numerically be evaluated with the iterative algorithm from [PF05]. This algorithm is known to give an exact numerical solution after a finite number of iterations with a worst-case complexity linear in the total number of eigenmodes NQ. This is in contrast to the interior point algorithms, for solving the power allocation problems (5.56) and (5.57), which have a polynomial worst-case complexity in NQ and terminate after a sufficient number

of iterations with an approximate solution [PJ06].

5.4. Chapter Summary

In this chapter it has been shown that appropriate resource allocation in wireless systems has significant influence on the performance of SC-MMSE FDE turbo equalization. The power and spectral efficiency can be increased when the transmitter possesses the available channel state information to adaptively allocate the resources transmission rate and power.

A simple algorithm for rate allocation in multiuser systems has been proposed that exploits the knowledge of the EXIT characteristics of the turbo equalizer. The algorithm adaptively selects the code parameters independently for each user with the objective to improve the system throughput. Numerical results of the throughput efficiency demonstrated the superiority of the proposed algorithm over non-adaptive schemes with fixed code rate ARQ.

Furthermore, when instead of partial CSI in the form of a feedback channel the long-term channel statistics are given at the transmitter, the allocation of transmission rates at the users can be performed with respect to the outage performance of the turbo equalizer. By means of Monte Carlo-based simulations the outage rate region of a two-user multiple access channel employing the SC-MMSE FDE at the receiver and rate-compatible channel coding at each transmitter has been numerically evaluated. With this region, we illustrated how the code parameters can be optimized at each user to meet a specific outage probability constraint of the turbo equalizer. In fact, it has been shown that the outage-based rate allocation scheme operates within a range of 0.3 bpc in sum rate away from the respective binary-input outage capacity region. Besides this, a framework for designing IRC channel coding schemes minimizing the outage probability of the SC-MMSE FDE has been developed. It was found that the optimization of the weighting coefficients of the IRC channel code can be formulated as a constrained non-convex program. By simulation, we found that the optimized IRC code achieves a coding advantage of more than 1.0 dB at an outage probability of $P_{\text{out}} = 10^{-1}$ over the regular RSC code when used in a turbo system.

Supposing perfect channel state information available at both the transmitter and receiver side, the turbo equalizer can be combined with a linear transmit precoder to enhance the power efficiency in MIMO systems. More specifically, in this work we have focused on an SVD-based precoder with transmit power allocation that explicitly takes into account the convergence constraints of the iterative receiver. The SVD-based precoder perfectly decouples the single-user MIMO ISI fading channel in

the spatial domain into a set of parallel ISI fading channels. For the minimization of the total transmission power over these parallel channels, four different design criteria based on the MSE, channel mutual information and output correlation at the equalizer have been considered. As a main result, it was found that a precoder optimizing the power levels subject to a target bit error rate of the turbo equalizer outperforms all other considered precoding schemes. Furthermore, this optimization can be formulated as a convex problem which can be solved very efficiently by standard numerical tools. We remark that a linear precoding and power optimization strategy for single-carrier signaling and turbo equalization has recently been proposed in [KCT+11]. However note that in contrast to [KCT+11] where multiple encoders and decoders are required for data transmission, the precoder in this work involves only a single error correcting channel code. Consequently, it offers a reduced complexity cost in the system implementation by avoiding multiple encoding and decoding.

6. Conclusions and Future Work

The aim of this thesis has been the development of efficient transmission strategies employing turbo equalization for single-carrier signaling over single or multiple-access block-fading channels with memory involving ISI. In particular, the focus has been on the design and analysis of low complexity and robust MMSE-based turbo equalizers operating in the frequency domain. Accordingly, the impact of different system configurations and channel settings on the convergence properties of the turbo equalizers has been studied and analytical bounds characterizing the average bit error rate and outage probability performance of the system have been derived. As a major contribution, two novel receiver designs improving the error performance over the existing SC-MMSE FDE [KM07], [YGWP08] have been proposed. Another special emphasis has been dedicated to adaptive transmit techniques, which aim to improve the power and spectral efficiency of turbo systems by efficiently exploiting the available resources at the transmitter side based upon the channel conditions. The challenging issue encountered in this context has been how the transmission rate and the power levels can be optimized while a specific convergence constraint of the iterative receiver and a QoS requirement are guaranteed. The main contributions are summarized as follows.

- A frequency domain turbo equalizer based on the framework of nonlinear MMSE symbol estimation, referred to as PDA SC-MMSE FDE, has been proposed for single-carrier block signaling. In contrast to the standard SC-MMSE FDE, the PDA SC-MMSE FDE merges *a priori* information from channel decoding and soft-decision feedback within the equalizer for ISI and MAI cancellation. Analytical and simulation results reveal that the proposed scheme provides SNR gains up to 2 dB in spatially uncorrelated MIMO channels as compared to the previously studied SC-MMSE turbo equalizer at the same order of computational complexity.

- With the aid of the EXIT and the correlation chart analysis tools, simple analytical expressions which are sufficiently accurate to predict the convergence properties of the SC-MMSE FDE and PDA SC-MMSE FDE in various single and multiuser propagation environments have been derived. Based on these expressions we have been able to gain insight into the convergence behavior

of the iterative receiver that helped to understand the impact of the internal equalizer iterations within the PDA SC-MMSE FDE on the overall performance of the system. Tight error bounds on the bit error and outage probabilities of MMSE-based FDEs have been derived as well. The error bounds provide simple, but effective tools for predicting and optimizing the performance of turbo systems. Moreover, they can be used to designing iterative systems with optimized channel coding, rate and power allocations targeting capacity-approaching performance.

- In practical multiuser scenarios, sparse scattering and/or very closely located users can cause very high spatial correlation between the different users' channels. In such situations the performance of the conventional SC-MMSE FDE may substantially be degraded and a more sophisticated equalizer may need to be applied for data detection. In this regard, a novel receiver design which is insensitive to spatial channel correlation has been presented. In particular, the proposed algorithm extends the SC-MMSE FDE to a hybrid technique by jointly performing groupwise frequency domain MMSE filtering and maximum *a posteriori* signal detection. Particular emphasis has been given on different greedy approaches for grouping the users to subgroups with respect to different MSE and channel correlation criteria. The suggested grouping schemes reduce noise enhancement of the groupwise interference suppression by allocating highly correlated user signals into the same subgroup. It was found that a simple correlation-based grouping method achieves similar performance than MSE-based methods at a significantly reduced complexity. Numerical results obtained by performance evaluations based on realistic channel sounding measurement data revealed a strong robustness of the hybrid turbo equalizer in MIMO channels with high spatial correlation. Typical performance gains achieved over the standard SC-MMSE FDE are in the range of 2 to 6 dB in SNR depending on the multiuser channel scenario.

- An EXIT chart based framework for transmission rate allocation in Gaussian multiple access ISI fading channels with SC-MMSE turbo equalization has been presented. The area property of EXIT functions has been used to derive a rate region upper bound of the iterative system. It was shown that maximizing the sum rate subject to the instantaneous channel state can efficiently be solved by variational methods. As a result of the sum rate optimization, a simple algorithm exploiting feedback information from the receiver to select independently for each user the optimal channel coding parameters with the objective to maximize the sum rate has been developed. Numerical results demonstrated that the adaptive rate allocation scheme achieves im-

proved throughput efficiency as compared to a standard method without rate adaption.

- The technique of rate adaption for multiuser turbo systems has been extended to an outage based rate allocation scheme. This approach optimizes the channel coding parameters with the intention to satisfy a specific outage probability constraint of the iterative receiver for a given channel fading distribution. The example of a rate-optimized two-user transmission showed that the proposed scheme operates close to its respective binary-input outage capacity region. Besides this, a novel design criterion for irregular channel codes has been proposed to improve the outage performance of single-user single-antenna turbo systems. It was shown that the application of optimized IRC codes for turbo equalization offers a coding gain of more than 1.0 dB in SNR compared to standard RSC coding over ISI fading channels with exponential delay-power profile.

- Finally, we have studied the application of linear transmit precoding for single-carrier signaling over MIMO ISI block-fading channels, where both the transmitter and receiver know perfectly the channel coefficients. More explicitly, we have concentrated on SVD-based precoding combined with transmit power optimization. Several power allocation strategies have been proposed. A convex optimization framework for optimizing the power levels over the frequency domain channel eigenmodes has shown to be superior over other existing power allocation methods. This result has been supported by results of BER performance evaluations with the different precoder schemes.

6.1. Future Work

In the course of this thesis, several interesting and import issues in the design and optimization of wireless communication systems have been addressed. However, many open research problems remain for future work. In the following some research directions that may be worth studying are described.

Rate and Power Allocation with Imperfect CSI

The application of the instantaneous rate and power allocation schemes of Sections 5.1 and 5.3 in real communication systems is limited in the sense that CSI is presumed to be perfectly available at the transmitter(s) and the receiver. However, the assumption of perfect knowledge of the instantaneous channel coefficients is unrealistic due to erroneous channel estimation (especially in fast-fading channels with

rapidly changing environments), and/or quantization, delay and errors introduced by a feedback channel. Consequently, a more realistic model for the transmitter and receiver that also covers imperfect CSI would be of practical relevance. Based on this model, the influence of channel uncertainty at the transmitter and the receiver side on the performance of the proposed rate and power allocation schemes should be thoroughly investigated. The obtained results may then be further used to extend the proposed approaches to robust resource allocation schemes which explicitly take into account the channel uncertainty at the transmitter and receiver.

Joint Rate and Power Optimization

In this work, we have concentrated on transmission rate and power optimization by focusing on two different design criteria: 1) maximizing the sum rate of multiuser systems subject to a fixed power allocation, and 2) minimizing the total transmission power of single-user systems subject to a fixed total power constraint and a fixed rate allocation. Therefore, an interesting extension would be the joint optimization of rate and power for single and multiuser transmissions under a fixed total power or rate constraint. This idea involves the joint design of channel coding schemes, transmit precoders and power allocations with a special focus on the convergence properties of the turbo equalizer. As examples, of particular interest are the problem of maximizing the rate for single-user transmissions subject to a total power constraint; the problem of sum rate maximization in multiuser systems subject to a total power or per user power constraint; the problem of minimizing the total power of all users subject to a fixed rate allocation; the problem of maximizing the minimum user rate subject to a total power constraint; and the problem of minimizing the maximum transmission power of the user subject to a fixed rate allocation. The development of efficient practical solutions to these optimization problems lead to new transmit strategies that aim to improve the overall performance, throughput and reliability of turbo equalization systems, and introduce fairness among users.

Extension to High Order Modulation

The proposed transmit rate and power allocation schemes as well as the receive algorithms have been developed for single-carrier signaling with BPSK modulation. By employing high order modulations with optimized mappings, the spectral efficiency of the system can be further increased. Thus, further work is required to extend the proposed transmit and receive techniques to be applicable in systems involving arbitrary signal constellations.

A. Proofs of Lemmas, Propositions and Theorems

A.1. Proof of Lemma 2.1

Assuming an exponential delay-power profile (2.18), the function $w(\Delta q)$ can expressed as $(L, Q) \to \infty$, as

$$\begin{aligned} w(\Delta q) &= \lim_{L\to\infty} \sum_{l=0}^{L-1} \sigma_l^2 \exp\left(-\sqrt{-1}\frac{2\pi}{L} l \Delta q\right) \\ &= \lim_{L\to\infty} \frac{c_{\exp}}{\tau_d} \sum_{l=0}^{L-1} \exp\left(-\frac{l}{L}\left(\sqrt{-1}2\pi\Delta q + \frac{1}{\Delta f \tau_d}\right)\right) \qquad (A.1) \\ &= \lim_{L\to\infty} \frac{c_{\exp}\left(1 - \exp\left(-(\sqrt{-1}2\pi\Delta q + \frac{1}{\Delta f\tau_d})\right)\right)}{(\Delta f\tau_d)L - (\Delta f\tau_d)L\exp\left(-\frac{1}{L}\left(\sqrt{-1}2\pi\Delta q + \frac{1}{\Delta f\tau_d}\right)\right)}, \qquad (A.2) \end{aligned}$$

where the expression in (A.2) has been derived using the exponential sum formula [GR07]. Using the fact that the mean energy of the delay-power profile per MIMO channel is normalized to one, we obtain

$$\begin{aligned} \lim_{L\to\infty} \sum_{l=0}^{L-1} \frac{c_{\exp}}{\tau_d}\left(-\frac{l}{\tau_d}\right) &= \lim_{L\to\infty} \frac{c_{\exp}\left(1 - \exp\left(\frac{1}{\Delta f\tau_d}\right)\right)}{(\Delta f\tau_d)L - (\Delta f\tau_d)L\exp\left(-\frac{1}{\Delta f\tau_d L}\right)} \\ &= c_{\exp}\left(1 - \exp\left(-\frac{1}{\Delta f\tau_d}\right)\right) \\ &= 1. \end{aligned}$$

The normalization constant $c_{\exp}$ can therefore be written as

$$c_{\exp} = \frac{1}{1 - \exp\left(-\frac{1}{\Delta f\tau_d}\right)}. \qquad (A.3)$$

Substituting (A.3) into (A.2) and taking the limit, we finally obtain

$$\begin{aligned} w(\Delta q) &= \lim_{L\to\infty} \frac{1}{(\Delta f \tau_d)L - (\Delta f \tau_d)L \exp\Big(-\frac{1}{L}\Big(\sqrt{-1}2\pi\Delta q + \frac{1}{\Delta f \tau_d}\Big)\Big)} \\ &= \frac{1}{1+\sqrt{-1}2\pi\Delta f\tau_d\Delta q} \\ &= \frac{1-\sqrt{-1}2\pi\Delta f\tau_d\Delta q}{1+(2\pi\Delta f\tau_d\Delta q)^2}. \end{aligned} \tag{A.4}$$

A.2. Proof of Lemma 3.6

To show that $\psi_n^{\mathrm{FD}}(\bar{\boldsymbol{\varphi}})$ is monotonically non-decreasing in $\bar{\boldsymbol{\varphi}}$, it suffices to show that

$$\frac{\partial \psi_n^{\mathrm{FD}}(\bar{\boldsymbol{\varphi}})}{\partial \bar{\varphi}_j} \geq 0 \text{ for all } \bar{\varphi}_j \in [0,1], \forall j. \tag{A.5}$$

Using (3.39), the first derivative of $\psi_n^{\mathrm{FD}}(\cdot)$ is obtained as

$$\frac{\partial \psi_n^{\mathrm{FD}}(\bar{\boldsymbol{\varphi}})}{\partial \bar{\varphi}_n} = \frac{\frac{\partial \gamma_n}{\partial \bar{\varphi}_n} - \gamma_n^2}{\frac{1}{2}(1-\gamma_n(1-\bar{\varphi}_n))^2} \text{ for } j = n, \tag{A.6}$$

$$\frac{\partial \psi_n^{\mathrm{FD}}(\bar{\boldsymbol{\varphi}})}{\partial \bar{\varphi}_j} = \frac{\frac{\partial \gamma_n}{\partial \bar{\varphi}_j}}{\frac{1}{2}(1-\gamma_n(1-\bar{\varphi}_n))^2} \text{ for } j \neq n, \tag{A.7}$$

where the partial derivatives $\partial\gamma_n/\partial\bar{\varphi}_j$ are given by

$$\frac{\partial \gamma_n}{\partial \bar{\varphi}_j} = Q^{-1}\mathrm{Trace}\Big(\boldsymbol{\Xi}_{c,j}^H \boldsymbol{\Psi}^{\mathrm{FD}-1}\boldsymbol{\Xi}_{c,n}\boldsymbol{\Xi}_{c,n}^H\boldsymbol{\Psi}^{\mathrm{FD}-1}\boldsymbol{\Xi}_{c,j}\Big). \tag{A.8}$$

We now immediately see that $\partial\gamma_n/\partial\bar{\varphi}_j \geq 0$ for all $j = 1,..,N$. Moreover, due to the block-diagonal structure of the covariance matrix $\boldsymbol{\Psi}^{\mathrm{FD}}$, the matrix $\mathbf{A} \equiv \boldsymbol{\Xi}_{c,n}^H\boldsymbol{\Psi}^{\mathrm{FD}-1}\boldsymbol{\Xi}_{c,n}$ is diagonal. Therefore, the numerator of (A.6) can be written as

$$Q^{-1}\sum_{q=0}^{Q-1}[\mathbf{A}]_{q,q}^2 - Q^{-2}\Big(\sum_{q=0}^{Q-1}[\mathbf{A}]_{q,q}\Big)^2. \tag{A.9}$$

As $\sum_q a_q^2 \geq Q^{-1}(\sum_q a_q)^2$, $a_q \geq 0$, $\forall q$, we obtain $\partial\gamma_n/\partial\bar{\varphi}_n \geq \gamma_n^2$. Therefore, we conclude that (A.5) holds true.

A.3. Proof of Theorem 3.13

To prove that a groupwise filter design based on MSE and SINR criteria lead to the same MAP decision metric $\rho_{g,q}$, we first explicitly express $\rho_{g,q}$ as a function of

the filter $\check{\mathbf{\Gamma}}_g$ and covariance matrix $\mathbf{R}_g$. By noting that $\mathbf{z}_{g,q}$ in (3.94) is given by $\mathbf{z}_{g,q} = \mathbf{S}_q \mathbf{F}_U^H \hat{\mathbf{\Gamma}}_g^H (\underline{\mathbf{r}} - \bar{\underline{\mathbf{r}}}) + \mathbf{U}_g \bar{\mathbf{t}}_{g,q}$, the MAP decision metric (3.97) can be written as

$$\begin{aligned}\rho_{g,q} &= -\Big(\mathbf{z}_{g,q} - \mathbf{U}_g \mathbf{x}\Big)^H \mathbf{R}_g^{-1} \Big(\mathbf{z}_{g,q} - \mathbf{U}_g \mathbf{x}\Big) \\ &= \Big(\mathbf{S}_q \mathbf{F}_U^H \hat{\mathbf{\Gamma}}_g^H (\underline{\mathbf{r}} - \bar{\underline{\mathbf{r}}}) - \mathbf{U}_g (\mathbf{x} - \bar{\mathbf{t}}_{g,q})\Big)^H \mathbf{R}_g^{-1} \Big(\mathbf{S}_q \mathbf{F}_U^H \hat{\mathbf{\Gamma}}_g^H (\underline{\mathbf{r}} - \bar{\underline{\mathbf{r}}}) - \mathbf{U}_g (\mathbf{x} - \bar{\mathbf{t}}_{g,q})\Big).\end{aligned} \tag{A.10}$$

The matrix product $\mathbf{S}_q \mathbf{F}_U^H \hat{\mathbf{\Gamma}}_g^H$ is obviously equivalent to the product $\check{\mathbf{\Gamma}}_g^H \mathbf{D}_q^H$, where $\mathbf{D}_q \equiv \Big(\mathbf{I}_M \otimes \mathrm{diag}\{\mathbf{e}_q^T \mathbf{F}\}\Big)$. Moreover, since $\mathbf{U}_g = Q^{-1} \check{\mathbf{\Gamma}}_g^H \mathbf{\Upsilon}_g$, we can further write (A.10) as

$$\rho_{g,q} = \Big(\mathbf{D}_q^H (\underline{\mathbf{r}} - \bar{\underline{\mathbf{r}}}) - Q^{-1} \mathbf{\Upsilon}_g \Big(\mathbf{x} - \bar{\mathbf{t}}_{g,q}\Big)\Big)^H \check{\mathbf{\Gamma}}_g \mathbf{R}_g^{-1} \check{\mathbf{\Gamma}}_g^H \Big(\mathbf{D}_q^H (\underline{\mathbf{r}} - \bar{\underline{\mathbf{r}}}) - Q^{-1} \mathbf{\Upsilon}_g \Big(\mathbf{x} - \bar{\mathbf{t}}_{g,q}\Big)\Big). \tag{A.11}$$

Consequently from (A.11), we see that it remains to show that the matrix product

$$\mathbf{Y}_g \equiv \check{\mathbf{\Gamma}}_g \mathbf{R}_g^{-1} \check{\mathbf{\Gamma}}_g^H \tag{A.12}$$

is identical for the MSE and SINR criteria. For the MSE criterion (3.87), $\mathbf{Y}_g$ in (A.12) can be expressed with (3.90) and (3.95) as

$$\begin{aligned}\mathbf{Y}_g &= \check{\mathbf{\Gamma}}_g \mathbf{R}_g^{-1} \check{\mathbf{\Gamma}}_g^H \\ &= \Big(\mathbf{\Psi}^{\mathrm{FD}-1} \mathbf{\Upsilon}_g \mathbf{\Theta}_g^{-1} \mathbf{\Omega}_g^{-1}\Big) \Big(Q^{-1} \mathbf{\Omega}_g^{-1} \mathbf{\Theta}_g^{-1} \mathbf{\Upsilon}_g^H \mathbf{\Psi}^{\mathrm{FD}-1} \mathbf{\Upsilon}_g \mathbf{\Omega}_g^{-1}\Big)^{-1} \Big(\mathbf{\Psi}^{\mathrm{FD}-1} \mathbf{\Upsilon}_g \mathbf{\Theta}_g^{-1} \mathbf{\Omega}_g^{-1}\Big)^H \\ &= Q \mathbf{\Psi}^{\mathrm{FD}-1} \mathbf{\Upsilon}_g \mathbf{\Theta}_g^{-1} \Big(\mathbf{\Upsilon}_g^H \mathbf{\Psi}^{\mathrm{FD}-1} \mathbf{\Upsilon}_g\Big)^{-1} \mathbf{\Upsilon}_g^H \mathbf{\Psi}^{\mathrm{FD}-1}.\end{aligned} \tag{A.13}$$

Let us now compute (A.12) for the SINR formulation (3.87). Using the filter in (B.17) and the covariance matrix in (B.19), we get

$$\mathring{\mathbf{\Gamma}}_g \mathring{\mathbf{R}}_g^{-1} \mathring{\mathbf{\Gamma}}_g^H = Q^2 \mathbf{N}_g^{-1} \mathbf{T}_g \mathbf{T}_g^H \mathbf{N}_g^{-H}. \tag{A.14}$$

From (B.16), we have

$$\mathbf{T}_g \mathbf{T}_g^H = Q^4 \mathbf{N}_g^{-H} \mathbf{Z}_{g,1} \mathbf{N}_g^{-1} \mathbf{T}_g \hat{\mathbf{K}}_g^{-2} \mathbf{T}_g^H \mathbf{N}_g^{-H} \mathbf{Z}_{g,1}^H \mathbf{N}_g^{-1} \tag{A.15}$$

and

$$\hat{\mathbf{K}}_g^{-1} = Q^{-2} \Big(\mathbf{\Upsilon}_g^H \mathbf{N}_g^{-1} \mathbf{T}_g\Big)^{-1} \Big(\mathbf{T}_g^H \mathbf{N}_g^{-H} \mathbf{\Upsilon}_g\Big)^{-1}, \tag{A.16}$$

where $\hat{\mathbf{K}}_g = \mathrm{diag}\{t_{g,1}, t_{g,2}, ..., t_{g,U}\}$ is the $U \times U$ diagonal matrix containing the U

nonzero diagonal elements of $\mathbf{K}_g$. Substituting (A.15) and (A.16) into (A.14) and using simple algebra, we obtain

$$\mathring{\mathbf{\Gamma}}_g \mathring{\mathbf{R}}_g^{-1} \mathring{\mathbf{\Gamma}}_g^H = Q^2 \mathbf{Z}_{g,2}^{-1} \mathbf{\Upsilon}_g \left(\mathbf{\Upsilon}_g^H \mathbf{Z}_{g,2}^{-1} \mathbf{\Upsilon}_g \right)^{-1} \mathbf{\Upsilon}_g^H \mathbf{Z}_{g,2}^{-1}.$$

Now, applying the matrix inversion lemma to $\mathbf{Z}_{g,2}^{-1} \mathbf{\Upsilon}_g$, we finally obtain

$$\begin{aligned} \mathring{\mathbf{\Gamma}}_g \mathring{\mathbf{R}}_g^{-1} \mathring{\mathbf{\Gamma}}_g^H &= Q \mathbf{\Psi}^{\mathrm{FD}-1} \mathbf{\Upsilon}_g \mathbf{\Theta}_g^{-1} \left(\mathbf{\Upsilon}_g^H \mathbf{\Psi}^{\mathrm{FD}-1} \mathbf{\Upsilon}_g \right)^{-1} \mathbf{\Upsilon}_g^H \mathbf{\Psi}^{\mathrm{FD}-1} \\ &= \mathbf{Y}_g, \end{aligned}$$

which is identical to (A.13).

A.4. Proof of Lemma 5.4

The functional in (5.15) can be written as

$$\int_0^1 Y(\mathbf{v}) \mathrm{d}t \approx c + \int_0^1 U_1(v_1) v_2' \mathrm{d}t + \int_0^1 U_2(v_2) v_1' \mathrm{d}t, \tag{A.17}$$

where $U_1(v_1) \equiv \beta_{2,1} v_1 + (\beta_{2,4} - \beta_{1,3}/2) v_1^2$ and $U_2(v_2) \equiv \beta_{1,2} v_2 + (\beta_{1,5} - \beta_{2,3}/2) v_2^2$ are quadratic polynomials in v_1 and v_2, respectively, and c is a constant. The Euler-Lagrange equation in (5.19) can hence be written as

$$\beta_{2,1} - \beta_{1,2} + (2\beta_{2,4} - \beta_{1,3}) I_{d,1} - (2\beta_{1,5} - \beta_{2,3}) I_{d,2} \stackrel{!}{=} 0. \tag{A.18}$$

In the case when (5.19) has no solution, the coefficients of the polynomials $U_1(p_1)$ and $U_2(p_2)$ satisfy:

$$\beta_{1,3} = 2\beta_{2,4}, \beta_{2,3} = 2\beta_{1,5}, \tag{A.19a}$$

$$\beta_{2,1} - \beta_{1,2} \neq 0. \tag{A.19b}$$

By (A.17) and (A.19), the variational problem in (5.14) becomes

$$R_{max} \approx c + \max_{\mathbf{v} \in \mathcal{V}} \left\{ (\beta_{1,2} - \beta_{2,1}) \int_{\mathbf{v}} I_{d,2} \mathrm{d} I_{d,1} \right\}. \tag{A.20}$$

Now, it is easy to confirm that the sum rate expression given by (A.20) is maximized, either for $\mathbf{v}(t) \in \mathcal{L}(a_0, a_1, a_2)$, for all $t \in \mathbb{D}$ if $\beta_{1,2} > \beta_{2,1}$ or $\mathbf{v}(t) \in \mathcal{L}(a_0, a_3, a_2)$, for all $t \in \mathbb{D}$ if $\beta_{1,2} < \beta_{2,1}$.

A.5. Proof of Theorem 5.5

For any admissible parametric curve $\mathbf{v} \in \mathcal{V}$, we can find a parametrization $\tilde{\mathbf{v}} \in \mathcal{V}$ of $\mathcal{S}$ and a partitioning $\bigcup_i [t_i, t_{i+1}]$ of the interval $\mathbb{D}$ such that for each interval $[t_i, t_{i+1}]$, one has $\mathbf{v}(t_i) = \tilde{\mathbf{v}}(t_i)$, $\mathbf{v}(t_{i+1}) = \tilde{\mathbf{v}}(t_{i+1})$, and $\mathbf{v}(t) \in \mathcal{G}_1$ or $\mathbf{v}(t) \in \mathcal{G}_2$, for all $t \in [t_i, t_{i+1}]$. An example of such a partitioning is shown in Fig. 5.4. Based on this partitioning, we can express the sum rate difference $R[\tilde{\mathbf{v}}] - R[\mathbf{v}]$ between $\tilde{\mathbf{v}}$ and $\mathbf{v}$ as

$$R[\tilde{\mathbf{v}}] - R[\mathbf{v}] = \sum_i \Big(\Delta R_i \equiv \int_{t_i}^{t_{i+1}} Y(\tilde{\mathbf{v}}) \mathrm{d}t - \int_{t_i}^{t_{i+1}} Y(\mathbf{v}) \mathrm{d}t \Big). \tag{A.21}$$

Each ΔR_i can be written as a line integral along the simple closed curve $\mathcal{Y}_i \equiv \Big\{ \mathbf{v}(t), \tilde{\mathbf{v}}(t) | t \in [t_i, t_{i+1}] \Big\}$ yielding

$$\Delta R_i = o_i \oint_{\mathcal{Y}_i} \hat{f}_{e,1}(\mathbf{I}_d) \mathrm{d}I_{d,1} + o_i \oint_{\mathcal{A}_i} \hat{f}_{e,2}(\mathbf{I}_d) \mathrm{d}I_{d,2}, \tag{A.22}$$

where $o_i = 1$ when $\mathbf{v}(t) \in \mathcal{G}_1$, for all $t \in [t_i, t_{i+1}]$, and $o_i = -1$ otherwise. Let each simple closed curve $\mathcal{Y}_i$ be oriented in the positive direction with the bounded region $\mathcal{M}_i$ in $\mathbb{D}^2$ on the left. Then, applying Green's theorem to (A.22) allows us to rewrite ΔR_i as $\Delta R_i = o_i \iint_{\mathcal{M}_i} T(\mathbf{I}_d) \mathrm{d}I_{d,1} \mathrm{d}I_{d,2}$. With conditions (5.20), we can state that $\Delta R_i \geq 0$ since either $\mathcal{M}_i \subseteq \mathcal{G}_1$ or $\mathcal{M}_i \subseteq \mathcal{G}_2$, as shown in Fig. 5.4. Thus, we can conclude that $R[\tilde{\mathbf{v}}] \geq R[\mathbf{v}]$ for any $\mathbf{v} \in \mathcal{V}$, which yields the optimality of the convergence curve $\mathcal{S}$.

A.6. Proof of Lemma 5.6

Using the integral expression in (A.17), we can express the sum rates $R_0(u)$ and $R_1(u)$ for $\mathcal{H}_0(u)$ and $\mathcal{H}_1(u)$, respectively, as functions of $u \in \mathbb{D}$, as

$$R_0(u) \equiv c + \int_0^u U_2(0) \mathrm{d}I_{d,1} + \int_0^1 U_1(u) \mathrm{d}I_{d,2} + \int_u^1 U_2(1) \mathrm{d}I_{d,1}, \tag{A.23}$$

$$R_1(u) \equiv c + \int_0^u U_1(0) \mathrm{d}I_{d,2} + \int_0^1 U_2(u) \mathrm{d}I_{d,1} + \int_u^1 U_1(1) \mathrm{d}I_{d,2}, \tag{A.24}$$

Integrating each term in (A.23) and (A.24) allows us to rewrite $R_0(u)$ and $R_1(u)$ as

$$R_0(u) = c + U_1(u) + (1-u) U_2(1), \tag{A.25}$$

$$R_1(u) = c + U_2(u) + (1-u) U_1(1). \tag{A.26}$$

Thus, the variational problem in (5.14) reduces to

$$R_{max} \approx \max_{l\in\{0,1\}} \max_{u\in[0,1]} \Big\{ R_l(u) \Big\}. \tag{A.27}$$

The solution of (A.27) can easily be obtained with the standard framework of classical calculus as the objective function is quadratic in u [Kre05].

A.7. Proof of Lemma 5.7

In order to proof that (5.57) is a convex optimization problem, we express the equalizer correlation function $f_e(\mathbf{p}, \varphi_d)$ using (5.50) in closed form as

$$f_e(\mathbf{p}, \varphi_d) = \frac{1}{N} \sum_{n=1}^{N} \phi\Big(\psi_n^{\mathrm{FDPr}}(\mathbf{p}_n, \varphi_d) \Big). \tag{A.28}$$

Let us denote the n-th term of the above sum by

$$S_n(\mathbf{p}, \varphi_d) \equiv \frac{1}{N} \phi\left(2QD_n(\mathbf{p}_n) - \frac{2}{1-\varphi_d} \right), \tag{A.29}$$

where $D_n(\mathbf{p}_n) \equiv L_{n,Q-1}(p_{n,Q-1}, L_{n,Q-2})$ is recursively defined by

$$L_{n,q}(p_{n,q}, L_{n,q-1}) \equiv \Big(l_{n,q}(p_{n,q})^{-1} + (L_{n,q-1})^{-1} \Big)^{-1}, \tag{A.30}$$

for $q = 0, .., Q-1$ with $(L_{k,-1})^{-1} \equiv 0$. The function $L_{n,q}(p_{n,q}, L_{n,q-1})$ is concave for $p_{n,q} \geq 0$ and $L_{n,q-1} > 0$, since its Hessian $\nabla^2 L_{n,q}$,

$$\nabla^2 L_{n,q} = -\frac{2}{(l_{n,q} + L_{n,q-1})^3} \begin{bmatrix} \frac{g_{n,q}}{\sigma^2} L_{n,q-1} \\ -l_{n,q} \end{bmatrix} \begin{bmatrix} \frac{g_{n,q}}{\sigma_0^2} L_{n,q-1} \\ -l_{n,q} \end{bmatrix}^T \preceq 0 \tag{A.31}$$

is negative semidefinite. It follows that $D_n(\mathbf{p}_n)$ is a composition of concave functions. Moreover, each $L_{n,q}(p_{n,q}, L_{n,q-1})$ is monotonically nondecreasing component-wise,

$$\frac{\partial L_{n,q}}{\partial p_{n,q}} = \frac{p_{n,q}^2}{\Big(p_{n,q} + L_{n,q-1} \Big)^2} \geq 0, \tag{A.32}$$

$$\frac{\partial L_{n,q}}{\partial L_{n,q-1}} = \frac{L_{n,q-1}^2}{\Big(p_{n,q} + L_{n,q-1} \Big)^2} \geq 0. \tag{A.33}$$

As $D_n(\mathbf{p}_n)$ is nondecreasing component-wise, it is concave in $\mathbf{p}_n$. Note that this property follows from the property that a composition of a concave function, which

is increasing component-wise with an n-tuple of linear/concave functions in its argument, is a concave function [BV04]. Also, as shown in Fig 3.4, $\phi(x)$ in (A.29) is monotonically nondecreasing and concave in x for $x \geq 0$. As a result, the functions $S_n(\mathbf{p}, \varphi_d)$ for $n = 1, .., N$ in (A.29) are concave functions. It follows that the equalizer correlation function $f_e(\mathbf{p}, \varphi_d)$ is a linear combination of concave functions with nonnegative coefficients and therefore, it is concave in $\mathbf{p}$. The feasible set of problem (5.57) is therefore convex. As a result, we minimize a linear objective function over a convex set. We can conclude that the optimization problem is convex which can be efficiently solved by standard interior-point methods that have a very low, polynomial, worst-case complexity [BV04]. For a detailed discussion on computational complexity of such methods and parameter choices, please refer to [BV04].

B. Derivation of Filter Coefficients

B.1. MMSE Frequency Domain Filter Coefficients

In order to characterize the optimal solution of (3.32), let us first define the two $QM \times 1$ vectors $\hat{\mathbf{\Gamma}}_n \equiv \mathbf{\Gamma}_n \mathbf{1}_Q$ and $\hat{\mathbf{\Xi}}_{c,n} \equiv \mathbf{\Xi}_{c,n} \mathbf{1}_Q$. Using these notations, the MSE in (3.28) can be written as

$$\begin{aligned}
\mathrm{MSE}_n^{\mathrm{FD}} &= Q^{-1}\mathrm{Trace}\Big(\mathbf{\Gamma}_n^H \mathbf{\Psi}^{\mathrm{FD}} \mathbf{\Gamma}_n\Big) - (1-\bar{\varphi}_n)|\mu_n|^2 \\
&= Q^{-1}\hat{\mathbf{\Gamma}}_n^H \mathbf{\Psi}^{\mathrm{FD}} \hat{\mathbf{\Gamma}}_n - (1-\bar{\varphi}_n) Q^{-2} \hat{\mathbf{\Gamma}}_n^H \hat{\mathbf{\Xi}}_{c,n} \hat{\mathbf{\Xi}}_{c,n}^H \hat{\mathbf{\Gamma}}_n \\
&= Q^{-1}\hat{\mathbf{\Gamma}}_n^H \Big(\mathbf{\Psi}^{\mathrm{FD}} - (1-\bar{\varphi}_n) Q^{-1} \hat{\mathbf{\Xi}}_{c,n} \hat{\mathbf{\Xi}}_{c,n}^H\Big) \hat{\mathbf{\Gamma}}_n \\
&= Q^{-1}\hat{\mathbf{\Gamma}}_n^H \mathring{\mathbf{\Psi}}^{\mathrm{FD}} \hat{\mathbf{\Gamma}}_n,
\end{aligned} \tag{B.1}$$

where we have defined $\mathring{\mathbf{\Psi}}^{\mathrm{FD}} \equiv \mathbf{\Psi}^{\mathrm{FD}} - (1-\bar{\varphi}_n) Q^{-1} \hat{\mathbf{\Xi}}_{c,n} \hat{\mathbf{\Xi}}_{c,n}^H$. Using (B.1), the optimization problem (3.32) can be reformulated as

$$\text{minimize } Q^{-1}\hat{\mathbf{\Gamma}}_n^H \mathring{\mathbf{\Psi}}^{\mathrm{FD}} \hat{\mathbf{\Gamma}}_n \text{ subject to: } Q^{-1}\hat{\mathbf{\Gamma}}_n^H \hat{\mathbf{\Xi}}_{c,n} = 1. \tag{B.2}$$

Obviously, (B.2) is a convex optimization problem. Hence, it has a unique solution given in terms of the Karush-Kuhn-Tacker (KKT) conditions applied to the Lagrangian function

$$L_G(\hat{\mathbf{\Gamma}}_n, \lambda) = Q^{-1}\hat{\mathbf{\Gamma}}_n^H \mathring{\mathbf{\Psi}}^{\mathrm{FD}} \hat{\mathbf{\Gamma}}_n + \lambda\Big(Q^{-1}\hat{\mathbf{\Gamma}}_n^H \hat{\mathbf{\Xi}}_{c,n} - 1\Big), \tag{B.3}$$

where λ is the Lagrangian multiplier. The KKT conditions to (B.3) are given by

$$Q^{-1}\mathring{\mathbf{\Psi}}^{\mathrm{FD}} \hat{\mathbf{\Gamma}}_n + Q^{-1}\lambda \hat{\mathbf{\Xi}}_{c,n} = \mathbf{0}, \forall n, \tag{B.4}$$

$$Q^{-1}\hat{\mathbf{\Gamma}}_n^H \hat{\mathbf{\Xi}}_{c,n} - 1 = 0, \forall n. \tag{B.5}$$

Using simple algebra, the optimal solution to (B.2) is obtained as

$$\hat{\mathbf{\Gamma}}_n = \frac{\mathring{\mathbf{\Psi}}^{\mathrm{FD}-1} \hat{\mathbf{\Xi}}_{c,n}}{Q^{-1}\hat{\mathbf{\Xi}}_{c,n}^H \mathring{\mathbf{\Psi}}^{\mathrm{FD}-1} \hat{\mathbf{\Xi}}_{c,n}}. \tag{B.6}$$

Applying the matrix inversion lemma to the nominator and denominator of (B.6), and rewriting the result in the diagonal-block form, the optimal MMSE filter is obtained by (3.33).

B.2. Groupwise MMSE Frequency Domain Filter Coefficients

The Lagrangian to the optimization problem in (3.89) is given by

$$L_G(\check{\mathbf{\Gamma}}_g, \boldsymbol{\lambda}) = Q^{-1}\text{Trace}\left(\check{\mathbf{\Gamma}}_g^H \mathbf{\Psi}_0^{\text{FD}} \check{\mathbf{\Gamma}}_g\right) + \boldsymbol{\lambda}^T\Big(Q^{-1}\text{diag}(\check{\mathbf{\Gamma}}_g^H \mathbf{\Upsilon}_g) - \mathbf{1}_U\Big), \tag{B.7}$$

where $\boldsymbol{\lambda} = [\lambda_1, \lambda_2, ..., \lambda_U]^T$ is a vector containing the Lagrangian multipliers. Let $\hat{\boldsymbol{\gamma}}_{g,u}$ be the uth column of $\check{\mathbf{\Gamma}}_g$. The optimization of (B.7) is equivalent to the optimization of the individual component-cost functions, indexed by u, separately. Therefore, Eqn. (B.7) also be written as

$$L_G(\check{\mathbf{\Gamma}}_g, \boldsymbol{\lambda}) = \sum_{u=1}^{U}\Big(Q^{-1}\hat{\boldsymbol{\gamma}}_{g,u}^H \mathbf{\Psi}_0^{\text{FD}} \hat{\boldsymbol{\gamma}}_{g,u} + \lambda_u\Big(Q^{-1}\hat{\boldsymbol{\gamma}}_{g,u}^H \mathbf{\Upsilon}_g \mathbf{e}_u - 1\Big)\Big). \tag{B.8}$$

The KKT conditions to (B.8) are given by

$$Q^{-1}\mathbf{\Psi}_0^{\text{FD}}\hat{\boldsymbol{\gamma}}_{g,u} + Q^{-1}\lambda_u \mathbf{\Upsilon}_g \mathbf{e}_u = \mathbf{0}, \forall u, \tag{B.9}$$

$$Q^{-1}\mathbf{e}_u^T \mathbf{\Upsilon}_g^H \hat{\boldsymbol{\gamma}}_{g,u} - 1 = 0, \forall u. \tag{B.10}$$

After some straightforward manipulations of (B.9) and (B.10), the optimal frequency domain filter for the uth component is obtained as

$$\hat{\boldsymbol{\gamma}}_{g,u} = Q\Big(\mathbf{e}_u^T \mathbf{\Upsilon}_g^H \mathbf{\Psi}_0^{\text{FD}-1} \mathbf{\Upsilon}_g \mathbf{e}_u\Big)^{-1} \mathbf{\Psi}_0^{\text{FD}-1} \mathbf{\Upsilon}_g \mathbf{e}_u. \tag{B.11}$$

Finally, applying the matrix-inversion lemma to (B.11) and rewriting the result in matrix-notation yields the expression in (3.90).

B.3. Groupwise SINR Filter Coefficients

The SINR for the gth subgroup can be expressed as

$$\begin{aligned}\mathrm{SINR}_g &\equiv \frac{\mathbb{E}\Big[\,\|\mathbf{M}_g\mathbf{t}_g\|^2\,\Big]}{\mathbb{E}\Big[\,\|\mathbf{z}_g-\mathbf{M}_g\mathbf{t}_g\|^2\,\Big]}\\ &= \frac{\mathrm{Trace}\left(\mathbf{M}_g\mathbf{M}_g^H\right)}{\mathrm{Trace}\left(\begin{array}{c}\Big(\mathbf{W}_g^H\overline{\mathbf{H}}_g-\mathbf{M}_g\Big)\mathbf{\Lambda}_g^{(1)}\Big(\mathbf{W}_g^H\overline{\mathbf{H}}_g-\mathbf{M}_g\Big)^H\\ +\mathbf{W}_g^H\,\overline{\overline{\mathbf{H}}}_g\mathbf{\Lambda}_g^{(2)}\overline{\overline{\mathbf{H}}}_g^H\mathbf{W}_g+\sigma_0^2\mathbf{W}_g^H\mathbf{W}_g\end{array}\right)}\\ &= \frac{\mathrm{Trace}\left(\Big(\mathbf{U}_g\otimes\mathbf{I}_U\Big)\Big(\mathbf{U}_g\otimes\mathbf{I}_U\Big)^H\right)}{\mathrm{Trace}\left(\widehat{\mathbf{\Gamma}}_g^H\mathbf{\Psi}^{\mathrm{FD}}\widehat{\mathbf{\Gamma}}_g-\mathbf{M}_g\mathbf{\Lambda}_g^{(1)}\mathbf{M}_g^H\right)}\\ &= \frac{\mathrm{Trace}\left(\check{\mathbf{\Gamma}}_g^H\mathbf{\Upsilon}_g\mathbf{\Upsilon}_g^H\check{\mathbf{\Gamma}}_g\right)}{\mathrm{Trace}\left(\check{\mathbf{\Gamma}}_g^H\Big(Q\mathbf{\Psi}^{\mathrm{FD}}-\mathbf{\Upsilon}_g\hat{\mathbf{\Lambda}}_g\mathbf{\Upsilon}_g^H\Big)\check{\mathbf{\Gamma}}_g\right)}.\end{aligned} \tag{B.12}$$

Based on (B.12), the problem of maximizing the SINR for each subgroup can be written as

$$\mathring{\mathbf{\Gamma}}_g=\arg\max_{\{\check{\mathbf{\Gamma}}_g\in\mathbb{C}^{MQ\times U}\}}\frac{\mathrm{Trace}\left(\check{\mathbf{\Gamma}}_g^H\mathbf{Z}_{g,1}\check{\mathbf{\Gamma}}_g\right)}{\mathrm{Trace}\left(\check{\mathbf{\Gamma}}_g^H\mathbf{Z}_{g,2}\check{\mathbf{\Gamma}}_g\right)}, \tag{B.13}$$

where $\mathbf{Z}_{g,1}\equiv\mathbf{\Upsilon}_g\mathbf{\Upsilon}_g^H\in\mathbb{C}^{QM\times QM}$ and $\mathbf{Z}_{g,2}\equiv Q\mathbf{\Psi}^{\mathrm{FD}}-\mathbf{\Upsilon}_g\hat{\mathbf{\Lambda}}_g\mathbf{\Upsilon}_g^H\in\mathbb{C}^{QM\times QM}$ are Hermitian and Hermitian positive definite, respectively. Therefore, Eqn. (B.13) can be expressed as a generalized eigenvalue problem, where the matrices $\mathbf{Z}_{g,1}$ and $\mathbf{Z}_{g,2}$ can be jointly diagonalized as [STS07]

$$\mathbf{X}_g^H\mathbf{Z}_{g,1}\mathbf{X}_g=\mathbf{K}_g \tag{B.14}$$

$$\mathbf{X}_g^H\mathbf{Z}_{g,2}\mathbf{X}_g=Q^2\mathbf{I}_{QM}. \tag{B.15}$$

Here, $\mathbf{K}_g=\mathrm{diag}(t_{g,1},t_{g,2},...,t_{g,U},0,...0)$ is an $QM\times QM$ diagonal matrix, containing the generalized non-negative eigenvalues $t_{g,1}\geq t_{g,2}\geq...\geq t_{g,U}$ listed in decreasing order, and $\mathbf{X}_g$ is the matrix of the corresponding generalized eigenvectors. Then, the optimal filter corresponds to the first U columns of $\mathbf{X}_g$. Similar to [MJLL10], the solution to (B.13) can be found by applying the Cholesky factorization to $\mathbf{Z}_{g,2}$, $\mathbf{Z}_{g,2}=\mathbf{N}_g^H\mathbf{D}_g$, and solving the standard eigenvalue problem

$$Q^2\mathbf{D}_g^{-H}\mathbf{Z}_{g,1}\mathbf{D}_g^{-1}=\mathbf{E}_g\mathbf{K}_g\mathbf{E}_g^H, \tag{B.16}$$

where $\mathbf{E}_g \in \mathbb{C}^{QM\times QM}$ is unitary. The optimal filter maximizing the above ratio is then given by

$$\mathring{\mathbf{\Gamma}}_g = Q\mathbf{N}_g^{-1}\mathbf{T}_g, \tag{B.17}$$

where $\mathbf{T}_g \in \mathbb{C}^{QM\times U}$ consists of the first U eigenvectors of $\mathbf{E}_g$ corresponding to the U nonzero eigenvalues of $\mathbf{K}_g$. Moreover, the SINR related to the gth subgroup is found to

$$\mathrm{SINR}_g = \frac{1}{UQ^2}\sum_{u=1}^{U} t_{g,u}. \tag{B.18}$$

Also, the equivalent channel matrix and covariance matrix of the filter output signal $\mathbf{z}_{g,q}$ in (3.94) are obtained, respectively, as

$$\mathring{\mathbf{U}}_g = Q^{-1}\mathbf{T}_g^H\mathbf{N}_g^{-H}\mathbf{\Upsilon}_g \text{ and } \mathring{\mathbf{R}}_g = \mathbf{I}_U. \tag{B.19}$$

From (B.19), we observe that the groupwise frequency domain SINR filter (B.17) is a noise-whitening filter that whitens the residual interference plus noise term.

C. Graph-based Algorithm

An approximate solution to (5.14) can also be obtained by transforming the continuous problem into an equivalent discrete dynamic programming problem [Ber05]. In particular, we first discretize the region $\mathbb{D}^2$ into a finite grid of points, which allows us to formulate the optimization problem by a path-search problem over a finite weighted graph. Each edge of the graph has its own specific cost and corresponds to a linear curve segment in $\mathbb{D}^2$. The admissible curves in this model are assumed to be piecewise linear functions, constrained by the grid points that have to be passed through. We then propose a simple algorithm based on the dynamic programming principle [Ber05], which may solve the maximum-cost path-search problem on this graph.

Let us denote by $\mathcal{Q}$ a uniform 2D grid of $\mathbb{D}^2$, $\mathcal{Q} \equiv \{ih, jh, 0 \leq i \leq B, 0 \leq j \leq B\} \subset \mathbb{D}^2$, where $h \in \mathbb{R}$, $h > 0$ determines the grid spacing in the respective coordinate, and i, j are integer values. Next, define a directed graph $G_R = (\mathcal{L}_G, \mathcal{M}_G)$ for the discrete problem with $\mathcal{L}_G$ denoting a set of $(B+1)^2$ vertices, $\mathcal{M}_G$ denoting a finite set of directed edges connecting neighboring pairs of vertices, and $\mathrm{co} : \mathcal{M}_G \to \mathbb{D}$ being a cost function over the edges. Each vertex $(i, j) \in \mathcal{L}_G$ of G_R is an ordered two-tuple and corresponds to a point (ih, jh) in the 2D grid $\mathcal{Q}$ as defined above. Moreover, we define, for any vertex $(i, j) \in \mathcal{L}_G$ of G_R, the set Neighb$[(i, j)]$ of its neighbors by: Neighb$[(i, j)] = \Big\{(i', j')|(i', j') \in \mathcal{L}_G, (i', j') = (i-1, j), (i, j-1), (i-1, j-1)\Big\}$. An edge of this graph is of the form $\Big((i', j'), (i, j)\Big) \in \mathcal{M}_G$ with $(i, j) \in \mathcal{L}_G$, and $(i', j') \in$ Neighb$[(i, j)]$.

Having defined the vertices and edges of G_R, we can now specify the cost co$(\cdot)$ for each edge. According to (5.15), a reasonable cost-definition is the sum rate increment that may be approximated for a small step-width τ_{STEP} between neighboring vertices (i', j') and (i, j) as

$$\int_{t'}^{t'+\tau_{\text{STEP}}} Y(\mathbf{v}(t))\mathrm{d}t \approx \tau_{\text{STEP}} \sum_{n=1}^{2} \hat{f}_{e,n}\left(p_1^{(i',i)}, p_2^{(j',j)}\right) \Delta p_n^{(i',i)} \equiv \mathrm{co}[((i', j'), (i, j))], \tag{C.1}$$

where the terms are defined as $p_1^{(i',i)} \equiv \frac{(i'+i)h}{2}$, $p_2^{(j',j)} \equiv \frac{(j'+j)h}{2}$, $\Delta p_1^{(i',i)} \equiv \frac{(i-i')h}{\tau_{\text{STEP}}}$ and $\Delta p_2^{(j',j)} \equiv \frac{(j-j')h}{\tau_{\text{STEP}}}$.

With the above definition of Neighb$[(i, j)]$, any discrete curve through $\mathcal{Q}$ from

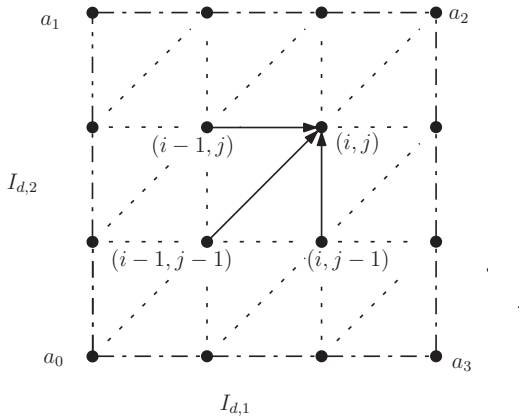

Figure C.1.: Discretization of the plane region $\mathbb{D}^2$. Each vertex $(i,j) \in \mathcal{L}_G$ (corresponding to grid point $(ih, jh) \in \mathcal{Q}$) has three (feasible) neighbors $(i-1,j)$, $(i,j-1)$ and $(i-1,j-1)$.

the bottom left corner (vertex $(0,0)$) to the top right corner (vertex (B,B)) is restricted to the direct three neighboring grid points, as illustrated in Fig. C.1. For given two neighboring points, their relative path angle $\varphi = \arctan(\Delta p_2^{(j',j)} / \Delta p_1^{(i',i)})$ is restricted to a multiple of $\pi/4$. Furthermore, any admissible path on G_R satisfies the monotonicity condition (5.11), since $\Delta p_1^{(i',i)} \geq 0$ and $\Delta p_2^{(j',j)} \geq 0$, $\forall((i',j'),(i,j)) \in \mathcal{M}_G$. The neighborhood structure may be extended beyond the nearest three grid points by extending the definition of the set Neighb$[(i,j)]$. The optimal choice of the destination grid is out of the scope of this work.

Next, a simple recursive dynamic programming algorithm is proposed which provides an efficient solution to the problem of finding the path with maximum cost from vertex $(0,0)$ to (B,B) on G_R. A pseudo-code implementation of the algorithm is shown in Algorithm C.1.

For each vertex $(i,j) \in \mathcal{L}_G$, the algorithm stores the total cost $d[(i,j)]$ of the maximum-cost path found so far between vertex (i,j) and $(0,0)$. Initially, $d[(i,j)] = 0$ for all $(i,j) \in \mathcal{L}_G$. The computation of $d[(i,j)]$ is performed by evaluating the edge costs of all neighboring vertices $(i',j') \in$ Neighb$[(i,j)]$ to vertex (i,j), and selecting the one yielding the highest edge cost. Additionally, a predecessor label is stored for each vertex (i,j) that represents the previous vertex (i^*,j^*) in the maximum-cost path to the current vertex (i,j). When the algorithm terminates the value $d[(B,B)]$ represents the maximum cost corresponding to the optimal path on G_R. Based on

Algorithm C.1 Pseudo-code for graph-based path-search

Initialize $d[(i,j)] = 0$ and $\mathrm{pre}[(i,j)] = \mathrm{none}$, $0 \le i \le B$, $0 \le j \le B$.
for $i = 0$ to B **do**
  for $j = 0$ to B **do**
    if $\mathrm{Neighb}[(i,j)] \neq \emptyset$ **then**
      Find the predecessor to vertex (i,j) with the highest cost value:

$$(i^*, j^*) = \arg \max_{(i',j') \in \mathrm{Neighb}[(i,j)]} \Big\{ d[(i',j')] + \mathrm{co}[((i',j'),(i,j))] \Big\}$$

      Save the predecessor to vertex (i,j): $\mathrm{pre}[(i,j)] = (i^*, j^*)$
      Update the cost $d[(i,j)]$ of vertex (i,j): $d[(i,j)] = d[(i^*,j^*)] + \mathrm{co}[((i^*,j^*),(i,j))]$
    end if
  end for
end for
Initialize the sequence $\mathbf{s}_G = \{(Bh, Bh)\}$.
$(i,j) \leftarrow (B,B)$
while $(i,j) \neq (0,0)$ **do**
  $(i,j) = \mathrm{pre}[(i,j)]$
  Insert the grid point (ih, jh) at the beginning of $\mathbf{s}_G$.
end while
Use linear interpolation between the grid points in $\mathbf{s}_G$ and output the corresponding convergence curve as a result.

the stored predecessor information back-tracing can be performed to construct the maximum-cost path to vertex $(0,0)$.

To estimate the computational complexity of Algorithm C.1, let us denote by s_G the maximal number of neighbors for each vertex $v_G \in \mathcal{L}_G$. For $\mathrm{Neighb}[(i,j)]$, $s_G \le 3$. At each vertex v_G, the edge cost-values of the s_G possible neighbors to v_G have to be computed and compared, which results in $O(s_G)$ computations. With a total number of $(B+1)^2$ vertices, we can conclude that Algorithm C.1 needs $O(s_G B^2)$ computations to solve the maximum-cost path search problem on G_R.

Notation

Throughout this thesis, the following notations are adopted. Normal letters represent scalar quantities, boldface lower-case and bold face uppercase letters designate vectors and matrices, respectively. Specific sets are denoted in blackboard type, e.g., $\mathbb{R}$. The probability of an event $\mathcal{O}$ is denoted by $\text{Prob}(\mathcal{O})$. In general, vectors are regarded as column vectors. The ith element of a vector $\mathbf{a}$ is denoted by $\mathbf{a}_i$. The notation $\mathbf{a} \geq \mathbf{b}$ for length-N vectors $\mathbf{a}$ and $\mathbf{b}$ means $a_n \geq b_n$ for $n = 1, .., N$. The (l, k)th entry of a matrix $\mathbf{A}$ is denoted by $[\mathbf{A}]_{l,k}$. The statistical expectation and variance of a scalar, vector, or matrix random variable are denoted by $\mathbb{E}(\cdot)$ and $\text{Var}(\cdot)$, respectively. The covariance and correlation of the two random vectors $\mathbf{x}_1$ and $\mathbf{x}_2$ are written as $\text{Cov}(\mathbf{x}_1, \mathbf{x}_2)$ and $\text{Corr}(\mathbf{x}_1, \mathbf{x}_2)$, respectively. The probability density function (PDF) of a single scalar random variable x and the joint PDF of a vector $\mathbf{x}$ are denoted by $p(x)$ and $p(\mathbf{x})$, respectively. Finally, the soft estimate of vector $\mathbf{a}$ and its frequency domain representation are denoted by $\bar{\mathbf{a}}$ and $\underline{\mathbf{a}}$, respectively.

Statistical Distributions

$\mathcal{CN}(\boldsymbol{\mu}, \boldsymbol{\Sigma})$	Multivariate complex Gaussian distribution with mean vector $\boldsymbol{\mu}$ and covariance matrix $\boldsymbol{\Sigma}$
$\mathcal{CN}(\mu, \sigma^2)$	Complex-valued Gaussian distribution with mean μ and variance σ^2
$\mathcal{N}(\mu, \sigma^2)$	Real-valued Gaussian distribution with mean μ and variance σ^2

Functions and Norms

$\delta(\cdot)$	Dirac delta function
$\exp[\cdot]$, $e^{\cdot}$	Exponential function
$\Gamma(\cdot)$	Gamma function
$\Gamma(\cdot, \cdot)$	Incomplete Gamma function
$\binom{a}{b}$	Binomial coefficient
$\log_{10}(\cdot)$	Logarithm to base 10
$\log_2(\cdot)$	Logarithm to base 2
$\mathbf{u}(\cdot)$, $\mathbf{g}(\cdot)$, $\mathbf{v}(\cdot)$	Vector function
$\mathbf{w}.(\cdot)$	Three dimensional space curve

$\mathcal{F}^1[\cdot,\cdot]$	Space of monotonically increasing, continuous and piecewise differentiable functions on an interval
$\operatorname{erfc}(\cdot)$	Complementary Gaussian error function
$\operatorname{Pol}(\cdot)$	Polynomial
$\operatorname{sgn}(\cdot)$	Signum function
$\omega(\cdot)$	Hermite rank
$\phi(\cdot)$	Integral function
$\phi_T(\cdot)$	Mapping function of correlation values to mutual information
$\psi_{\cdot}^{\mathrm{FD}}(\cdot)$, $\psi_{\cdot}^{\mathrm{NL}}(\cdot)$, $\psi_{\cdot}^{\mathrm{FDPr}}(\cdot,\cdot)$	SNR function of *extrinsic* LLRs at equalizer output
$\tanh(\cdot)$	Hyperbolic tangent function
$\varphi(\cdot)$	Correlation function
$C^{\mathrm{MIMO}}(\cdot)$, $C_{\mathrm{BPSK}}(\cdot)$	Capacity
$d(\cdot)$	Overall impulse response of the transmit and receive filtering
$E_1(\cdot)$	Exponential integral function
$f_{\cdot}(\cdot)$	Equalizer or decoder correlation function
$g_{\cdot,\cdot}(\cdot,\cdot)$	Continuous channel gain between transmit/receive antenna pair
$g_{e,\cdot}(\cdot)$	Projected equalizer correlation function
$h(\cdot)$	Differential entropy function
$I(\cdot,\cdot)$	Mutual information
$I_0(\cdot)$	Modified zero-order Bessel function of the first kind
$J(\cdot)$	J-function
$L(\cdot)$	Log-likelihood ratio
$q_{\cdot}(\cdot)$	Cross-correlation function
$r^{\cdot,\cdot}(\cdot)$	Covariance function
$U(\cdot)$	Unit step function
$w(\cdot)$	Cross-correlation function of complex channel coefficients
$\hat{f}_{P_{\cdot,\cdot}}^{(\cdot)}(\cdot)$	Projected equalizer EXIT function
$\hat{f}_{\cdot}(\cdot)$	Equalizer or decoder EXIT function

Operators

$(\cdot)^*$	Complex conjugation
$(\cdot)^+$	Maximum of argument and zero
$(\cdot)^H$	Hermitian transposition
$(\cdot)^T$	Transposition
$\arg\max(\cdot)$	Argument maximizing the expression in the brackets

$\arg\min(\cdot)$	Argument minimizing a expression in the brackets
$\det(\cdot)$	Determinant of a matrix
$\Im\{\cdot\}$	Imaginary part of a complex number
$\mathbf{A} \otimes \mathbf{B}$	Kronecker product of matrices $\mathbf{A}$ and $\mathbf{B}$
$\mathbf{A}^{-1}$	Inverse of square matrix $\mathbf{A}$
$\mathrm{circ}_Q\{\cdot\}$	Circulant matrix of size $Q \times Q$ with the elements of a vector argument on its first column
$\mathrm{ddiag}\{\cdot\}$	Square diagonal matrix having the diagonal elements of a matrix argument on its main diagonal
$\mathrm{diag}(\cdot)$	Vector with elements equal to the diagonal elements of a square matrix argument or square diagonal matrix with elements equal to the entries of a vector argument
$\mathrm{Trace}(\cdot)$	Trace of a matrix
$\mathrm{vec}(\cdot)$	Vectorization of a matrix
$\partial\mathcal{A}$	Boundary of the closed set $\mathcal{A}$
$\Re\{\cdot\}$	Real part of a complex number
f^{-1}	Inverse of function f

Sets

$\mathbb{C}$	Set of all complex numbers
$\mathbb{D}$	Set of all real numbers in the interval $[0, 1]$
$\mathbb{R}$	Set of all real numbers
$\mathbb{S}$	Set of binary input vectors
$\mathbb{Z}$	Set of all integer numbers
$\mathcal{C}$	Set of codes
$\mathcal{C}^{\mathrm{MAC}}(\cdot,\cdot)$	Rate region of the multiple access channel
$\mathcal{C}^{\mathrm{MAC}}_{\mathrm{con,out}}(\cdot)$	Outage rate region of the multiple access channel with constraint inputs
$\mathcal{C}^{\mathrm{MAC}}_{\mathrm{con}}$	Rate region of the multiple access channel with constraint inputs
$\mathcal{C}^{\mathrm{MAC}}_{\mathrm{erg}}(\cdot)$	Outage rate region of the multiple access channel
$\mathcal{C}^{\mathrm{MAC}}_{\mathrm{out}}(\cdot)$	Outage rate region of the multiple access channel
$\mathcal{D}$	Convergence region of the turbo equalizer
$\mathcal{J}$	Set of discrete correlation values
$\mathcal{L}(\cdot)$	Union of straight line segments
$\mathcal{Q}$	2D grid
$\mathcal{R}^{\mathrm{out}}_{\mathrm{MAC}}$	Outage rate region
$\mathcal{S}$, $\mathcal{H}.(\cdot)$	Convergence curve

$\mathcal{T}(\cdot)$	Set of rate pairs for a specific convergence curve
$\mathcal{U}$	Plane region
$\mathcal{V}$	Set of admissible parametric curves

Frequently Used Sequences

$\nu_{\cdot,\cdot}$, $\bar{\nu}_{\cdot,\cdot}$, $\bar{\bar{\nu}}_{\cdot,\cdot}$	Interference and noise component
$a_{\cdot}$	Information bit
$b_{\cdot,\cdot}[\cdot]$	Data symbol before precoding
$c'_{\cdot}$	Coded bit of SCCC
$c_{\cdot}$	Coded bit
$d_{\cdot,\cdot}[\cdot]$	Data symbol after precoding
$e'_{\cdot}$	Interleaved bit
$e_{\cdot}$	Interleaved bit
$n_{\cdot}[\cdot]$, $n_{\cdot,\cdot}[\cdot]$	Additive white Gaussian noise sample
$r_{\cdot,\cdot}[\cdot]$	Received symbol
$s_{\cdot}[\cdot]$	Transmit symbol
$x_{\cdot,\cdot}[\cdot]$	Binary symbol
$y_{\cdot}[\cdot]$	Received symbol
$z_{\cdot,\cdot}[\cdot]$	Estimated symbol

Specific Vectors and Matrices

$\mathbf{0}_Q$	All-zero $Q \times 1$ vector
$\mathbf{1}_Q$	All-one $Q \times 1$ vector
$\mathbf{C}$	Diagonal matrix containing variances of channel coefficients
$\mathbf{e}_k$	All-zero column vector with the kth entry being one
$\mathbf{F}$	Discrete Fourier matrix
$\mathbf{G}$	Diagonal matrix containing the eigenvalues of the MIMO ISI channel
$\mathbf{I}_Q$	Identity matrix of size $Q \times Q$
$\mathbf{J}$	Spatial-temporal correlation matrix of the channel
$\mathbf{R}$	Channel correlation matrix at receiver side
$\mathbf{S}$	Channel correlation matrix at transmitter side
$\mathbf{U}$	Unitary matrix
$\mathbf{V}$	Unitary matrix

Frequently Used Variables and Parameters

α	Correlation coefficient

$\alpha_{\cdot,\cdot}$, $\varphi_{\cdot,\cdot}$	Correlation between a transmit signal and its conditional estimate
Δf	Normalized frequency separation between adjacent subchannels
Δq	Frequency separation between subchannels
$\delta_{\cdot}$	Eigenvalue
$\delta_{\Delta q}$	Correlation coefficient of frequency domain channel gains
$\epsilon_{\cdot}$	Weighting coefficient
$\kappa(\cdot)$	Frequency domain channel gain
$\lambda_{\cdot}[\cdot]$	Extrinsic log-likelihood ratio
$\mathbf{I}_d^*$	Mutual information limit point
$\mathring{\mu}_{\cdot}$	Mean
$\mathring{\sigma}_{\cdot}^2$	Variance
$\mathrm{MSE}_{\cdot}^{\mathrm{FD}}$, $\mathrm{MSE}_{\cdot}^{\mathrm{GrFD}}$	Mean-square-error
$\mathrm{SINR}_{\cdot}$	Signal-to-Interference-plus-Noise Ratio of a subgroup
$\mathrm{TP}^{\star}$	Throughput efficiency
$\mu_{\cdot,\cdot}$, $\bar{\mu}_{\cdot}$, $\bar{\bar{\mu}}_{\cdot}$	Equivalent channel gain
$\rho_{\cdot,\cdot}$	MAP decision metric
ρ_{SNR}	Inverse of noise variance
$\sigma_{\cdot}^2$	Noise variance or variance of a channel tap component
$\sigma_{\nu,\cdot,\cdot}^2$, $\sigma_{\tilde{\nu},\cdot,\cdot}^2$	Variance of interference and noise component
$\tau_{\cdot,\cdot}(\cdot)$	Frequency domain channel coefficient
τ_d	Root mean square channel delay spread
$\theta_{\cdot}[\cdot]$	A Posteriori log-likelihood ratio
$\varphi_d^{\mathrm{target}}$	Target correlation value
$\zeta_{\cdot}[\cdot]$	A Priori log-likelihood ratio
$A_{\cdot}$	Area under correlation or EXIT function
C_{con}	Constellation constrained capacity
E_s	Signal power at the transmitter
G	Number of subgroups
$g_{\cdot}$, $g_{\cdot,\cdot}$	Eigenvalue
$h_{\cdot,\cdot}[\cdot,\cdot]$	Discrete-time channel coefficient
$I_d, I_{d,\cdot}$, $I_e, I_{e,\cdot}$	Average mutual information
L	Effective discrete-time channel memory length
M	Number of outputs of MIMO system
N	Number of inputs of MIMO system
N_0	Noise power
N_b	Number of data blocks per frame
N_c	Number of coded bits per frame

N_i	Number of information bits per frame
N_p	Total number of resolvable discrete delays
N_s	Number of fixed data symbols per frame and per transmit antenna or user
P	Guard interval length
P_0	Total power
$p_{\cdot}$	Power value
$P_{\text{out}},\ P_o, P_o^{\star}(\cdot)$	Outage probability
P_b	Bit error probability
P_r	Normalized total receive power
Q	Block length
r	Rank of channel matrix
$R,\ R_{\cdot},\ \mathring{R}$	Information rate
$r'_{c,\cdot},\ r_{c,\cdot}, r_c$	Code rate
$R_{\text{con}}^{\text{MAC}}$	Constellation-constrained sum rate
$R_{\text{sum}}^{\text{MAC}}$	Information sum rate
$R_{\text{MAC}}^{\text{out}}$	Outage sum rate
T	Symbol duration
t	Absolute time
T_d	Number of decoding iterations
T_e	Number of turbo iterations
U	Number of users per subgroup
$\bar{\rho}_{\cdot,\cdot}$	Pairwise normalized channel correlation coefficient
$\bar{\varphi},\ \bar{\varphi}_{\cdot},\ \bar{\bar{\varphi}}_{\cdot}$	Average power of soft symbol estimates

Frequently Used Matrices and Vectors

$\boldsymbol{\Omega}_{\cdot,\cdot}(\cdot)$	Covariance matrix
$\overline{\boldsymbol{\Xi}}_{\cdot}$	Frequency domain channel matrix of a subgroup
$\overline{\mathbf{H}}_{\cdot}$	Block circulant channel matrix of a subgroup
$\boldsymbol{\tau}_{\cdot,\cdot}$	Frequency domain channel response
$\boldsymbol{\alpha}_{\cdot}$	Input correlation parameter vector
$\boldsymbol{\varphi}_{\cdot}$	Output correlation parameter vector
$\widehat{\boldsymbol{\Gamma}}_{\cdot},\ \widehat{\boldsymbol{\Gamma}}_{\cdot,\cdot},\ \check{\boldsymbol{\Gamma}}_{\cdot}$	Frequency domain block filtering matrix of a subgroup
$\boldsymbol{\Gamma}_{\cdot},\ \boldsymbol{\Gamma}_{\cdot,\cdot}$	Frequency domain block filtering matrix
$\boldsymbol{\Lambda},\ \boldsymbol{\Lambda}_{\cdot},\ \hat{\boldsymbol{\Lambda}}_{\cdot}$	Covariance matrix
$\boldsymbol{\Phi}_{\cdot},\ \mathbf{M}_{\cdot}$	Equivalent channel matrix after filtering
$\boldsymbol{\Sigma}^{\text{TD}},\ \boldsymbol{\Sigma}^{\text{NL}}$	Time domain covariance matrix of residual signal
$\boldsymbol{\Xi},\ \underline{\boldsymbol{\Xi}}_{\cdot}$	Frequency domain channel matrix

$\boldsymbol{\Xi}_c$, $\boldsymbol{\Xi}_{c,\cdot}$	Frequency domain compound channel matrix
$\mathbf{a}$, $\mathbf{a}_\cdot$	Information bit vector
$\mathbf{b}$, $\mathbf{b}_\cdot$	Transmit data symbol vector
$\mathbf{d}$, $\mathbf{d}_\cdot$	Transmit data symbol vector after precoding
$\mathbf{e}$	Interleaved bit vector
$\mathbf{f}_\cdot$	Transmit data symbol vector for all subgroups except the desired subgroup
$\mathbf{H}$, $\mathbf{H}_\cdot$	Circulant channel matrix
$\mathbf{h}_{\cdot,\cdot}[\cdot]$	Vector of discrete-time channel coefficients
$\mathbf{h}_{\text{vec}}[\cdot]$	Vector containing the coefficients of the MIMO channel
$\mathbf{H}_c$, $\mathbf{H}_{c,\cdot}$	Compound circulant channel matrix
$\mathbf{n}$, $\mathbf{n}_\cdot$	Noise symbol vector
$\mathbf{O}_\cdot$	Time domain block filtering matrix
$\mathbf{P}$	Power allocation matrix
$\mathbf{p}$, $\mathbf{p}_\cdot$	Power loading vector
$\mathbf{Q}$, $\mathbf{Q}_\cdot$	Covariance matrix of transmit vector
$\mathbf{Q}_F$	Frequency domain covariance matrix of transmit vector
$\mathbf{r}$, $\mathbf{r}_\cdot$	Received data symbol vector
$\mathbf{R}_\cdot$	Covariance matrix of interference and noise component of a subgroup
$\mathbf{S}_\cdot$, $\hat{\mathbf{S}}_\cdot$	Selection matrix
$\mathbf{T}$, $\mathbf{T}_\cdot$	Precoding matrix
$\mathbf{t}_\cdot$	Transmit data symbol vector for a subgroup
$\mathbf{U}_\cdot$	Equivalent frequency domain channel matrix after filtering
$\mathbf{w}_{\cdot,\cdot}$	Time domain MMSE filter vector
$\mathbf{W}_\cdot$, $\mathbf{W}_{\cdot,\cdot}$	Time domain block filtering matrix for a subgroup
$\mathbf{Y}$	Covariance matrix of receive vector
$\mathbf{z}_\cdot$, $\mathbf{z}_{\cdot,\cdot}$	Estimated data symbol vector
$\boldsymbol{\Delta}_{\cdot,\cdot}(\cdot)$	Interference component vector
$\boldsymbol{\Psi}^{\text{FD}}$, $\boldsymbol{\Psi}_0^{\text{FD}}$, $\boldsymbol{\Psi}^{\text{NL}}$	Frequency domain covariance matrix of residual signal
$\overline{\overline{\boldsymbol{\Xi}}}_\cdot$	Frequency domain channel matrix
$\overline{\overline{\mathbf{H}}}_\cdot$	Block circulant channel matrix
$\boldsymbol{\lambda}_\cdot[\cdot]$	Vector of *extrinsic* LLRs
$\boldsymbol{\zeta}_\cdot[\cdot]$	Vector of *a priori* LLRs

Abbreviations

2D	Two dimensional
3D	Three dimensional
3GPP	3rd Generation Partnership Project
AP	Access Point
ARQ	Automatic Repeat Request
AWGN	Additive White Gaussian Noise
BCJR	Bahl-Cocke-Jelinek-Raviv
BEC	Binary Erasure Channel
BER	Bit Error Rate
BICM	Bit Interleaved Coded Modulation
BICM-ID	Bit Interleaved Coded Modulation Iterative Detection
bit	Binary digit
bpc	Bit Per Channel Use
BPSK	Binary Phase Shift Keying
BS	Base Station
CAI	Co-Antenna Interference
CDF	Cumulative Density Function
CDMA	Code Division Multiple Access
CIR	Channel Impulse Response
CP	Cyclic Prefix
CSI	Channel State Information
DFT	Discrete Fourier Transformation
EM	Expectation-Maximization
EXIT	Extrinsic Information Transfer
FDD	Frequency-Division-Duplex
FDE	Frequency Domain Equalizer
FER	Frame Error Rate
FFT	Fast Fourier Transformation
FIR	Finite Impulse Response
GAD	Group Antenna Detection
GD	Group Detector
GS	Group Selection
GSM	Global Standard for Mobile Communications

IFFT	Inverse Fast Fourier Transformation
IGI	Inter-Group Interference
i.i.d	Independent Identically distributed
IRC	Irregular Recursive Convolutional
ISI	Inter-Symbol Interference
LDPC	Low Density Parity Check Codes
LLR	Log-Likelihood Ratios
LOS	Line of Sight
LS	Least Squares
LUT	Look Up Table
MAI	Multiple Access Interference
MAP	Maximum A Posteriori
MFB	Matched Filter Bound
MF	Matched Filter
MIMO	Multiple-Input Multiple-Output
MLD	Maximum Likelihood Detection
ML	Maximum Likelihood
MMSE	Minimum Mean-Squared Error
MSE	Mean-Square-Error
MT	Mobile Terminal
NLOS	Non Line of Sight
NMMSE	Nonlinear Minimum Mean-Squared Error
OFDM	Orthogonal Frequency Division Multiplex
P2P	Point-to-Point
PDA	Probabilistic Data Association
PDF	Probability Density Function
QoS	Quality-of-Service
QPSK	Quaternary-Phase Shift Keying
RLS	Recursive Least Squares
RMS	Root Mean Square
RSC	Recursive Systematic Convolutional
Rx	Receiver
SCCC	Serially Concatenated Convolutional Code
SCC	Single Convolutional Code
SC-MMSE	Soft Interference Cancellation and Minimum-Mean Squared-Error
SCM	Spatial Channel Modeling
SDMA	Space-Division Multiple-Access
SfISfO	Soft-In Soft-Out
SIC	Soft Interference Cancellation
SIMO	Single-Input Multiple-Output
SINR	Signal-to-Interference-plus-Noise Ratio

SISO	Single-Input Single-Output
SNR	Signal to Noise Ratio
STTrC	Space-Time Trellis-Coded
SVD	Singular Values Decomposition
TDD	Time-Division-Duplex
TDE	Time Domain Equalizer
TP	Throughput
Tx	Transmitter
UCA	Uniform Circular Array
ULA	Uniform Linear Array
UMTS	Universal Mobile Telecommunications System
UW	Unique Word
WCDMA	Wide band Code Division Multiple Access
WLAN	Wireless Local Area Network
ZP	Zero Padding

List of Publications

Journal Papers:

- M. Grossmann and C. Schneider, "Groupwise Frequency Domain Multiuser MMSE Turbo Equalization for Single Carrier Block Transmission over Spatially-Correlated Channels," *IEEE Journal of Selected Topics in Signal Processing*, vol. 5, no. 8, pp. 1548-1562, Dec. 2011.

- M. Grossmann, "Outage Performance Analysis and Code Design for Three-Stage MMSE Turbo Equalization in Frequency-Selective Rayleigh Fading Channels," *IEEE Transactions on Vehicular Technology*, vol. 60, no. 2, pp. 473-484, Feb. 2011.

- M. Grossmann, T. Ortlepp and T. Matsumoto, "Rate Allocation for 2-User MAC with MMSE Turbo Equalization," *IEEE Transactions on Wireless Communications*, vol. 5, no. 5, pp. 1033-1043, March 2010.

- M. Grossmann, "SVD-based Precoding for Single Carrier MIMO Transmission with Frequency Domain MMSE Turbo Equalization," *IEEE Signal Processing Letters*, vol. 16, no. 5, pp. 418-421, May 2009.

- M. Grossmann and T. Matsumoto, "Nonlinear Frequency Domain MMSE Turbo Equalization using Probabilistic Data Association," *IEEE Communications Letters*, vol. 12, no. 4, pp. 295-297, April 2008.

- M. Grossmann and T. Matsumoto, "Hybrid Turbo Multiuser Detection for OFDM Transmission with Spatially-Correlated Channels," *IEEE Communications Letters*, vol. 11, no. 5, pp. 420-422, May 2007.

Conference Papers:

- M. Grossmann and T. Matsumoto, "On the Outage Probability of MMSE Turbo Equalization in Frequency-Selective Rayleigh Fading Channels," *In Proc. International IEEE ITG Workshop on Smart Antennas (WSA 2010)*, Bremen, Germany, February 2010.

- M. Grossmann and T. Matsumoto, "Rate Allocation for K-User MAC with Turbo Equalization," *In Proc. International ITG Workshop on Smart Antennas (WSA 2009)*, Berlin, Germany, February 2009.

- M. Grossmann, C. Schneider and R. Thomä, "Turbo Equalization for MIMO-OFDM Transmission with Insufficient Guard Interval," *In Proc. International IEEE Zurich Seminar on Communications (IZS 2006)*, Zurich, Switzerland, February 2006.

- M. Särestöniemi, T. Matsumoto and M. Grossmann, "Coded Space-Time Single Carrier Transmission with MMSE MIMO Turbo Equalization," *In Proc. International IEEE Symposium on Wireless Communication Systems*, Valencia, Spain, September 2006.

- J. Karjalainen, C. Schneider, M. Grossmann, T. Matsumoto and R. Thomä, "Evaluation of Joint over Antenna Detection with ST-WNRA Coded MU MIMO Transmission in Realistic Channels," *In Proc. International IEEE ITG Workshop on Smart Antennas (WSA 2006)*, Ulm, Germany, March 2006.

- C. Schneider, M. Grossmann and R. Thomä, "Measurement based Performance Evaluation of MIMO-OFDM with Turbo-Equalization," *In Proc. IEEE Vehicular Technology Spring (VTC 2005)*, Stockholm, Sweden, June 2005.

- C. Schneider, M. Grossmann, K. Kansanen, T. Matsumoto and R. Thomä, "Measurement based Throughput Performance Evaluation of Antenna Variable Modulation for Broadband Turbo MIMO Transmission," *In Proc. International Symp. on Wireless Personal and Multimedia Communication (WPMC) 2004*, Abano Terme, Italy, September 2004.

- C. Schneider, M. Grossmann and R. Thomä "Performance of Antenna Variable Modulation for Turbo MIMO Transmission in Frequency-Selective Channels," *In Proc. International IEEE ITG Workshop on Smart Antennas (WSA 2004)*, Munich, Germany, March 2004.

Bibliography

[80207] IEEE Standard 802.11. *Wireless LAN Medium Access Control (MAC) and Physical Layer (PHY) Specifications*. IEEE, 2007.

[AAK01] M. S. Alouini, A. Abdi, and M. Kaveh. Sum of gamma variates and performance of wireless communication systems over Nakagami-fading channels. *IEEE Transactions on Vehicular Technology*, 50, no. 11, pp. 1471-1480, Nov. 2001.

[AD01] N. Al-Dhahir. Fir channel shortening equalizers for MIMO ISI channels. *IEEE Transactions on Communications*, 49, no. 2, pp. 819-828, Feb. 2001.

[ADU02] A. Amraoui, S. Dusad, and R. Urbanke. Achieving general points in the 2-user gaussian MAC without time-sharing or rate-splitting by means of iterative coding. *in Proc. IEEE Int. Symp. Information Theory, Lausanne, Switzerland*, July 2002.

[AGR98] P. D. Alexander, A. J. Grant, and M. C. Reed. Performance analysis of an iterative decoder for code-division multiple-access. *European Transactions on Telecommunications*, 9, pp. 419-426, Sept. 1998.

[AJL07] K. Amis, L. Josse, and C. Laot. Efficient frequency-domain MMSE turbo equalization derivation and performance comparison with the time-domain counterpart. *in Proc. IEEE ICWMC 2007, Lausanne, Guadeloupe, France, pp. 65-69*, March 2007.

[AKtB04] A. Ashikhmin, G. Kramer, and S. ten Brink. Extrinsic information transfer functions: model and erasure channel properties. *IEEE Transactions on Information Theory*, 50, no. 11, pp. 2657-2673, Nov. 2004.

[AM03] T. Abe and T. Matsumoto. Space-time turbo equalization in frequency-selective MIMO channels. *IEEE Transactions on Vehicular Technology*, 52, no. 3, pp. 469-475, May 2003.

[Arc94] M. A. Arcones. Limit theorems for nonlinear functionals of a stationary Gaussian sequence of vectors. *The Annals of Probability*, 22, no. 4, pp. 2242-2274, 1994.

[Ari00] S. L. Ariyavisitakul. Turbo space-time processing to improve wireless channel capacity. *IEEE Transactions on Communications*, 48, no. 8, pp. 1347-1359, Aug. 2000.

[BC02] J. Boutros and G. Caire. Iterative multiuser joint decoding: unified framework and asymptotic analysis. *IEEE Transactions on Information Theory*, 48, no. 8, pp. 1772-1793, July 2002.

[BCJR74] L. R. Bahl, J. Cocke, F. Jelinek, and J. Raviv. Optimal decoding of linear block codes for minimizing symbol error rate. *IEEE Transactions on Information Theory*, 20, no. 3, pp. 284-287, March 1974.

[BDFT10] N. Benvenuto, R. Dinis, D. Falconer, and S. Tomasin. Single carrier modulation with nonlinear frequency domain equalization: an idea whose time has come-again. *Proceeding IEEE*, 98, no. 1, pp. 69-96, Jan. 2010.

[BDMP98] S. Benedetto, D. Divsalar, G. Montorsi, and F. Pollara. Serial concatenation of interleaved codes: performance analysis, design, and iterative decoding. *IEEE Transactions on Information Theory*, 44, no. 3, pp. 909-926, May 1998.

[BDU06] M. Botsch, G. Dietl, and W. Utschick. Iterative multi-user detection using reduced-complexity equalization. *in Proc. Int. Symp. on Turbo Codes and Rel. Topics*, Brest, Fance, April 2006.

[Bel63] P. A. Bello. Characterization of randomly time-variant linear channels. *IEEE Transactions on Communications*, 11, no. 12, pp. 360-393, Dec. 1963.

[Ber05] D. P. Bertsekas. Dynamic programming and optimal control. *3th ed. Athena Scientific, Belmont, MA*, 2005.

[BF98] G. Bauch and V. Franz. A comparison of soft-in/soft-out algorithms for 'turbo detection'. *in Proc. Int. Conf. Telecomm.*, pp. 259-263, June 1998.

[BGBF03] J. Boutros, N. Gresset, L. Brunel, and M. Fossorier. Soft-input soft-output lattice sphere decoder for linear channels. *in Proc. IEEE GLOBECOM, pp. 1583-1587*, San Fransisco, USA, Dec. 2003.

[BGT93] C. Berrou, A. Glavieux, and P. Thitimajshima. Near shannon limit error-correcting coding and decoding: Turbo-codes. *in Proc. IEEE Int. Conf. on Communications*, Geneva, Switzerland 1993.

[BHW03] S. Bäro, J. Hagenauer, and M. Witzke. Iterative detection of MIMO transmission using a list-sequential (LISS) detector. *in Proc. IEEE International Conference on Comm., pp. 2653-2657*, Anchorage, AK, May 2003.

[BN07] K. Bhattad and K. R. Narayanan. An MSE-based transfer chart for analyzing iterative decoding schemes using a gaussian approximation. *IEEE Transactions on Information Theory*, 53, no. 1, pp. 22-38, Jan. 2007.

[BPS98] E. Biglieri, J. Proakis, and S. Shamai. Fading channels: information-theoretic and communication aspects. *IEEE Transactions on Information Theory*, 44, no. 6, pp. 2619-2992, Oct. 1998.

[BRG05] F. Braennstroem, L. K. Rasmussen, and A. J. Grant. Convergence analysis and optimal scheduling for multiple concatenated codes. *IEEE Transactions on Information Theory*, 51, no. 9, pp. 3354-3364, Sept. 2005.

[BV04] S. Boyd and L. Vandenberghe. *Convex Optimization*. Cambridge University Press, Cambridge, March 2004.

[Cho07] J. Choi. A correlation based analysis for approximate MAP detectors and iterative receivers. *IEEE Transactions on Wireless Communications*, 6, no. 5, pp. 1764-1773, May 2007.

[CL94] T. Coleman and Y. Li. On the convergence of reflective newton methods for large-scale nonlinear minimization subject to bounds. *Mathematical Programming*, 67, no. 2, pp. 189-224, 1994.

[CL96] T. Coleman and Y. Li. An interior trust region approach for nonlinear minimization subject to bounds. *SIAM Journal on Optimization*, 6, pp. 418-445, 1996.

[CMT04] G. Caire, R. Müller, and T. Tanaka. Iterative multiuser joint decoding: Optimal power allocation and low-complexity implementation. *IEEE Transactions on Information Theory*, 50, no. 9, pp. 950-1973, Sept. 2004.

[Cox72] D. C. Cox. Delay Doppler characteristics of multipath propagation at 910 MHz in a suburban mobile dario environment. *IEEE Transactions on Antennas and Propagation*, 20 no. 5, pp. 625-635, Sept. 1972.

[CRU01] S. Y. Chung, T. Richardson, and R. Urbanke. Analysis of the sum product decoding of low-density parity-check codes using a Gaussian approximation. *IEEE Transactions on Information Theory*, 47, no. 2, pp. 657-670, Feb. 2001.

[CST07] A. Clark, P. Smith, and D. Taylor. Instantaneous capacity of OFDM on Rayleigh-fading channels. *IEEE Transactions on Information Theory*, 53, no. 1, pp. 355-361, Jan. 2007.

[CT91] T. M. Cover and J. A. Thomas. *Elements of Information Theory*. John Wiley &. Sons, Inc., New York, 1991.

[CTB98] G. Caire, G. Taricco, and E. Biglieri. Bit-interleaved coded modulation. *IEEE Transactions on Information Theory*, 44, no. 5, pp. 927-946, May 1998.

[CTB99] G. Caire, G. Taricco, and E. Biglieri. Optimal power control over fading channels. *IEEE Transactions on Information Theory*, 45, no. 5, pp. 1468-1489, July 1999.

[CV93] R. S. Cheng and S. Verdu. Gaussian multiaccess channels with ISI: capacity regions and multiuser water-filling. *IEEE Transactions on Information Theory*, 39, no. 5, pp. 773-785, May 1993.

[DDP01] D. Divsalar, S. Dolinar, and F. Pollara. Iterative turbo decoder analysis based on density evolution. *IEEE Journal on Selected Areas in Communications*, 19, pp. 891-907, May 2001.

[DGE01] L. Deneire, B. Gyselinckx, and M. Engels. Training sequence versus cyclic prefix - a new look on single carrier communication. *IEEE Communications Letters*, 5, no. 7, pp. 292-294, Jul. 2001.

[DJB+95] C. Douillard, M. Jezequel, C. Berrou, A. Picart, P. Didier, and A. Glavieux. Iterative correction of intersymbol interference: turbo equalization. *European Trans. Telecomm.*, vol. 6, pp. 507-511, Sept. 1995.

[DV02] A. Dejonghe and L. Vandendorpe. Turbo-equalisation for multilevel modulation: an efficient low-complexity scheme. *in Proc. IEEE Int. Conf. Commun., vol 3, pp. 1863-1867*, 2002.

[EPP06] A. Elkhazin, K. N. Plataniotis, and S. Pasupathy. Reduced-dimension MAP turbo-BLAST detection. *IEEE Transactions on Communications*, 54, no. 1, pp. 108-118, Jan. 2006.

[EQ88] M. V. Eyuboglu and S. H. Qureshi. Reduced-state sequence estimation with set partitioning and decision feedback. *IEEE Transactions on Communications*, 36, no. 1, pp. 13-21, Jan. 1988.

[FG98] G. J. Foschini and M. J. Gans. On limits of wireless communications in a fading environment when using multiple antennas. *Wireless Personal Communications*, 6, pp. 311-335, 1998.

[For72] G. D. Forney. Maximum-likelihood sequence estimation of digital sequences in the presence of intersymbol interference. *IEEE Transactions on Information Theory*, 18, no. 5, pp. 363-378, May 1972.

[GH99] S. Gollamudi and Y.-F. Huang. Iterative nonlinear MMSE multiuser detection. *in Proc. Int. Conf. Acoust., Speech, Signal Process.*, Phoenix, AZ, March 1999.

[GH01] H. E. Gamal and A. Hammons. Analyzing the turbo decoder using the Gaussian approximation. *IEEE Transactions on Information Theory*, 47, no. 2, pp. 671-686, Feb. 2001.

[GL81] A. Gersho and T. L. Lim. Adaptive cancellation of intersymbol interference for data transmission. *Bell Syst. Tech. J.*, 60, pp. 1997-2021, Nov. 1981.

[GLL97] A. Glavieux, C. Laot, and J. Labat. Turbo equalization over a frequency selective channel. *in Proc. Int. Symp. on Turbo Codes and Rel. Topics*, Brest, Fance, Sept. 1997.

[GM07] M. Grossmann and T. Matsumoto. Hybrid turbo multiuser detection for OFDM transmission with spatially-correlated channels. *IEEE Communications Letters*, 11, no. 5, pp. 420-422, May 2007.

[GM08] M. Grossmann and T. Matsumoto. Nonlinear frequency domain MMSE turbo equalization using probabilistic data association. *IEEE Communications Letters*, 12, no. 4, pp. 295-297, April 2008.

[GM09] M. Grossmann and M. Matsumoto. Rate allocation for k-user MAC with turbo equalization. *in Proc. International ITG Workshop on Smart Antennas*, Berlin, Germany, Feb. 2009.

[GM10] M. Grossmann and T. Matsumoto. On the outage probability of MMSE turbo equalization in frequency-selective rayleigh fading channels. *in Proc. International IEEE ITG Workshop on Smart Antennas (WSA 2010), Bremen, Germany*, Feb. 2010.

[GOM10] M. Grossmann, T. Ortlepp, and M. Matsumoto. Rate allocation for 2-user MAC with MMSE turbo equalization. *IEEE Transactions on Wireless Communications*, 5, no. 5, pp. 1033-1043, May 2010.

[GPH09] Q. Guo, L. Ping, and D. Huang. A low-complexity iterative channel estimation and detection technique for doubly selective channels. *IEEE Transactions on Wireless Communications*, 8, no. 8, pp. 4340-4349, Aug. 2009.

[GR07] I. S. Gradshteyn and I. M. Ryzhik. *Table of Integrals, Series and Products*. 7th ed. New York Academic, 2007.

[Gro09] M. Grossmann. SVD-based precoding for single carrier MIMO transmission with frequency domain MMSE turbo equalization. *IEEE Signal Processing Letters*, 16, no. 5, pp. 418-421, May 2009.

[Gro11] M. Grossmann. Outage performance analysis and code design for three-stage MMSE turbo equalization in frequency-selective Rayleigh fading channels. *IEEE Transactions on Vehicular Technology*, 60, no. 2, pp. 473-484, Feb. 2011.

[GS01] A. J. Grant and C. B. Schlegel. Convergence of linear interference cancellation multiuser receivers. *IEEE Transactions on Communications*, 49, no. 10, pp. 1824-1834, Oct. 2001.

[GS11] M. Grossmann and C. Schneider. Groupwise frequency domain multiuser MMSE turbo equalization for single carrier block transmission over spatially-correlated channels. *IEEE Journal of Selected Topics in Signal Processing*, 5, no. 8, pp. 1548-1562, Dec. 2011.

[GSS+03] D. Gesbert, M. Shafi, D. Shiu, P. J. Smith, and A. Naguib. An overview of MIMO space-time coded wireless systems. *IEEE Journal on Selected Areas in Communications*, 21, no. 3, pp. 218-302, April 2003.

[GT06] G. A. Gupta and S. Toumpis. Power allocation over parallel Gaussian multiple access and broadcast channels. *IEEE Transactions on Information Theory*, 52, no. 7, pp. 3274-3282, July 2006.

[HA04] J. Haipeng and A. Acampora. Bounds on the outage-constrained capacity region of space-division multiple-access radio systems. *EURASIP Journal on Applied Signal Processing*, 2004, no. 9, pp. 1288-1298, 2004.

[Hag04] J. Hagenauer. The EXIT chart - introduction to the extrinsic information transfer in iterative processing. *in Proc. 12th Europ. Signal Proc. Conf. (EUSIPCO)*, Vienna, Austria, Sept. 2004.

[Han02] L. Hanzo. *Turbo Coding, Turbo Equalisation and Space-Time Coding for Transmission over Fading Channels*. John Wiley & Sons, Inc. New York, NY, USA, 2002.

[Hay02] S. Haykin. *Adaptive Filter Theory*. 4th Edition, Prentice Hall, 2002.

[HEM01] J. Hokfelt, O. Edfors, and T. Maseng. A turbo code interleaver design criterion based on the performance of iterative decoding. *IEEE Communications Letters*, 5, no. 2, pp. 52-54, Feb. 2001.

[HJ85] R. A. Horn and C. R. Johnson. *Matrix Analysis*. Cambridge University Press, 1985.

[HK07] J. Hagenauer and C. Kuhn. The list-sequential (LISS) algorithm and its application. *IEEE Transactions on Communications*, 55, no. 5, pp. 919-928, May 2007.

[HLS00] P. Hoeher, I. Land, and U. Sorger. Log-likelihood values and Monte Carlo simulation - some fundamental results. *in Proc. Int. Symp. on Turbo Codes and Rel. Topics*, Brest, France, Sept. 2000.

[HOP96] J. Hagenauer, E. Offer, and L. Papke. Iterative decoding of binary block and convolutional codes. *IEEE Transactions on Information Theory*, 42, no. 2, pp. 429-445, Mar. 1996.

[HS05] C. Hermosilla and L. Szczecinski. Performance evaluation of linear turbo receivers using analytical extrinsic information transfer functions. *EURASIP Journal on Applied Signal Processing*, 6, pp. 892-905, 2005.

[HtB03] B. M. Hochwald and S. ten Brink. Achieving near-capacity on a multiple-antenna channel. *IEEE Transactions on Communications*, 51, no. 3, pp. 389-399, Mar. 2003.

[Hub02] J. Huber. Grundlagen der Wahrscheinlichkeitsrechnung für iterative Decodierverfahren. *e & i Elektrotechnik und Informationstechnik*, 119, no. 11, pp. 386-394, Nov. 2002.

[Jak94] W. C. Jakes. *Microwave Mobile Communications*. New York, NY: IEEE Press, 1994.

[JLA08a] N. L. Josse, C. Laot, and K. Amis. Efficient series expansion for matrix inversion with application to MMSE equalization. *IEEE Communications Letters*, 12, no. 1, pp. 310-312, Jan. 2008.

[JLA08b] N. L. Josse, C. Laot, and K. Amis. MMSE turbo equalization using a low complexity series expansion to approximate the matrix inversion in frequency selective MIMO channels. *in Proc. Int. Symp. on Turbo Codes and Rel. Topics*, Brest, Fance, April 2008.

[JLJ98] J. Jost and X. Li-Jost. *Calculus of variations*, volume 64. Cambridge Studies in Advanced Mathematics, Cambridge University Press, Cambridge, 1998.

[JLML08] J. Jeong, H. Lee, S. H. Moon, and I. Lee. Enhanced group detection with a new receiver combiner for spatial multiplexing MIMO systems. *in Proc. IEEE Veh. Technol. Conf. Fall 2008*, Calgary, Canada, Sept. 2008.

[JPSL04] S. Jiang, L. Ping, H. Sun, and C. S. Leung. Modified LMMSE turbo equalization. *IEEE Communications Letters*, 8, no. 3, pp. 174-176, March 2004.

[JW04] M. Jensen and J. Wallace. A review of antennas and propagation for MIMO wireless communications. *IEEE Transactions on Antennas and Propagation*, 52 no. 11, pp. 2810-2824, Nov. 2004.

[JW05] Y. Jong and T. J. Willink. Iterative tree search detection for MIMO wireless systems. *IEEE Transactions on Communications*, 53, no. 6, pp. 930-935, June 2005.

[Kan05] K. Kansanen. Wireless broadband single-carrier systems with MMSE turbo equalization receivers. *Doctoral thesis, University of Oulu*, Oulu, Finland 2005.

[KC09] Y. Kim and K. Cheun. A reduced-complexity tree search detection algorithm for MIMO systems. *IEEE Transactions on Signal Processing*, 57, no. 6, pp. 2420-2424, June 2009.

[KCT+11] J. Karjalainen, M. Codreanu, A. Tölli, M. Juntti, and T. Matsumoto. EXIT chart-based power allocation for iterative frequency domain

MIMO detector. *IEEE Transactions on Signal Processing*, 59, no. 4, pp. 1624-1641, April 2011.

[KFL01] F. R. Kschischang, B. J. Frey, and H. A. Loeliger. Factor graphs and the sum-product algorithm. *IEEE Transactions on Information Theory*, 47, no. 2, pp. 498-519, Feb. 2001.

[KKHN09] A. Kammoun, M. Kharouf, W. Hachem, and J. Najim. BER and outage probability approximations for LMMSE detectors on correlated MIMO channels. *IEEE Transactions on Information Theory*, 55, no. 10, pp. 4386-4397, Oct. 2009.

[KM03] K. Kansanen and T. Matsumoto. A computationally efficient MIMO turbo-equalizer. *in Proc. IEEE Veh. Techn. Conference*, Jeju, Korea, April 2003.

[KM07] K. Kansanen and T. Matsumoto. An analytical method for MMSE MIMO turbo equalizer EXIT chart computation. *IEEE Transactions on Wireless Communications*, 6, no. 1, pp. 59-63, Jan 2007.

[Kre05] E. Kreyszig. *Advanced Engineering Mathematics*. John Wiley &. Sons, Inc., New York, 2005.

[KSMT05] K. Kansanen, C. Schneider, T. Matsumoto, and R. Thomä. Multilevel-coded QAM with MIMO turbo-equalization in broadband single-carrier signaling. *IEEE Transactions on Vehicular Technology*, 54, no. 3, pp. 954-966, May 2005.

[KSP+03] J. P. Kermoal, L. Schumacher, K. I. Pedersen, P. E. Mogensen, and F. Frederiksen. A stochastic MIMO radio channel model with experimental validation. *IEEE Journal on Selected Areas in Communications*, 20, no. 8, pp. 1211-1226, Aug. 2003.

[Lan05] I. Land. Reliability information in channel decoding. *PhD thesis, Christian-Albrechts-University Kiel, Kiel, Germany*, Sept. 2005.

[LC98] S. Lin and D. Costello. *Error Control Coding: Fundamentals and Applications*. Prentice Hall, Englewood Cliffs, NJ, 1998.

[LHG03] I. Land, P. Hoeher, and S. Gligorevic. Computation of symbol-wise mutual information in transmission systems with LogAPP decoders and application to EXIT charts. *in Proc. Int. Symp. on Turbo Codes and Rel. Topics*, Brest, Fance, Sept. 2003.

[LHLF00] X. Li, H. C. Huang, A. Lozano, and G. J. Foschini. Reduced-complexity detection algorithms for systems using multi-element arrays. *in Proc. IEEE GLOBECOM' 00*, 2, pp. 1072-1076, 2000.

[Loe04] H. A. Loeliger. An introduction to factor graphs. *IEEE Signal Processing Magazine*, pp. 28-41, Jan. 2004.

[LP04] L. Liu and L. Ping. An extending window MMSE turbo equalization algorithm. *IEEE Signal Processing Letters*, 11, no. 11, pp. 891-894, Nov. 2004.

[LPWH01] J. Luo, K. R. Pattipati, P. K. Willett, and F. Hasegawa. Near optimal multiuser detection in synchronous CDMA using probabilistic data association. *IEEE Communication Letters*, 5, no. 9, pp. 361-363, Sept. 2001.

[LR97] X. Li and J. Ritcey. Bit-interleaved coded modulation with iterative decoding. *Electronic Letters*, 1, pp. 169-171, 1997.

[LS03] S-J. Lee and A. C. Singer. Convergence analysis for linear turbo equalization. *in Proc. Annual Asilomar Conf. Signals, Syst., Comp*, pp. 667-671, 2003.

[Mal03] R. K. Malik. On multivariate Rayleigh and exponential distributions. *IEEE Transactions on Information Theory*, 49, no. 6, pp. 1499-1515, June 2003.

[MDEJ03] R. K. Martin, M. Ding, B. L. Evans, and C. R. Johnson. Efficient channel shortening equalizer design. *EURASIP Journal on Applied Signal Processing*, 13, no. 2, pp. 1279-1290, 2003.

[MJLL10] S. H. Moon, J. Jeong, H. Lee, and I. Lee. Enhanced groupwise detection with a new receive combiner for spatial multiplexing MIMO systems. *IEEE Transactions on Communications*, 58, no. 9, pp. 2511-2515, Sept. 2010.

[MP07] V. Mai and A. Paulraj. MIMO wireless linear precoding. *IEEE Signal Processing Magazine*, 24, no. 5, pp. 86-105, Sept. 2007.

[MWG+02] B. Muquet, Z. Wang, G. Giannakis, M. de Courville, and P. Duhamel. Cyclic prefixing or zero padding for wireless multicarrier transmissions? *IEEE Transactions on Communications*, 50, no. 12, pp. 2136-2148, Dec. 2002.

[NWY05] K. R. Narayanan, X. Wang, and G. Yue. Estimating the PDF of the SIC-MMSE equalizer output and its applications in designing LDPC codes with turbo equalization. *IEEE Transactions on Wireless Communications*, 4, no. 1, pp. 278-287, Jan. 2005.

[OAM01] H. Omori, T. Asai, and T. Matsumoto. A matched filter approximation for SC/MMSE iterative equalizers. *IEEE Communications Letters*, 5, no. 7, pp. 310-312, Jul. 2001.

[OHW+03] H. Ozcelik, M. Herdin, W. Weichselberger, J. Wallace, and E. Bonek. Deficiencies of 'Kronecker' MIMO radio channel model. *Electronics Letters*, 39 no. 16, pp. 1209-1210, Aug. 2003.

[OSV03] E. Onggosanusi, A. Sayeed, and B. Veen. Efficient signaling schemes for wideband space-time wireless channels using channel state information. *IEEE Transactions on Vehicular Technology*, 52, no. 1, pp. 1-13, Jan. 2003.

[PCL03] D. Palomar, J. Cioffi, and M. Lagunas. Joint Tx-Rx beamforming design for multicarrier MIMO channels: A unified framework for convex optimization. *IEEE Transactions on Signal Processing*, 51, no. 9, pp. 2381-2401, Sep. 2003.

[PF05] D. P. Palomar and J. R. Fonollosa. Practical algorithms for a family of waterfilling solutions. *IEEE Transactions on Signal Processing*, 53, no. 2, pp. 686-595, Feb. 2005.

[PGNB04] A. J. Paulraj, D. A. Gore, R. U. Nabar, and H. Boelcskei. An overview of MIMO communications - a key to gigabit wireless. *Proceeding IEEE*, 92, no. 2, pp. 198-218, Feb. 2004.

[PJ06] D. P. Palomar and Y. Jiang. MIMO transceiver design via majorization theory. *Foundations and Trends in Communication and Information Theory*, 3, Dec. 2006.

[PNG03] A. J. Paulraj, R. Nabar, and D. Gore. *Introduction to Space-Time Wireless Communications*. Cambridge University Press, 2003.

[PP02] A. Papoulis and S. U. Pillai. *Probability, Random Variables and Stochastic Processes*. 4th ed. New York: McGraw-Hill, 2002.

[PR06] T. H. Peng and L. K. Rasmussen. Asymptotically optimal nonlinear MMSE multiuser detection based on multivariate Gaussian approximation. *IEEE Transactions on Communications*, 54, no. 9, pp. 1427-1438, Sept. 2006.

[Pro01] J. G. Proakis. *Digital Communications*. 4th ed. New York: McGraw-Hill, 2001.

[PS04] S. Pfletschinger and F. Sanzi. Iterative demapping for OFDM with zero-padding or cyclic prefix. *in Proc. IEEE Int. Conf. on Commun. (ICC) 2004*, Paris, France, June 2004.

[PSS01] H. D. Pfister, J. B. Soriaga, and P. H. Siegel. On the achievable information rates of finite state ISI channels. *in Proc. IEEE GLOBECOM*, pp. 2992-2996, San Antonio, USA 2001.

[PSU05] H. D. Pfister, I. Sason, and R. Urbanke. Capacity-achieving ensembles for the binary erasure channel with bounded complexity. *IEEE Transactions on Information Theory*, 51, no. 7, pp. 2352-2379, July 2005.

[PV97] H. V. Poor and S. Verdu. Probability of error in MMSE multiuser detection. *IEEE Transactions on Information Theory*, 43, no. 5, pp. 858-871, May 1997.

[Qur85] S. U. Qureshi. Adaptive equalization. *Proc. IEEE*, 73, pp. 1349-1287, Sept. 1985.

[RD07] A. Roumy and D. Declercq. Characterization and optimization of LDPC codes for the 2-user gaussian multiple access channel. *EURASIP Journal on Wireless Communications and Networking*, 2007, Article ID 74890, 10 pages, 2007.

[RG75] L. R. Rabiner and B. Gold. *Theory and application of digital signal processing*. Englewood Cliffs, N.J., Prentice-Hall, Inc., 1975.

[RHV07] V. Ramon, C. Herzet, and L. Vandendorpe. A semi-analytical method for predicting the performance and convergence behaviour of a multiuser turbo equalizer. *IEEE Transactions on Signal Processing*, 55, no. 3, pp. 1104-1117, March 2007.

[RKS10] V. Raghavan, J.-H. Kotecha, and A.-M. Sayeed. Why does the Kronecker model result in misleading capacity estimates? *IEEE Transactions on Information Theory*, 56 no. 10, pp. 4843-4864, Oct. 2010.

[RLM06] O. Rousseaux, G. Leus, and M. Moonen. Estimation and equalization of doubly selective channels using known symbol padding. *IEEE Transactions on Signal Processing*, 54, no. 3, pp. 979-990, Mar. 2006.

[RSU01] T. Richardson, A. Shokrollahi, and R. Urbanke. Design of capacity-approaching irregular low-density parity-check codes. *IEEE Transactions on Information Theory*, 47, no. 2, pp. 619-637, Feb. 2001.

[RU96] B. Rimoldi and R. Urbanke. A rate-splitting approach to the gaussian multiple-access channel. *IEEE Transactions on Information Theory*, 42, no. 2, pp. 364-375, Mar. 1996.

[RU01] T. Richardson and R. Urbanke. The capacity of low-density parity-check codes under message-passing decoding. *IEEE Transactions on Information Theory*, 47, no. 2, pp. 599-618, Feb. 2001.

[RU06] T. Richardson and R. Urbanke. *Modern Coding Theory*. Cambridge University Press, 2006.

[SB06] F. Schreckenbach and G. Bauch. Bit-interleaved coded irregular modulation. *European Transactions on Telecommunications (ETT)*, 17, pp. 269-282, March 2006.

[SB10] C. Studer and H. Bölcskei. Soft-input soft-output single tree-search sphere decoding. *IEEE Transactions on Information Theory*, 56, no. 10, pp. 4827-4842, Oct. 2010.

[SBR06] D. P. Shepherd, F. Brännström, and M. C. Reed. Fidelity charts and stopping/termination criteria for iterative multiuser detection. *in Proc. Int. Symp. on Turbo Codes and Rel. Topics*, Munich, Germany, April 2006.

[SCG05] J. Del Ser, P. M. Crespo, and O. Galdos. Asymmetric joint source-channel coding correlated sources with blind HMM estimation at the receiver. *EURASIP Journal on Wireless Communications and Networking: Special Issue on Wireless Sensor Networks*, pp. 483-492, Sept. 2005.

[SGHB03] F. Schreckenbach, N. Görtz, J. Hagenauer, and G. Bauch. Optimization of symbol mappings for bit-interleaved coded modulation with iterative decoding. *IEEE Communications Letters*, 7, no. 12, pp. 593-595, Dec. 2003.

[SGK+04] C. Schneider, M. Grossmann, K. Kansanen, T. Matsumoto, and R. Thomä. Measurement based throughput performance evaluation of antenna variable modulation for broadband turbo MIMO transmission. *in Proc. International Symp. on Wireless Personal and Multimedia Communication (WPMC) 2004, Abano Terme, Italy*, Sept. 2004.

[SGT04] C. Schneider, M. Grossmann, and R. Thomä. Performance of antenna variable modulation for turbo MIMO transmission in frequency-selective channels. *In Proc. International IEEE ITG Workshop on Smart Antennas*, Munich, Germany, March 2004.

[Skl97] B. Sklar. Rayleigh fading channels in mobile digital communication systems part I: Characterization. *IEEE Communications Magazine*, 35, no. 7 pp. 90-100, 1997.

[SLW03] B. Steingrimsson, Z. Q. Luo, and K. M. Wong. Soft quasi-maximum likelihood detection for multiple-antenna wireless channels. *IEEE Transactions on Signal Processing*, 51, no. 11, pp. 2710-2719, Nov. 2003.

[SM07] H. Steendam and M. Moeneclaey. Different guard interval techniques for OFDM: Performance comparison. *in Proc. IEEE Multicar. Spread Spectrum Conf. 2007*, pp. 11-14, Herrsching, Germany 2007.

[SPS05] A. Sanderovich, M. Peleg, and S. Shamai (Shiz). LDPC coded MIMO multiple access with iterative joint decoding. *IEEE Transactions on Information Theory*, 51, no. 4, pp. 1437-1450, April 2005.

[SS01] Z. Shi and C. Schlegel. Joint iterative decoding of serially concatenated error control coded CDMA. *IEEE Journal on Selected Areas in Communications*, 19, no. 8, pp. 1646-1653, August 2001.

[SSB06] C. Schlegel, Z. Shi, and M. Burnashev. Optimal power/rate allocation and code selection for iterative joint detection of coded random CDMA. *IEEE Transactions on Information Theory*, 52, no. 9, pp. 4286-4294, Sept. 2006.

[SSP01] H. Sampath, P. Stoica, and A. Paulraj. Generalized linear precoder and decoder design for MIMO channels using the weighted MMSE criterion. *IEEE Transactions on Communications*, 49, no. 12, pp. 2198-2206, Dec. 2001.

[SSS04] S. Song, A. C. Singer, and K. Sung. Soft input channel estimation for turbo equalization. *IEEE Transactions on Signal Processing*, 52, no. 10, pp. 2885-2894, Oct. 2004.

[StB06] J. Shi and S. ten Brink. Exact EXIT functions for convolutional codes over the binary erasure channel. *in Proc. 44th Annual Allerton Conf. Commun., Control, and Computing*, Monticello, IL, pp. 431-437, 2006.

[STS07] M. Sadek, A. Tarighat, and A. H. Sayed. A leakage-based precoding scheme for downlink multi-user MIMO channels. *IEEE Transactions on Wireless Communications*, 6, no. 5, pp. 1711-1721, May 2007.

[tB01] S. ten Brink. Convergence behavior of iteratively decoded parallel concatenated codes. *IEEE Transactions on Communications*, 49, no. 10, pp. 1727-1737, Oct. 2001.

[tBK03] S. ten Brink and G. Kramer. Design of repeat-accumulate codes for iterative detection and decoding. *IEEE Transactions on Communications*, 51, no. 11, pp. 2764-2772, Nov. 2003.

[tBKA04] S. ten Brink, G. Kramer, and A. Ashikhmin. Design of low-density parity-check codes for modulation and detection. *IEEE Transactions on Communications*, 52, no. 4, pp. 670-678, April 2004.

[tBSY98a] S. ten Brink, J. Speidel, and R. Yan. Iterative demapping and decoding for multilevel modulation. *in Proc. IEEE Globecom Conf. 1998*, pp. 579-584, Sydney, Australia 1998.

[tBSY98b] S. ten Brink, J. Speidel, and R. Yan. Iterative demapping for QPSK modulation. *Electronic Letters*, 34, pp. 1459-1460, July 1998.

[Tüc04] M. Tüchler. Design of serially concatenated systems depending on the block length. *IEEE Transactions on Communications*, 52, no. 2, pp. 209-218, Feb. 2004.

[Tel99] I. E. Telatar. Capacity of multi-antenna Gaussian channels. *European Transactions on Telecommunications*, 10, no. 6, pp. 585-596, Nov. 1999.

[TH98] D. Tse and S. Hanly. Multiaccess fading channels-part I: Polymatroid structure, optimal resource allocation and throughput capacities. *IEEE Transactions on Information Theory*, 49, no. 11, pp. 2796-2815, Nov. 1998.

[TH02] M. Tüchler and J. Hagenauer. Turbo equalization: principles and new results. *IEEE Transactions on Communications*, 50, no. 5, pp. 754-767, May 2002.

[THR+01] R. S. Thomä, D. Hampicke, A. Richter, G. Sommerkorn, and U. Trautwein. MIMO vector channel sounder measurement for smart antenna system evaluation. *European Transactions on Telecommunications*, 12, no. 5, pp. 427-438, 2001.

[TJVW04] T. Tian, C. Jones, J. Villasenor, and R. Wesel. Selective avoidance of cycles in irregular LDPC code construction. *IEEE Transactions on Communications*, 52, no. 8, pp. 1242-1247, Aug. 2004.

[TKS04] M. Tüchler, R. Koetter, and A. Singer. Graphical models for coded data transmission over intersymbol interference channels. *European Transactions on Communications*, 15, pp. 307-321, August 2004.

[Ton03] A. M. Tonello. MIMO MAP equalization and turbo decoding in interleaved space time coded systems. *IEEE Transactions on Communications*, 2, no. 2, pp. 155-160, Feb. 2003.

[TR02] E. Tungsrisaguan and R. Rajatheva. Turbo equalization with sequential sequence estimation over multipath fading channels. *IEEE Communications Letters*, 6, no. 3, pp. 93-95, March 2002.

[TSK02] M. Tüchler, A. Singer, and R. Koetter. Minimum mean squared error equalization using a priori information. *IEEE Transactions on Signal Processing*, 50, no. 3, pp. 673-683, March 2002.

[TST05] U. Trautwein, C. Schneider, and R. Thomae. Measurement based performance evaluation of advanced MIMO transceiver designs. *EURASIP Journal on Applied Signal Processing*, pp. 1712-1724, Jan. 2005.

[TtBH02] M. Tüchler, S. ten Brink, and J. Hagenauer. Measures for tracing convergence of iterative decoding algorithms. *in Proc. 4th Int. ITG Conf. Source and Channel Coding*, Berlin, Germany, Jan. 2002.

[TWN+08] S. Tan, J. Wang, S. X. Ng, S. Chen, and L. Hanzo. Three-stage turbo MBER multiuser beamforming receiver using irregular convolutional codes. *IEEE Transactions on Vehicular Technology*, 57, no. 3, pp. 1657-1663, May 2008.

[Var95] M. K. Varanasi. Group detection for synchronous Gaussian code-division multiple-access channels. *IEEE Transactions on Information Theory*, 41, no. 7, pp. 1083-1096, July 1995.

[VB03] R. Visoz and A. O. Berthet. Iterative decoding and channel estimation for space-time BICM over MIMO block fading multipath awgn channel. *IEEE Transactions on Communications*, 51, no. 8, pp. 1358-1367, Aug. 2003.

[VBC06] R. Visoz, A. O. Berthet, and S. Chtourou. Frequency-domain block turbo-equalization for single-carrier transmission over MIMO broadband wireless channel. *IEEE Transactions on Wireless Communications*, 54, no. 12, pp. 2144-2149, Dec. 2006.

[VMJ04] N. Veselinovic, T. Matsumoto, and M. Juntti. Iterative MIMO turbo multiuser detection and equalization for STTrC-coded systems with unknown interference. *EURASIP Journal on Wireless Communications and Networking*, 2, pp. 309-321, Dec. 2004.

[WIN08] WINNER. WINNER II channel models. *Tech. Rep. IST-4-027756 WINNER II D1.1.2 V1.2*, Feb. 2008.

[WKTM05] R. Wohlgenannt, K. Kansanen, D. Tujkovic, and T. Matsumoto. Outage-based LDPC code design for SC/MMSE turbo equalization. *in Proc. IEEE Veh. Technol. Conf., pp. 505-509*, May 2005.

[WMG02] Z. Wang, X. Ma, and G. Giannakis. Optimality of single-carrier zero padded block transmissions. *in Proc. IEEE Wirel. Commun. and Ntwor. Conf. 2002*, vol. 2, pp. 660-664, France, Mar. 2002.

[WNYH06] J. Wang, S. X. Ng, L. Yang, and L. Hanzo. Combined serially concatenated codes and MMSE equalization: An EXIT chart aided perspective. *in Proc. IEEE Veh. Technol. Conf.-Fall, pp. 1-5*, Sept. 2006.

[WP99a] X. Wang and H. V. Poor. Iterative (turbo) soft-interference cancellation and decoding for coded CDMA. *IEEE Transactions on Communications*, 47, no. 7, pp. 1046-1061, July 1999.

[WP99b] X. Wang and H. V. Poor. Space-time multiuser detection in multipath CDMA channels. *IEEE Transactions on Signal Processing*, 7, no. 9, pp. 2356-2374, Sept. 1999.

[XP03] W. Xiang and S. S. Pietrobon. On the capacity and normalization of ISI channels. *IEEE Transactions on Information Theory*, 49, no. 9, pp. 2263-2268, Sept. 2003.

[XWL+04] C. Xiao, J. Wu, S.-Y. Leong, Y. R. Zheng, and K. B. Letaief. A discrete-time model for triply selective MIMO Rayleigh fading channels. *IEEE Transactions on Wireless Communications*, 3 no. 5, pp. 1678-1688, Sept. 2004.

[YGWP08] X. Yuan, Q. Guo, X. Wang, and L. Ping. Evolution analysis of low-cost iterative equalization in coded linear systems with cyclic prefixes. *IEEE Journal on Selected Areas in Communications*, 26, no. 2, pp. 301-310, Feb. 2008.

[YRBC04] W. Yu, W. Rhee, S. Boyd, and J. Cioffi. Iterative water-filling for Gaussian vector multiple access channels. *IEEE Transactions on Information Theory*, 50, no. 1, pp. 145-151, Jan. 2004.

[ZDK04] Z. Zhang, T. M. Duman, and E. M. Kurtas. Achievable information rates and coding for MIMO systems over ISI channels and frequency-selective fading channels. *IEEE Transactions on Communications*, 52, no. 10, pp. 1698-1710, Oct. 2004.

[Zeh92] E. Zehavi. 8-PSK trellis codes for a Rayleigh channel. *IEEE Transactions on Communications*, 40, no. 5, pp. 873-884, May 1992.

[ZM07] J. Zyren and W. McCoy. Overview of the 3GPP long term evolution physical layer. *Freescale Semiconductor, Inc., white paper*, July 2007.